Cretaceous and Cenozoic basin evolution based on decompacted sediment thickness from petroleum wells around New Zealand.

Louise Jane Christie

A thesis submitted to the
School of Geography, Environmental and Earth Science
Victoria University of Wellington,
in partial fulfillment of the degree of

Master of Science
in Geology

Victoria University of Wellington
2007

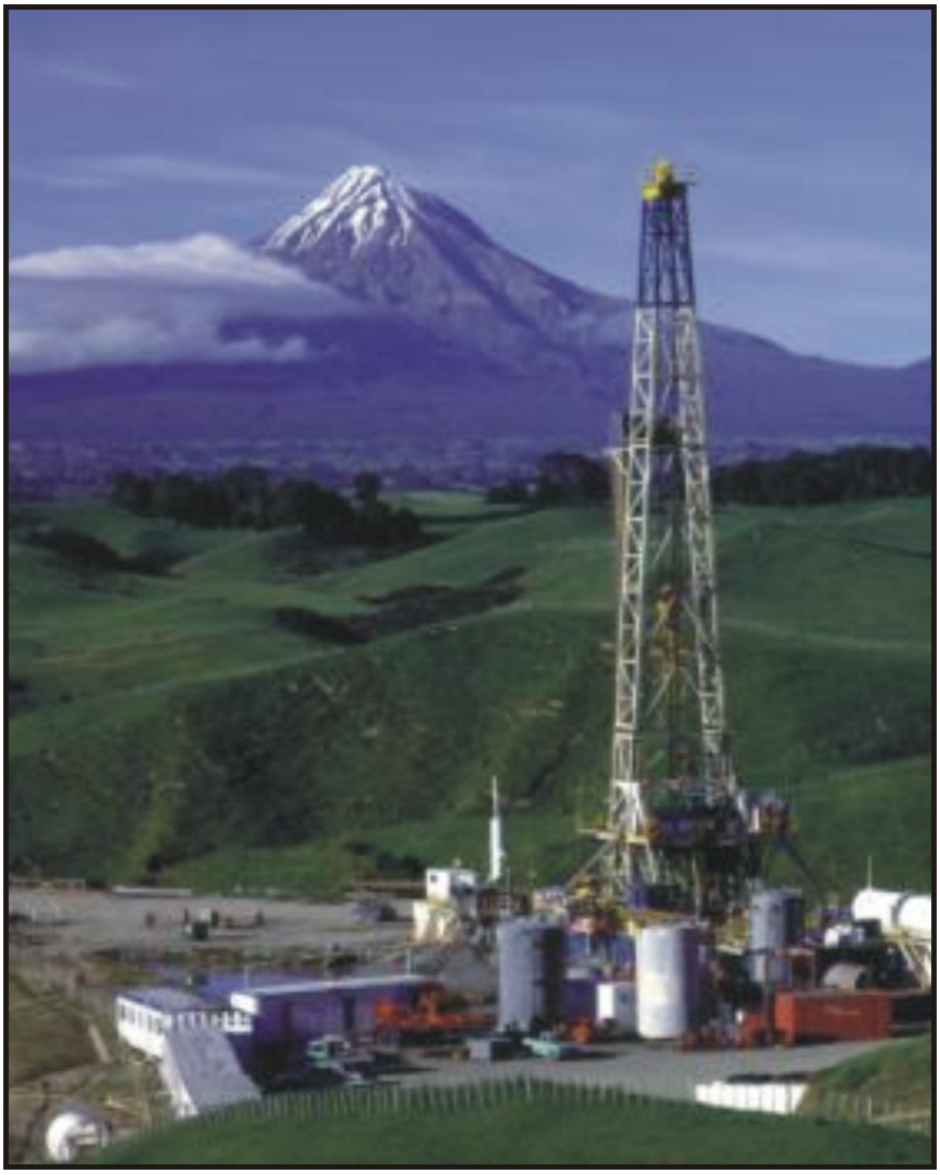

Frontispiece: Drilling near Mount Taranaki, New Zealand.

ABSTRACT

Decompacted sedimentary data from 33 New Zealand exploration wells is used to investigate basin evolution and tectonics from around New Zealand. This analysis is directed to both a comparison of basin behaviour and a search for common subsidence signatures. Common to almost all New Zealand basin subsidence curves is a sedimentary signature associated with rifting of the Gondwana super-continent (80-65 Ma). In the Great South Basin a second rifting event is inferred at 51 ± 2 Ma, illustrated by a rapid increase in subsidence rates (with a maximum rate of 190 $m.Myr^{-1}$ at Pakaha-1). Coinciding with the cessation of Tasman Sea rifting (~53 Ma), and with the onset of rifting in the Emerald Basin (~ 50 Ma), it is assumed that the event is related to the tectonic plate reorganization.

An increase in sedimentation is noted at ~20 Ma in most South Island wells. Convergence on the Alpine Fault, leading to increased erosion is cited as a mechanism for this period of basin growth, consistent with the Cande and Stock (2004) model of plate motions. A second increase in sedimentation occurs at ~6 Ma in almost all wells around New Zealand. Climate-driven erosion resulting in isostatic uplift is thought to contribute to this event.

Hiatuses in the sedimentary record for the Canterbury, Great South and Western Southland Basins during the late Oligocene are interpreted as the Marshall Paraconformity. It appears that the break in sedimentation located within a regional transgressional mega-sequence was caused by mid Oligocene glacio-eustatic fall and related oceanic current processes.

Loading by the Northland Allochthon, in conjunction with paleobathymetry and subsidence data, is used to demonstrate the mechanical properties of the lithosphere. A lithospheric rigidity of 1.5×10^{22} Nm is estimated, with an elastic thickness of 12 km. Considerably lower than elastic thickness values previously calculated for the Plio-Pleistocene loading of the Taranaki Platform. It is noted that the Northland value represents a younger, hotter crust at the time of load emplacment.

With the exception of the central Taranaki and Great South Basins, stretching factors (β) for the sedimentary basins surrounding New Zealand are below 2. This suggests crustal thickness prior to rifting was between 35 and 50 km, consistent with data from conjugate margins of Australia and Antarctica. An increase in water depth in the Taranaki Basin at 25 ± 3 Ma is confirmed by this study. This coincides with a similar signature on the West Coast of the South Island at 26 ± 2 Ma. It is suggested that a mantle flow caused by the initiation of the subduction zone at ~25 Ma extends over a broader region (>750 km) than previously thought.

ACKNOWLEDGEMENTS

" I no doubt deserve my enemies, but I don't believe I deserve my friends."

Walt Whitman

First, **Mr Davey**, my high school teacher. You made rocks interesting to a fifteen year-old! Teachers like you are capable of changing the world, you've certainly changed mine. I wish you all the best in your retirement.

Tim Stern, for sticking with the world's worst procrastinator. I wouldn't have made it without your guidance. **Mike Hannah**, thanks for getting involved in many aspects of my project (You'll know what I mean). The university and your students are lucky to have you. **Gill** in the Library, for your smiles whenever, wherever. And for helping me to fill in forms, find things I'd misplaced, and for buying me books. **Euan Smith**, for a hug when I REALLY needed one.

My officemates through the years, **Jess, Mike**, **Lee**, **Karryn**, **Calfy**, **Woody**, **Sebastian**, **Suz**, and **Danny boy**. Thank you for providing distractions when I needed them (I'm sorry some of you didn't need as many as I did). My team of proof readers, **Matt, Tom, Kim, Chris, Hannu** and **Liz**, thanks for your last minute effort. **Katie**, your strength got me through the start of the year. **Anya, Anya, Anya, Anya** (Four mentions). For all your help and for making me smile.

Sarah and **Anna**, thank you for not doing geology, I'll see you at Moo Moo's. **Iain**, **Driver**, and **Mac**. Thanks for listening and for the cuddles, even when I had to force you to give me them. **Caell and Shasta**, I'm terrible at keeping in touch, but I know we will be friends forever!

Grandma, for slipping me cash and petrol vouchers when mum and dad weren't looking. **Pud**, for the use of your computer and some good nights out, I owe you a tequila night.

Jodi, the worlds greatest friend, you have literally kept me sane. It isn't possible to put into words what you mean to me, so I'll stop here. I love you .

Finally, **Mum and Dad**. I can never thank you enough for your help, your hugs, your money, your food, your petrol, your house (and in Mum's case, even the clothes off your back!), but most importantly for your love and unconditional support. I love you. I owe you my first oil well!

TABLE OF CONTENTS

LIST OF FIGURES

CHAPTER 1: INTRODUCTION

CHAPTER 2: BACKGROUND

CHAPTER 3: METHODS

CHAPTER 4: CANTERBURY BASIN

CHAPTER 5: GREAT SOUTH BASIN

CHAPTER 6: WESTERN SOUTHLAND BASINS

CHAPTER 7: WEST COAST BASIN

CHAPTER 8: TARANAKI BASIN

CHAPTER 9: NORTHTLAND BASIN

CHAPTER 10: DISCUSSION

LIST OF TABLES

CHAPTER 1: INTRODUCTION

1. 1: PRELUDE

Tectonic investigations typically focus on the horizontal motions of tectonic plates over the Earth's surface, however, the associated vertical motions also play an important role in the evolution of our planet. Subsidence/uplift histories are typically more difficult to determine, and therefore studies typically focus on lateral motions. Improvements made in paleontology during the seventies and eighties resulted in advancements in geohistory analysis, allowing for better resolution of events and estimations of paleobathymetry. By taking into account sedimentation rate, subsidence/uplift rate and paleo-bathymetry, geohistory analysis can provide answers to the how, when and why of sedimentary basin formation. The resulting graphical representations offer clues to the driving force behind basin formation, and the overall tectonic regime prevailing at that time, enabling comparisons both within the same basin, and with other basins. Subsidence histories are becoming increasingly important in an energy hungry world as another tool in the petroleum geologists belt, allowing estimations of hydrocarbon maturity, reservoir potential, and of the timing of oil migration.

1. 2: PRESENT SETTING

Present day New Zealand straddles the boundary between the Australian Plate to the west, and the Pacific Plate to the east. The current land area, which covers 250,000 km^2, represents only a small portion of a much larger submerged continent, covering approximately 3,500,000 km^2 (Fig. 1.1). Subduction of the Pacific Plate under the Australian Plate at the Tonga-Kermadec Trench and Hikurangi Trough is linked to subduction of opposing polarity (Puysegur Trench) via a zone of oblique continental convergence through the South Island, known as the Alpine Fault (Norris et. al., 1990). Located around New Zealand are a number of basins, many of which formed during the Cretaceous break-up of Gondwana. Exceptions include the South Fiji Basin, of Oligocene age; the Harve Trough, which formed during the Pliocene to Recent (Walcott, 1987); and the Emerald and Solander Basins, which formed during the Eocene (Sutherland, 1995).

Figure 1.1: Map showing the major features of the New Zealand continent.

1. 3: NEW ZEALAND'S SEDIMENTARY BASIN HISTORY

The New Zealand sub-continent is well endowed with sedimentary basins that have formed over the last 100 M.a. (Cook and Gregg, 1997). The sedimentary rocks that fill these basins contain all of New Zealand's hydrocarbons and most of its non-metallic raw materials (Nathan et. al., 1986). The Cretaceous to the Cenozoic was a tectonically active period, with most basins displaying multiple phases of deformation (King, 2000). Basin development surrounding New Zealand can be broadly divided (from oldest to youngest) into phases of rifted margin, passive margin and convergent margin episodes, which reflect the tectonic development of the New Zealand sub-continent (Explore New Zealand Petroleum, 2003).

The breakup of Gondwana led to rapid subsidence and the formation of rift basins (Laird, 1993), which filled with syn-rift terrestrial and transgressive marine sediments (Stagpoole et. al., 2002). By the Paleocene subsidence led to widespread marine flooding.

The cessation of spreading in the Tasman Sea by Eocene meant that New Zealand was remote from any active plate boundary (Stagpoole, 2002), heralding the passive margin phase of basin development. The area surrounding New Zealand underwent regional post-rift thermal subsidence, resulting in the deposition of fine grained clastics and increasingly carbonaceous sediments (Balance, 1993).

The convergent margin phase began with a major reconfiguration of several tectonic plates in the middle Eocene. The southward propagation of subduction on the Australian-Pacific margin coincides with deposition of carbonate rich sediments, reflecting widespread submergence (Stagpoole, 2002). During the Neogene the Alpine Fault developed, forming a link between subduction in the north and oblique extension in the southwest of New Zealand (King, 2000). Sea-floor spreading in the south became increasingly oblique, eventually superseded by strike-slip motion and subduction of the Australian Plate beneath the Pacific Plate (Stagpoole, 2000). The ensuing compression on the plate boundary caused uplift and erosion, resulting in rapid deposition and infilling of new and previously formed depocentres (Explore New Zealand Petroleum, 2003).

This project focuses primarily on the sedimentary basins immediately surrounding New Zealand (Fig 1.2). Their close proximity to land means these basins have been explored in more detail than distant basins. They are penetrated by considerably more wells, are the

subject of numerous seismic cruises, and therefore their evolutionary history is better understood. Their location close to existing infrastructure also means that these basins are likely to prove most important to hydrocarbon exploration in the near future.

The East Coast Basin has been omitted for this investigation. This is due to the highly faulted nature of the sediment, related to subduction immediately to the east of the basin. While this deformation may prove profitable to the oil industry in the future, the wells in the region are not ideal for geohistory analysis due to the number of breaks in the sedimentary record.

Figure 1.2: New Zealand's sedimentary Basins (from Explore New Zealand Petroleum 2003, Ministry of Economic Development, Crown Minerals, 2003).

1. 4: THESIS AIMS

The primary aim of this investigation is to provide a region-by-region analysis of basin subsidence and extension factors (β values) in order to determine characteristic tectonics. New Zealand is fortunate that legislation requires petroleum exploration companies to make public their findings. This thesis seeks to make use of this information by utilizing petroleum well data compiled by Crown Minerals, a branch of the Ministry of Economic Development.

Almost all the basins have been examined individually using a variety of methods. This means comparisons of geohistory between basins is made difficult by inconsistent methods. This study provides comparable subsidence curves for a number of petroleum wells. As well as a systematic and general study of basins from around New Zealand, this study addresses the following specific questions:

- Is the subsidence noted in the Taranaki Basin by Stern and Holt (1994) seen outside of the Taranaki region? If so what is the wavelength and timing of this process?
- When did the plate boundary propagate through the South Island? Do data support Cande and Stock (2004), or Walcott (1998)?
- Do subsidence curves provide evidence of convergence on the Alpine Fault prior to 8-6 M.a., as suggested by Cande and Stock (2004)?
- Could the increase in sedimentation seen in sedimentary basins at 6 M.a. be the result of a change in climate, as suggest by Molnar (2004), or a change from submarine to sub-aerial erosion?
- Can geohistory analysis provide hints to the nature of the Marshall Paraconformity, a controversial break in the Oligocene stratigraphic record?
- What is the wavelength of flexure due to loading by the Northland Allocthon?

1. 5: THESIS OUTLINE

The following is a brief description of the layout for this thesis.

Chapter 2: Background

Included within this chapter is background information and theory that will aid in the understanding of the geohistory analysis in the following chapters.

Chapter 3: Methodology

This chapter briefly covers the methods used to create the curves used for analysis.

Chapter 4: Canterbury Basin

The first of the analysis chapters, this will provide the reader with a basic stratigraphic understanding, followed by the results of analysis, a section of interpretation and finally conclusions. The Canterbury Basin chapter is the first of six chapters, each covering a different basin, each of which will follow the same format, they are listed below:

Chapter 5: Great South Basin

Chapter 6: Western Southland Basin

Chapter 7: West Coast Basin

Chapter 8: Taranaki Basin

Chapter 9: Northland Basin

Chapter 10: Discussion

The discussion chapter will return to major points made in the individual basin chapters, and elaborate further by comparing results from other basins.

Chapter 11: Conclusions

This chapter provides a brief list of the conclusions made by this investigation.

Appendix

Included within the appendix are the stratigraphic columns and data used for each petroleum well examined.

CHAPTER 2: BACKGROUND

2. 1: INTRODUCTION

Sedimentation and subsidence curves can provide clues to nature of basin formation. In order to estimate the subsidence history of a sedimentary basin, however, present-day stratigraphic thicknesses must first be corrected to account for the loss of porosity due to loading from sediment above. This section will explain the principles of basin formation and subsidence, and theory behind decompaction and backstripping used in this investigation.

2. 2: MECHANISMS OF BASIN FORMATION

2. 2. 1: Isostasy

The application of Archimedes' principle to the earth suggests that continents are buoyed up by a force equal to the weight of the displaced mantle (Turcotte and Schubert, 1982). The result is that adjacent blocks of varying thickness and/or density will have different relief. Below a certain depth there is no density contrast between the two adjacent rock columns, and asthenosphere of equal density underlies both columns. The weight of the columns above this depth of compensation must therefore be equal (Kearey and Vine, 1996) (Fig. 2.1).

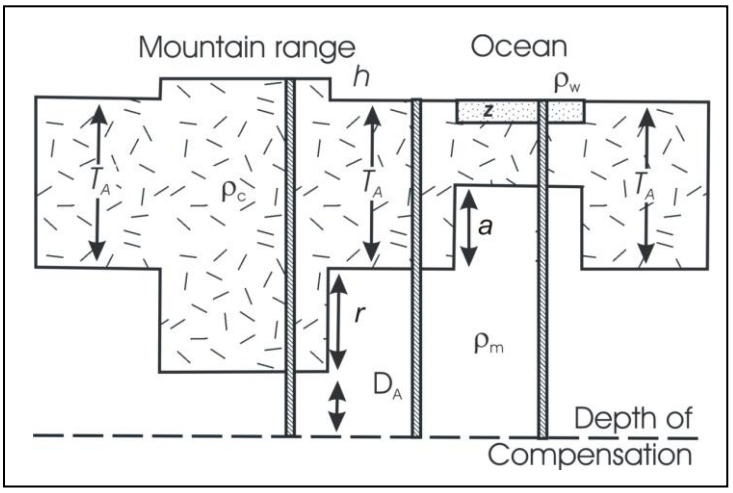

Figure 2.1: Airy mechanism of isostatic compensation. h, height of mountain above sea level; z, depth of water of density ρ_w; T_A, normal thickness of crust of density ρ_c; r, thickness of root; a, thickness of antiroot; D_A, depth of compensation below root; ρ_m, density of mantle.

Isotasy has implications in basin development where thickness or density of the crust is changed. This can happen in a number of ways, including stretching of the lithosphere, removal of the crust by erosion or tectonic processes, emplacement of denser material (e.g. dykes, thrust ophiolites), or filling a depression with denser material (e.g. replace water with sediment).

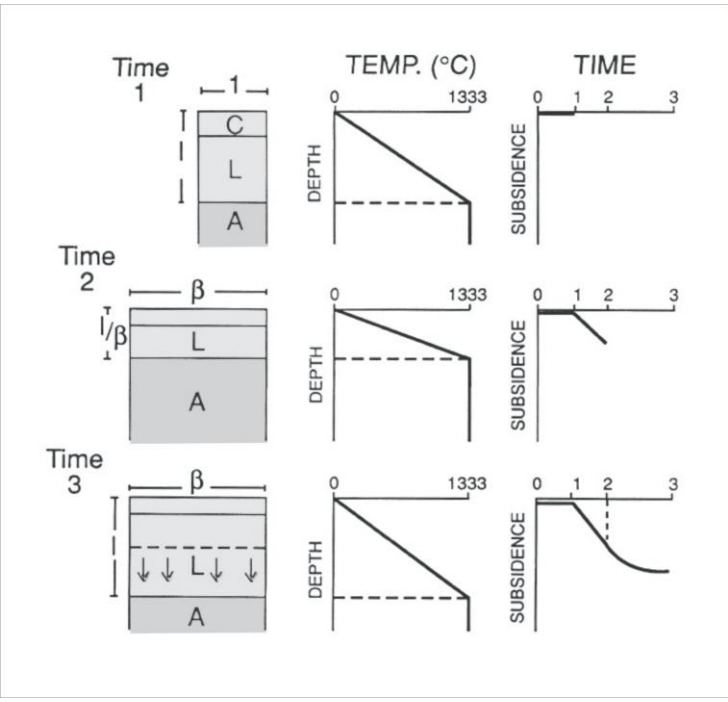

Figure 2.2: The thermal and subsidence effects of lithospheric extension. (Modified from McKenzie, 1978).

Figure 2.2 is a simple model showing initial isostatic rifting and subsequent thermal subsidence (to be discussed in a following section). At time $t = 1$ the lithospheric column of one unit height consists of crust (C), and mantle lid (L), and asthenosphere (A). The column has a simple geothermal gradient from the surface of the crust to the base of the lithosphere. If between $t = 1$ and $t = 2$ the lithosphere is stretched by a factor of β, the lithosphere will thin to $1 / \beta$ (McKenzie, 1978). Denser asthenosphere replaces the thinned crust, resulting in subsidence. This initial subsidence is not thermal, but the result of local isostatic processes. When the initial crustal thickness is over about 18 km, this subsidence is sufficient to overcome the relative uplift forces caused by the thinning of the mantle lid (McKenzie, 1978).

2. 2. 2: Flexure

Flexure is the long wavelength deflection of a lithosphere of finite strength caused by the application of an external force system (Allen and Allen, 2005). Isostasy explained above assumes that loading of the lithosphere is compensated for locally, as if the earth's crust consists of a series of free-floating pistons (Fig. 2.3), however, the lithosphere has a finite strength, therefore rigidity (Watts et. al, 1975). If deformation caused by a load spreads beyond the lateral extent of the load, then flexure is at work. Because the crust bends like an elastic beam, the bent plate is buoyed up by the weight of the displaced mantle and the by the strength of the surrounding lithosphere. The surrounding lithosphere is in turn held down by the weight of the nearby load (Lynch and Morgan, 1987). The higher the rigidity of the crust, the broader and shallower the depression created by loading. With a less rigid crust, the depression created is deep, but narrow (Coward, 1994).

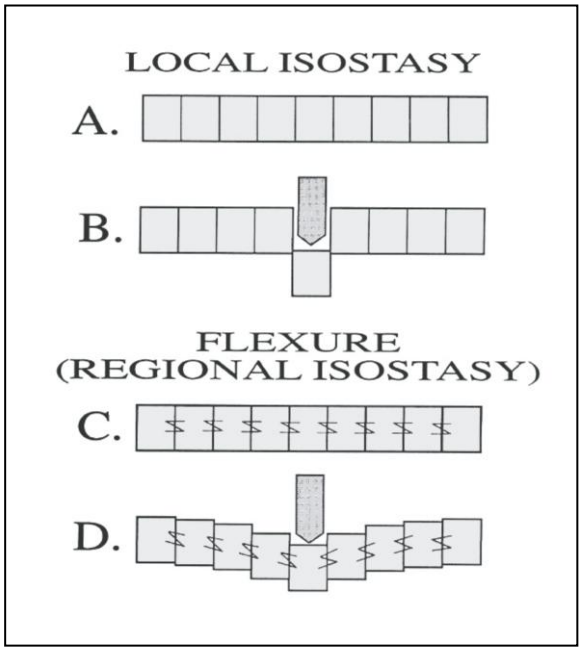

Figure 2.3: Comparison of local isostasy verses flexure (regional isostasy).
In local isostasy (A), the lithosphere is composed of separate blocks. As a load is placed on the surface of the earth (B), only the block immediately beneath the load subsides. In reality the earth has lateral strength (C), as if the blocks are attached to each other by springs. Emplacement of a load on the surface causes subsidence (D), but is compensated over a larger area due to the rigidity of the lithosphere.

2. 2. 3: Thermal subsidence

Again related to isostasy, thermal changes result in an adjustment of the density structure of the crust. The earth crust is capable of heating relatively quickly via the emplacment of intrusions or lithospheric thinning, however, cooling that occurs primarily by conduction is a much slower process (Allen and Allen, 2005). Returning to figure 2.2, after time $t = 2$ the subsidence occurring is due to thermal processes, as warm asthenosphere converts into cool lithosphere the region subsides. By the end of this process the original geothermal gradient is restored.

2. 3: INSTANTANEOUS RIFTING THEORY

2. 3. 1: The McKenzie (1978) model

A history of continental rifting is often provided by sediments deposited on the continental margin. Typically, these sediments record a decrease in subsidence with time. In order to explain these sedimentary deposits it is necessary to consider the effects of continental extension.

In 1974, Falvey stated that extension in both the crust and the subcrustal lithosphere could be used to explain the subsidence histories of various continental rift basins and margins. His theory assumed that the crust failed by brittle fracture, while plastic flow was responsible for subcrustal lithospheric thinning. McKenzie (1978) further developed this theory, creating a quantitative model of extension, assuming the amount of crustal and lithospheric stretching to be the same (uniform stretching). McKenzie's theory stated that the total subsidence of an extensional basin was comprised of two components: An initial isostatic element, where lithospheric material is replaced by asthenospheric material, which is dependent on the initial thickness of the crust and the amount of stretching β; and a subsequent thermal subsidence, caused by cooling and hence slow contraction, dependent solely on the amount of stretching. While the initial rifting is assumed to be instantaneous, the rate of thermal subsidence decreases exponentially with time, a result of a decrease in heat flow with time.

2. 3. 2: Derivation of the model

The initial subsidence can be calculated by assuming the 'before' and 'after' columns to be in isostatic equilibrium:

$$y_c\rho_c + (y_l - y_c)\rho_{sc} = y_s\rho_s + (y_c/\beta)\rho_c + (y_l - y_c)(1/\beta)\rho_{sc} + (y_l - y_s - y_l/\beta)\rho_m \qquad (2.1)$$

where ρ_c is the average density of the crust, ρ_{sc} is the average density of the subcrustal lithosphere, ρ_m is the density of the mantle, ρ_s is the density of water or sediment filling the basin, y_c is the thickness of the crust, y_l is the thickness of the lithosphere, y_s is the thickness of sediment, water or air filling the basin and β is the stretching factor.

Rearranging this equation gives an expression for the initial subsidence:

$$y_s = \frac{(1-1/\beta)}{(\rho_m - \rho_s)}\{\rho_m y_l - y_c\rho_c - (y_l - y_c)\rho_{sc}\} \qquad (2.2)$$

This initial isostatic rifting is shown for various β values in the first part of figure 2.4

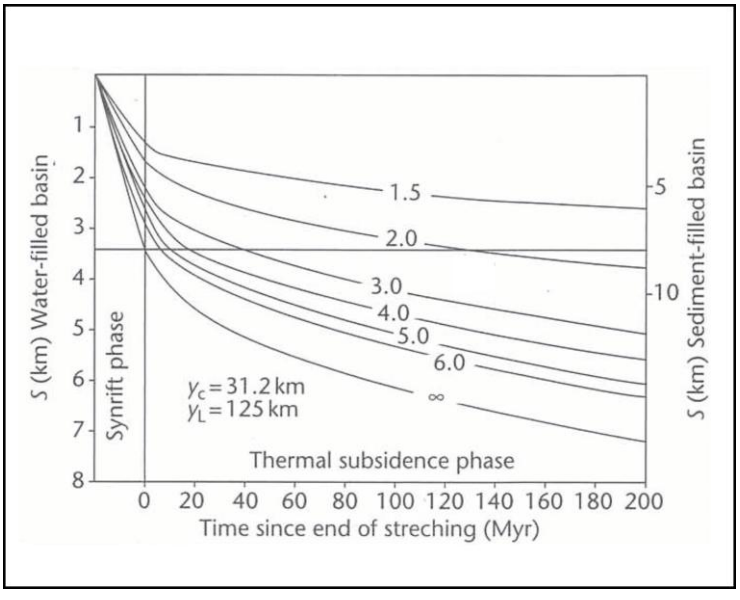

Figure 2.4: Elevation change with time for a water-filled and sediment-filled basins. The curve shows the initial linear subsidence related to isostatic changes, and the exponential form of subsidence due to thermal contraction. (From Allen and Allen, 2005)

Following the instantaneous increase in heat flow accompanying rifting in the McKenzie model the heat flow decreases exponentially with time. We know two boundary conditions: T = 0 at the surface; and T = T_m at the base of the lithosphere. It is assumed that cooling of the lithosphere is governed by one-dimensional vertical thermal conduction. This means that the heat transport via convection and lateral conduction is ignored. The unsteady (time-dependent) heat flow equation is

$$\frac{\partial T}{\partial t} = K\frac{\partial^2 T}{\partial y^2} \tag{2.3}$$

Where the curvature of the geotherm, as it relaxes to its prestretched gradient, is provided by the second derivative, and κ is the thermal diffusivity. The temperature at any depth and time (T(y,t)) can be calculated using an equation with two parts: First, a steady state solution $s(y)$ = (T_m(1 – y/y_l), which applies to a linear geotherm in the lithosphere; and second, an unsteady component $u(y,t)$, the general solution of which is:

$$u(y,t) = \sum_{n=0}^{\infty} An \sin\left(\frac{n\pi y}{y_l}\right)\exp\left(\frac{-n^2\pi^2\kappa t}{y_l^2}\right) \tag{2.4}$$

Where A is a constant and n is an integer that expresses the order of the harmonic of the Fourier transform, and κ is the thermal diffusivity. As n tends to ∞ the negative exponential decreases, ceasing to contribute to the unsteady temperature field. As a gross approximation it is frequently satisfactory to consider only n = 1. The constant A is constrained by the amount of stretching and the asthenospheric temperature (T_m). At t = 0,

$$An = \left\{\frac{2}{n}(-1)^{n+1}\frac{\beta}{n\pi}\sin\left(\frac{n\pi}{\beta}\right)T_m\right\} \tag{2.5}$$

Assuming n = 1, the full solution for T(y,t) is therefore the sum of the steady and unsteady components,

$$T(y,t) = T_m\left(1-\frac{y}{y_l}\right)+\left\{\frac{2}{\pi}\frac{\beta}{\pi}\sin\left(\frac{\pi}{\beta}\right)T_m\right\}\exp\left(-\frac{\pi^2\kappa t}{y_l^2}\right)\sin\left(\frac{\pi y}{y_l}\right) \tag{2.6}$$

Which simplifies to

$$\frac{T(y,t)}{T_m} = \left(1 - \frac{y}{y_l}\right) + \frac{2}{\pi}\frac{\beta}{\pi}\sin\left(\frac{\pi}{\beta}\right)\exp\left(-\frac{t}{\tau}\right)\sin\left(\frac{\pi y}{y_l}\right) \tag{2.7}$$

where $\tau = y_l^2 / \pi^2 \kappa$ and is known as the thermal time constant of the lithosphere. The surface heat flux is given by Fourier's law, which states that the flux is the temperature gradient times the thermal conductivity. For $n = 1$, this is

$$q = \frac{KT_m}{y_l}\left\{1 + \frac{2\beta}{\pi}\sin\left(\frac{\pi}{\beta}\right)e^{-t/\tau}\right\} \tag{2.8}$$

the subsidence given by thermal contraction is given by

$$S(t) \approx E_0 \frac{\beta}{\pi}\sin\left(\frac{\pi}{\beta}\right)(1 - e^{-t/\tau}) \tag{2.9}$$

where

$$E_0 = 4y_l\rho_{m^*}\alpha_v T_m / \pi^2(\rho_{m^*} - \rho_s) \tag{2.10}$$

where α_v is the volumetric coefficient of thermal expansion.

The result of these equations is that the amount of stretching strongly controls heat flux, with the dependency becoming insignificant after about 50 Myr. Heat flux with time is shown in figure 2.5, while subsidence due to thermal relaxation is shown in the second part of figure 2.4. The outcome of this complicated arithmetic is that if the subsidence history of a particular basin is known, it is possible to estimate the β from the thermal subsidence curve.

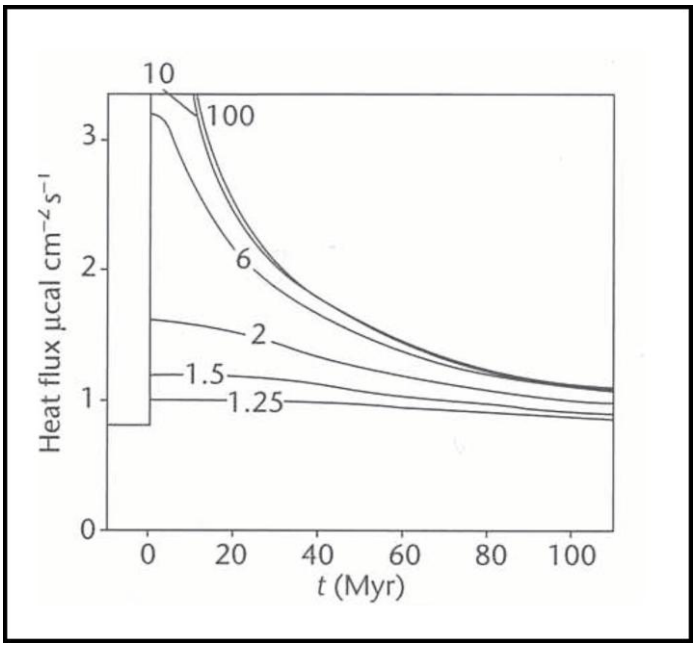

Figure 2.5: Plot shows the relationship between heat flux and time for different β values. Note that after ~50 Myr the heat fluxes are similar for all values of β. (From McKenzie, 1978)

2. 3. 3: Assumptions in the calculations

Obviously, models such as this are grossly oversimplified approximations of the real world. A number of assumptions occur in the model, increasing the likelihood of error in the calculations.

2. 3. 3. 1: Instantaneous rifting

The major assumption in the McKenzie (1978) model is that rifting is instantaneous. Jarvis and McKenzie (1980) reconsidered the instantaneous rifting model, to allow for protracted periods of stretching. However, it was found that, provided stretching of the entire lithosphere occurred in less than 20 Myr, the instantaneous model provided similar results. Extension and rifting responsible for the break-up of Gondwana and the formation of New Zealand's major basins occurred from the late Cretaceous to the Paleocene (King and Thrasher, 1996), a period of ~20 Myr. For this reason the instantaneous model of McKenzie (1978) is used for this investigation.

2. 3. 3. 2: Uniform stretching

It is assumed in the McKenzie model, that the crust and mantle lithosphere stretch by the same amount (Fig. 2.6(a)). Two models have been developed to provide alternatives to the uniform stretching model. The first (Fig. 2.6(b)), shows the discontinuous model, where there is a discontinuity or decoupling between two layers with differing β values (Royden and Keen, 1980). A second alternative is the continuous model, where there is a smooth transition in the stretching throughout the lithosphere (Royden and Sahagian, 1986).

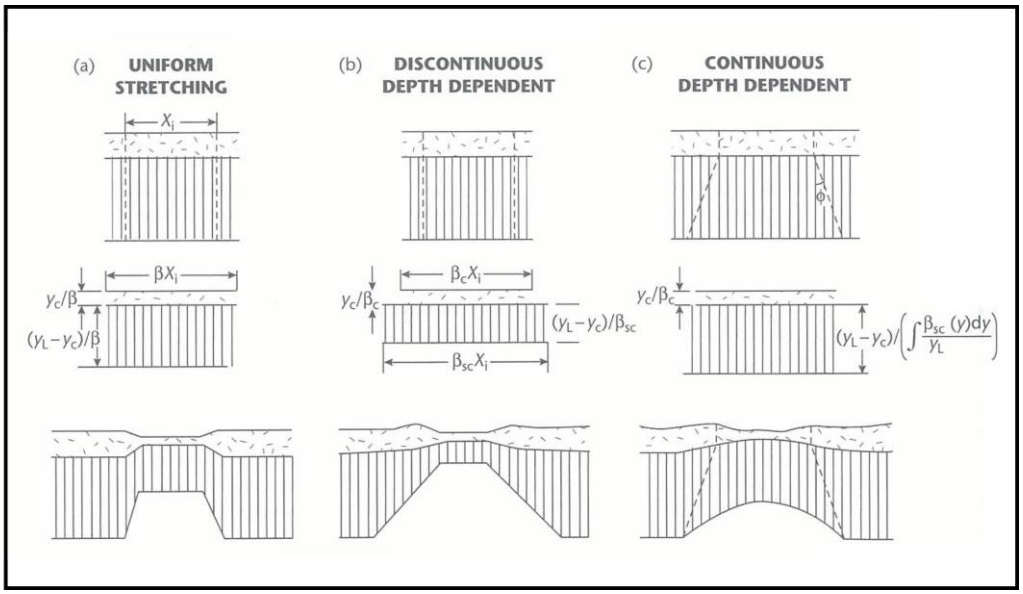

Figure 2.6: (a) Uniform stretching, where the crust and mantle lithosphere are stretched by the same β value.
(b) Discontinuous stretching, where there is a discontinuity between the two layer, each stretched by a different amount.
(c) Continuous stretching, where stretching is a function of depth. (From Allen and Allen, 2005)

These complex models have been developed to explain why some regions that have undergone extension apparently show no initial subsidence, but instead show uplift or doming. Uplift or doming will only occur where there is a large discrepancy in β values with depth, and ultimately, the amount of tectonic subsidence is still controlled by the amount of crustal thinning (Angevine et. al, 1990).

2. 3. 3. 3: Pure verses simple shear

The McKenzie model assumes pure shear (Fig. 2.7(a)), where a symmetrical lithospheric cross-section results from an upper brittle layer, overlying a lower dutile layer. However the lithosphere may extend asymmetrically, with displacement occurring on a large scale gently-dipping shear zone that traverses the entire lithosphere (Wernicke, 1981). Extension is relayed along the shear zone from the upper crust in one region to the lower crust and mantle lithosphere in another region. This results in a physical separation of the zone of fault controlled extension from the zone of upwelled asthenosphere and is known as 'simple shear' (Fig. 2.7(b)). This senario may lead to uplift and the formation of core complexes above the upwelled asthenosphere. It is also possible that simple shear in the upper crust and pure shear in the lower crust and mantle lithosphere may result in a hybrid model (Kusznir, 1991)(Fig. 2.7(c)).

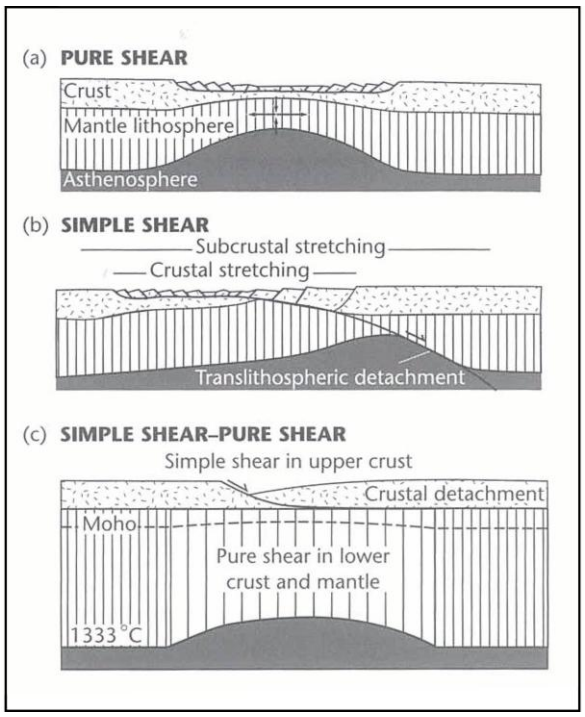

Figure 2.7: (a) Pure shear, where an upper brittle layer overlies a lower ductile layer.
(b) Simple shear, where a low-angle detachment separates the lithosphere into a hangingwall and footwall.
(c) Simple shear-pure shear hybrid, with simple shear by way of listric faults in the upper crust and pure shear in the ductile lower crust and mantle lithosphere. (From Allen and Allen, 2005).

2. 3. 3. 4: Lateral heat flow

One dimensional (vertical) heat flow is assumed by the McKenzie model, where as, it is clear that heat from the rift will be conducted laterally, as well as vertically. Lateral heat flow causes an increased rate of heat loss, particularly at the basins margins, where the horizontal temperature gradients are the largest (Cochran, 1983). This results in the model underestimating the amount of subsidence, at least during the early stages of thermal subsidence.

2. 3. 3. 5: Other Assumptions

A number of other assumptions are built into the McKenzie model these include:

- The necking depth is zero: Necking may actually be centred on strong layers deeper in the midcrust or upper mantle lithosphere.
- Airy isostasy is assumed to operate throughout: The continental lithosphere, however, has a finite elastic strength and flexural rigidity, partially in the post-rift thermal subsidence stage.
- There is no radiogenic heat production: However, the crust provides an additional important source of heat.
- There is no magmatic activity: Intrusion of melt modifies the heat flow history and therefore affects thermal subsidence.
- The asthenosphere has a uniform temperature at the base of the lithosphere: It is known that the temperature at the base of the lithosphere may be strongly varied due to the presence of convection systems.

2. 4: COMPACTION AND POROSITY LOSS

Burial of sediment during basin subsidence results in a number of physical and chemical processes, ultimately leading to changes in porosity. Porosity loss is effected by three sets of interrelated process (Giles, 1997):

- Mechanical compaction: This encompasses processes such as rearrangement and compression of grains in response to loading.
- Physiochemical compaction: This includes processes such as pressure solution and the alteration of feldspars.
- Cementation: The precipitation of minerals in pore spaces. This process is the result of temperature changes with burial, rather than loading.

The total volume of a sedimentary rock is represented by the equation:

TOTAL VOLUME = SOLID VOLUME + PORE VOLUME (2.11)

While compaction results in a major reduction in pore space and a small loss of solid volume due to compression, it is important to note that cementation results in an increase in the solid volume, by filling available pore space.

2. 5: POROSITY CHANGE WITH DEPTH

In order to restore porosity to that of the time of deposition it is important to understand the relationship between the porosity and depth of burial. A number of factors affect the porosity-depth relationship (Allen and Allen, 2005):

- Gross lithology; with shales compacting quickly compared to sandstones.
- Depositional facies; which controls grain size, sorting and clay content, therefore initial porosity.
- Composition of framework grains; for example pure quartz arenites differ from lithic arenites containing ductile fragments.
- Temperature; which strongly affects chemical diagenesis.
- Time; porosity loss may require sufficiently long periods of time.

Observations and estimates from a wide range of lithologies show that in normally pressured sediments porosity decreases exponentially with depth (Figure 2.8).

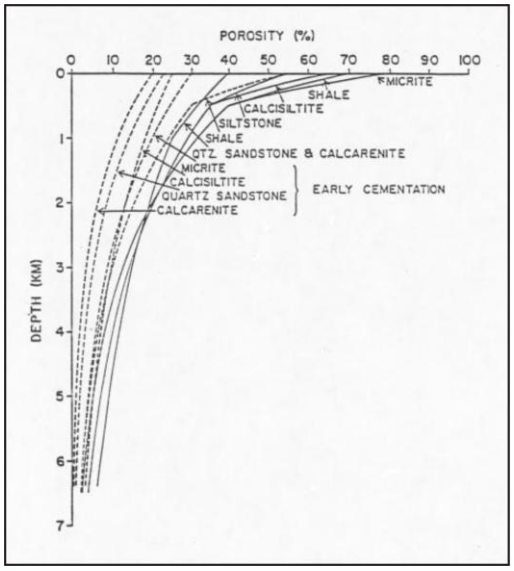

Figure 2.8: Graph showing changes in porosity with burial for different lithologies. (From Angevine, Heller and Paola, 1990)

There are a number of equations to represent this relationship, however this investigation uses the equation given by Athy (1930):

$$\phi = \phi_0 \exp^{-cz} \tag{2.12}$$

Where $\varnothing_0$ is the porosity at the surface eg. at the time of deposition, c is a coefficient determining the slope of the porosity-depth curve and z is the depth. This relationship can then be applied to any lithology, each with its own value for c. The values for c and $\varnothing_0$ used in this investigation are shown in Table 2.1

Lithology	$\varnothing_0$	c	Source
Conglomerate	0.45	3.3×10^{-4}	Stagpoole (2006)
Sandstone	0.45	3.3×10^{-4}	Funnel et. al. (1996)
Mudstone	0.5	4.4×10^{-4}	Armstrong et. al. (1998)
Siltstone	0.56	3.9×10^{-4}	Sclater and Christie (1980)
Limestone	0.7	7.1×10^{-4}	Stagpoole (2006)

Table 2.1: Porosity and compaction corrections used in this study, along with their source.

2. 6: CALCULATING THICKNESS OF COMPACTED UNITS

Most decompaction corrections used assume no loss of total solid volume, that is to say, the change in the stratigraphic thickness of the unit is due solely to a loss in the volume of the total pore space. The effects of pressure solution, cementation and overpressuring of pore fluids are ignored, these are discussed in the sources of error section in the methods chapter.

To remove the results of compaction the layer is effectively moved up the appropriate porosity-depth curve. At each incremental step the youngest overlying unit is removed and the next youngest unit is decompacted. This process is represented by the 'Progressive Decomp thickness' column in appendix B. Here, the method of Van Hinte (1978) is followed, whereby the original thickness is related to the present-day thickness by the equation:

$$T_0 = \frac{T_N(1-\phi_N)}{1-\phi_0} \tag{2.13}$$

Where $\varnothing_0$ is the original porosity at the time of deposition, and T_N and $\varnothing_N$ are the present day thickness and porosity of the unit. Figure 2.9 shows the effects of decompaction on a simple sediment accumulation curve. Figure 2.10 is an example

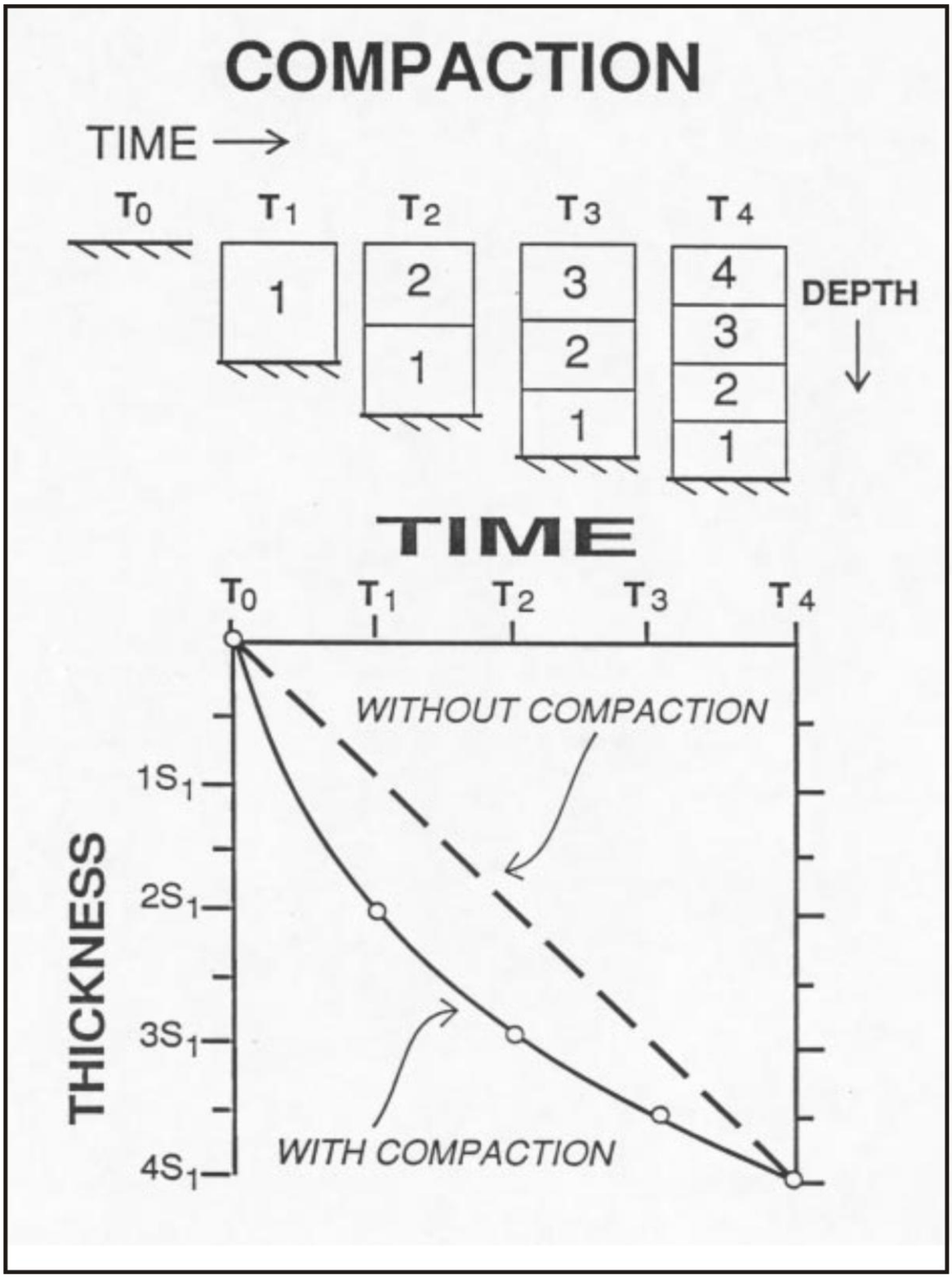

Figure 2.9: Removing the effects of compaction in geohistory analysis, by applying a 'compaction' correction. (From Angevine, Heller and Paola, 1990)

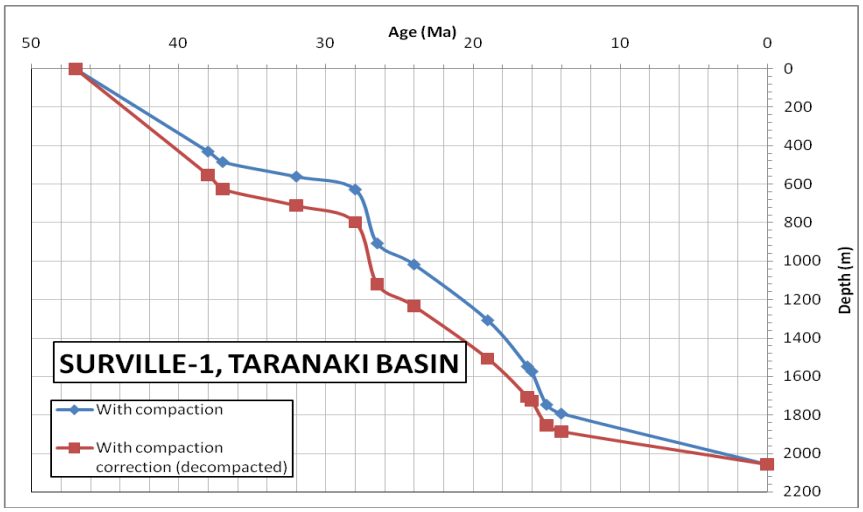

Figure 2.10: An example showing the effects of the 'compaction' correction on actual data from Surville-1, Taranaki Basin, New Zealand.

using data from Surville-1, a well located in the Taranaki Basin, which was utilized in this study. Note that in both figures the two curves meet at T_0. This is based on the assumption that the youngest unit is not compacted until an overlying unit is deposited on top. The weight of the overlying unit is deemed necessary for compaction to occur. In reality this is not the case, as the sediment at the base of any unit is compacted by the weight of younger material within the same unit, however this is a basic assumption of the 'backstripping' process.

2. 7: CALCULATING TOTAL SUBSIDENCE

Once compaction corrections have been applied, paleobathymetry for each unit is added in order to calculate total subsidence. This is added because calculations assume that the sedimentary basin is always filled to sea level, the datum used to show subsidence. If only the preserved thickness of the stratigraphic unit is used, the total subsidence of the basin is underestimated by the depth of the overlying water. Figure 2.11 provides decompacted sedimentation (without water depth) and total subsidence (with maximum water depth). Sedimentation in the basin appears to be linear, however, changes in the depth of deposition must be accounted for. These changes are included in the total subsidence curve, and show that the subsidence history of the basin has been sporadic. For this study 'total subsidence' is considered an intermediary step, therefore the results are not provided in the geohistory figures for the wells.

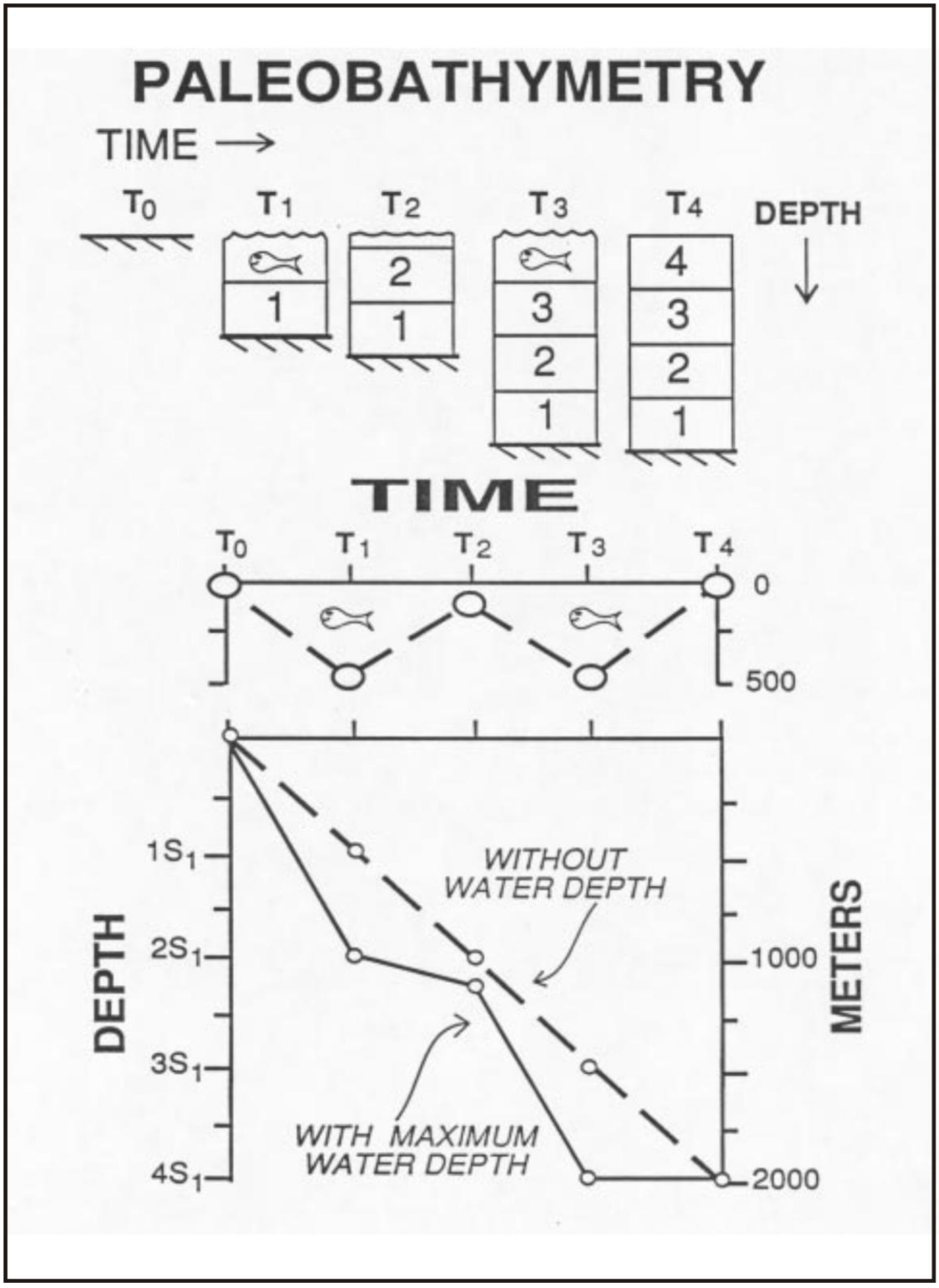

Figure 2.11: Incorporating paleobathymetry into the geohistory. (From Angevine, Heller and Paola, 1990)

2. 8: CALCULATING TECTONIC SUBSIDENCE

Included within the 'total subsidence' curve are the effects of all factors which control basin subsidence: Tectonic loads, sediment loads and sea level changes. As this study is concerned with the implications of tectonics on the basin history, it is necessary to remove the effects of sediment loading and sea level change. Known as 'backstripping', the loading effect of the sediments can be treated as a problem of a local (Airy) isostatic balance, where sediment is replaced by an equivalent column of water. The following equation is used to remove the effects of sedimentary loading:

$$Z = \left(\frac{\rho_a - \rho_s}{\rho_a - \rho_w} \right) S \tag{2.14}$$

Where Z is the depth to basement, measured from sea level (i.e. the amount of tectonic subsidence), ρ_a, ρ_w and ρ_s are the densities of the asthenosphere, the sediment column and water, and S is the total thickness of the decompacted sediment column

Figure 2.12 explains the derivation of the above equation.

By adding paleobathymetry to the above 'backstripping' equation one can effectively predicts the depth of the water-filled basin if the sedimentary rocks were removed.

$$Z = \left(\frac{\rho_a - \rho_s}{\rho_a - \rho_w} \right) S + W_d \tag{2.15}$$

Where W_d is the paleowater-depth.

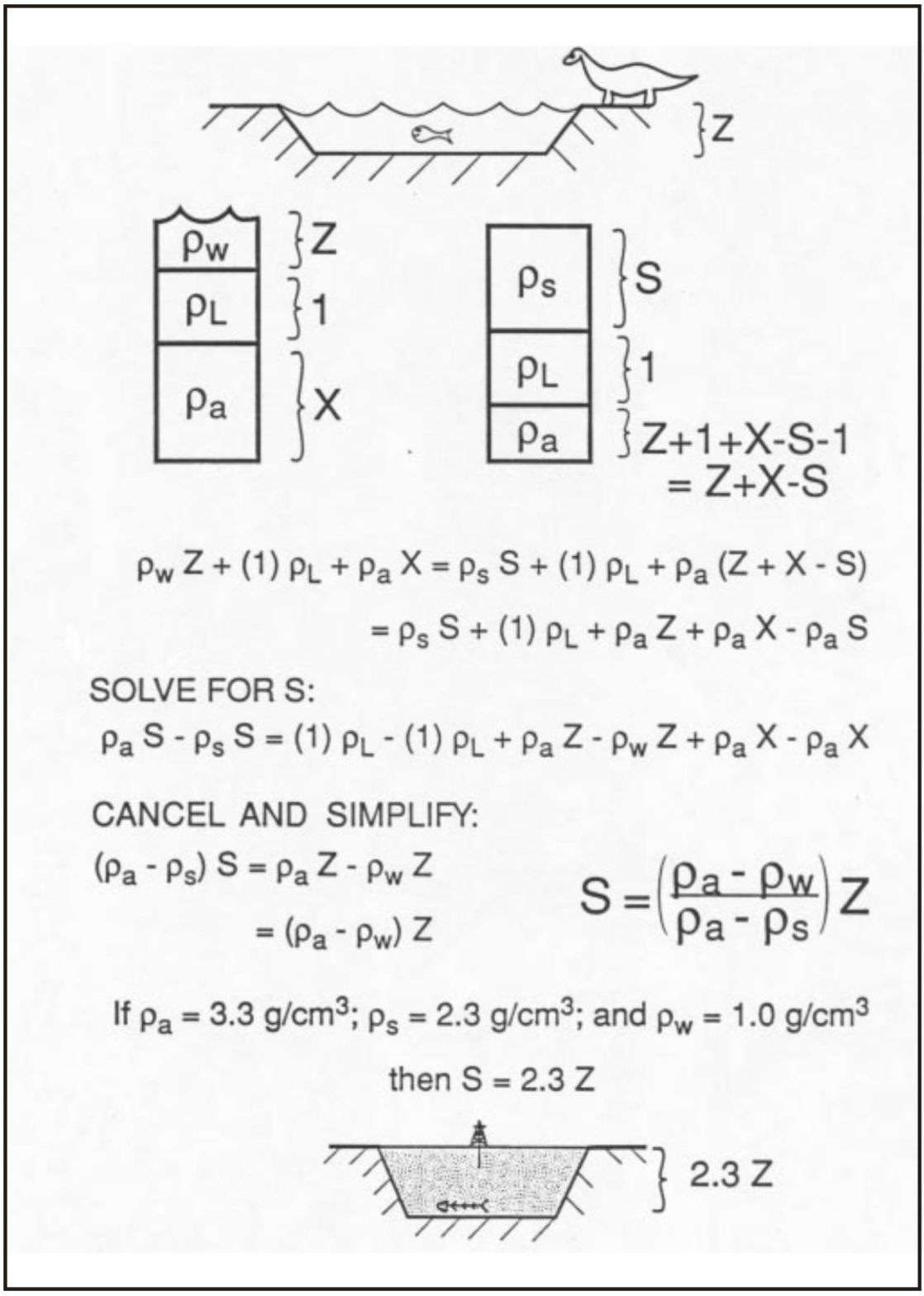

Figure 2.12: Figure showing column balancing, and the derivation of the backstripping equation. (From Angevine, Heller and Paola, 1990).

2. 9: BASIN CLASSIFICATION

A graphical presentation of a basins' geohistory is an important tool in determining the mechanism of formation and the likely plate tectonic setting. This section will provide an overview of basins' types and their characteristic subsidence cures (Fig. 2.13), as presented by Dickinson (1976).

2. 9. 1: Passive / rifted margins

Atlantic-type margins and back-arc basins typically form by crustal extension and if they continue to completion, the formation of oceanic crust (Kearey and Vine, 1996). The geohistory plots for these basins are characterised by an early extensional period, associated with an initial isostatic subsidence in response to crustal thinning. This phase is followed by post-rift thermally driven subsidence as heat is loss by conduction. McKenzie (1978) proposed that as long as extension is instantaneous (i.e. less than 20 My) the initial subsidence will be complete before thermal subsidence begins. Geohistory plots of post-rift subsidence show a convex-down pattern. This pattern is typical of the early Tertiary stages of formation in most of New Zealand's major basins.

2. 9. 2: Transform basins

These pull-apart basins are associated with strike-slip faults, and share some characteristics with passive margin sequences. However these features are much smaller and shorter lived, rarely continuing to completion. Where the basin affects the mantle lid the smaller dimensions of the basin mean heat is loss faster than at passive margins. Because of this thermal heat loss and subsidence occurs at the same time as subsidence due to crustal thinning. The resulting geohistory plot generally shows rapid nearly linear subsidence, with a short tail of slower subsidence, presumably representing cooling of the remaining thermal anomaly once the fault ceases to be active (Angevine et. al., 1990). In many cases the mantle lid is not affected, with rapid subsidence purely the result of crustal extension and thinning, equivalent to the initial subsidence seen in passive/rifted margins.

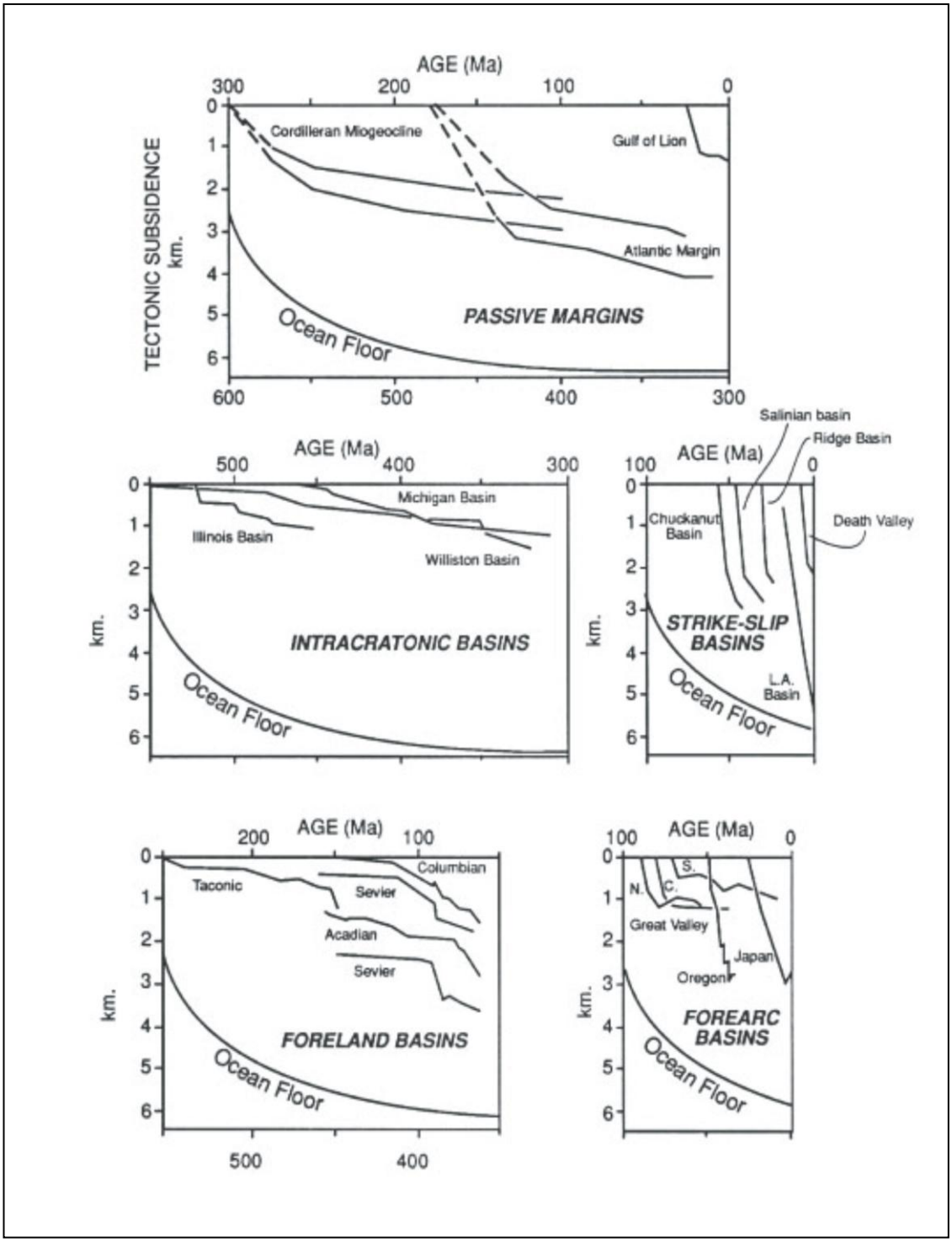

Figure 2.13: Representative tectonic subsidence histories of basins from different tectonic settings (from Angevine et. al., 1990).

2. 9. 3: Foreland basins

Foreland basins form by flexure of the lithosphere due to the emplacement of a thrust belt load (Coward, 1996)). The sedimentation and subsidence rate in foreland basins reflect the rate of thrusting in the adjacent orogenic belt. As the belts migrates into the basin subsidence increases, resulting in a convex-up subsidence curve (Allen and Allen, 2005). Eroded sediment from the thrust belt further distribute the load across the basin, forcing the subsidence to migrate across the basin over time. At the cessation of thrusting erosion may result in the removal of the load, leading to flexural uplift.

2. 9. 4: Forearc basins

The formation of forearc basins is not well understood, it is possible they are the result of multiple complex mechanisms. However, subsidence curves appear to show abrupt stepping in the rate of subsidence, very rapid initial subsidence, or progressive loading. For example, loading could be the result of an accretionary wedge or volcanic arc (Silver and Reed, 1988).

2. 9. 5: Intra-continental basins

Once again the mechanisms responsible for the formation of intra-continental basins are not well known. These large basins are typically circular in shape, and are characterised by slow sedimentation over tens to hundreds of millions of years. Many believe (Haxby et. al., 1976; Heidlauf elt. al., 1986; Coakley and Gurnis, 1995; in Angevine et. al, 1990) that the basins have a thermal origin, however, this fails to explain the stepped subsidence history of some basins, again suggesting a complex cause.

CHAPTER 3: METHODS

3. 1: CROWN MINERALS DATA SOURCE

The Resource Data Unit of Crown Minerals, a branch of the Ministry of Economic Development has complied a comprehensive collection of data from the 680 wells drilled within New Zealand's Exclusive Economic Zone since the 1880's. Data include seismic data, well data, drill cores and cuttings. These open-file data, which are available on the Crown Minerals website (www.crownminerals.govt.nz), have been utilized in this study in order to analysis the subsidence history of New Zealand's sedimentary basins.

3. 2: STRATIGRAPHIC COLUMNS

Information necessary for geohistory analysis was collected from petroleum reports on the Crown Minerals website. Stratigraphic columns were created for the petroleum wells deemed suitable (See appendix). For geohistory analysis wells had to fit a number of criteria:

- A sedimentary record reaching back to the Cretaceous
- Thick homogenous sedimentary units
- Minimum faults or unconformities
- Precise dating of sediments
- Accurate estimation of environment of deposition

Few, if any wells met all these criteria. Attempts were made to minimize error, and these methods will be explained in a following section.

3. 3: DATA ENTRY

Data from the stratigraphic columns was entered into Microsoft Excel spreadsheets (See appendix). The depth corresponding to each unit represents the depth to the base of the lithological unit. Ages represent the age at the base of the unit, assumed to be the start of the given New Zealand series, as presented by fig. 3.1. Where depth to a certain lithological horizon was given but an age was not, it was assumed that sedimentation was constant over the period to the next known age.

GLOBAL GEOCHRONOLOGICAL SCALE			NEW ZEALAND TIMESCALE				
Era-them	System	Series	Series	Stage	Symbol	Age of base, Ma	Durat-ion, Ma
CENOZOIC	Quaternary	Holocene	Wanganui Series	Haweran	Wq	0.34	0.34
		Pleistocene		Castlecliffian	Wc	1.63	1.29
	Neogene	Pliocene		Nukumaruan	Wn	2.4	0.77
				Mangapanian	Wm	3.03	0.63
				Waipipian	Wp	3.6	0.57
				Opoitian	Wo	5.28	1.68
		Miocene	Taranaki Series	Kapitean	Tk	6.5	1.22
				Tongaporutuan	Tt	11.0	4.5
			Southland Series	Waiauan	Sw	13.2	2.2
				Lillburnian	Sl	15.1	1.9
				Clifdenian	Sc	16.0	0.9
			Pareora Series	Altonian	Pl	19.0	3
				Otaian	Po	21.7	2.7
	Paleogene	Oligocene	Landon Series	Waitakian	Lw	25.2	3.5
				Duntroonian	Ld	27.3	2.1
				Whaingaroan	Lwh	34.3	7
		Eocene	Arnold Series	Runangan	Ar	35.8	1.5
				Kaiatan	Ak	37.0	1.2
				Bortonian	Ab	43.0	6
			Dannevirke Series	Porangan	Dp	46.2	3.2
				Heretaungan	Dh	49.5	3.3
				Mangaorapan	Dm	53.0	3.5
				Waipawan	Dw	55.5	2.5
		Paleocene		Teurian	Dt	65.0	9.5
MESOZOIC	Cretaceous		Mata Series	Haumurian	Mh	84.5	19.5
				Piripauan	Mp	86.5	2
			Raukumara Series	Teratan	Rt	89.0	2.5
				Mangaotanean	Rm	92.0	3
				Arowhanan	Ra	95.0	3
			Clarence Series	Ngaterian	Cn	100.0	5
				Motuan	Cm	103.0	3
				Urutawan	Cu	108.0	5
			Taitai Series	(Korangan)	Uk	(117)	9
				(no stages designated)	U	144.2	27.2
	Jurassic		Oteke Series	Puaroan	Op	148.5	4.3
			Kawhia Series	Ohauan	Ko	153.5	5
				Heterian	Kh	157.5	4
				Temaikan	Kt	178.0	20.5
			Herangi Series	Ururoan	Hu	190.0	12
				Aratauran	Ha	200.0	10

Table 3.1: New Zealand Geological Timescale.

3. 4: SEDIMENT ACCUMULATION AND SUBSIDENCE

Decompaction was carried out using a computer software program called DECOMPACT, which was developed by Dr. David Waltham of Royal Holloway, University of London in 2001. DECOMPACT is based on the equations described in the previous chapter. By entering the age and depth at the base of the unit, along with the initial porosity and corresponding c-value, it calculates the depth to the base of each decompacted unit. The data representing the contact between basement and the overlying sediments was then plotted graphically as 'decompacted sediment accumulation' for each well.

As mentioned in an earlier chapter, total subsidence is considered as an intermediate step, and is not shown in this investigation. Using the equation explained in the preceding chapter, 'tectonic subsidence' is calculated. This is presented graphically for each well.

3. 5: PALEOBATHYMETRIC CLASSIFICATION

Edwards (1979) classification of marine environments was used (Fig 3.1). An older classification scheme was chosen, due to the age of many wells. For this analysis paleobathymetries were taken from the individual well reports. Due to the inherent uncertainty of paleobathymetric determination, in most cases a depositional range of environments were given e.g: outer shelf to upper bathyal. In this case the depth plotted corresponded to the depth between the two environments e.g: 200 m, and the extent of the error bars represent the minimum and maximum depths of these environments e.g: 120 m to 500 m. Where a specific environment was given e.g: inner shelf, which ranges from 20 m to 50 m, the middle of the environment was plotted e.g: 35 m, with the error bars at the limits of the environment. The paleobathymetry for each well is presented on graph along with decompacted sediment accumulation and tectonic subsidence.

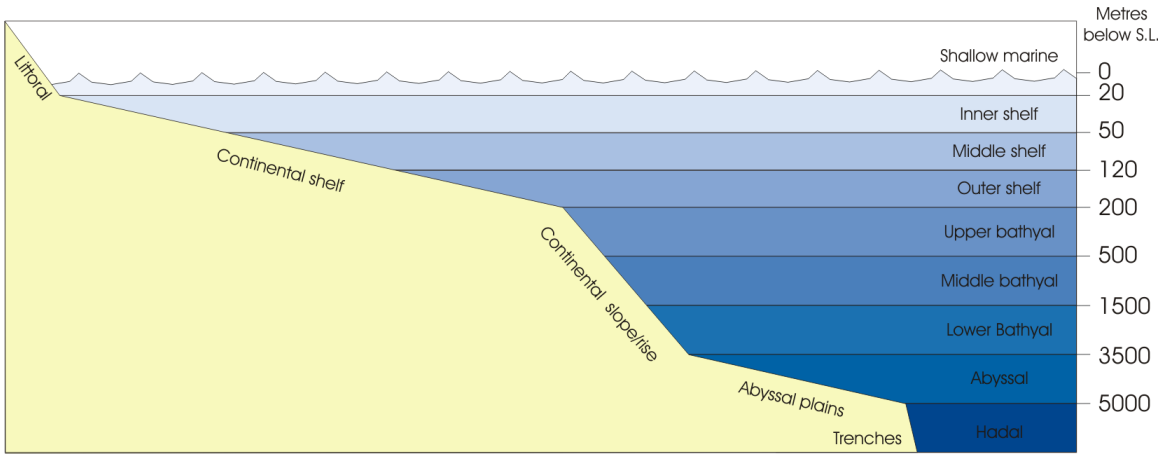

Figure 3.1: Definitions of marine environments, as given by Edwards (1979).

3. 6: SOURCES OF ERROR

Decompaction and back-stripping are common methods used in sedimentary basin analysis, however a number of uncertainties and assumption mean the resulting curve is only an estimate of the subsidence history. This section briefly describes the main factors that cause inaccuracy.

3. 6. 1: Paleontological data

In this investigation paleontological data are used to date the units, and to provide an indication of the paleo-environment in which that sediments were deposited, unfortunately it is also likely to contribute to the greatest source of imprecision.

While it is possible to compare fossils species with extant species to estimate depths of inhabitation, this method is indirect, and sources of error increase with the age of the fossil (Hayward and Wood, 1989). The micro-fossils used to estimate paleo-water depths are an significant source of imprecision. These diagnostic marine organisms are in many cases planktonic, and capable of inhabiting a wide range of water depths. To remedy this error bars have been applied to the paleobathymetric data.

Ages of sediments have been shown to vary markedly between different dating methods (e.g., radiogenic, magnetic, biostratigraphic etc) (Angevine, Heller and Paola, 1990). By using the only the paleontological timescale, this investigation has removed the likelihood of disagreement between differing types of dating techniques. The age of many of the well reports may mean they were published before amendments to the biochronology (Hayward, 1987). Due to the condensed nature of the available older well reports, the New Zealand age is given, while the specie/species responsible for the attributed age has not, making correction impossible. It is likely this affects a small number of wells, and due to the high precision of the timescale, the adjustments made are likely to be insignificant.

Far more likely to contribute error is the fact that in many cases dating and paleo-environmental data were based on the presence of only a few specimens of micro-flora and fauna. Equipment contamination, down-hole slumping and sediment reworking have the ability to distort the apparent age of sediments by millions of years.

3. 6. 2: Assumptions in the calculations

The compaction corrections used to 'decompact' the sediment are based on porosity-depth relationships, with a number of constants for each lithology. These constants have generally been derived from investigation in individual areas, making them site-specific. Even if the calculated values represent an average, there are likely to be unaccounted for variations in porosity and grain size, affecting the thickness of the 'decompacted' section. Where possible New Zealand corrections have been applied.

The calculations also assume that the units are at normal pressure, there has been no alteration of individual grain size, or shape, and that no cementation or dissolution has occurred. While this is idealistic, there is no way to correct for these changes, as they can vary markedly both laterally, vertically and through time.

3. 6. 3: Faults and Unconformities

The nature of petroleum deposits means that many of these wells have been drilled in areas which have been heavily faulted and folded, resulting in unconformities. A

reverse fault causes a repetition of strata, while a normal fault will produce an apparent loss of data. Both of these outcomes obviously affect the final back-stripped column. Little can be inferred over these periods, however, the observed change in water depth does provide a minimum rate of subsidence/uplift.

3. 6. 4: Sea-level effects

Sea-level is the datum from which subsidence is established. This investigation takes into account regional changes in sea-level, due to tectonics, while ignoring eustatic sea-level fluctuations. This is for two reasons. First, there is no consensus on global sea-level variation; and second, by working with relatively thick units, this study is focused on larger scale tectonic events. This study considers eustatic sea-level fluctuations as relatively high frequency, and low amplitude events superimposed on the tectonic signal of each basin.

3. 6. .5: Terrestrial deposits

Lithological features used to indicate terrestrial environments of deposition also create a source of inaccuracy. Certain features denote certain facies, however without further investigation it is often impossible to tell whether a fluvial unit was deposited on a glacial outwash plain high in the mountains, or on a flood plain just above sea level. In this investigation all terrestrial deposits are assumed to have been deposited at 0 m above sea level. While unrealistic, this means that minimum values of subsidence/uplift can be calculated.

CHAPTER 4: CANTERBURY BASIN

4. 1: INTRODUCTION

Reaching from the Alpine and Hope Faults in the northwest, to approximately 74° 50' longitude, the offshore portion of the Canterbury Basin (Fig. 4.1) encompasses an area ~30,000 km^2, while the onshore extension, represented by the Canterbury Plains covers ~12,500 km^2. The basin is bound to the north by the broad Chatham Rise, and is linked to the Great South Basin in the south.

4. 2: STRATIGRAPHY

The basal section of the Canterbury Basin is comprised of a series of grabens and half-grabens formed during the mid Cretaceous (Fig. 4.2); these features have trapped up to 6 km of Cretaceous and Cenozoic sediments in the main depocentre, known as the Clipper Sub-basin (Sutherland and Browne, 2003). Despite the close proximity to the Alpine Fault, a major plate boundary, the majority of the basin has been tectonically inactive since the late Cretaceous, however, a number of localized late Eocene to Oligocene and Miocene igneous centers are present (Fulthorpe and Carter, 1991).

The stratigraphy deposited atop basement can be broken into three regions: Northern, central and southern Canterbury (Browne and Field, 1985; Andrews et. al., 1987).

4. 2. 1: Northern Canterbury

This region reaches from the Ashley River in the south, to the Hope Fault in the north, with Kowai-1 (Fig. 4.3) being the only studied well within the vicinity. The eight groups that outcrop in the region are:

- Mt Somers Volcanic Group (Early late Cretaceous)
- Mandamus Igneous Complex (Early late Cretaceous)
- Iwitahi Group (Late Cretaceous)
- Eyre Group (Late Cretaceous to early Oligocene)
- A late Cretaceous to Mid Oligocene limestone

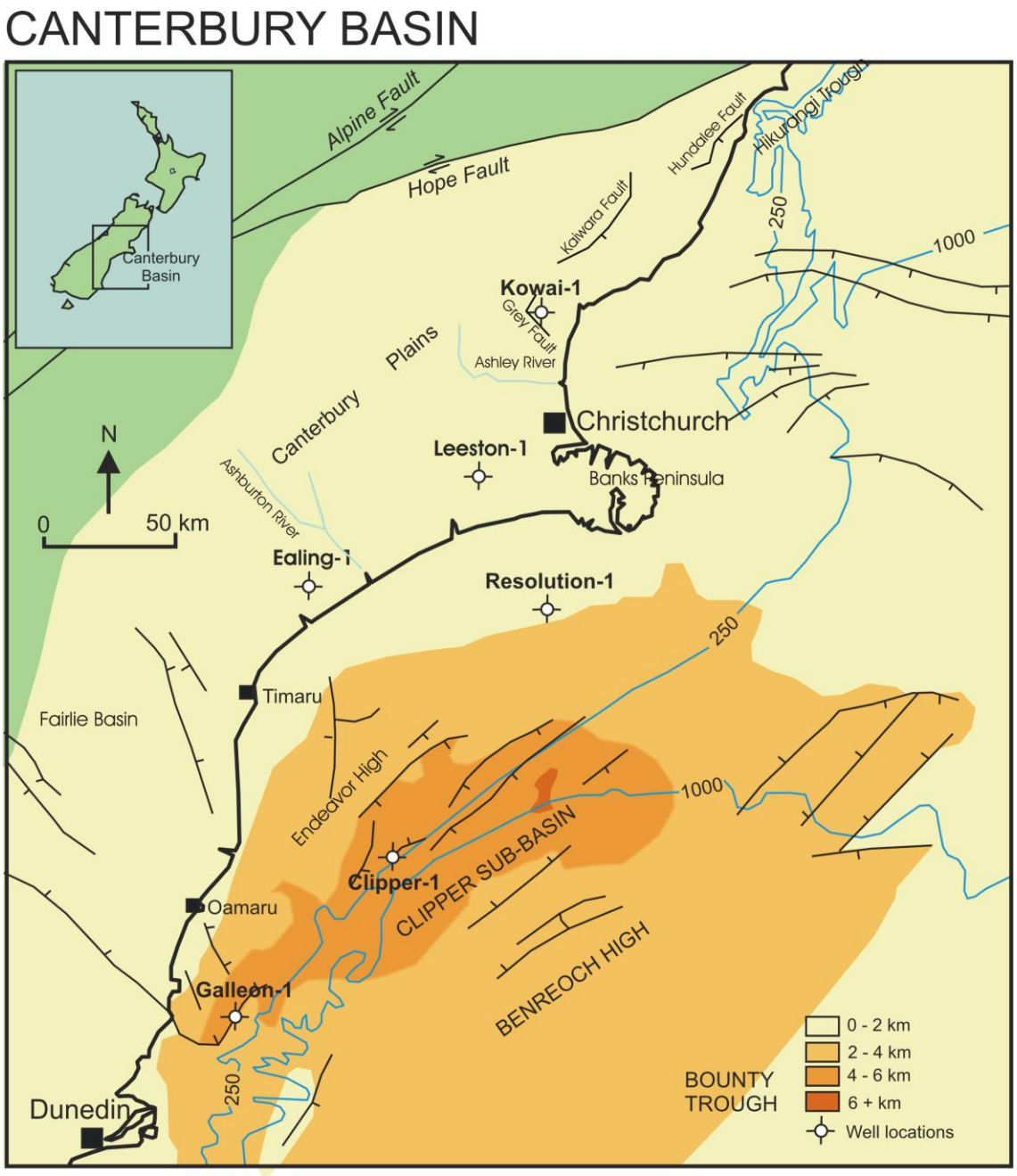

Figure 4.1: Map of the Canterbury Basin, showing location of wells, sediment thickness and major faults, including the Alpine and Hope Faults (from Explore New Zealand Petroleum 2003, Ministry of Economic Development, Crown Minerals, 2003).

- Cookson Volcanic Group (Mid Oligocene)
- Porter Group (Oligocene)
- Motunau Group (Late Oligocene to Pleistocene)

Most of these groups outcrop in very limited areas. For this reason only the most laterally extensive, the Eyre and Motunau Groups, and the limestone, will be discussed here.

4. 2. 1. 1: The Eyre Group

This group contains 17 formations, including conglomerates, sandstones, siltstones, mudstones, greensands, volcanics and limestones. There is a general transgressive trend and the group fines upwards. The base is represented by high energy, near shore, perhaps even terrestrial siltstones, conglomerates and quartzose sandstones with lignite seams; and passes up into mudstones, greensands and detrital sandstones, deposited in outer shelf conditions (Browne and Field, 1985). Deposition occurred from the Haumurian (84 Ma) to the Whaingaroan (27 Ma).

4. 2. 1. 2: The late Cretaceous to mid Oligocene Limestone

Technically not a group, this widespread pelagic limestone is known as the Amuri Limestone Formation. It consists of cm to deci-cm beds, which are indurated and bioturbated. Bioclasts consist of predominately coccoliths, with foraminifera also present. A lack of clastic material suggests the unit was deposited some distance from shore (Browne and Field, 1985).

4. 2. 1. 3: The Motunau Group

Like the Eyre group, the Motunau also consists of a diverse range of sediment types, with limestone, greensands, sandstone, siltstone, mudstone and conglomerate all present within the nine formations. The units were deposited from the Duntroonian (27 Ma) to the Castlecliffian (2 Ma). Sediment types typically represent a shallow marine environment, with a regression from late Miocene to Pleisocene times (Browne and Field, 1985).

LINE CB82-30

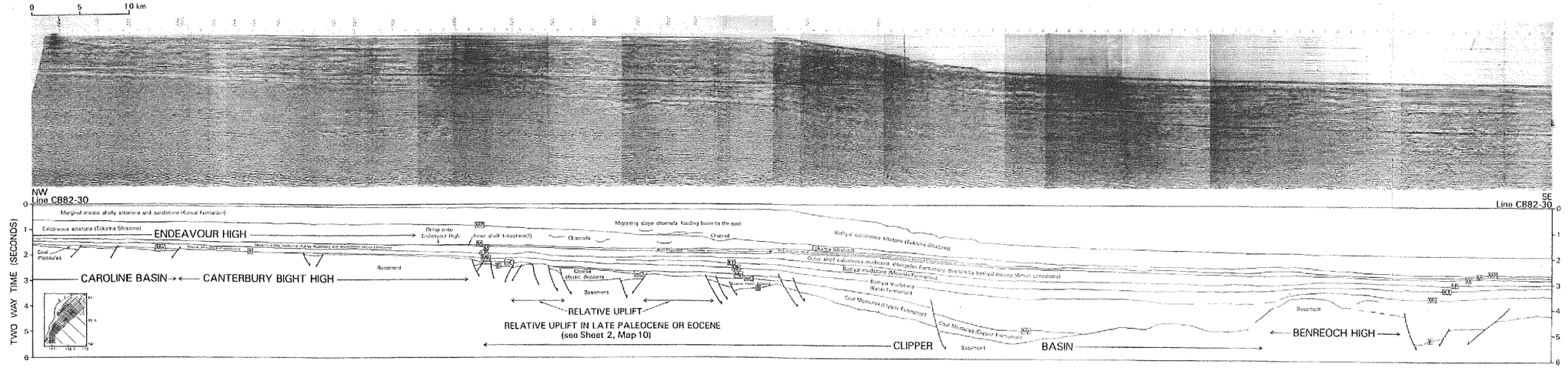

Figure 4. 2: Seismic section across the Canterbury Basin (From BP Shell Todd, 1982).

Horizon B = Top of basement, MC = mid Cretaceous, Mp = near base of Piripauan,
Mh = intra-Haumurian, KT = near base of Paleocene, LP = Late Paleocene,
O = Oligocene, M = early to mid Miocene, Mp = late Miocene-Pliocene horizon.

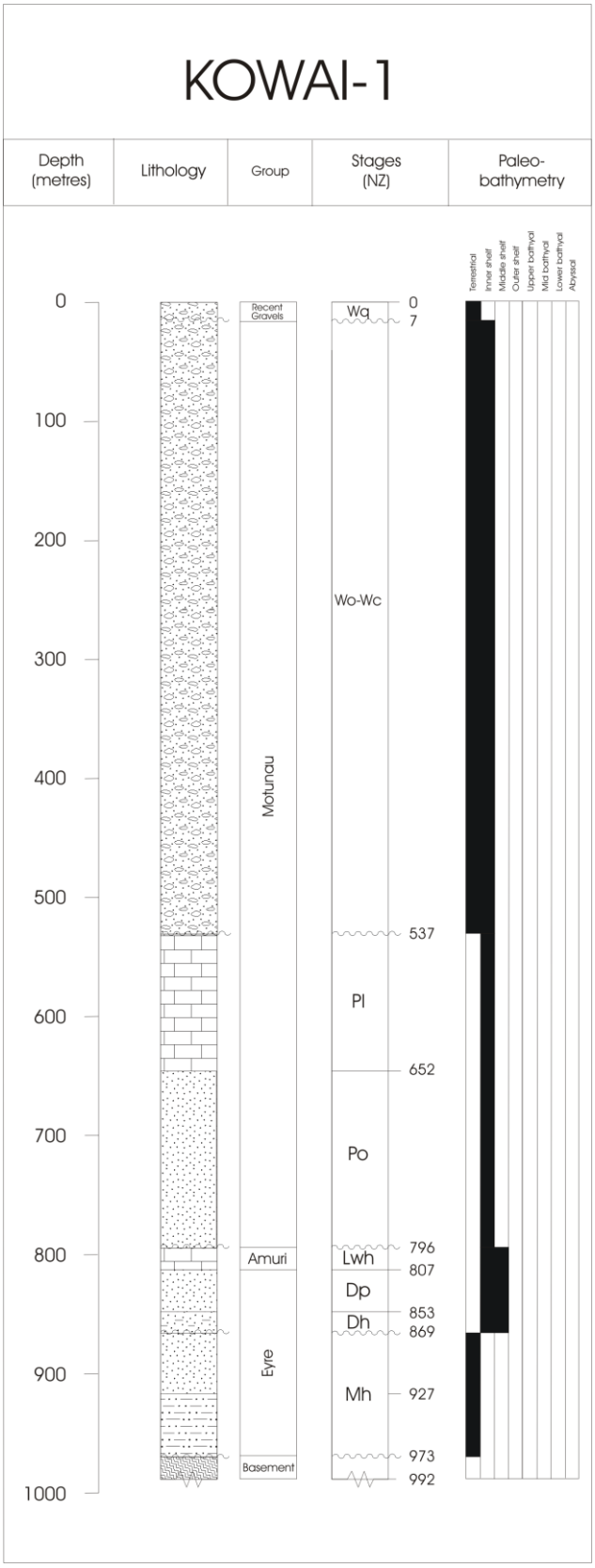

Figure 4.3: Stratigraphic column for Kowai-1, typical of Northern Canterbury, New Zealand.

4. 2. 2: Central Canterbury

Eight groups outcrop in the region stretching from the Ashley River in the north, to the Ashburton River in the south. Leeston-1 (Fig. 4.4) and Resolution-1 are located in this area. The eight outcropping units are:

- Mount Somers Volcanic Group (early late Cretaceous)
- Eyre Group (late Cretaceous to late Eocene)
- An early to middle Oligocene Limestone
- Motunau Group (late Oligocene to Quaternary)
- Burnt Hill Group (Miocene)
- Lyttleton Group (Miocene to Pliocene)
- Akaroa Group (Miocene to Pliocene)
- Diamond Harbour Group (Miocene to Pliocene)

Many of these units occur only in small areas, therefore only the Mount Somers Volcanic Group and the Burnt Hill Group will be discussed in this section. The voluminous Eyre Group and the Amuri Limestone were covered in the previous section.

4. 2. 2. 1: The Mount Somers Volcanic Group

This group unconformably overlies the Torlesse Supergroup, and consists of rhyolite, ignimbrite, dacite, andesite and dolerite, as intrusions, flows and tephras. Deposited in a terrestrial environment, this unit outcrops more commonly in the southwest of the region, however the volcanic rocks of Banks Peninsula are also included in this group (Andrews et. al., 1987).

4. 2. 2. 2: The Burnt Hill Group

Miocene in age, this group is comprised of non-calcareous marine and estuarine rocks. It includes a number of volcanic units, both of air-fall and flow nature; and a number of minor detrital interbedded units (Andrews et. al., 1987).

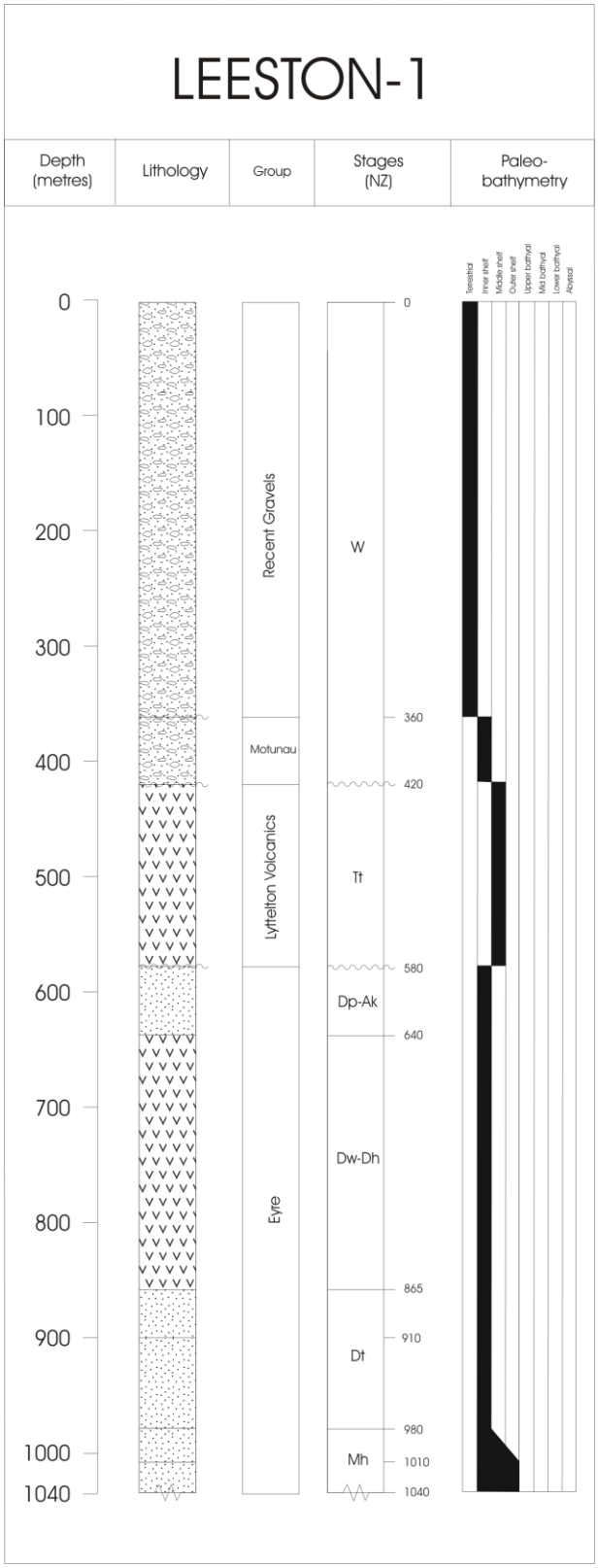

Figure 4.4: Stratigraphic column for Leeston-1, typical of Central Canterbury, New Zealand.

4. 2. 3: Southern Canterbury

The area referred to as southern Canterbury extends from the Waitaki River in the south to the Rakaia River in the north. Clipper-1, Ealing-1 (Fig. 4.5), and Galleon-1 are located within this region. The groups which outcrop in this area are:

- Mount Somers Group (early to late Cretaceous)
- Eyre Group (mid to late Cretaceous)
- Alma Group (mid to late Eocene)
- Early to mid Oligiocene Limestone
- Otiake Group (mid Oligocene to mid Miocene)
- Motunau Group (late Oligocene to late Miocene)
- Kurow Group (mid Miocene to Pleistocene)

Only the Otiake and Kurow groups will be discussed in this section, as the remaining units have been identified in earlier sections.

4. 2. 3. 1: Otiake Group

The Otiake Group extends from Oamaru to the Rakaia River. Deposited during the mid Oligocene to mid Miocene period in shallow to mid shelf depths, this unit is moderately to highly calcareous. The group includes limestones, calcareous sandstones, mudstones and greensands. The Brothers Volcanics, also included within the Otiake Group encompass all late Oligocene volcanic bodies and volcanogenic sediments in the Mount Somers district.

4. 2. 3. 2: Kurow Group

The Kurow Group is a terrestrial to shallow marine group, deposited unconformably over rocks of Waitakian (25 Ma) age or older. In northern Canterbury rocks of this age are included within the Motunau Group, however, the unconformity in southern Canterbury provides a convenient group boundary. This unit includes lignite, clay, sands and conglomerates.

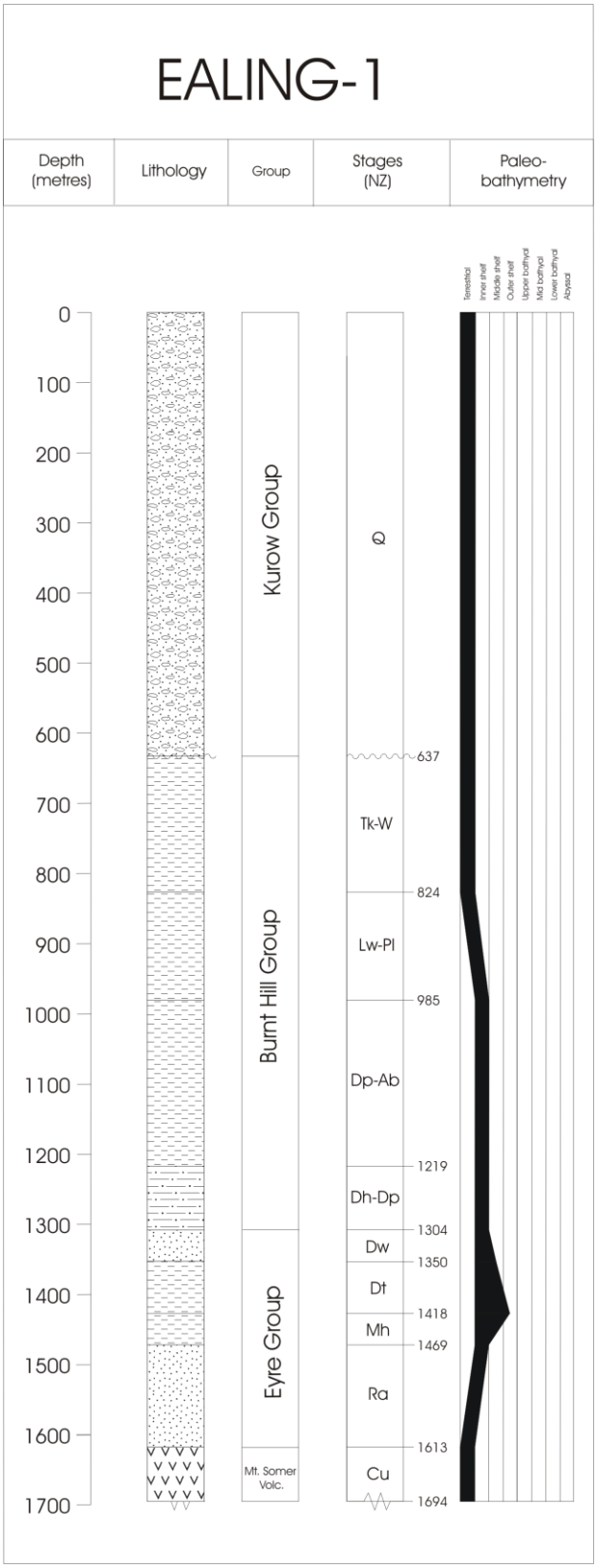

Figure 4.5: Stratigraphic column for Ealing-1, typical of southern Canterbury, New Zealand.

4. 3: LOCATION OF WELLS

Well	Lat/ Long	Date spudded
Clipper-1	44 58’ 14.84” S 171 53’ 48.25” E	1984
Ealing-1	44 03’ 20.1” S 171 28’ 97.1” E	2000
Galleon-1	45 29’ 18.82” S 171 09’ 49.85” E	1985
Kowai-1	43 09’ 61.68” S 172 36’ 10.02” E	1978
Leeston-1	43 40’ 66.68” S 172 18’ 03.36” E	1969
Resolution-1	44 11’ 16.20” S 172 38’ 09.69” E	1975

Table 4.1: Location and the year of drilling for Canterbury Basin petroleum wells used in this study. Clipper-1, Galleon-1 and Resolution-1 are all located offshore, while Ealing-1, Kowai-1 and Leeston-1 are onshore.

4. 4: QUALITY OF DATA FROM WELLS

The information used in this section is based on data published in the individual well completion reports. In the case of Clipper-1 and Resolution-1 these data are derived from foraminifera, nannofossils and palynoflora. Galleon-1 and Kowai-1 rely solely on foraminifera. The age of the fossils suggests there are likely to be dating errors built into the age estimations. There are also likely to be age differences between the wells drilled in the 1970s and those from the 1980s, due to a revision of the International and New Zealand timescales in 1982. With the exception of Ealing-1, Leeston-1 and Resolution-1, all wells were drilled to basement.

4. 5: RESULTS

The geohistory of the Canterbury Basin is summarized in figure 4.6 and 4.7. Figures 4.8 and 4.9 show the results from the individual wells located within Canterbury Basin.

4. 5. 1: Clipper-1

The sediment overlying basement rock was deposited during the Raukumara series (95-85 Ma). Initially, rapid sedimentation and subsidence slowed towards the end of the Cretaceous (fig. 4.8), where water depth reached a maximum of upper bathyal. The Paleocene saw an increase in sedimentation, but little tectonic subsidence. Tectonic subsidence and sediment accumulation slowed during the Eocene period. During the late Eocene to early Oligocene there is a change in the shape the curve; it is over this period that the curve transitions from essentially concave-up to concave-down. Rates of sedimentation and subsidence began to accelerate, while there was a decrease in water depth. During the Miocene rates continued to rise. An unconformity has removed sediment most likely representing the beginning of the middle Miocene. Over this period tectonic subsidence resulted in an increase from outer shelf water depths to upper bathyal. Preceding this event both sedimentation and tectonic subsidence rates continued to increase, reaching a maximum during the Pliocene period.

β values were determined using tectonic subsidence over the period between 75 and 37 Ma. Using a minimum subsidence of 410m, and a maximum of 630m, a β value of 1.8 $\pm$ 0.2 was calculated.

4. 5. 2: Ealing-1

Begining during the Urutawan (108 Ma), deposition was originally slow at a rate of 4 $m.Myr^{-1}$ (Fig. 4.8). At 84 Ma an increase in water depth was accompanied by an increase in sedimentation and subsidence rate. Deposition remained about the same until 46 Ma. Slight uplift at a rate of 3 $m.Myr^{-1}$ appears to have occurred from 56 to 46 Ma, accompanied by a decrease in water depth. From 46 Ma sedimentation and subsidence increased for 3 Myr, before an unconformity removes much of the Eocene and Oligocene data. Sedimentation resumes at 25 Ma, before another break in the record occurs from 16 to 7 Ma. From this period shallow water conditions occur, while

sedimentation and subsidence rate the maximum rates seen in this well (245 m.Myr^{-1} and 108 m.Myr^{-1}).

Assuming thermal subsidence occurred between 84 and 56 Ma, with a minimum of 100 m, and a maximum of 300 m, a β value of 1.4 ± 0.15 was calculated.

4. 5. 3: Galleon-1

After an initial period of uplift beginning during the late Cretaceous, the shape of the geohistory plot of Galleon-1 is similar to that of Clipper-1 (Fig. 4.8). Sedimentation and tectonic subsidence rates decreased until late Oligocene, where once again the curve changes from concave-up to concave-down. The unconformity (19-15 Ma) seen in the record from Clipper-1 is also represented in the data from Galleon-1. The paleobathymetry of Galleon-1 however is simpler than that from Clipper-1. Barring the brief period of uplift, which resulted in water depths increasing from shelfal depths to terrestrial, the water depth at Galleon-1 increased until outer shelf conditions were reached during the Paleogene. Water depth has remained approximately stable until present.

Using a minimum of 395m of tectonic subsidence, and a maximum of 475m between 65 Ma and 39 Ma, a β value of 1.8 ± 0.05 was calculated for Galleon-1.

4. 5 .4: Kowai-1

The geohistory plot of Kowai-1 is similar in shape to that of Clipper-1 (Fig. 4.9), however the presence of four unconformities has resulted in compression of the curve. Sediment deposited during these periods is not accounted for. Little can be inferred about the periods of erosion or non-deposition, this has lead to compression of the curve. The resulting curve therefore shows minimum values of sediment accumulation and tectonic subsidence. Sediment deposition and subsidence rates show the familiar pattern of slowing until the Oligocene, and increasing afterwards. However, there is a short period of uplift during the Oligocene at a rate of 10 m.Myr^{-1}, which is not seen in either Clipper-1 or Galleon-1.

It was impossible to calculate reliable β values for Kowai-1 due to an unconformity, which ranged from 65 to 50 Ma, s significant portion of the post-extension period.

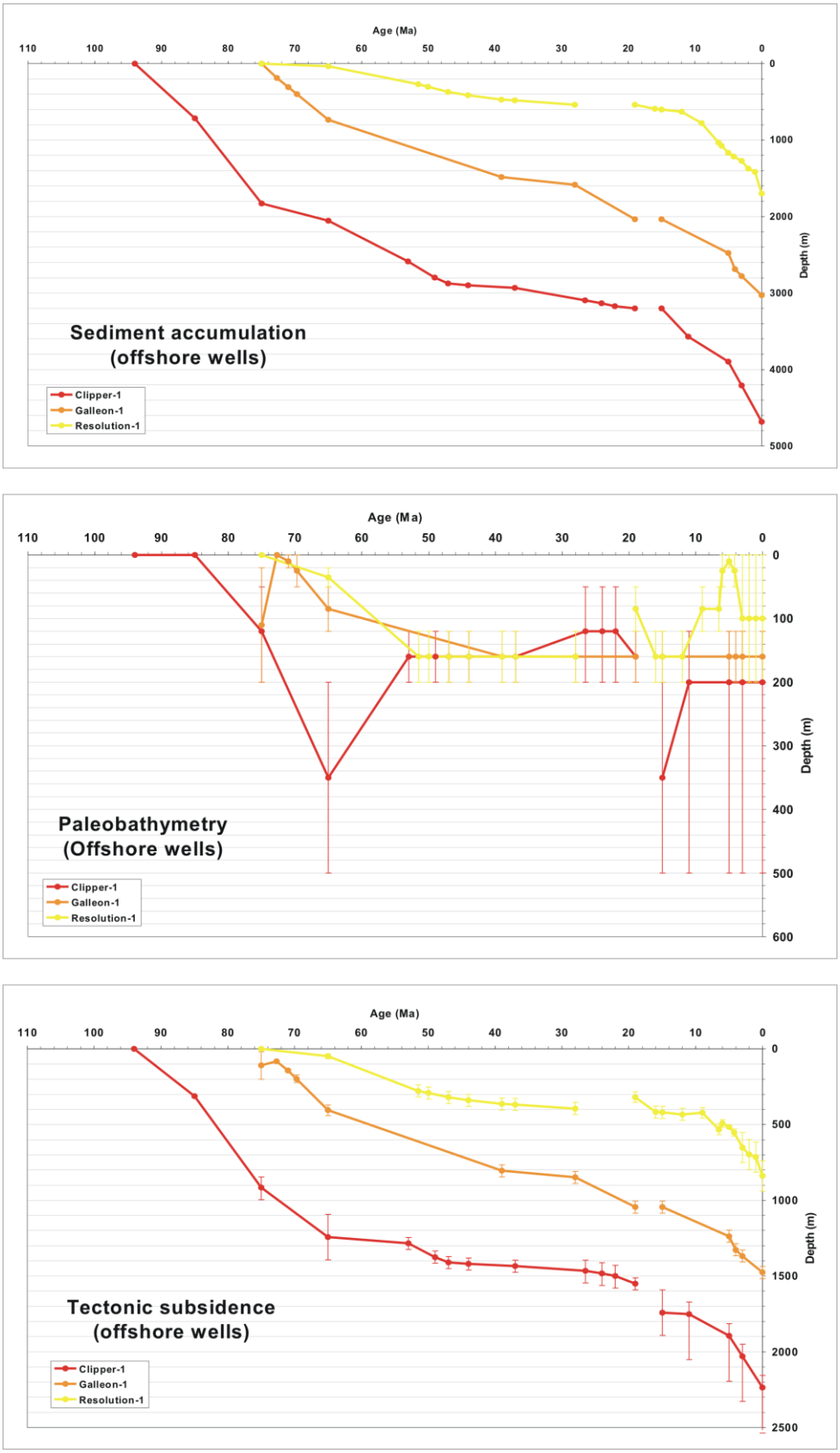

Figure 4.6: Geohistory plots for the wells located offshore, Canterbury Basin.

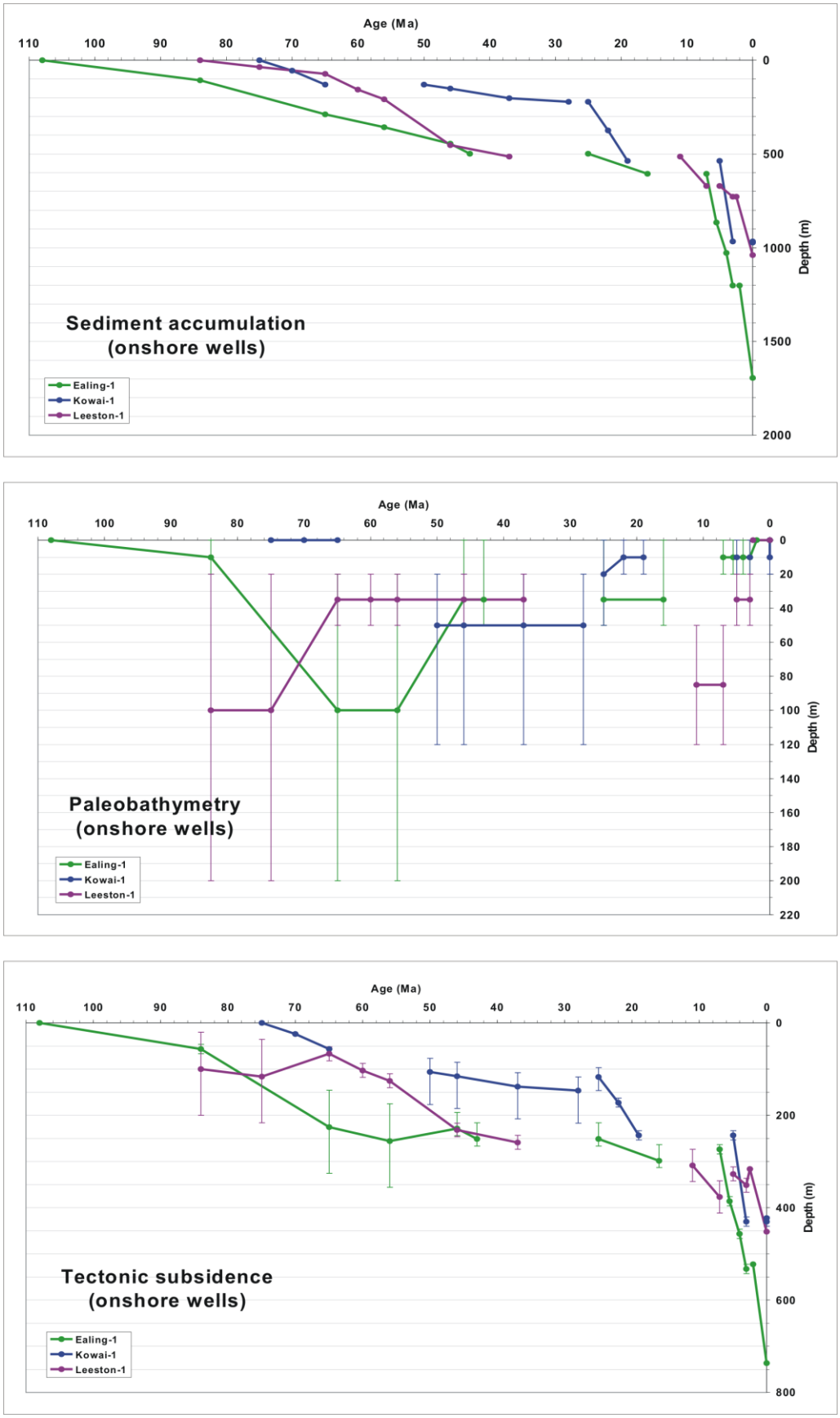

Figure 4.7: Geohistory plots for the wells located onshore, Canterbury Basin.

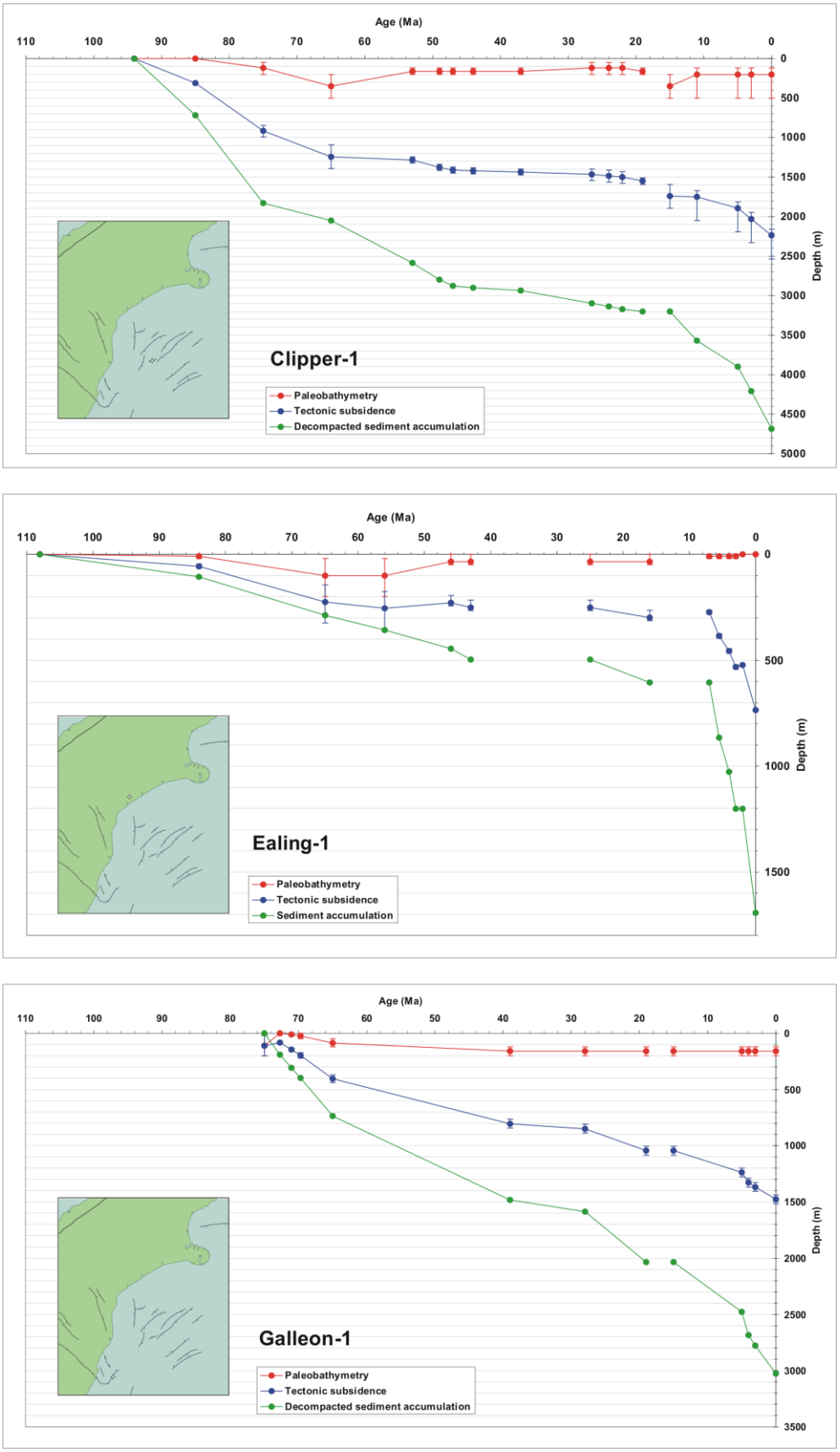

Figure 4.8: Geohistory Plots for Clipper-1, Ealing-1 and Galleon-1, Canterbury Basin.

4. 5. 5: Leeston-1

Sedimentation began during the Haumurian (84 Ma) on the inner continental shelf. Uplift resulted in decreasing water depths until 65 Ma, while sedimentation occurred at 4m.Myr^{-1}.

From 65 Ma deposition and subsidence increased to 25 m.Myr^{-1} and 11m.Myr^{-1} respectively, until 46 Ma (Fig. 4.9). At this point rates decreased until 37 Ma. The Oligocene and much of the Miocene are missing from the record, however, changes in paleobathymetry over this break show atleast 2 m.Myr^{-1} of subsidence occurred. From 12 Ma paleobathymetry and tectonic subsidence show brief periods of rapid uplift, while sediment accumulation reaches a maximum (125 m.Myr^{-1}).

4. 5. 6: Resolution-1

Sediment accumulation and tectonic subsidence follow a similar pattern to the Canterbury wells previously mentioned (Fig. 4.9). An unconformity has removed data corresponding to the period between the late Oligocene and the middle of the early Miocene, and it appears likely the transition from concave-up to concave down occurred over this interval. A change in water depth from outer shelf to middle shelf suggests a period of uplift. However, this maybe due to poor depth determination as the data suggests an immediate return to outer shelfal depths. Other periods of uplift appear to occur between 12 and 9 Ma, as well as between 7 and 6 Ma, however these may also be the result of a similar problem.

Using 20 m as the minimum amount of tectonic subsidence and 170 m as the maximum, a value of 1.6 ± 0.15 was calculated for the period from 52 to 37 Ma.

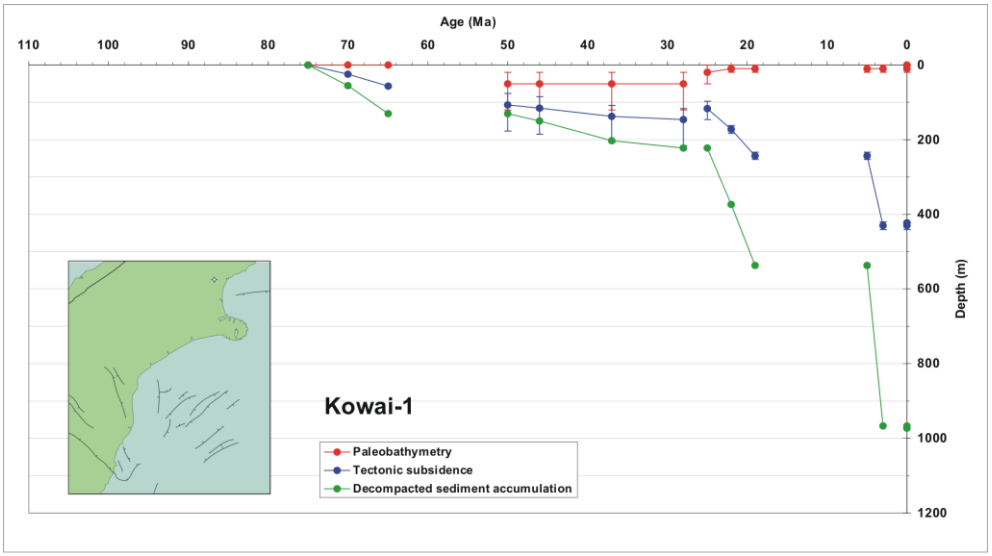

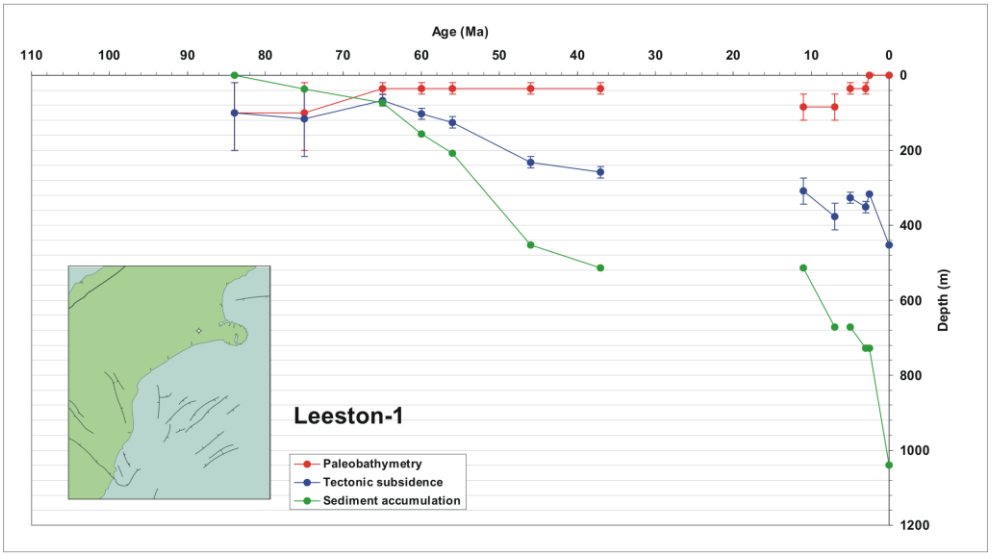

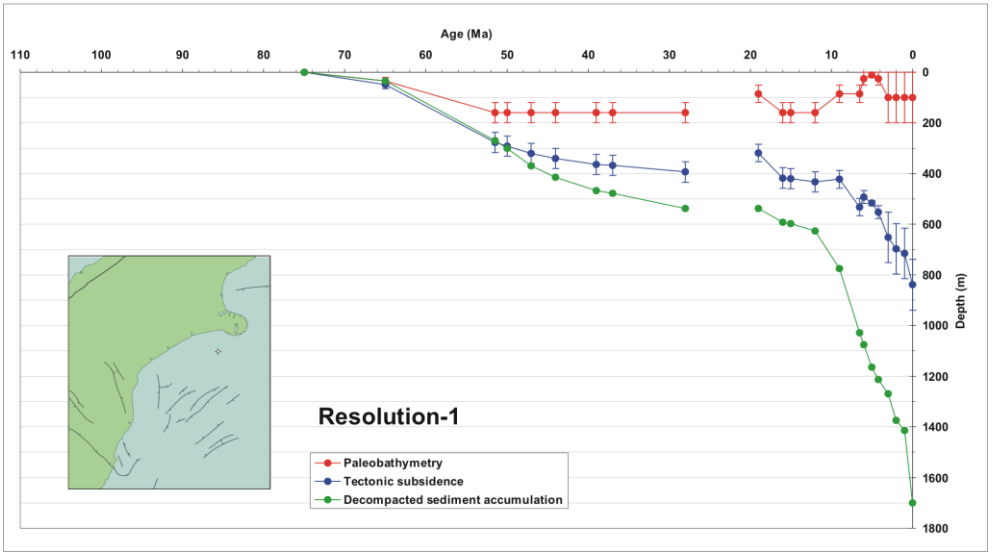

Figure 4.9: Geohistory Plots for Kowai-1, Leeston-1 and Resolution-1, Canterbury Basin.

4. 6: INTERPRETATION AND DISCUSSION

Figure 4.10 shows the characteristic curve for the Canterbury Basin. The curve clearly shows McKenzie style thermal subsidence following the break up of Gondwana during the Cretaceous. A change in tectonic style is seen during near the Oligocene-Miocene boundary, perhaps representing convergence on the Alpine Fault. Tectonic subsidence also increases at ~6 Ma, the cause of which will be elaborated on further below, and also in the discussion chapter.

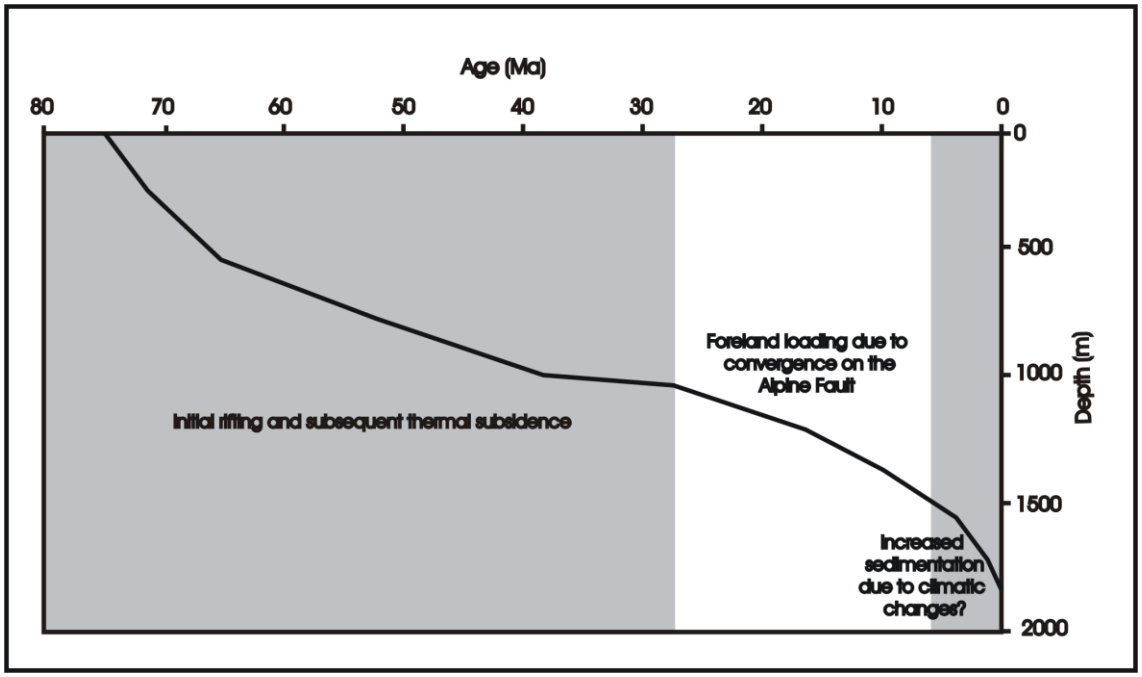

Figure 4.10: Tectonic subsidence curve for the Canterbury Basin, with inferred driving forces.

4. 6. 1: Mid to Late Cretaceous

There is little doubt that the formation of the Canterbury Basin is related to the late Cretaceous break-up of Gondwana, however, the basin history data seems to suggest an extended period of subsidence. The presence of three distinct faulting domains (Fig. 4.11) suggests more than one influence on basin formation.

Break-up of Gondwana resulted in the formation of a number of fault bound grabens and half grabens of varying orientation. These subaerial features filled with coarse

conglomerates, and the bounding faults played an important role in the initial subsidence of the basin (Field and Browne, 1989).

Field and Browne et. al. (1989) separated the mid to late Cretaceous normal faults in and surrounding the Canterbury Basin into three separate domains based on fault orientation. (Fig. 4.11). However, the origin of these faults is disputed. Field and Browne et. al. agree with Bradshaw (1989) that the faults in the Clipper domain, where Clipper-1 and Galleon-1 are located, were caused by NW-SE crustal extension, related to the separation of New Zealand from Antarctica. They also concur that the faulting in the North Otago and Chatham Rise domains are parallel to the dominant structural grain of basement, and are reactivations of earlier features. As a less probable alternative Field and Browne (1989) also suggest that the faulting in all domains may be due to the N-S extension parallel to the Bounty Trough, and the southern margin of the Chatham Rise. Laird (1993) suggested that the faulting in the North Otago is parallel to, and therefore related to, the spreading axis of the Tasman Sea, and the Lord Howe Rise. Using Kamp's (1986) reconstruction, Laird demonstrated that basin and fault orientations have changed, and that the Chatham Rise faults also used to be parallel to the Lord Howe Rise and Tasman Sea spreading axis, perhaps representing an extension of the Lord Howe Rift System through New Zealand. Due to the complicated tectonics of the late Cretaceous, it is difficult to prove or disprove these theories based solely on the subsidence history of the four wells presented in this chapter. Nevertheless, what the subsidence data do show is a rift history that had finished by 65 Ma, then a long (~30 Myr) period of what is interpreted to be thermal subsidence.

Subsidence began initially in the present day center of the basin, where Clipper-1 has since been drilled. Subsidence at Galleon-1 began after Clipper-1, but before the other wells located closer to the edge of the basin. As sediment accumulated and loaded the basin center, flexure of the crust resulted in the growth of the basin, an increase in water depth, and the subsidence of the outer wells. At Clipper-1 sedimentation slowed from ~75 Ma, with increasing water depth. This may be due to either increased distance from the sediment source, or a change in the uplift rates in the source area providing sediment.

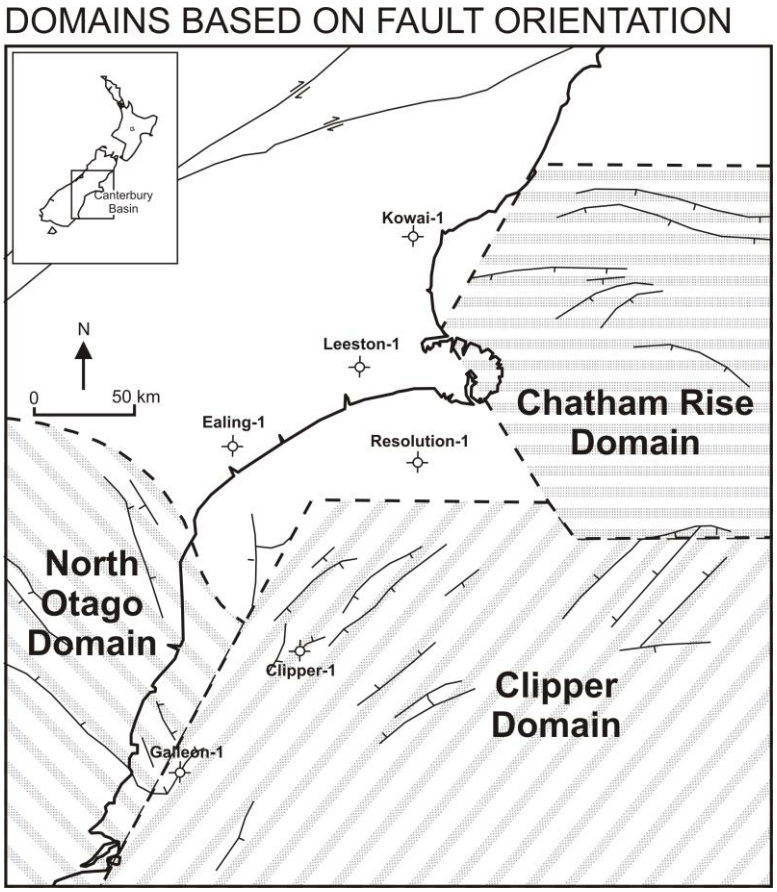

Figure 4.11: Cretaceous faulting domains (from Field and Browne et. al., 1989)

At Galleon-1 subsidence began in ~100m of water before tectonic uplift exposed the area. It is possible that this is an over-estimation of water depth, perhaps representing sporadic marine incursions, rather than a totally marine environment.

From the geohistory plot of Resolution-1, it appears that tectonic subsidence is more rapid than sedimentation, i.e, subsidence is largely expressed by increased paleobathymetry. It is feasible that sediment source area was low-lying, providing little output, while thermal subsidence continued. A second scenario is that water depth has simply been overestimated. When the shallowest depth in the possible range is used the results are more in keeping with the other studied wells.

The shape of the subsidence curves for the Cretaceous suggests that this basin represents a passive margin based on the Dickinson classification system (1976) (Fig 2.13), and the decreasing subsidence rate is characteristic of a simple thermally subsiding basin. As the crust cooled and subsided, accommodation space for sediments was created. As the rate of cooling slowed, so too did the rate of subsidence and therefore sedimentation.

4. 6. 2: Paleocene

This was a period of relative tectonic quiescence. Spreading in the Tasman ceased during early to mid Paleocene, and New Zealand continued to passively drift away from Antarctica. Faulting during the Paleocene was limited to local movement of Cretaceous faults (Field and Browne et. al., 1989). Sediments were derived from a low lying landmass to west of the basin, and from the subaerial Chatham Rise to the north (Wood et. al., 1989).

In the center of the basin Clipper-1 showed a decrease in sedimentation, with a much smaller decrease in subsidence. This subsequently lead to the filling of the basin and decrease in water depth. This is likely to be due to a decrease in the rate of cooling of the rifted crust slowing subsidence. Nearer the edge of the basin, Resolution-1 showed a slight increase in sedimentation, subsidence, and also water depth. This is possibly due to a combination of thermal relaxation, isostatic adjustment of the crust to the loading, and Resoulution-1's proximity to the subaerial Chatham Rise sediment source. Kowai-1 remained terrestrial during this time, and the observed unconformity is likely due to subaerial erosion.

4. 6. 3: Eocene

This was a period of increased tectonic activity. At approximately 50 Ma a new plate boundary propagated into southern New Zealand along a zone of Cretaceous oceanic transform faults, the Emerald Fracture Zone (Molnar et. al., 1975; Sutherland, 1999). This event lead to renewed movement of extensional faults in the Canterbury Basin, and the formation of the Fairlie Basin to the west at ~42 Ma (Field and Browne et. al., 1989).

Subsidence curves in the Great South Basin clearly show this rifting event as a rapid increase in subsidence and sedimentation (Carter, 1988; Baxter, 1993). An increase is noted at Clipper-1, and in Resolution-1, and is most probably related to this event. Carter (1988), suggested that the geohistory plots for Canterbury are not as simple as they initially appear, and in fact represent two superimposed heat decay curves: one beginning in at ~100 Ma, related to Gondwana rifting and initial basin formation; and a second beginning at ~60 Ma, related to the propagating plate boundary. He cites widespread volcanic activity in the region as evidence of this deformation and heating event. Warping and/or faulting preceding this event could explain the increase in sedimentation seen at Clipper-1 beginning at about 65 Ma. A lack of data points in the other wells prevents it from being recognized, however. This second phase is inferred by Field and Browne (1989) at Endevour-1, also located in the Canterbury Basin, and Carter (1988) shows it in his study of Galleon-1.

4. 6. 4: Oligocene

New Zealand continued to slowly drift northwards during the Oligocene, however this was another period dominated by tectonics. Once again the region can be divided into tectonic domains (Field and Browne, 1993). Kowai-1 is located in the northwestern domain (fig. 4.12), which is influenced by a developing transpressive system, and associated uplift and erosion. Data from Kowai-1 most clearly shows the effects of this transpressional phase.

The unconformities in Ealing-1, Kowai-1, Leeston-1 and Resolution-1 represent the Marshal Paraconformity, a controversial chronostratigraphic break probably caused by climate change. Global cooling and subsequent glaciation in the Oligocene caused a major fall in sea level at 29 Ma (Vail and Hardenbol, 1979; Haq, 1987, 1988). It is likely that the break seen in Kowai-1 and Resolution-1 is a period of non-deposition caused by the oceanic cooling and density-driven strengthening of current activity, creating unfavourible conditions for limestone production (Fulthorp et. al., 1996). Lewis suggested that the localized areas surrounding Leeston-1 and Ealing-1 were subaerial exposed, with older sediments eroded, explaining why the stratigraphic break begins much earlier at these sites, however this has been debated by Carter (1985).

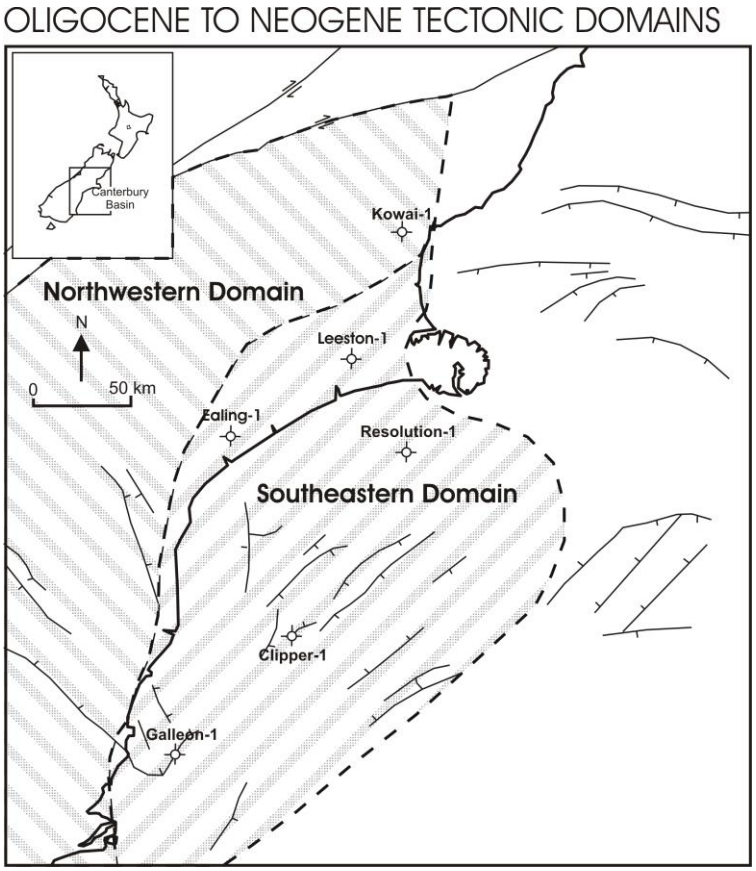

Figure 4.12: Oligocene and Neogene tectonic domains (After Field and Browne, 1993)

In the southeastern domain there is little faulting or folding, and subsidence dominates the sedimentary record. Differential subsidence, rather than block faulting lead to the development of the Endeavor High, a NE-SW trending sub-marine region (Field and Browne et. al., 1989). Proximity to this feature likely prevented currents depositing clastic sediments in the region, as the Oligocene record is dominated by carbonate production (Stagpoole et. al., 2002).

4. 6. 5: Miocene

It is during this time that the tectonic loading signature of the basin becomes most apparent, but the timing of this event is debated. Walcott (1998) inferred plate motion between the Pacific and Australian plates based on magnetic anomalies and fracture zone data. He proposed a pronounced clockwise change in the convergence direction

between these two plates at approximately 6 Ma (Fig. 4.13). While Clipper-1, Galleon-1 and Resolution-1 show a rapid increase in both sedimentation and subsidence at this time, the curves show a definite increase considerably earlier. The increase that the geohistory plots show begins at 20 ± 3 Ma, which is consistent with the onset of convergence as suggested by Cande and Stock (2004).

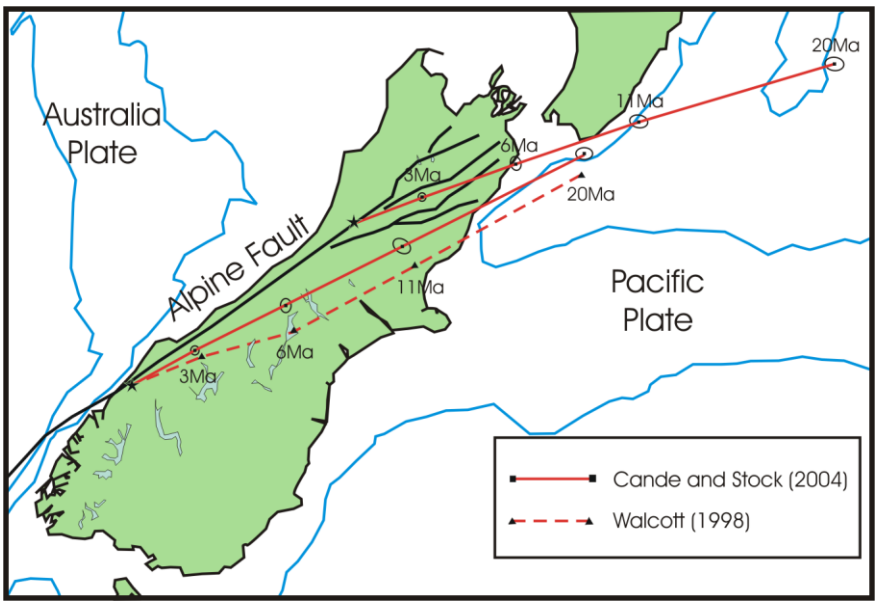

Figure 4.13: Predicted plate motion trajectories for the Pacific plate relative to the Australian plate based on data from Walcott (1998) and from Cande and Stock (2004). (From Cande and Stock, 2004)

Cande and Stock (2004) pointed out that Walcott's conclusion were based on an interpolation between two different data sources. They recalculated the convergence direction and found that there has been little change in the direction of convergence over the past 20 Myr, however, they do note a small kinematic change at 6 Ma, in keeping with the increase seen in the geohistory plots at this time.

Sediment deposited during the Miocene was dominantly clastic, presumably due to an influx of sediment from the rapidly rising Southern Alps. This lead to the increase in sedimentation and subsidence in all wells in the region, and the rapid enlargement of the

basin. The sediments fine towards the east, and seismic sections show that they form a prograding wedge, that was accompanied by subsidence during deposition.

During the late Miocene the E-W compression in northern Canterbury also led to the formation of a number of anticlinal ridges, bound to the west by high angle faults and accompanying troughs. This explains the unconformities Kowai-1 and Resolution-1. The periods of non-deposition in Clipper-1 and Galleon-1 maybe due to re-working of sediments by localized currents present on the continental shelf. A number of channels visible on the seismic lines presented in Field and Browne et. al. provide evidence for these currents.

It is during this time that the Marlborough Fault System formed. Initially the faults formed as Riedel shears to the compression, through later movement was related to the formation of the Hikurangi Trough (Field and Browne et. al., 1989).

At the end of the Miocene, Resolution-1 underwent a brief period of uplift. This may have resulted from poor paleobathymetic determination, however, the timing of the event coincides with the emplacement of the Banks Peninsula Volcanics in the region between 12 and 5.8 Ma. Field and Browne et. al. suggest that the warping and uplift associated with the volcanics probably occurred prior to deposition, providing a possible mechanism for the event.

4. 6. 6: Pliocene to Recent

During this period the Canterbury Basin received the most sediment since the early Cretaceous, however as discussed earlier, the reason why is controversial. Faulting and folding were basically restricted to the north and to the west, close to the plate boundary, while deposition and subsidence were basin wide.

Present day estimations of exhumation adjacent to the Alpine Fault have been calculated to be up to 10 mm/yr (Wellman, 1979; Beavan et. al., 2002), however, as mentioned earlier, there may have been little change in convergence rates on the Alpine Fault since 20 Ma. But something during this period resulted in the fastest period of sedimentation and subsidence in the basin's history, as seen in all wells, and further eastward propagation of

the alluvial piedmonts. The most commonly accepted theory is that increased faulting and folding due to motion on the Alpine Fault lead to increased erosion and deposition, however, a second theory, climate change, is gaining supporters.

Using data from the Deep-Sea Drilling Project (DSDP) and the Ocean Drilling Project (ODP), Hay et. al. (1988), calculated that global sediment accumulation for the past 5 Myr has been approximately three times that of any other 5 Myr period in the past 65 Ma. They suggested the increase was due to falling sea level, which exposed previously submerged areas of continental shelf to subaerial erosion. However, Molnar (2004) noted that many basins in central Asia also showed an increase during the period, these areas being located significant distances from the coast. Similar evidence found in low latitudes e.g. Northern Australia and the Amazon Basin, excludes glaciation as the sole cause of the sediment flux. Instead, Molnar suggests that increasing frequency and amplitude of climate change in the Pliocene led to increased erosion, as geomorphic processes struggle to reach equilibrium with such frequent climate cycles.

The Hikurangi Trough was rapidly propagating southwards, to its present position just north of the Chatham Rise. The structural grain of the still forming North Canterbury Fold and Fold Belt was approximately parallel to this feature (Field and Browne, et. al., 1989). During the late Quaternary the compressional forces acting caused reverse throws on formerly normal faults such as the Kaiwara, Hundalee and Grey Faults, providing a sediment source for the rapidly subsiding sub-basins.

4. 6. 7: β Values

The β values in the Canterbury Basin range from 1.4 to 2. Using wide angle reflection data, Henrys et. al. calculated a depth of ~25 km to the Moho beneath the Canterbury Basin, giving a pre-rift crustal thickness of 35-50 km. As expected, the thickest sediments are located near the area with the highest β value. In this case more sediment has accumulated near Clipper-1, where the extension was greatest, than near Resolution-1 on the edge of the basin, which has a lower stretching factor. Based on calculated β values, Figure 4.14 shows a contoured map of the area.

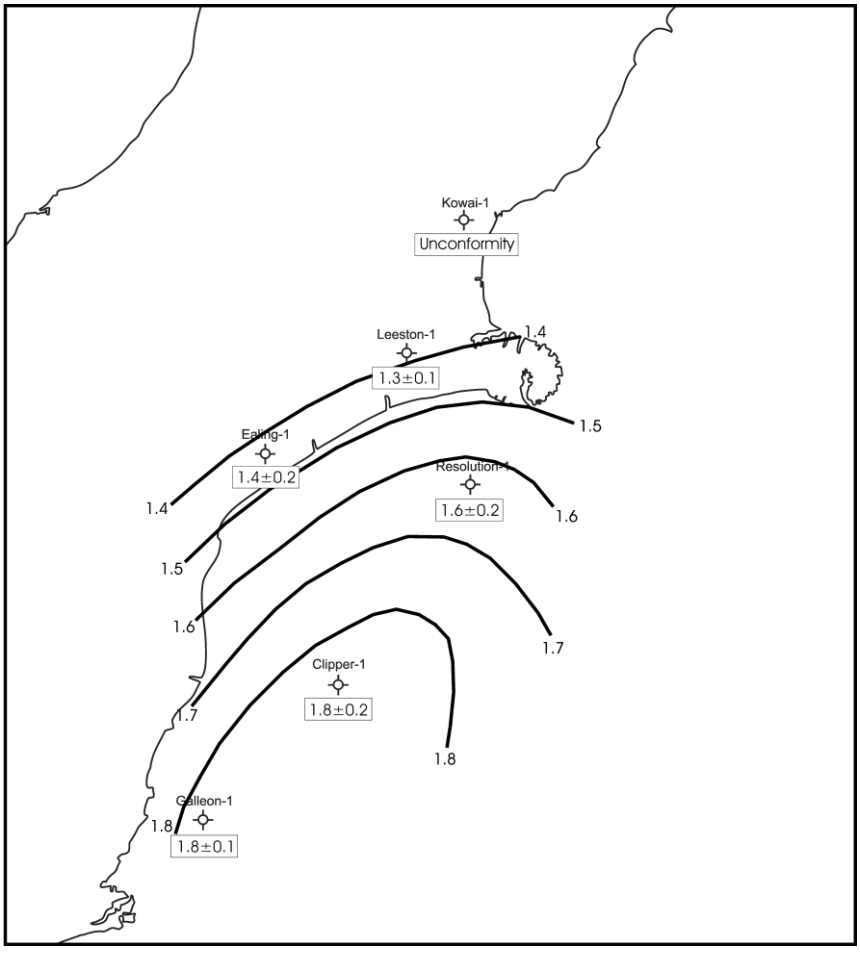

Figure 4.14: Map showing distribution of β values in the Canterbury Basin. β values approximately correlate with isopach thicknesses shown in Fig. 4. 1.

4. 7: CONCLUSIONS

- The signature of the Canterbury basin shows an initial rifting period beginning from about 100 to 90 Ma.
- This is followed by approximately 50 Ma of thermal subsidence.
- There is a possibility that an increase in subsidence and sedimentation seen at ~50 Ma represents another period of extension caused by the formation of the southern plate boundary at this time.
- Sedimentation and subsidence increases from about 20 Ma, it is probable that this is the result of convergence on the Australian-Pacific plate boundary, as proposed by Cande and Stock (2004).
- Another increase in sedimentation and subsidence at 6 Ma is noted, this likely represents a slight change in direction of convergence, as noted by Cande and Stock (2004), and more notably by Walcott (1998), combined with climatic forcing, suggested by Molnar (2004).
- β extension values for the region range from 1.8 ± 0.2 near the center of the sedimentary basin, to 1.3 ± 0.1 closer to the flanks, suggesting crustal thickness was between 35 and 50 km thick prior to rifting.

CHAPTER 5: GREAT SOUTH BASIN

5. 1: INTRODUCTION

Located to the southeast of the South Island, the Great South Basin (Fig. 5.1) covers over 100,000 km^2, making it one of the biggest basins on the continental portion of New Zealand. With an average water depth of over 700m the Great South Basin is poorly studied due to its position entirely offshore, its lack of related exposures onshore and only a handful wells drilled.

5. 2: STRATIGRAPHY

Like the adjoining Canterbury Basin, the Great South Basin has a complex horst and graben style, formed during a period of mid Cretaceous rifting relating to the breakup of Gondwana. Normal faulting created a number of structural highs and sub-basins (Fig. 5.2), which have collected up to 8.6 km of Cretaceous and Cenozoic sediments (Fig. 5.3). The presence of a nearby active plate boundary for most of the Great South Basin's history further complicates interpretations of tectonics and subsidence.

Beggs (1993) broke the stratigraphy of the Great South basins into four major groups:
The Hoiho group represents sediments deposited during the rifting phase of basin development, prior to the late Cretaceous period. The sediments are sandy terrestrial deposits and coal measures, which were deposited in NE trending graben and half-graben systems (Beggs, 1993). Conglomerates are present close to graben-bounding faults. The presence of fault scarp fans are marked in figure 5.2.

The Pakaha group, which ranges from Campanian to Teurian (86-55 Ma) in age, and is characterised by a period of transgression (Beggs, 1993). Deposition coincides with sea-floor spreading between Western Antarctica and the Campbell Plateau (Beggs, 1993). The majority of the Pakaha deposits are shallow sandstones, however the presence of terrestrial coal measures and intercalcated marginal marine facies in the northwest suggest terrestrial conditions prevailed there (Beggs, 1993).

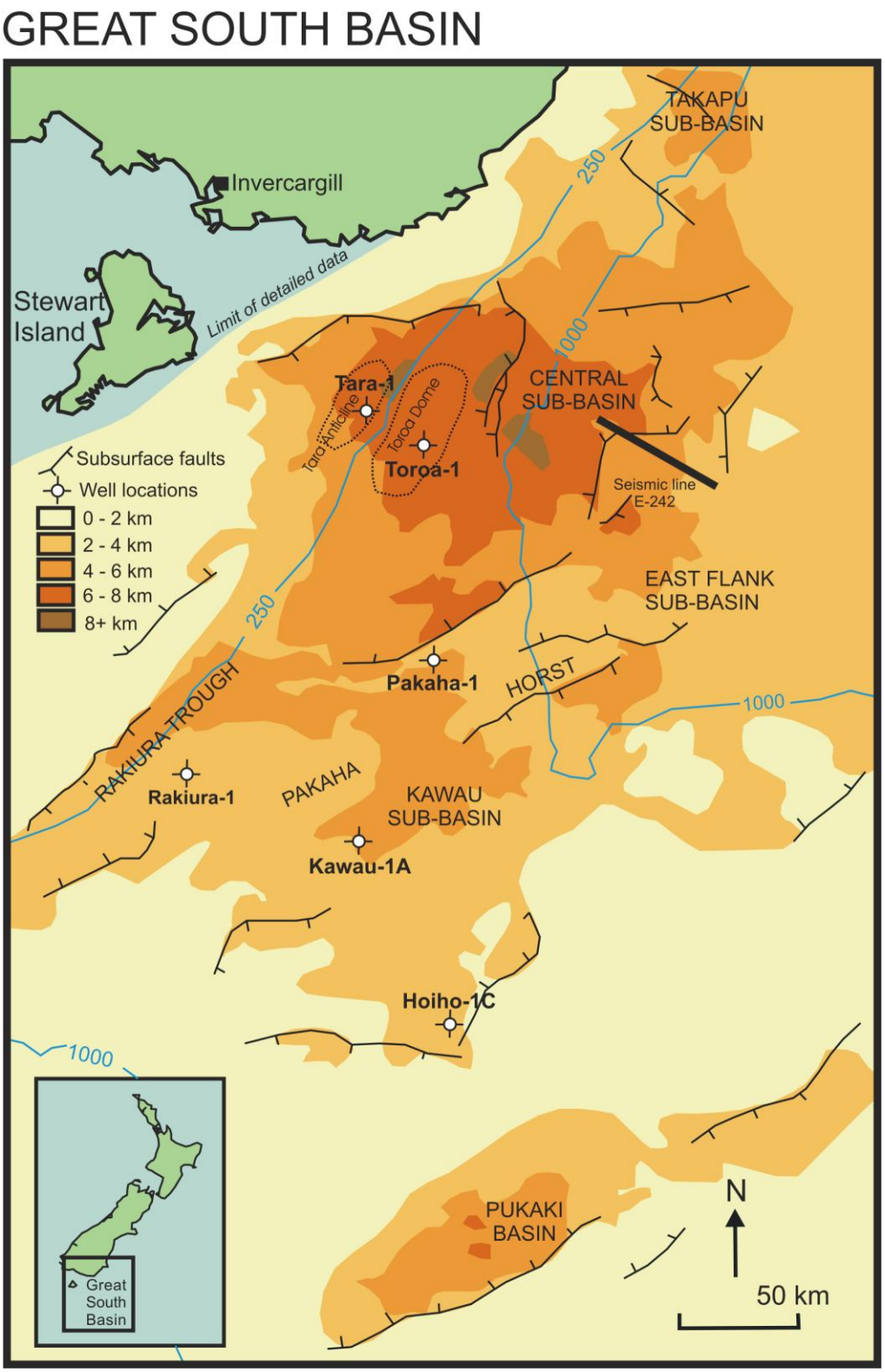

Figure 5.1: Map of the Great South Basin, showing location of wells, sedimentary thickness and major faults (from Explore New Zealand Petroleum 2003, Ministry of Ecomonic Development, Crown Minerals, 2003).

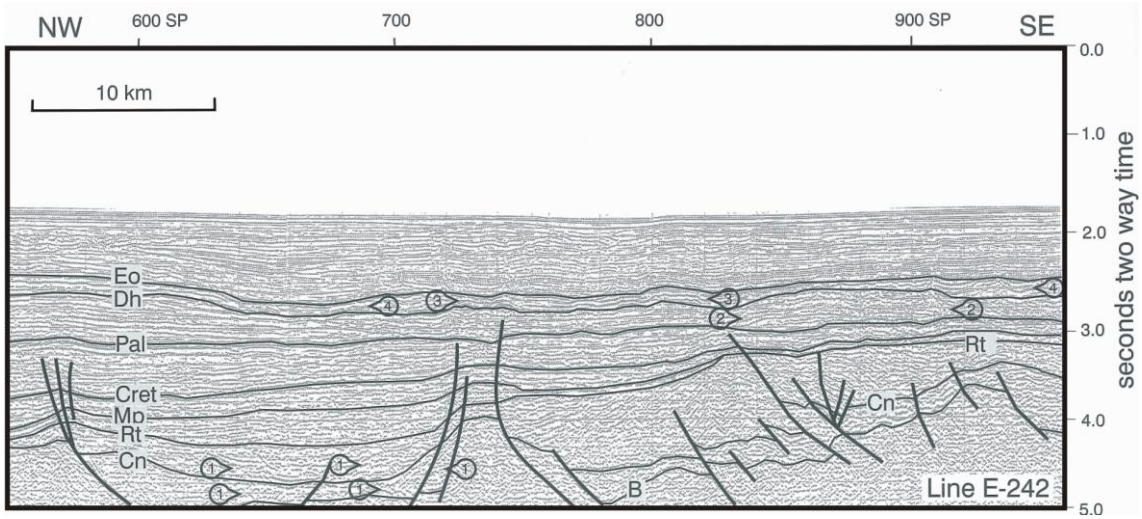

Figure 5.2: Seismic section across the East Flank sub-basin. B = top of basement, Cn = top Clanence Series, Rt = top Raukumara Series, Mp = top Piripauan (top Hoiho Group), Cret = top Cretaceous, Pal = top Paleocene (top Pakaha Group), Dh = top Heretaungan, Eo = top Eocene (top Rakiura Group). 1 = fault scarp fan, 2 = turbidite fan, 3 = mounded seismic facies representing carbonate drift build-up, 4 = late Eocene channeling (From Cook et. al., 1999).

The Rakiura group, which is Teurian to late Oligocene in age (55-28 Ma), is represented by increased carbonate sedimentation, represented by mounded carbonate drift build-up (fig. 5.2). A progressive westward stepping of the shoreline along the western edge of the Great South Basin occurred at this time (Beggs, 1993). Thermal subsidence resulted in the total flooding of the basin and sediment source area during the late Eocene to early Oligocene. However, Beggs (1993), attributed some of the subsidence to the initiation of the late Cenozoic plate boundary into New Zealand.

Finally the Penrod group, a thin veneer of mainly carbonate sediments deposited during a compressional regime from the middle of the Oligocene to present. The drilling returns from this sequence are poor (Beggs, 1993), however, figure 5.2 shows extensive late Eocene channeling. These groups will be referred to during the following sections.

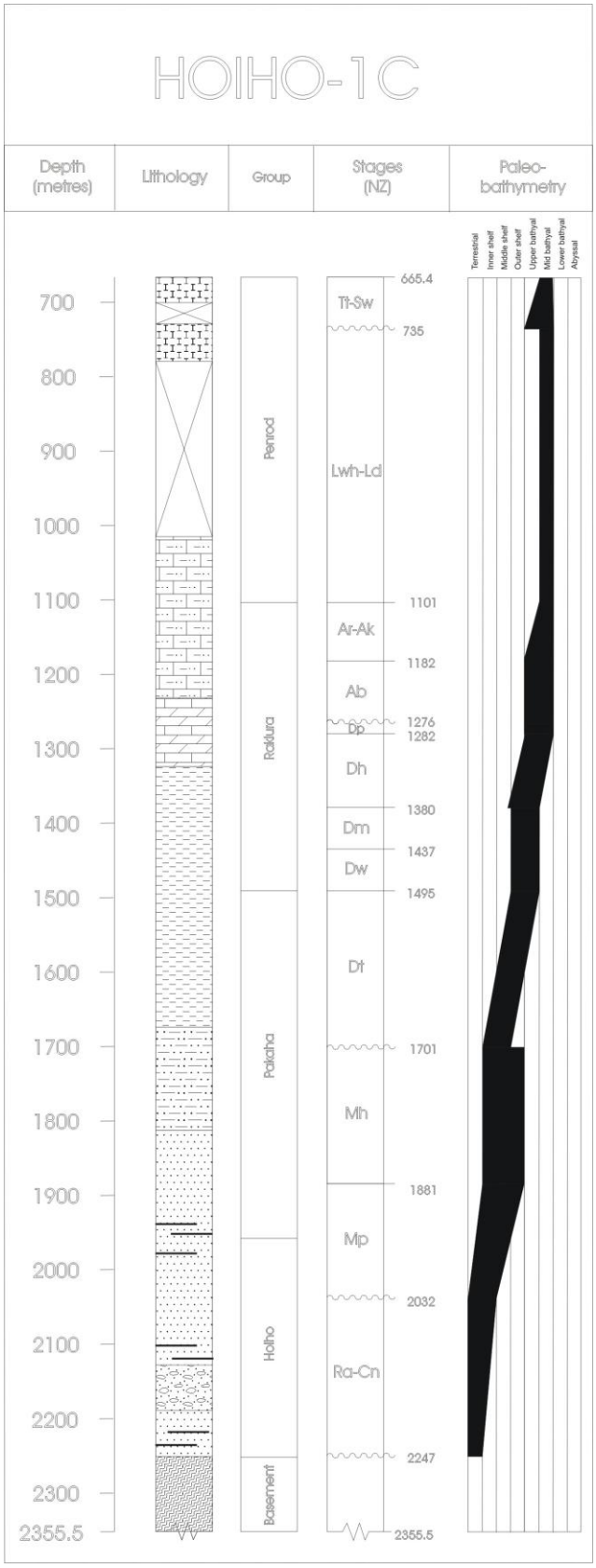

Figure 5.3: Stratigraphic column for Hoiho-1C, typical of the Great South Basin, New Zealand.

5. 3: LOCATION OF WELLS

Well	Lat/Long	Date spudded
Hoiho-1C	49° 36’ 54.5” S 169° 37’ 22.1” E	1978
Kawau-1	48° 55’ 44.34” S 169° 06’ 04.08” E	1977
Pakaha-1	48° 14’ 56.53” S 169° 32’ 58.19” E	1977
Rakiura-1	48° 39’ 52.53” S 168° 08’ 46.54” E	1983
Tara-1	47° 19’ 06.07” S 169° 10’ 06.32” E	1978
Toroa-1	47° 26’ 46” S 169° 29’ 15” E	1976

Table 5.1: Location and age of Great South Basin petroleum wells used for this study

5. 4: QUALITY OF DATA FROM WELLS

The information used in this section is based on data published in the individual well completion reports. The fossils were dated and paleo-environments estimated based on paleontology, palynology and to a lesser extent electrical logging and matching to the general Great South Basin stratigraphic sequence. In the Toroa-1 well report, the oldest well used here, the biostratigrapher states that there are a number of conflicts between the different data sources, and therefore a large error in dating and depth should be assumed. The age of the data (i.e.: > 90 Ma) suggests there are likely to be dating errors built into the age estimations. There is also likely to be age differences between the wells drilled in the 70’s and those from the 80’s, due to a revision of the International and New Zealand timescales in 1982. With the exception of Toroa-1, all wells were drilled to basement.

5. 5: RESULTS

The geohistory of the Great South Basin is summarised in figure 5.4. Figures 5.5 , and 5.6 show the results from the individual wells located within the Great South Basin.

5. 5. 1: Kawau-1A

In this study Kawau-1A (Fig. 5.5) is the well with the oldest preserved sediments. Subsidence and accumulation appears to have begun during the Motuan (103-100 Ma). Initially basin development was slow. Rates picked up during the mid Cretaceous. By the end of the mid Cretaceous the rates of deposition and subsidence had returned to 11 $m.Myr^{-1}$ and 5 $m.Myr^{-1}$ respectively, before an unconformity led to the removal of rocks pertaining to earliest late Cretaceous. Rates had once more slowed by the close of the Cretaceous. The Paleocene and early to mid Eocene are characterized by higher rate of sediment accumulation and subsidence. Once more sedimentation rates dropped during mid Eocene to mid Miocene. Shallowing of water depth during the mid Miocene was accompanied by a sudden increase in both sedimentation and subsidence with rates of sedimentation reaching rates of 306 $m.r^{-1}$ and subsidence of 133 $m.Myr^{-1}$.

An unconformity of the period representing thermal subsidence means it is impossible to calculate a β value at Kawau-1.

6. 5. 2: Pakaha-1

Curves from this well show a similar shape to Kawau-1A (Fig. 5.5), reflecting their position in the Kawau sub-basin. Sediment accumulation at Pakaha-1 seem to begin during the Haumurian (84-65 Ma), approximately 30 Myr after it began at Kawau-1A. Despite this time lag the curves shows the same features, however sedimentation and subsidence rate are slightly higher at Pakaha-1. This is most apparent during the mid Eocene, where Pakaha-1 subsides considerably faster, while sedimentation remains only slightly faster. The late Eocene uplift seen in Kawau-1A occurs 7 Myr earlier in Pakaha-1. Unlike Kawau-1A, Pakaha-1 shows bathymetric deepening from the Miocene, however this is likely due to a lack of data in the Neogene.

Assuming a minimum of 660m tectonic subsidence between 65 and 49 Ma, results in a minimum β value of 5, an unreasonably high value, the implications of which will be discussed further in this chapter.

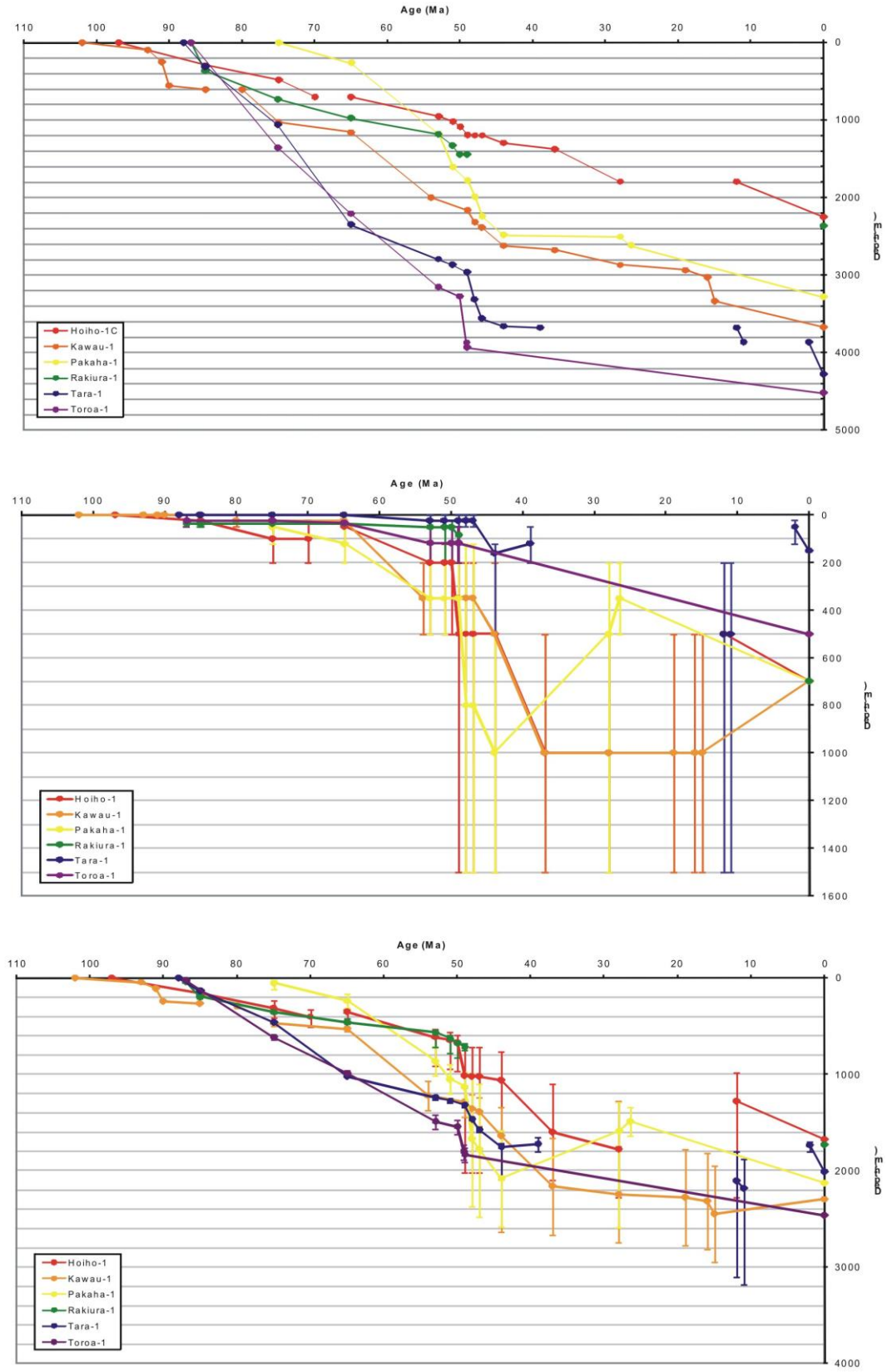

Figure 5. 4: Geohistory plots for the Great South Basin.

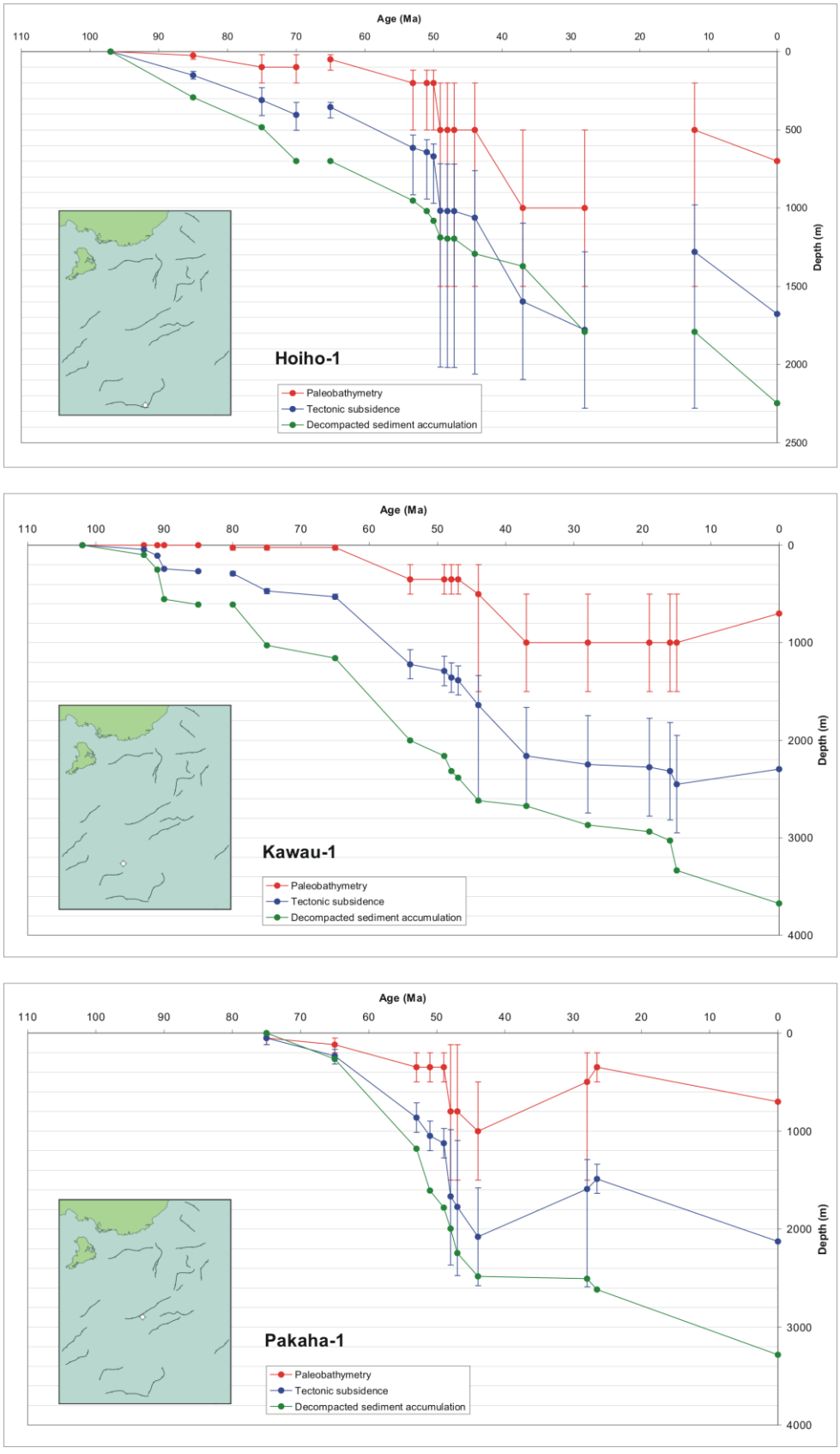

Figure 5.5: Geohistory plots for Hoiho-1C, Kawau-1, and Pahaka-1, Great South Basin.

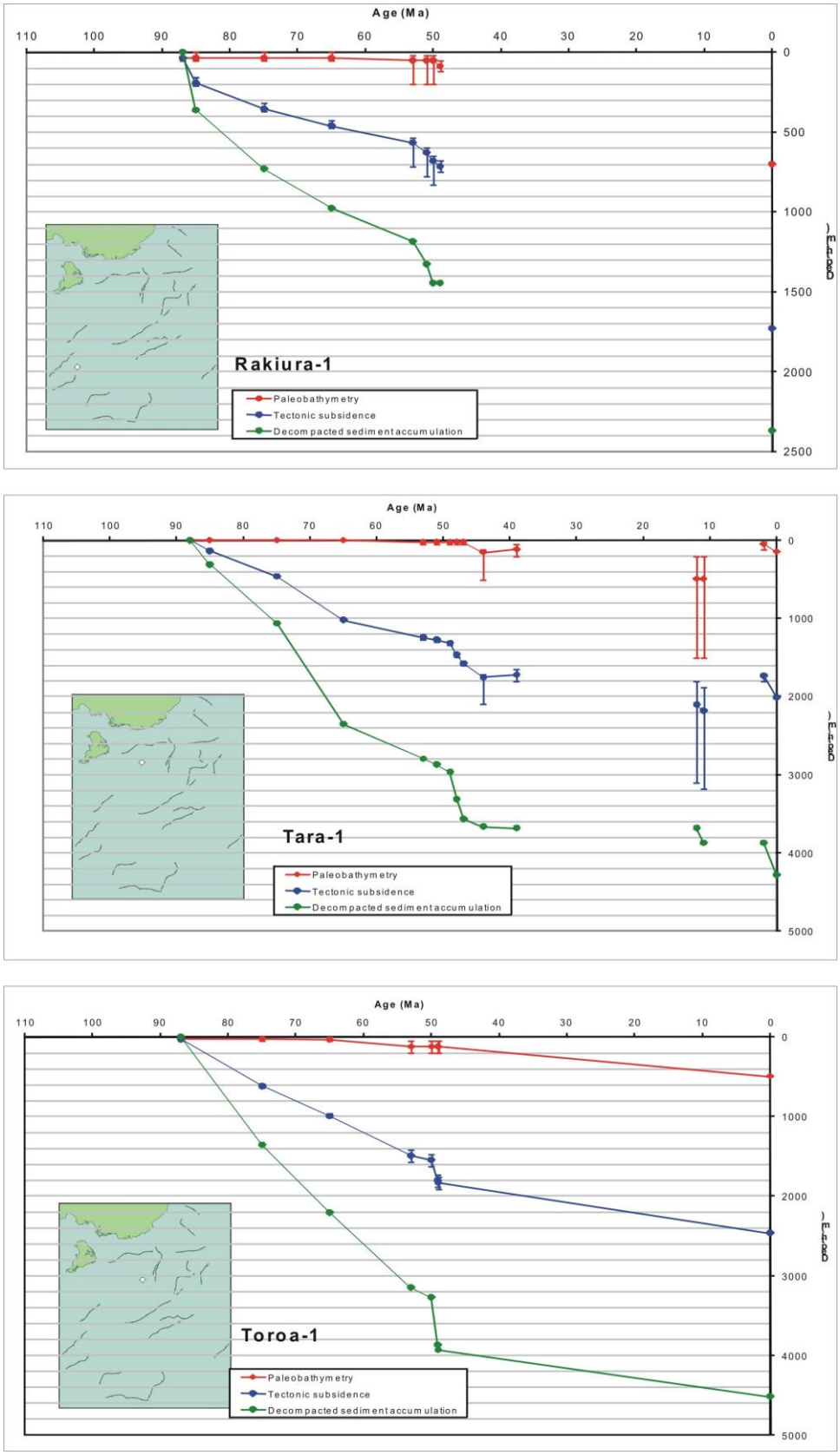

Figure 5.6: Geohistory plots for Rakiura-1, Tara-1 and Toroa-1, Great South Basin.

5. 5. 3: Toroa-1

The sedimentary record began during the Piripauan (87-84 Ma) at this location (Fig. 5.6). Both subsidence and sediment accumulation were rapid until the Eocene, with rates ranging from 79 to 113 m.Myr^{-1} of deposition, and 37 to 49 m.Myr^{-1} of subsidence. At the beginning of the Eocene a short period of deceleration was immediately followed by extreme deposition and subsidence, with rates of 663 m.Myr^{-1} of sedimentation and 288 m.Myr^{-1} of subsidence. A lack of returns during drilling means the data for this well ends during the Eocene.

Even using the most conservative subsidence values, β values range from 5 to 7, and are unreasonably high.

5. 5. 4: Tara-1

Due to the central location of both Tara-1 (Fig. 5.6) and Toroa-1 the curves are very similar. Like Toroa-1, Tara-1 shows rapid sedimentation and subsidence from the beginning of the record in the Teratan (89-87 Ma). Rates of both sedimentation and subsidence are similar during the Cretaceous, however basin development at Tara-1 quickens with respect to Toroa-1 during latest Cretaceous, before slowing during the Paleocene. The sudden increase in sedimentation and subsidence is seen in Tara-1 as well, and is followed by a period of uplift during the middle Eocene. This uplift event which is also seen in Kawau-1A and Pakaha-1 is slower, at a rate of 6 m.Myr^{-1}, and appears to last for a shorter duration, however an unconformity does result in the removal of sediment representing late Eocene to middle Miocene. A brief period of rapid deposition and subsidence is recorded after the unconformity, which is in turn followed by another unconformity. A decrease in water depth during this second interruption suggests a second period of uplift.

Assuming a minimum of 227 m subsidence and a maximum of 277 m between 65 and 51 Ma, a β value of 2.0 ± 0.1 was calculated.

5. 5. 5: Rakiura-1

Deposition in this well began during the Teratan (89-87 Ma). The curves (Fig. 5.6) show an initial pulse of rapid sedimentation and subsidence during the mid Cretaceous, at rates of 106 m.Myr^{-1} and 46 m.Myr^{-1} respectively. Rapid sedimentation at this time is only seen in the wells near the basin center, this may be the result of poor dating of sediment. Approximately 30 Myr of slow, steady basin development followed this event. As seen in all other wells, Rakiura-1 shows a period of acceleration in both sediment accumulation and subsidence during the early to mid Eocene. Once again a lack of data returned during drilling led to a termination of the record immediately following this event, perhaps erasing the decrease in water depth seen in Hoiho-1C.

A β value of 1.55 ± 0.25 was calculated, based on a minimum of 330 m of tectonic subsidence and a maximum of 560 m between 85 and 53 Ma.

5. 5. 6: Hoiho-1C

A similar location on the outer edge of the basin, means that the curves (Fig. 5.5) produced for Hoiho-1C mirror those of Rakiura-1. As mentioned above, this well does not show the pulse of sedimentation and subsidence seen at Rakiura-1. The sedimentary record begins during the Ngaterian (100-95 Ma), and shows slow subsidence and sedimentation until disrupted by an unconformity in the late Cretaceous. Changes in water depth over this period suggest uplift at a rate of 10 m.Myr^{-1}. Deposition and subsidence resume after this break, with rates slightly faster than those seen in Rakiura-1. Once again the early Eocene sees a brief period of rapid subsidence, however sedimentation rates show much less change. This event is followed by a short period of very slow sedimentation and subsidence, which is in turn followed by a return to rapid subsidence at a rate of between 20 to 76 m.Myr^{-1}, though little change in sedimentation rates. An unconformity has deleted the record from late Oligocene to middle Miocene, during which time uplift occurred, at an average rate of 31 m.Myr^{-1}.

An unconformity over the period of McKenzie-style thermal decay prevents the calculation of a β value at Hoiho-1C.

5. 6: INTERPRETATION AND DISCUSSION

Figure 5.7 shows the tectonic subsidence curve which is characteristic of the Great South Basin. Thermal subsidence follows the break up of Gondwana during the Cretaceous period. Rifting in the Emerald Basin at 51 ± 2 Ma resulted in an increase in subsidence, following which thermal subsidence continued. Similar to the Canterbury Basin, an increase in subsidence is seen from 6 Ma, perhaps related to climatic changes occurring at the time.

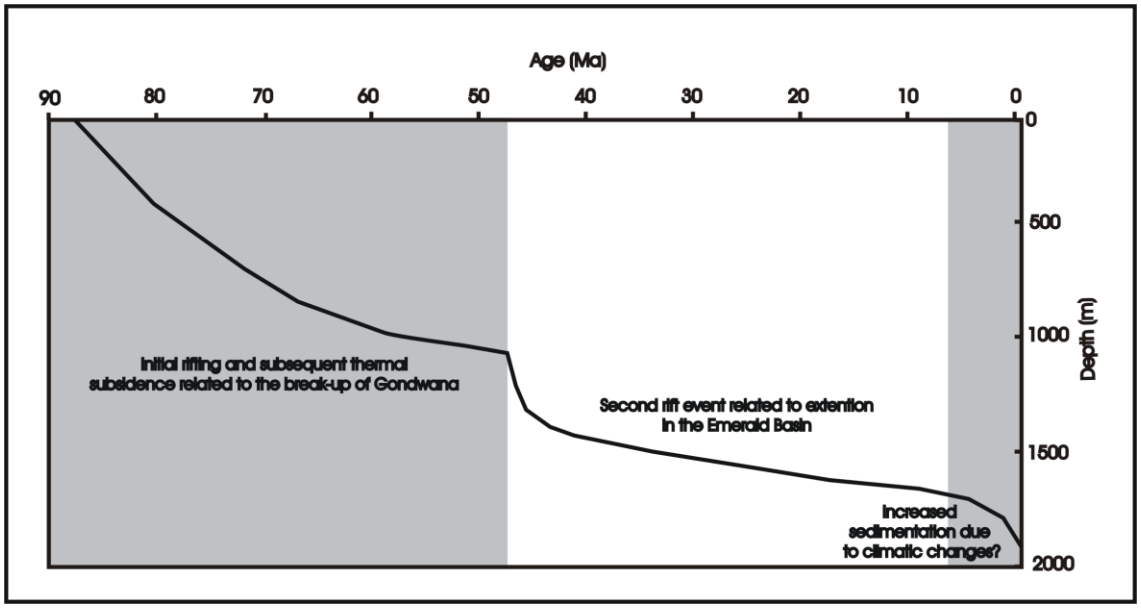

Figure 5.7: Characteristic tectonic subsidence curve for the Great South Basin.

5. 6. 1: Mid to late Cretaceous

During the Cretaceous the tectonics of the Great South Basin changed from subduction to extension due to the breakup of Gondwana. Rifting took place, forming the Tasman Sea, and separating the Lord Howe Rise and East Antarctica from Australia. This resulted in a series of NE to E trending fault controlled grabens and half-grabens, parallel to the rifting axis between New Zealand and Antarctica (Laird, 1981).

The Raukumaran (95-87 Ma) saw rapid basin development, with the sedimentation and subsidence beginning at the southern three wells. The curves show that sedimentation began later at the Central sub-basin (Tara-1 and Toroa-1) than at Pakaha-1. During this period the Pakaha Horst was uplifted and eroded (Cook, et. al., 1999), explaining why the sedimentary record in Pakaha does not begin until late Cretaceous. The onset of sedimentation and subsidence was rapid (191 $m.Myr^{-1}$ and 83 $m.Myr^{-1}$ respectively) at Rakiura-1, this maybe due to an overestimated decompaction correction, or more likely, due to a dating error.

As there was no longer physical barriers between the individual depocenters (Cook, et. al., 1999), the Piriauan (87-84 Ma) was a time of basin-wide subsidence, with subsidence beginning at Pahaka-1, Tara-1 and Toroa-1. As faulting only cuts the base of the Pakaha group, this subsidence was probably related, primarily, to thermal changes in the crust.

An unconformity is noted in Hoiho-1C between 75 and 70 Ma. Due to the mid to outer shelf environment it is likely that this is the result of reworking by currents. An unconformity is also noted in the Kawau-1 record (85-80 Ma). During this time the area was emergent, so subaerial erosion is the likely cause. The Kawau-1 sediments also recorded two pulses of increased sedimentation and subsidence, the first period starting at 93 Ma, and the second at 80 Ma. It is possible that these events were caused by changes in plate motion, related to the break-up of Gondwana. However, there is no evidence for these changes in the other wells studied and they are not noted by Cook et. al. (1999). They are therefore, likely due to dating or decompaction errors.

With the exception of Hoiho-1C, the paleobathymetry of the wells remained stable during the Cretaceous period. Hoiho-1C, however, showed a increasing water-depth from 97 Ma until 75 Ma. It remained steady until 70 Ma, and was followed by uplift, coinciding with the previously mentioned unconformity.

By 79 Ma the Emerald fracture zone had formed (Cook, et. al., 1999). This zone of transform faulting formed to accommodate a major offset between the Lord Howe Rise and Campbell Plateau spreading centers, which developed during rifting.

5. 6. 2: Paleocene

As seen throughout the majority of New Zealand's sedimentary basins, the Paleocene was a period of tectonic quiescence. However, numerous tectonic boundaries were still active. The northern section of the Emerald Fracture Zone may have accommodated strike-slip motion during this period, joining the Tasman and Pacific spreading centers south of New Zealand, resulting in minor rifting and deformation in the western South Island (Laird, 1994). Marks and Stock (1997) suggested that plate reconstructions required movement along a boundary in the Ross Embayment, active prior to 53 Ma. Sea floor spreading in the south-east Indian Ocean is also likely to have influence the Tasman and Pacific spreading centers near the Emerald Fracture Zone (Gaina et. al., 1998).

Paleobathymetry shows a period of basin wide transgression beginning at ~65 Ma, much earlier than shown by other studies (Baxter 1993; Cook et. al. 1999), maybe because of a lack of data over this period. Cook et. al. (1999), also show this increase in water depth, but their data suggest that it began 8 to 11 Myr later. It is important to note that, while the data presented here may not have the resolution to show the exact timing of the event, in almost all cases the data are within the error estimations made by Cook et. al. (1999).

The general shape of the geohistory plots for the wells investigated suggests that for the Cretaceous and Paleocene periods the basin represents a stuttering passive margin, with decreasing sedimentation and subsidence rates related to thermal relaxation of the crust.

5. 6. 3: Eocene

It is evident that the Eocene was a period of renewed tectonism, and an event during this time stands out on the geohistory plots. During this time a new plate boundary propagated north from the southeast Indian Ridge, up the Emerald Fracture Zone (Fig. 5.8), before stepping to the right, and following the western margin of the Campbell Plateau (Sutherland, 1995; Wood et. al., 1996).

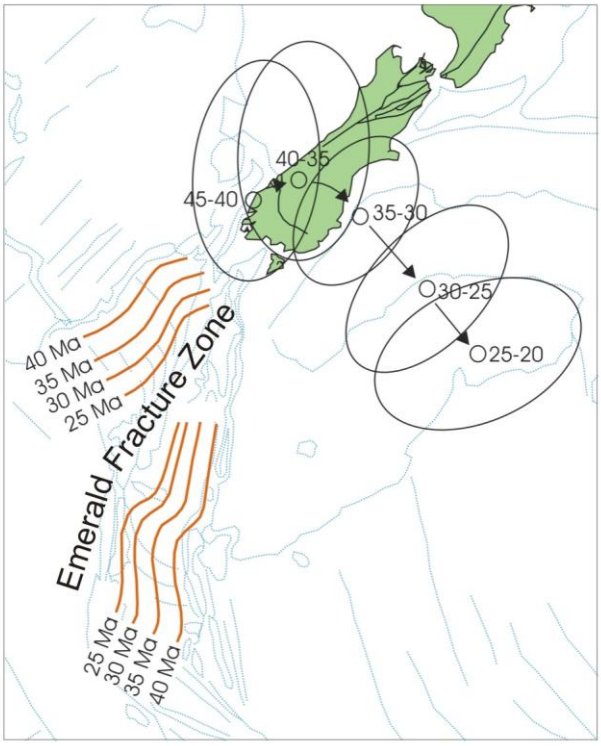

Figure: 5.8: Movement of the Australia-Pacific instantaneous pole with time (GEOS-NZ results 45-20 Ma; GEOS-3P results 20-0 Ma) and estimated isochrones for ocean crust south of New Zealand. (From Sutherland, 1995).

An extrapolation of sea floor spreading rates suggests that the oldest sea floor is 46 to 42 Ma (Wood et. al, 1996), however data from these wells suggests that crustal thinning was beginning to be felt earlier in the Great South Basin, at 51 ± 2 Ma. It is at this time that all wells show an increase in sedimentation and subsidence, with exponential decay, characteristic of a passive rifting event (Fig. 2.13).

Cook et. al (1999) proposed that this change in tectonics resulted from changes in drainage. They suggested that a major drainage system that previously was depositing vast amounts of sediment in the Great South Basin, as seen during the early Eocene, was rerouted to the developing Solander Basin and Trough in Western Southland. This perhaps explains the sudden decrease in sedimentation seen in all wells during the late Eocene. For example, an unconformity appears in the record at Tara-1, starting at 39

Ma, this may be due to the rerouting of drainage systems, or due to subaerial erosion, related to a global drop in sea level.

Carter (1988) also noted Eocene to Oligocene tilting along the northwest margin of the basin. Although the exact date of inception is controversial, it is probable that the early development of the Toroa Dome and Tara Anticline began during this time. Tara-1 (44-39 Ma) and Pahaka-1 (45-29 Ma) show uplift during the late Eocene. It is probable that the uplift at Pahaka-1 occurred at a faster rate, over a shorter time period, however, a lack of data prevent better resolution of the event. Cook et. al. (1999) show this uplift event occurring at Pahaka-1 from 36-33 Ma, and also an event at Takapu-1 from 36-24 Ma. These compressional features are almost certainly the result of stresses related to motion on the developing Alpine Fault.

It appears that water depth has been over estimated during the Eocene (44-37 Ma) at Hoiho-1C. The result is that tectonic subsidence is an order of magnitude to large, clearly visible in the geohistory plot (Fig. 5.5). While probably over-estimated, this event cannot be ignored, as similar deepening also occurs at Tara-1 and Kawau-1. Occurring at 45 ± 2 Ma, this coincides with the timing of Wood's (1996) proposed crustal failure, and creation of the oldest sea-floor.

5. 6. 4: Oligocene

The tectonic tempo began to increase during the Oligocene. The pole of instantaneous rotation was located close to the South Island during the Oligocene to Miocene (Fig. 5.8). This resulted in a gradual shift from extension to strike-slip motion and local compression, which was manifest in the continuation of the tilting and folding. However, the close proximity of the pole (Fig. 5.8) meant that the rates of displacement were slow (<15 mm/yr) (Cook et. al., 1999). During which time there was reactivation of Cretaceous faults. In the northwest of the basin Carter (1988) noted reverse faulting and folding. Apparent uplift is seen in the three southern-most wells during this time. Localised volcanism was also occurring (Gage, 1957; Ward and Lewis, 1975).

At Hoiho-1C an unconformity breaks the record from 28 to 12 Ma, over which time up to 500 m of uplift appears to have occurred. It is likely that paleobathymetry was over-estimated prior to the hiatus. Cook et. al. (1999) show only 200 m of uplift from 27 to 11 Ma.

During the Oligocene there is little data from Pahaka-1, Rakiura-1 and Toroa-1, primarily due to the sediments being too immature to warrant hydrocarbon exploration. This lack of fossil dating prevents the distinction of events. There is, however, a general trend of continued sedimentation and subsidence. However, Cook et. al. (1999) distinguish a period of uplift over the Oligocene (28-22 Ma) at Toroa-1, but a lack of error bars suggests it is an inference without fossil proof.

5. 6. 5: Miocene

During this period the sea floor spreading to the south of New Zealand became highly oblique, and eventually evolved into oblique convergent strike-slip (Lamarche et. al, 1997). Sutherland (1995) proposes 600 km of strike-slip motion through the South Island since the early Miocene. The component of compression caused continued movement on the reactivated reverse faults. Increased uplift led to an increased sediment supply, and rapid shelf progradation, however strong currents across the Campbell Plateau isolated the southern and eastern parts of the basin from significant amounts of terrigenous sediment. These reworking currents are the likely cause of the periods of non-deposition seen at Hoiho-1C and Tara-1.

A lack of cores returned from Pakaha-1 and Toroa-1 during drilling has resulted in a poor record for the Miocene to Recent. The record from Kawau-1 is more complete, and shows an increase in sedimentation and subsidence from 19 Ma. This suggests uplift on the Alpine Fault (and associated fault systems), was supplying the basin with eroded sediment. A brief period of increased sedimentation and subsidence is also visible between the two unconformities in Tara-1. Between 12 and 11 Ma a sedimentation rate of 188 $m.Myr^{-1}$ occurred, accompanied by subsidence at 82 $m.Myr^{-1}$. At Hoiho-1C, a lack of data mean the rates are averaged. Nevertheless, the rates are elevated over the period from 12 Ma until present, especially if this time period contains

uplift events, as seen in the other southern wells (Kawau-1 and Rakiura-1). This is consistent with events seen in the Canterbury Basin, and with Cande and Stock's (2004) proposal that convergence on the Alpine Fault began at 20 Ma.

5. 6. 6: Pliocene to Recent.

Progressively increasing convergence within the South Island means the Southern Alps are now at their maximum height and extent (Sutherland, 1995). Compression has led to continued faulting and folding in the basin, however sedimentation is still controlled by strong currents. As mentioned above, the sedimentary record is poor during the Pliocene to Recent, however Kawau-1, Rakiura-1 and Tara-1, show uplift during the Pliocene. Tara-1 shows uplift during a period of non-deposition, followed by subsidence from 2 Ma until present. As mentioned earlier, the lack of data mean the geohistory plots only show averaged trends, this is the case for Hoiho-1C, Pahaka-1and Toroa-1.

5. 6. 7: Beta values

As expected, β values increase towards the center of the basin. An unconformity on the basins flanks during the Cretaceous prevents the determination of β values at Hoiho-1C and at Kawau-1. Rakiura-1, located near the edge of the basin has a relatively low value of 1.55 ± 0.25. Pakaha-1, Tara-1 and Toroa-1 located in the basin center show considerably higher values, which have been confirmed by other authors (ie: Cook et. al., 1999). If these values were correct one would expect the crust to be much thinner, and to have subsided considerably more, hence have a lower surface elevation. It is possible that the values at Pakaha-1, Tara-1 and Toroa-1 are overestimated due to an assumption that rifting is instantaneous, an unrealistic assumption. It is also likely that thinning of the crust occurred over an extended period prior to the formation of sea floor interpreted here at 51 ± 2 Ma, interrupting the thermal subsidence related to the initial rifting event.

Cook et. al, (1999) note that the southern wells (Pahaka-1, Kawau-1A, Rakiura-1 and Hoiho-1C) deviate from the classic subsidence curve models, which is confirmed by this study. First, they note that these wells do not show good exponential form; and

second, the magnitude of post-rift subsidence is larger than expected from model curves based on varying stretching factors. They use dynamic topography as a possible explanation. The anomalous subsidence can be rationalized if 400-800 m of uplift occurred during rifting, dieing away in the period following. Figure 5.9 shows the calculated stretching factors if 600 m of uplift is assumed, with values reaching a maximum of 2.5. Gravity profiles (Smith and Sandwell, 1995) across the basin suggest that crustal thickness ranges from between 15 km in the center of the basin to 25-30 km near present day coastline. Based on the β value of 2.5 at the centre of the basin, the original crustal thickness was ~38 km.

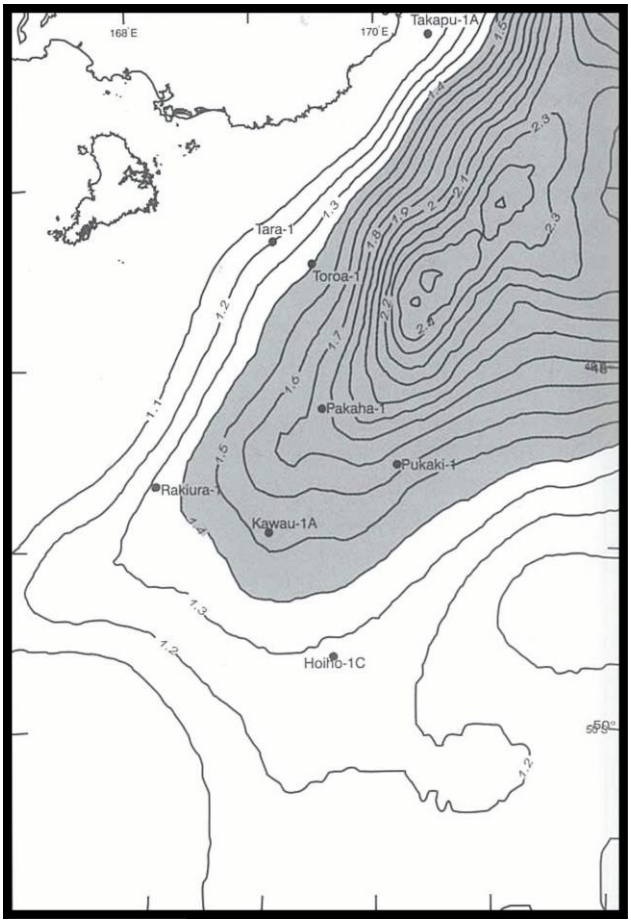

Figure 5.9: Map showing calculated stretching factors assuming 600 m of topographic uplift associated with rifting (From Cook et. al., 1999**).**

5. 7: CONCLUSIONS

- Rifting began in the southern wells (Hoiho-1C and Kawau-1) between 100-90 Ma. Rifting at the other wells began at 90-80 Ma, except at Pakaha-1, where the position on the Pakaha Horst prevented deposition until 75 Ma.
- At all wells, thermal subsidence followed rifting until 51 ± 2 Ma, where increased sedimentation and subsidence suggests a second rifting event. This is likely related to the plate boundary forming to the south of New Zealand
- From the Oligocene, uplift suggests the wells are affected by the formation of the plate boundary, with assumed distributed surface uplift and exhumation.
- An increase in sedimentation and subsidence seen at Kawau-1, Tara-1 and possibly Hoiho-1 suggests convergence on the Alpine Fault was underway by 19 Ma, supporting Cande and Stock (2004), and evidence from the Canterbury Basin.
- Using the McKenzie (1978) method, β values are overestimated in the center of the basin, due to assumptions in the subsidence model, and the effects of a second rifting event.
- Assuming 600 m of dynamic topographic uplift associated with rifting, a maximum β value of 2.5 was calculated for the basin center, meaning the crustal thickness prior to rifting was ~38 km.

CHAPTER 6: WESTERN SOUTHLAND BASINS

6. 1: LOCATION

The region discussed in the following chapter is comprised of a number of small, fault-controlled basins (Fig 6.1). These basins are adjacent to the Fiordland Complex, a fault-bound block of metamorphic and plutonic rock of Paleozoic and Mesozoic age (Norris and Turnbull, 1993). To the east of the crystalline block, located onshore, is the Te Anau and Waiau Basins, and Solander Basin offshore. The Balleny Basin lies offshore to the south. While separated from the plate boundary by the Fiordland Complex, the stresses of the Alpine fault, and Hollyford and Moonlight Systems have resulted in uplift, affecting the evolution of the basins (Carter and Norris, 1976).

6. 2: STRATIGRAPHY

Extension of the New Zealand plateau during the Cretaceous resulted in the separation of Gondwana, but also the formation of a series of fault-controlled basins in western Southland (Fig 6.2). The subaerial environment of the region in this time meant little accommodation space was available for sediment deposition, however, the Puysegur Group was laid down during the Cretaceous period. This group consists of non-marine conglomerates overlaid by interbedded sandstones and mudstones, interpreted as river channel-flood plain deposits, grading up into a lacustrine fan delta complex (Norris and Turnbull, 1993). The Puysegur Group outcrops in few places, namely the Balleny and Puysegur Basins, likely because of erosion during the Paleocene and Eocene (Turnbull and Uruski, 1993).

A second period of deposition occurred during the latest Cretaceous. These sediments are known as the Ohai Group, and are geographically isolated from the Puysegur Group. This unit also has few outcrop locations, but has been shown to continue at depth below the Waiau Basin. This unit represents a fluvial system, consisting of conglomerate with minor sand and mudstone interbeds, which is overlain by crossbedded sandstone and mudstone, containing a number of bituminous coal seams (Norris and Turnbull, 1993).

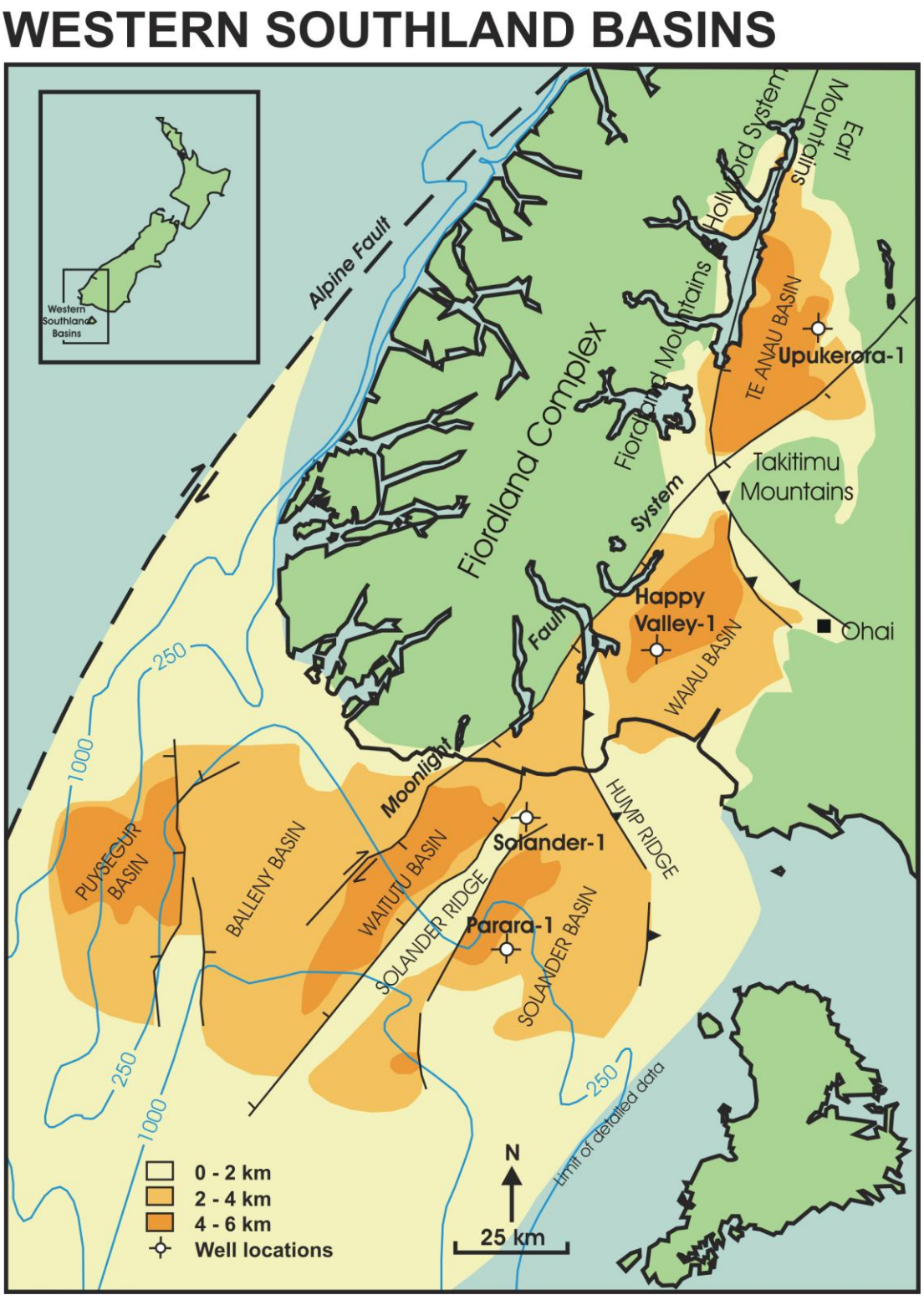

Figure 6. 1: Map of the Western Southland Basins, showing location of wells, sediment thickness and major faults, including the Alpine Fault and the Moonlight Fault System. (from Explore New Zealand Petroleum 2003, Ministry of Economic Development, Crown Minerals, 2003).

LINE B209

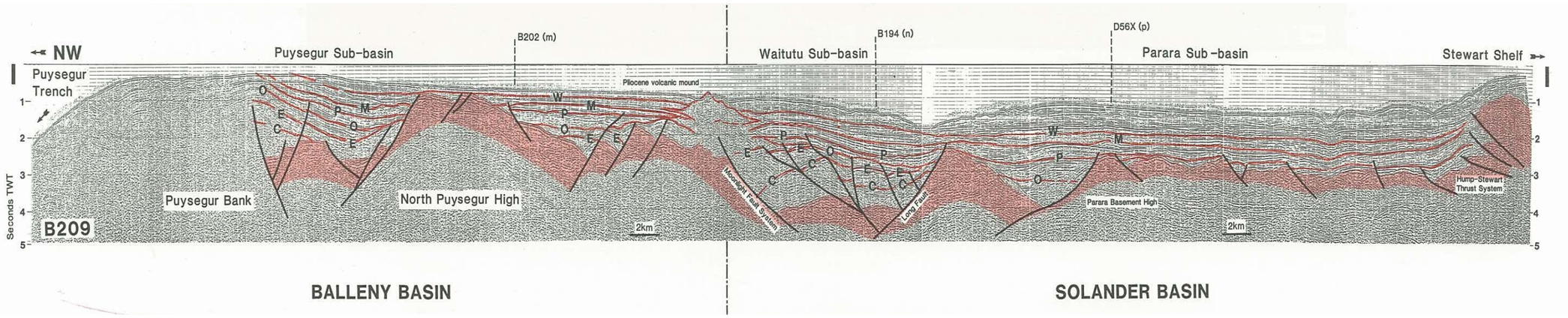

Figure 6. 2: Seismic section across offshore Western Southland, with interpretation by Turnbull and Uruski et. al (1993)

Figure shows the formation of Cretaceous sub-basins.
W - Top Waipipian, M - Top Miocene, P - Top Pareora Series (Early Miocene),
O - Top Oligocene, E - Top Eocene, C - Top Cretaceous, Basement is shaded red.

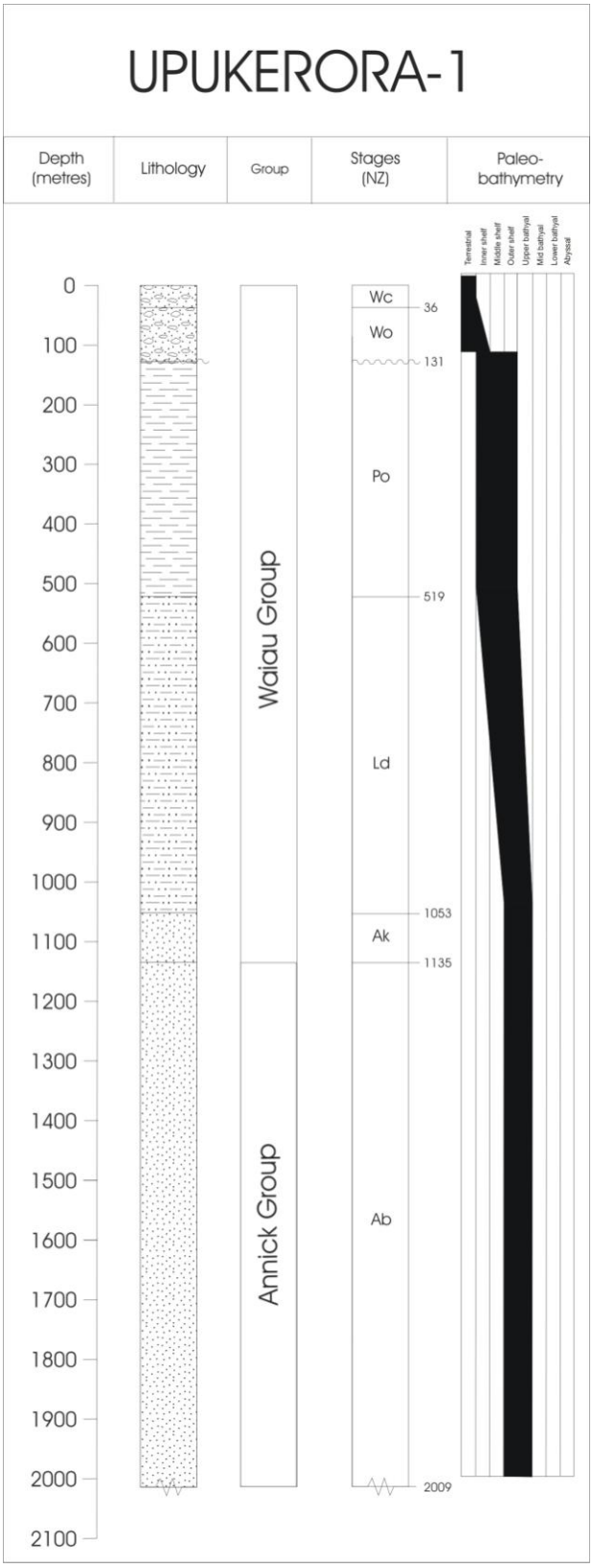

Figure 6.3: Stratigraphic column of Upukerora-1, located in the Te Anau Basin, typical of deposits in Western Southland, New Zealand.

An erosional unconformity separates the Ohai Group from the late Eocene sediments of the Balleny, Nightcaps, and Annick Groups (Fig. 6.3). No rocks of Paleocene to early Eocene are known in the region.

The Balleny Group, restricted to the Balleny Basin has been poorly studied, due to its offshore location. However, seismic data suggests that by the close of the Miocene the deposition of the Balleny Group resulted in the growth of the basin, covering a number of pre-existing highs (Turnbull and Uruski, 1993).

The Nightcaps group, restricted to the Waiau Basin, is of late Eocene to early Oligocene. The unit represents a range of environments, ranging from a braided sandy fluvial system near Ohai, to back-swamp and flood plains, and lacustrine to lagoonal. Such a variety of depositional environments has resulted in a number of litholgies, however, sandstone dominates with conglomerates, mudstones, carbonaceous mudstones, oil shales and coal seams all appearing in places (Turnbull et. al. 1989).

The Annick Group appears in the Te Anau Basin and in the area to the north. The group consists of a basal marine conglomerate, which grades up into a sand and mudstone. This is then overlain by a crossbedded sandstone, containing minor conglomerates, carbonaceous mudstone and thin coal seams. This unit is thought to have accumulated in a rapidly subsiding, tectonically active marine basin (Turnbull et. al., 1989)

The final group deposited in the region is the Waiau Group. In the Waiau Basin the group was deposited from earliest Oligocene to late Pliocene, while in the Te Anau Basin deposition took place from early Oligocene to late Miocene. The laterally extensive unit has been described as a ‘background’ mudstone, divided by numerous small areas of other lithologies (Turnbull et. al., 1989). Deposited in a fault controlled basinal environment, with submarine fan deposits around the margins, the basin shows evidence of shallowing with time (Turnbull et. al., 1989).

6. 3: LOCATION OF WELLS

Well	Lat / Long	Date spudded
Happy Valley-1C	167° 29’ 18.35” E 46° 01’ 05.91” S	1988
Parara-1	167° 10’19.14” E 46° 37’ 29.17” S	1976
Solander-1	167° 09’ 12.49” E 46° 21’ 14.68” S	1986
Upukerora-1	167° 55’ 34.0” E 45° 21’ 22.0” S	1988

Table 6.1: Location and the year of drilling for the Western Southland Basins petroleum wells used in this study. Solander-1 and Parara-1 are located offshore, while Happy Valley-1 and Upukerora-1 are onshore.

6. 4: QUALITY OF DATA

The data used in this region is taken from the individual well completion reports, and based on foraminifera presence and abundance. Basement was reached in Parara-1 and Solander-1, but not in Happy Valley-1C or Upukerora-1. The data from Parara-1 is over ten years older than the other wells, and therefore may show variation due to reworking of the geological timescale.

6. 5: RESULTS

The geohistory of the Western Southland Basins is summarised in figure 6.4. Figures 6.5 and 6.6 show the results from the individual wells located within the Western Southland region.

6. 5. 1: Happy Valley-1C

The sedimentary record at this location begun in the Bortonian (43 Ma) series (Fig. 6.5). Deposition was initially very rapid, reaching accumulation rates of 280 m.Myr^{-1}. Rapid subsidence appears to accompany the rapid deposition. It is possible however, that this feature is the result of poor dating, leading to the steepening of the curves. By late Eocene these rates dropped considerably. Basin development continued until middle Miocene. At this point sedimentation slowed to 11 m.Myr^{-1}, while subsidence slowed to 5 m.Myr^{-1}.

Using a minimum of 110 m of tectonic subsidence and a maximum of 250 m, between 27 and 19 Ma, a β value of 1.6 ± 0.2 was calculated.

6. 5. 2: Parara-1

Parara-1 has the longest sedimentary record of the wells studied in this basin, with sedimentation beginning in the Haumurian (84 Ma) (Fig. 6.5). Deposition and subsidence was reasonably steady during the late Cretaceous to early Miocene, with an acceleration of sediment deposition during the Oligocene. Rates increased during the Miocene. This was followed by a period of slower basin development during the late Miocene, which in turn was followed by another pulse lasting from the Pliocene to Recent.

Assuming thermal subsidence from 65 to 28 Ma, with a minimum of 465 m, and a maximum of 545 m, the β value calculated was 1.55 ± 0.05.

6. 5. 3: Solander-1

The curves representing this area are similar to those of Parara-1, reflecting the position of both wells in the Solander sub-basin (Fig. 6.5). Deposition begins much later in Solander-1, with the oldest rocks being of Kaiatan age (37 Ma). Like Parara-1,

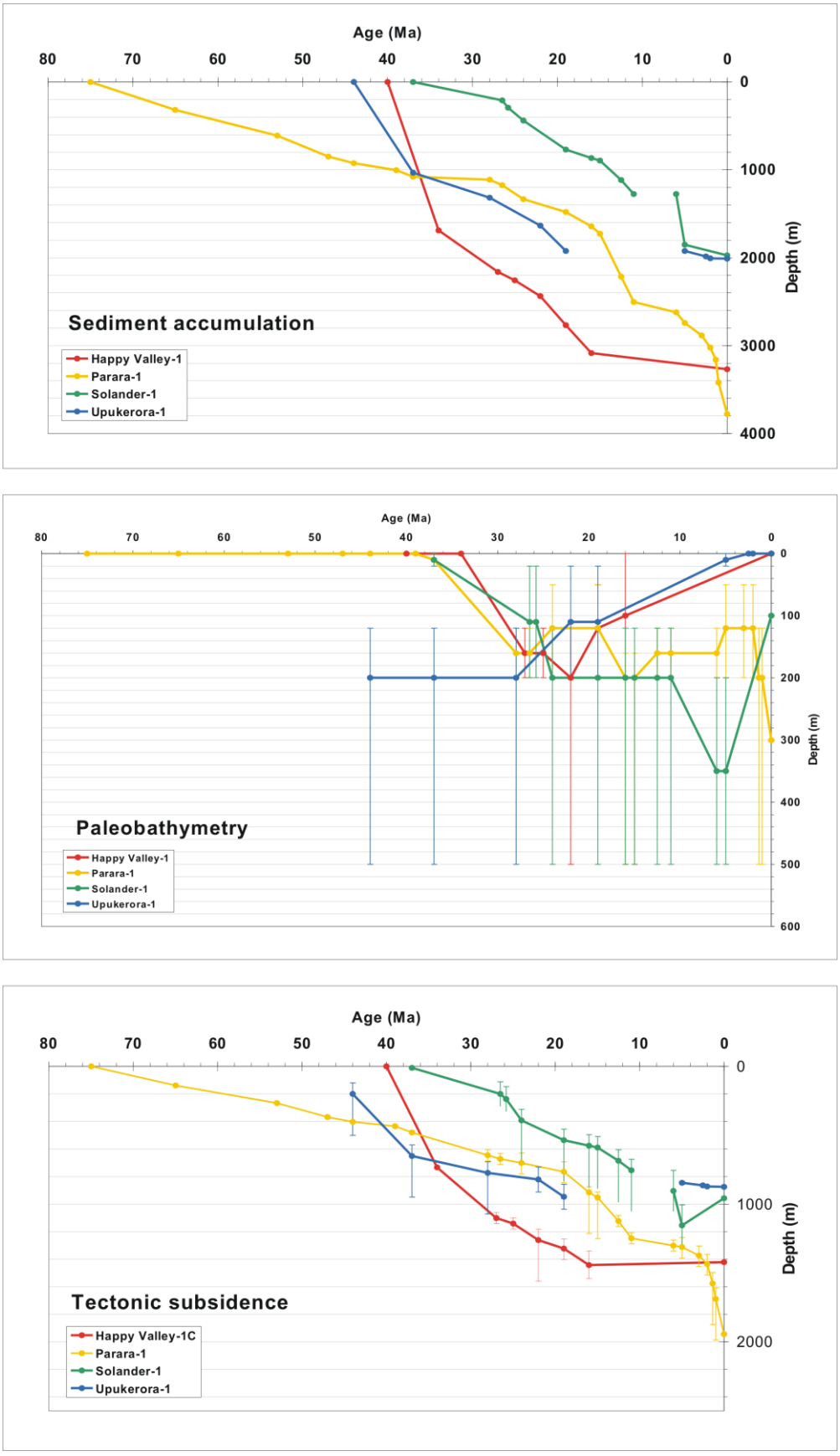

Figure 6.4: Geohistory plots for the wells located in the Western Southland Basins.

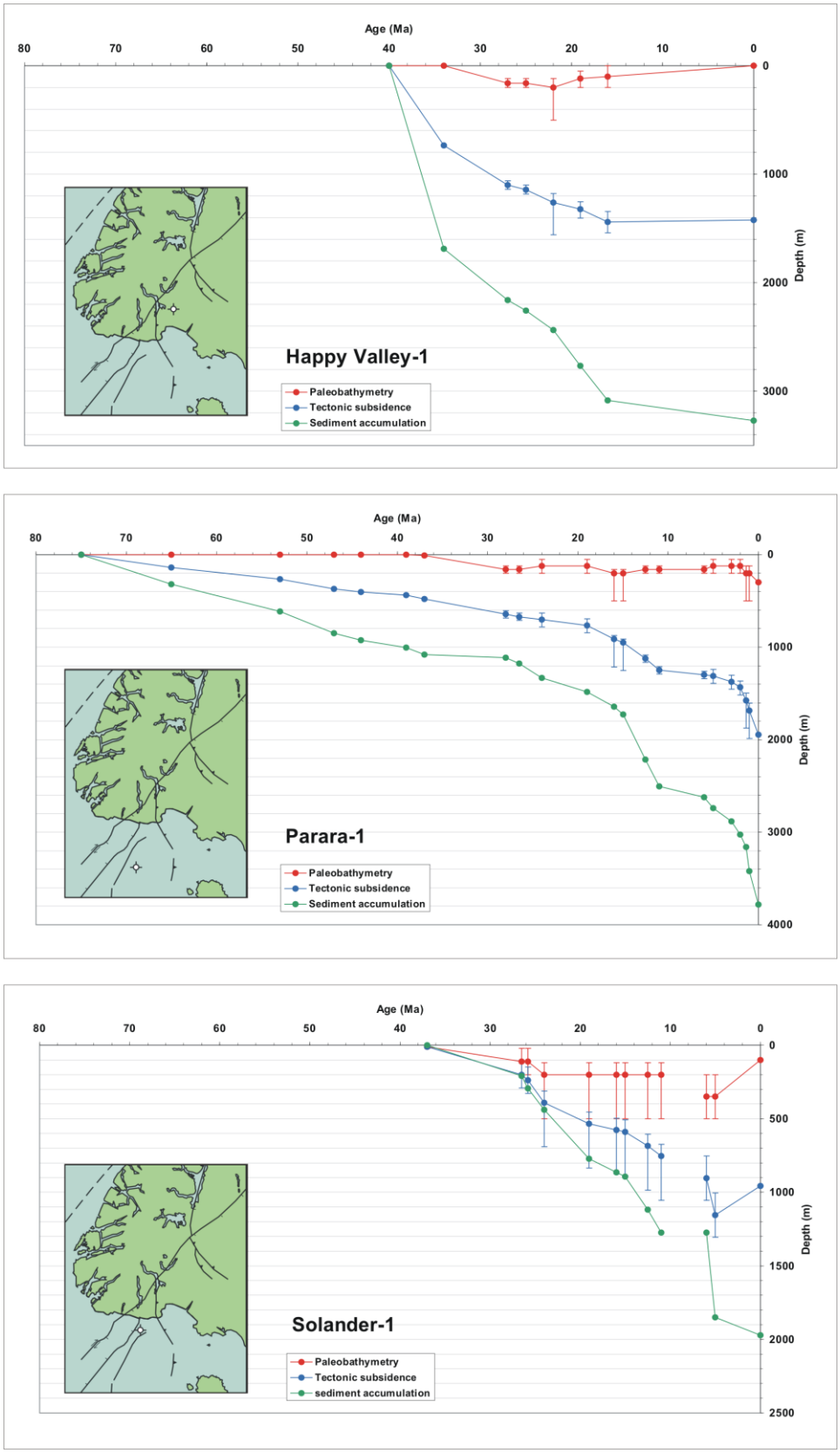

Figure 6.5: Geohistory Plots for Happy Valley-1, Parara-1 and Solander, Western Southland Basins.

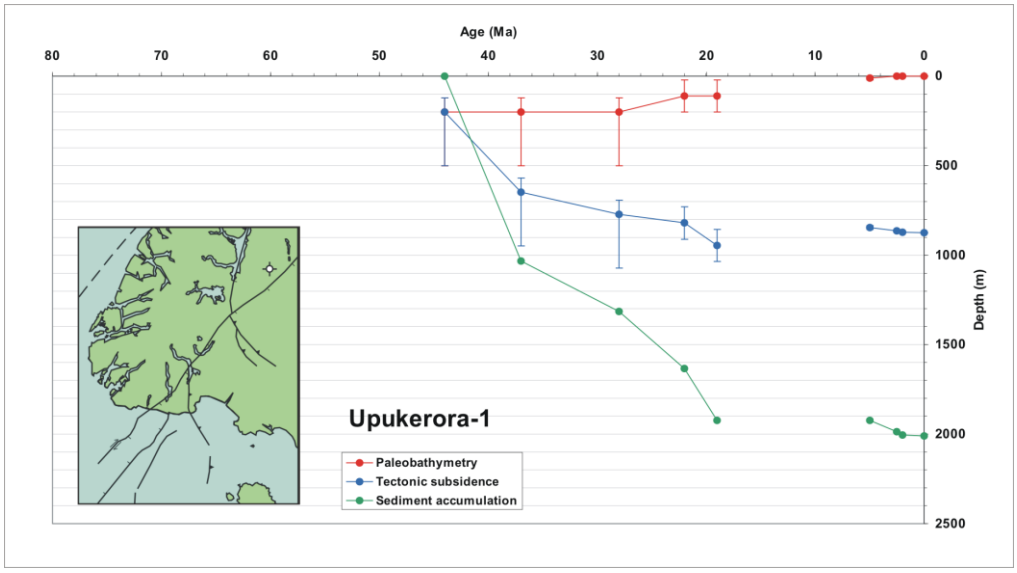

Figure 6.6: Geohistory Plot for Upukerora-1, Western Southland Basins.

deposition and subsidence were initially slow, however rates were slightly faster at Solander-1. The Miocene sees the same acceleration in rates seen in Parara-1, before a deceleration, which appears to begin 6 Ma later, however an unconformity removed part of the late Miocene, perhaps eliminating the signal. Solander-1 does not show the increase in sedimentation and subsidence seen in Parara-1 during the Pliocene to Recent.

Sediment which accumulated at Solander-1 post dates extension, instead representing a period of compression. For this reason a β value is not calculated.

6. 5. 4: Upukerora-1

Deposition at Upukerora-1 began in the Porangan (46 Ma), slightly earlier than at Happy Valley-1C (Fig. 6.6). However the Upukerora-1 curves shows a similar shape to Happy Valley-1C. After an initial pulse of rapid sedimentation and subsidence rates dropped with regards to both accumulation and subsidence by late Eocene. An unconformity removed sediment of mid to late Miocene age, and a change in water depth appears to record a period of uplift at a rate of 7 $m.Myr^{-1}$ Sedimentation and subsidence following the hiatus continued at rates similar to those preceding the break.

Using a minimum of 150 m of tectonic subsidence, and a maximum of 340 m between 37 and 22 Ma, a β value of 1.5 ± 0.2 was calculated.

6. 6: INTERPRETATION AND DISCUSSION

Figure 6.7 shows a generic tectonic subsidence curve for the Western Southland Basins. Producing a representative curve for the region is difficult due to the complex nature of the numerous sub-basins. For this reason, individual well histories may vary from the composite curve produced here.

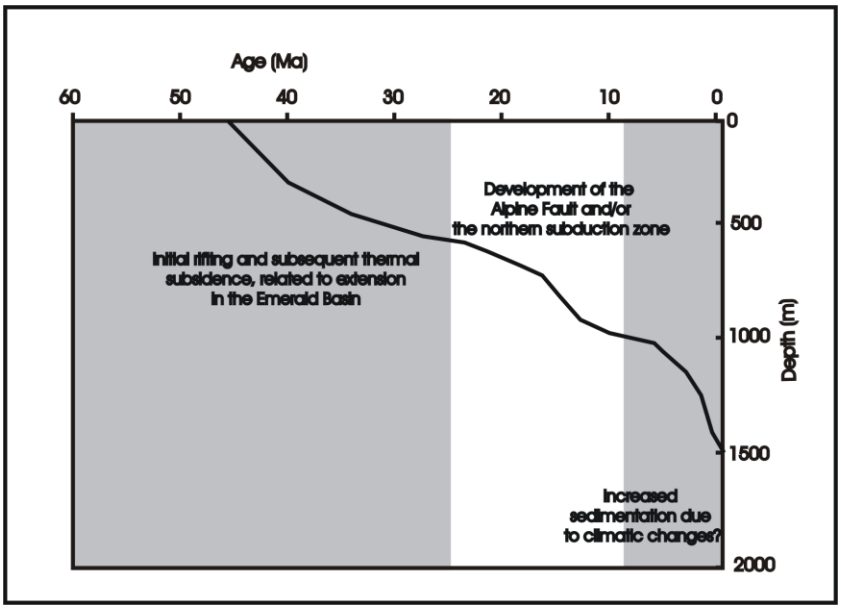

Figure 6.7: Composite tectonic subsidence curve for western Southland

Sub basins typically show McKenzie style thermal subsidence following the formation of sea-floor in the Emerald Basin. A change to concave down occurs at ~ 25 Ma, possibly due to platform subsidence related to subduction to the northeast of New Zealand at this time. A second increase in subsidence during the latest Miocene may represent changes in climatic conditions at the time.

6. 6. 1: Early to late Cretaceous

For most of the Cretaceous a convergent margin was present near New Zealand, but this is believed to have stopped around 105 Ma. , and was rapidly followed by a period of extension (Laird, 1981). All sediments deposited during the Cretaceous are interpreted

as continental rift deposits associated with this mid-Cretaceous breakup of Gondwana (Turnbull and Uruski et. al., 1993).

Syn-tectonic deposition occurred in a number of fault controlled extensional basins. The orientation of the listric faults bounding the tensional basins was northeast southwest, and related to the rifting between New Zealand and Antarctica (Laird, 1981; Kosch and Wellman 1988). The only sediment of this age is preserved at Parara-1, showing that deposition was certainly being deposited in the Solander Basin. Turnbull and Uruski et al (1993) suggest that sedimentation was occurring in most other basins, however a period of Paleocene to late Eocene uplift resulted in the removal of the record in the other wells studied.

6. 6. 2: Paleocene

One explanation for the lack of sediment representing the Paleocene is that the region was uplifted and eroded during this time. Bott (1975) suggested that this widespread hiatus may be the result of initial thermal rebound, resulting from the upwelling of magma which accompanied the plate separation and onset of spreading in the Tasman Sea. Western Southland's location, away from the immediate vicinity of the spreading axis, but close enough to have been effected by initial thermal uplift meant that the thermal uplift was followed by erosion and isostatic uplift, rather than thermal and isostatic subsidence observed in other regions (Turnbull and Uruski et. al., 1993). This uplift meant that the Western Southland region was probably the source of sediment deposited in the Great South Basin during this time (Anderton et. al., 1982).

6. 6. 3: Eocene

Tension stresses once again dominated the Eocene. A new extensional plate boundary propagated north, up the line of the Emerald Fracture Zone (Fig. 5.8, Great South Basin Chapter), causing the formation of the Moonlight Fault System between the Fiordland, Te Anau and Balleny Basins in the west, and the Waiau and Solander Basins to the east (Turnbull and Uruski et. al., 1993). The movement along this fault system was dextral strike-slip, and was driven by the anticlockwise rotation of the Pacific Plate relative to the Australian plate (Stock and Molnar, 1982).

The Cretaceous fault blocks were broken by faults, creating a series of northeast-southwest trending full graben basins. Syn-tectonic deposition began in the Parara sub-basin and the Te Anau Basin. The north to northwest trending faults that bound these features were reactivations of Cretaceous faults present in the underlying basement.

By late Eocene sediment had begun to accumulate in the northernmost wells. The initial pulse of rapid deposition and subsidence seen at Happy Valley-1C, and to a lesser degree in Upukerora-1 may be the result of poor dating and paleo-bathymetric estimations, rather than an actual event, however the formation of the Moonlight Fault System would have resulted in uplift, and elevated sediment levels. It has also been suggested that during this time a major drainage system discharging into the Great South Basin was diverted into Western Southland (Turnbull and Uruski, et. al., 1993). Rapid subsidence at a rate of 500 $m.Myr^{-1}$ was recorded at Lill Burn, located in the Waiau Basin, and at 350 $m.Myr^{-1}$ at Earl Mountain in the Te Anau Basin (Turnbull and Uruski et. al., 1993), suggesting it is probably an actual event. During this time sedimenatation was slow at Solander-1 and Parara-1 as this region was terrestrial, and probably hilly (Turnbull and Uruski et. al., 1993).

6. 6. 4: Oligocene

During the Oligocene the extensional regime existing since the Cretaceous decreased in intensity. Activity during the early Oligocene was restricted to fewer, much larger master faults such as the Moonlight and Hollyford systems, and the Solander Fault (Turnbull and Uruski et. al., 1993). Sedimentation during this early period took place in interconnected fault-controlled basins, of which the Balleny Basin and southern Waitutu were open to oceanic inflences. In the curves this period is represented by slow sedimentation and subsidence and increasing water depths.

By the close of the Oligocene, the Pacific Plate pole of rotation moved southeast(Fig. 5.8, Great South Basin Chapter)(Sutherland, 1995; Wood et. al., 1996). This resulted in strike-slip motion along the Alpine Fault, with an increasing component of convergence The compression resulted in local uplift and erosion, none of which is seen in the

curves, however the sudden increase in sedimentation at Solander-1 and Parara-1 may be the result of erosion on the upthrown Solander Ridge. The increase in sedimentation at Upukerora-1 is likely to be due to uplift on the Moonlight Fault System. This increase is more dramatic than at Happy Valley-1 due to currents carrying sediment from a river system, flowing into the Te Anau Basin (Turnbull and Uruski et. al., 1993).

6. 6. 5: Miocene

By the end of the Miocene almost the entire region was covered by sediment, however this simple sedimentary picture is the result of complex tectonic elements. The Miocene was dominated by compression, and the development of subduction along the Macquarie Ridge, which began by middle Miocene (Davey and Smith, 1983). This feature resulted in the uplift of the Balleny Basin, perhaps explaining the sudden increase in sediment deposited in the adjacent Solander Basin, as seen on the curves. The growth of anticlines was also common (Fig. 6.8(a)), as seen at Upukerora-1, where much of this period is missing, with uplift occurring over the unconformity. By Miocene the Alpine Fault had assumed the role of plate boundary, with dextral strike-slip occurring on it, and also on several major splays (Turnbull and Uruski et. al., 1993).

Bends in the fault systems (Fig. 6.8(b)) resulted in a number of ‘flower’ structures, and a possible pull-apart basin in the Waitutu Sub-basin (Turnbull and Uruski et. al., 1993). Compressional, as well as dextral strike-slip movement fits well with plate reconstructions (Carter and Norris, 1976). The volume of mass flow and slump deposits suggest that the compressional rates peaked in the late Miocene (Turnbull and Uruski et. al., 1993).

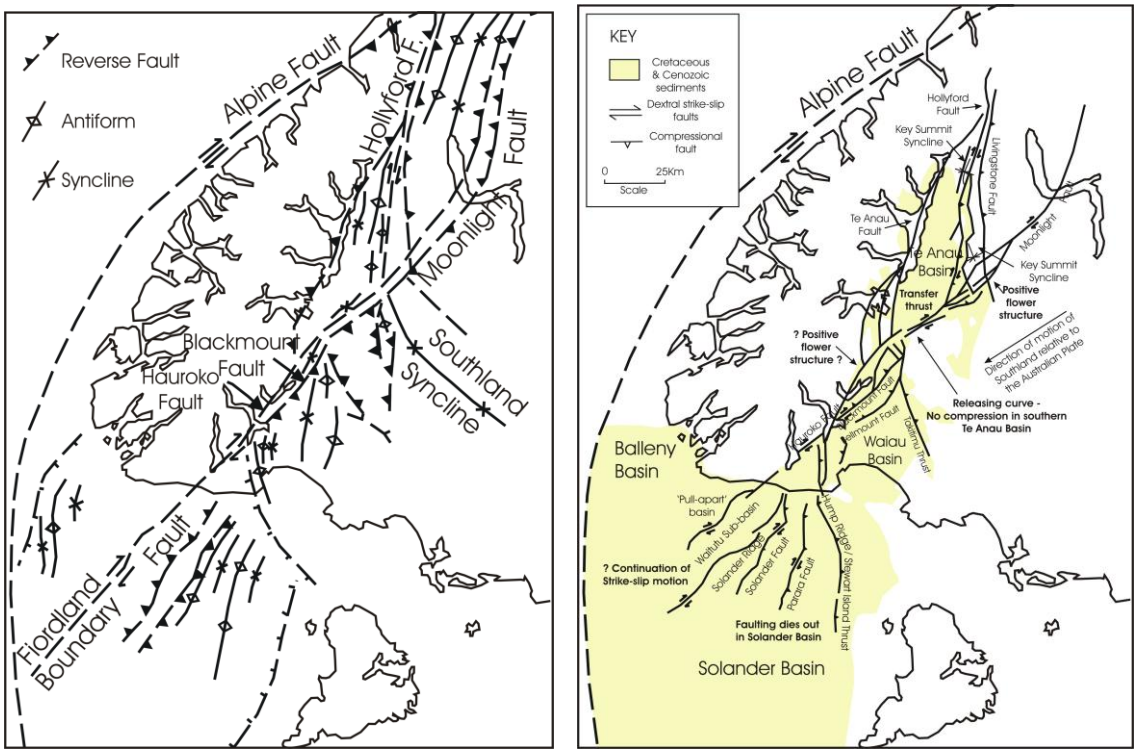

Figure 6.8: Map of Western Southland showing
(a): location of antiforms and synforms during the Miocene (From Norris and Turmbull, 1993).
(b): active faults, and the presence of restraining curves and pull apart basins (From Turnbull and Uruski et. al., 1993)

There is an increase in both sedimentation and subsidence in the Solander Basin during the mid to late Miocene. This is possibly due to back-arc tension adjacent to the subducting Puysegur Trench (Field and Uruski, 1991). Localised uplift on faults misaligned with the developing Alpine Fault may have also contributed sediment.

It is also worth considering the position of the region relative to the convergent subduction zone in the north. A tectonic reconstruction by King (2000)(Fig. 6.9) shows that the Western Southland region was much closer to the plate boundary during the Miocene. It is possible that the increase in sedimentation is due to uplift related to convergence in the adjacent regions. A considerable increase in subsidence and sedimentation is also noted in wells in the Taranaki region. The increase in

sedimentation and subsidence potentially represents the southernmost effects of this subduction event.

Figure 6.9: Tectonic reconstruction at 25 Ma, showing the northern position of the Western Southland region at this time. (From King, 2000).

6. 6. 6: Pliocene to Recent

By beginning of this period the Western Southland region looked similar to the present day configuration, however the Fiordland and Takitimu Mountains were lower (Ward 1988). The basement blocks that surround the basins have continued to rise until present day. A number of volcanic bodies have been imaged on seismic data pertaining to this period, and are related to subduction (Turnbull and Uruski et. al., 1993).

6. 6. 7: Beta Values

The β values in Western Southland range from 1.5 ± 0.2 to 1.6 ± 0.2. Seismic reflection data show that the crust below the Solander Basin is ~20 km thick, increasing to ~30 km on the Stewart Island shelf (Sutherland and Melhuish, 2000), hence the crust in the region was between 30 and 45 km thick prior to rifting.

There appears to be little pattern to the β values calculated for the western Southland basin. This likely reflects the complex mechanisms that formed the basins. The highest β value is found at Happy Valley-1, perhaps due to the Waiau Basin being bound by faults on three side, resulting in prolonged extension, even when the direction of extension changed. The narrow geometry (<30 km) of the basins in Western Southland means that lateral heat conduction likely played an important part in the thermal decay of the region, a process not taken into account by the McKenzie model used here. It is likely that this has lead to an overestimation of β values in Western Southland.

6. 7: CONCLUSIONS

- With the exception of Parara-1, the Western Southland sedimentary record begins during the Eocene. This may be due to subaerial erosion removing any earlier sedimentation.
- The formation of the Moonlight Fault system during the Eocene, and possibly a change in drainage supplied the initial sediment pulse in the Te Anau and Waiau Basins.
- Sedimentation and subsidence slowed during the Oligocene in Western Southland, while water depth appears to increase.
- An increase in sedimentation during the Miocene at Solander-1 probably represents erosion of the upthrown Solander Ridge.
- Uplift of the Balleny Basin, caused by the development of the subduction zone during the late Miocene may also have contributed to increased deposition in the adjacent Solander Basin
- β values range from 1.5 to 1.6, which suggest that prior to rifting the crust was 30 to 40 km thick.
- There appears to be no pattern to the calculated β values, reflecting complex mechanisms responsible for individual basin formation.

CHAPTER 7: WEST COAST BASIN

7. 1: INTRODUCTION

For the purpose of this investigation the West Coast is defined as the area of the South Island to the west of the Alpine Fault and the Waimea-Flaxmore Fault System, and includes the immediately adjacent continental shelf south of 40° 20' (Fig. 7.1). While structurally complex, this region is commonly broken into two tectonically distinct units, the Western Platform, and the West Coast Basin-and-Range Province, with the current coastline providing a convenient boundary between the undeformed Western Platform, and the heavily faulted West Coast Basin-and-Range Province.

7. 2: STRATIGRAPHY

The tectonic basement of the West Coast region, like the rest of New Zealand, was affected by rifting from Gondwana during the mid Cretaceous (Laird, 1993). The syn-rift Pororari Group was deposited in the resulting fault-angled depressions (Fig. 7.2). These sediments represent coarse terrestrial fanglomerates and more distal fluvial sediments (Laird, 1993). It is likely these sediments were widely distributed, however uplift and subsequent erosion during the early part of the late Cretaceous has led to removal of all but a small area of Beeby Conglomerate in the northeast.

During the latest Cretaceous to Paleocene, deposition was restricted to three small fault-controlled basins, the Pakawau and Greville Basins and the Paparora Trough and the South Westland Embayment. During this period coal measures and conglomerates were deposited in the basins (Fig. 7.3), with the Paparoa and Brunner Coal measures being laid in the Paparoa Trough (Laird, 1993). In the Pakawau Basin the Pakawau Group was deposited. Sedimentation in the Greville Basin is thought to be similar in lithology to the Pakawau Group (Nathan and others, 1986). On the South Westland Embayment continued subsidence led to a transgressive sequence, passing from the terrestrial Tauperikaka Coal Measures, into the Whakapohai Sandstone and finally the Tauperikaka formation, a deep-marine mudstone (Nathan and others, 1986). The rest of the region at this time is thought to have been emergent, leading to peneplanation.

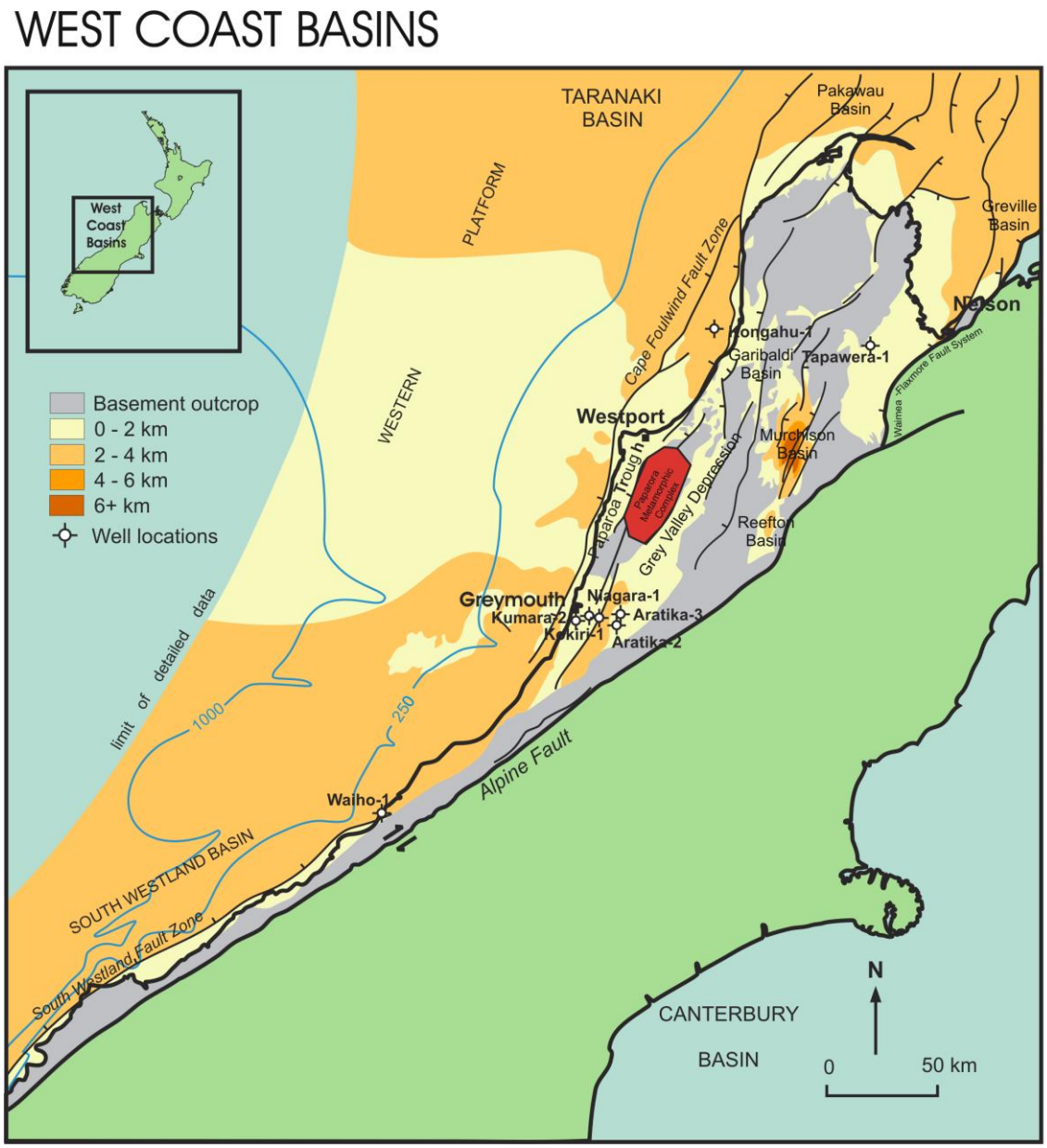

Figure 7.1: Map of the West Coast Basin showing location of wells, sediment thickness and major faults including the Alpine Fault (from Explore New Zealand Petroleum 2003, Ministry of Economic Development, Crown Minerals, 2003).

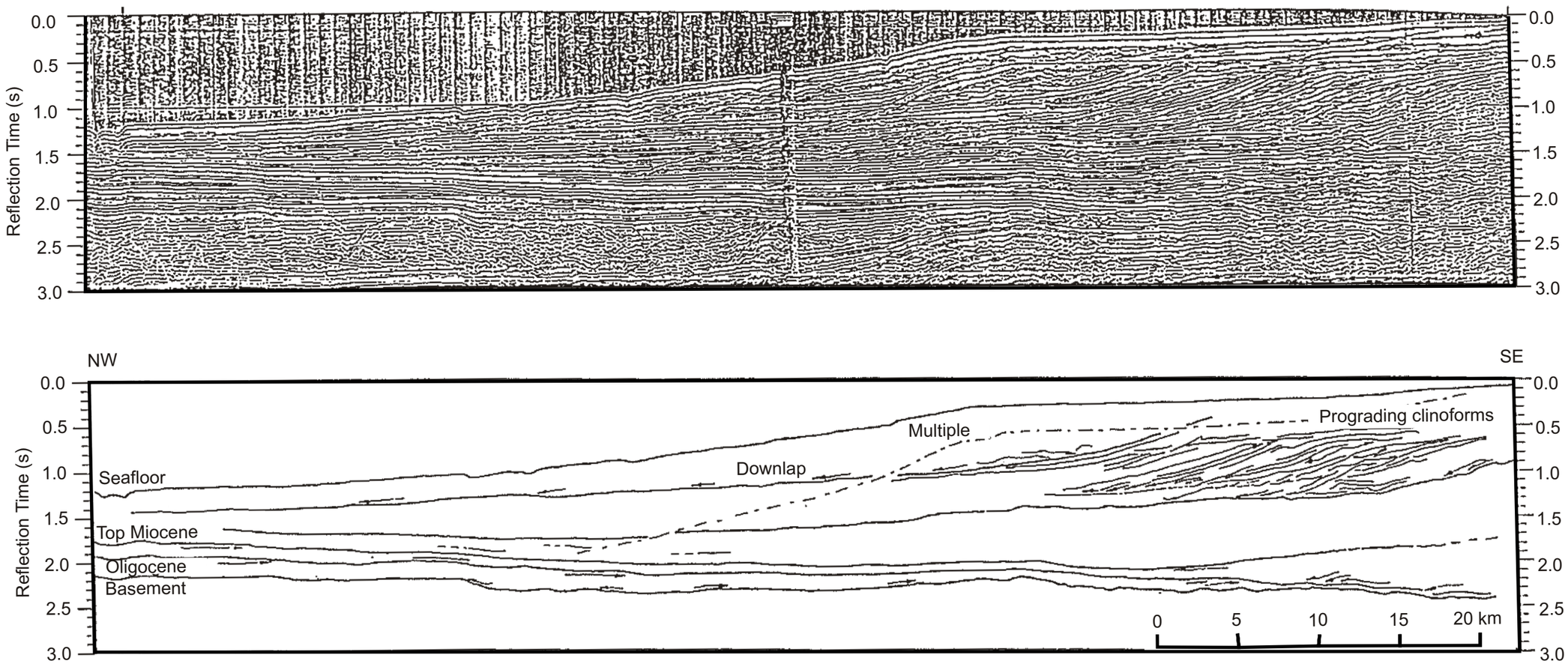

Figure 7. 2: Seismic profile across the Western Platform, West Coast, with interpretation by Sircombe (1993).

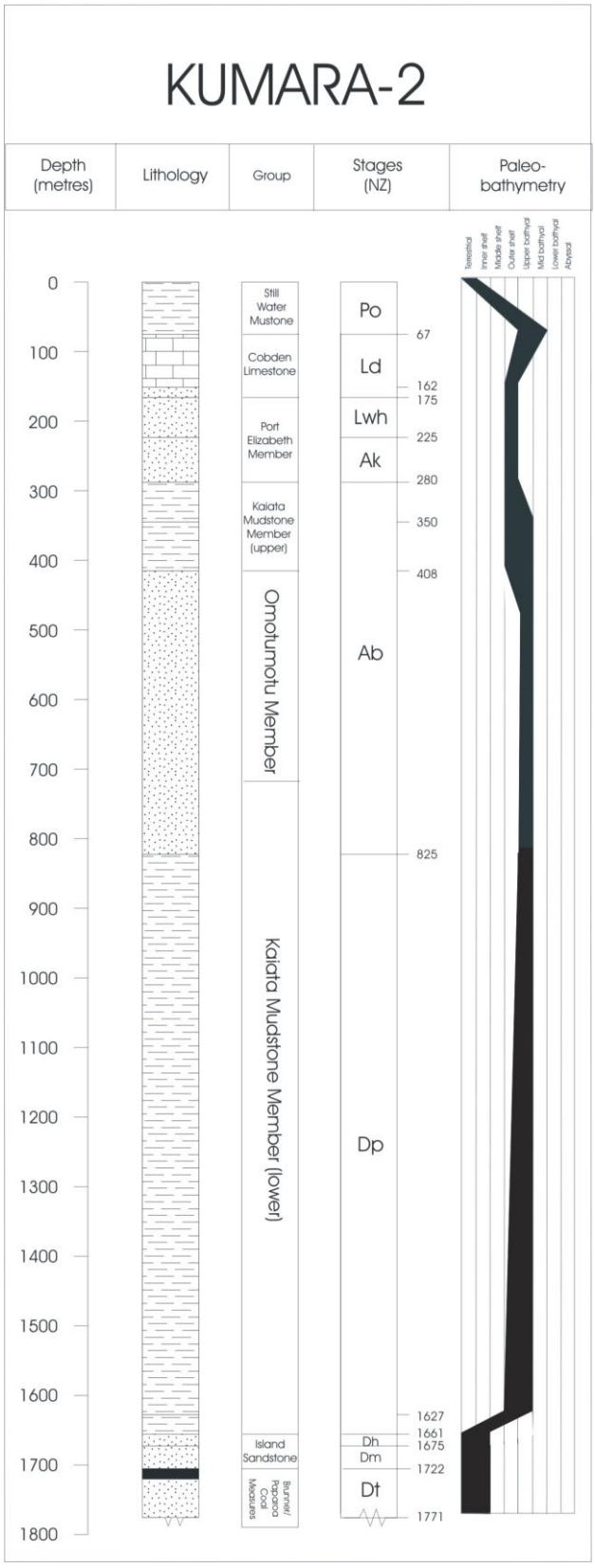

Figure 7. 3: Stratigraphic column of Kiwa-1, typical of basin deposits on the West Coast, New Zealand.

During the early Eocene a thin sequence was deposited in the center of the Paparoa Trough, and sedimentation continued on the South Westland Embayment, with the deposition of a deep water marine sequence. Elsewhere subaerial erosion continued, leading to a subdued topography (Nathan and others, 1986).

Middle to late Eocene saw the development of the Reefton, Murchison and Garibaldi Basins. A regional transgression was superimposed on the basin subsidence, with the Brunner Coal Measures representing the basal section of basin stratigraphy conformably overlain by shallow marine sediments, namely the Kaiata Formation and Garibaldi Sandstone. Calcareous deposition dominated the Oligocene period (King et. al., 2000). Calcareous muds such as the Matiri Formation and Cobden Limestone are present in the basins, while bioclastic limestones such as the Takaka Limestone were deposited on the intervening highs (Nathan and others, 1986).

At all basins expect for the Murchison Basin, subsidence stopped at the Oligocene-Miocene boundary. Deposition began in new basins, the Grey Valley Trough and the Taranaki Graben, both controlled by N-NNE faults (Kamp et. al., 1996). In the Murchison Basin sedimentation reached a maximum, the thick, flysch-type Mangles Formation being the result (Nathan and others, 1986).

The Grey Valley Trough and Taranaki Graben became established during the middle Miocene. Uplift on the Alpine Fault during this time resulted in a series of overlapping alluvial fans extending north and west from the Southern Alps (Nathan and others, 1986). Examples of these conglomerates are the Moutere and Port Hills Gravels in the Moutere Depression, the Longford Formation in the Murchison Basin, and the Old Man Group of the Grey Valley Trough.

Differential uplift superimposed on regional uplift occured during the Quaternary. Block-uplift has led to the topography seen in the ‘Basin and Range’ province with erosion of uplifted regions, and deposition of predominately gravels on the down-thrown areas (Nathan and others, 1986).

7. 3: LOCATION OF WELLS

Well	Lat/Long	Date spudded
Aratika-2	171° 25’ 99.8” E 42° 32’ 71.68” S	1977
Aratika-3	171° 29’ 16.66” E 42° 33’ 08.34” S	1978
Kokiri-1	171° 22’ 84.98” E 42° 28’ 85.1” S	1980
Kongahu-1	171° 52’ 46.28” E 41° 14’ 84.16” S	1984
Kumara-2	171° 11’ 74.08” E 42° 34’ 53.36” S	1985
Tapawera-1	172° 48’ 88.32” E 41° 22’ 30.02” S	1988
Waiho-1	170° 2’ 23.27” E 43° 18’ 16.68” S	1972

Table 7. 1: Location and age of West Coast Basin petroleum wells used for this study.

Kongahu-1 is located offshore, all other wells are onshore.

7. 4: QUALITY OF DATA FROM WELLS

The information used in this study was sourced from individual petroleum well completion reports. Age and paleobathymetry estimations were based on paleonology, palynology, stratigraphic matching to outcrops and to a lesser extent electrical logging. The age of fossils suggests there are likely to be dating errors in age estimations. Difference in the timescales used are also likely to contribute errors.

Only Aratika-2 and Kongahu-1 were drilled to basement.

7. 5: RESULTS

The geohistory plots for the West Coast region are presented in figures 7.4 and 7.5. Figures 7.6, 7.7 and 7.8 show the results from the individual wells.

7. 5. 1: Aratika-2

This well contains the oldest rocks studied in this basin with deposition beginning in the Mata (86 Ma) series. Subsidence and accumulation were initially slow (Fig. 7.6). Erosion removed sediment pertaining to the Paleocene and the majority of the Eocene. Sediment accumulated at a slower rate during the Oligocene and the early Miocene, before reaching a maximum rate of deposition of 140 $m.Myr^{-1}$ during the middle Miocene. Accumulation and subsidence had slowed by the end of the middle Miocene, where erosion removed almost all rocks younger than this. A episode of uplift occurred over this period, with an average rate of $14m.Myr^{-1}$.

Assuming 70 m of tectonic subsidence over the period from 73 to 65 Ma, a minimum β value of 1.25 was calculated.

7. 5. 2: Kumara-2

The overall shape of this curve is quite distinct from the other curves in the West Coast Basin (Fig. 7.7). Deposition began at this site during the Teurian (65 Ma). As at Aratika-2, subsidence and accumulation were initially slow. Rates were steady until the middle Eocene, where there was a rapid increase in both accumulation and subsidence. Sediment accumulation during this period reached rates of almost 300 $m.Myr^{-1}$. Rapid subsidence which accompanied sedimentation occurred over a very brief period, and by the close of the period the rates had returned to those seen prior to the mid Eocene event. At approximately 26 Ma there is rapid increase in water depth and therefore total subsidence at Kumara-2, this is not followed by an increase in sedimentation. An unconformity immediately following this event means all rocks postdating this event are absent. However from the change in water depth it is known that there has been uplift over this period.

A β value of 1.1 ± 0.2 was calculated at Kumara-2, assuming 55 m of tectonic subsidence from 53 to 44 Ma.

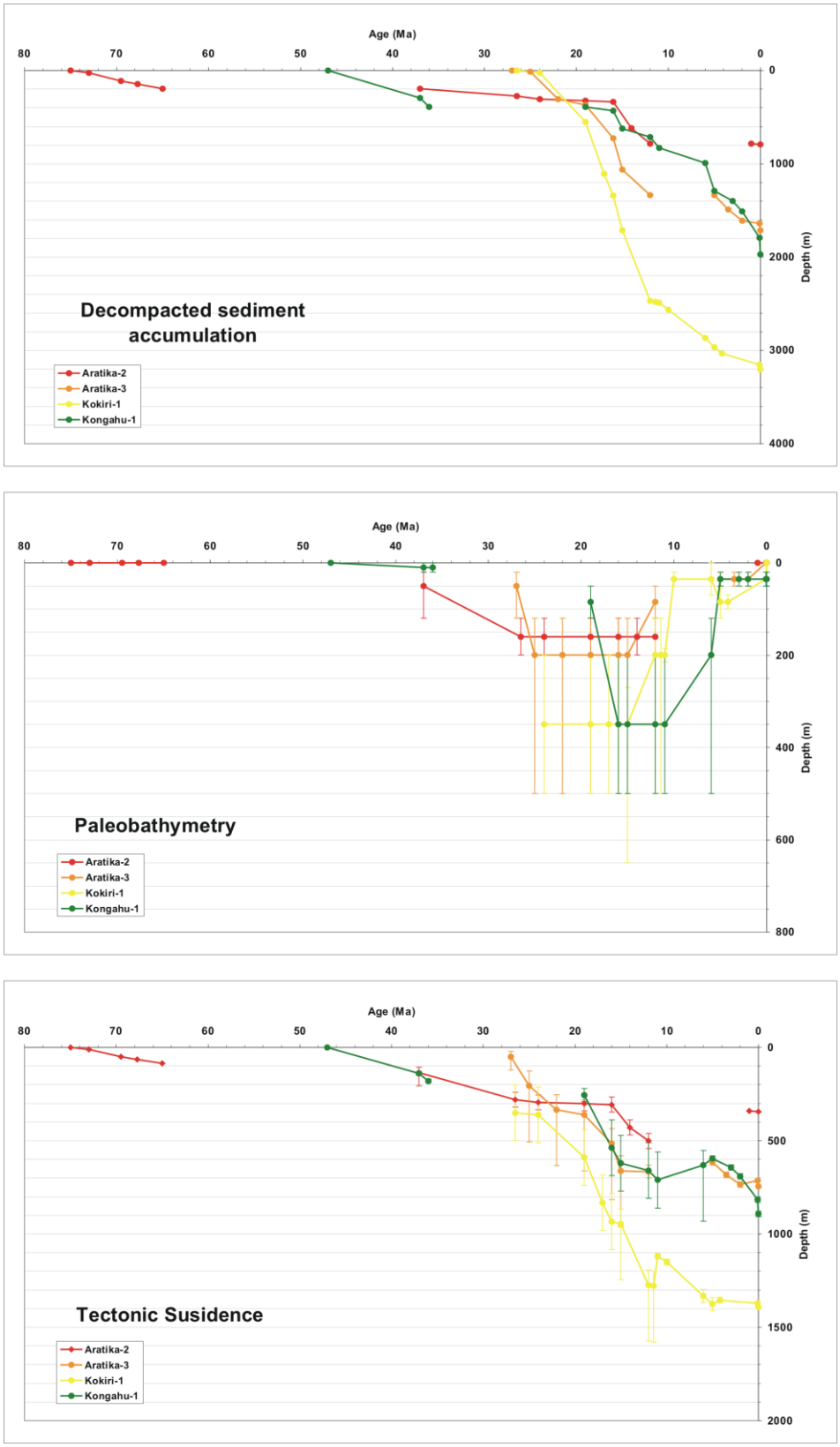

Figure 7.4: Geohistory plots for Aratika-2, Aratika-3, Kokiri-1 and Kongahu-1, West Coast

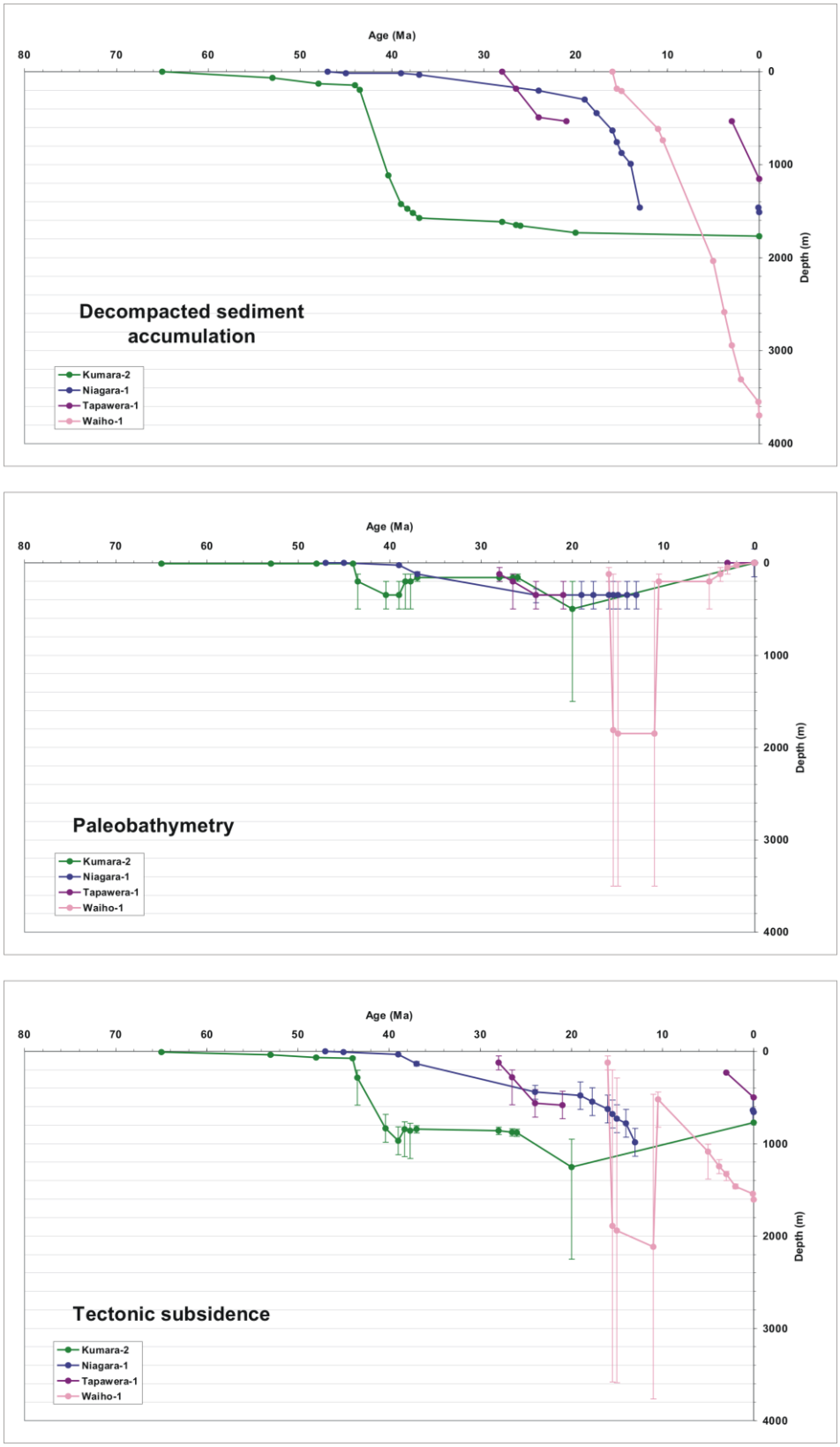

Figure 7.5: Geohistory plots for Kumara-2, Niagara-1, Tapawera-1 and Waiho-1, West Coast

7. 5. 3: Kongahu-1

Subsidence at Kongahu-1 began in the middle Eocene, and at a faster rate than at the three previous wells (Fig. 7.7). Prior to an unconformity which lasts the duration of the Oligocene, rates of accumulation reached 93 m.Myr^{-1} and subsidence rates of 40 m.Myr^{-1} were reached. In the same way as the other wells, bar Kumara-2 and Tapawera-1, sedimentation and subsidence rapidly increased during the middle Miocene. Sedimentation rates dropped following this event, before increasing again at 6Ma. A period of uplift lasting from 11 Ma to 5 Ma followed the episode of subsidence. Unlike most wells the sedimentary record from late Miocene to today appears to be intact.

7. 5. 4: Kokiri-1

Once again the shape of this curve is unique in this basin (Fig. 7.6). Deposition began at Kokiri-1 during the late Oligocene in a bathyal environment. Sediment accumulation and subsidence were rapid during the Miocene, reaching rates of 374 m.Myr^{-1} and over 120 m.Myr^{-1} respectively. Deposition rates decreased, but remained high up until the Quaternary.

7. 5. 5: Aratika-3

Slow sedimentation began in the middle Oligocene and was accompanied by rapid subsidence at a rate of 78 m.Myr^{-1} (Fig. 7.6). By the beginning of the Miocene accumulation had increased to 117 m.Myr^{-1}, while the rate of subsidence had dropped. Once again a middle Miocene event is seen, with sedimentation rates of 336 m.Myr^{-1}, subsidence at rates of 146 m.Myr^{-1}. These rates decrease until a brief period of non-deposition and uplift, at about 7 m.Myr^{-1}. This is immediately followed once again by subsidence and sediment accumulation.

7. 5. 6: Tapawera-1

Rapid sedimentation and subsidence beginning in the middle Oligocene is followed by an unconformity lasting almost the entire Miocene (Fig. 7.8). There is slow subsidence over this period, and rapid uplift immediately following.

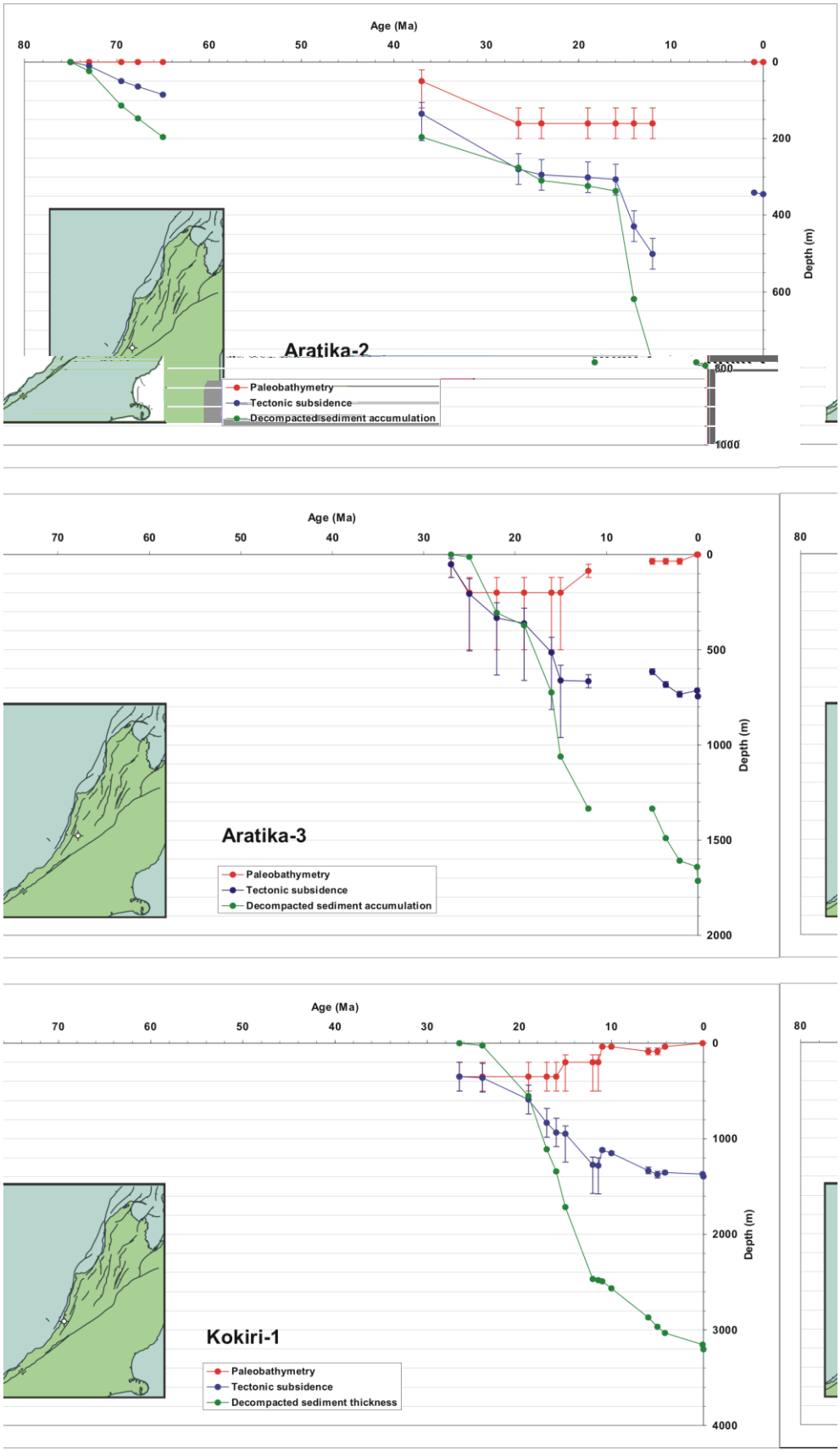

Figure 7.6: Geohistory plots for Aratika-2, Aratika-3 and Kokiri-1, West Coast.

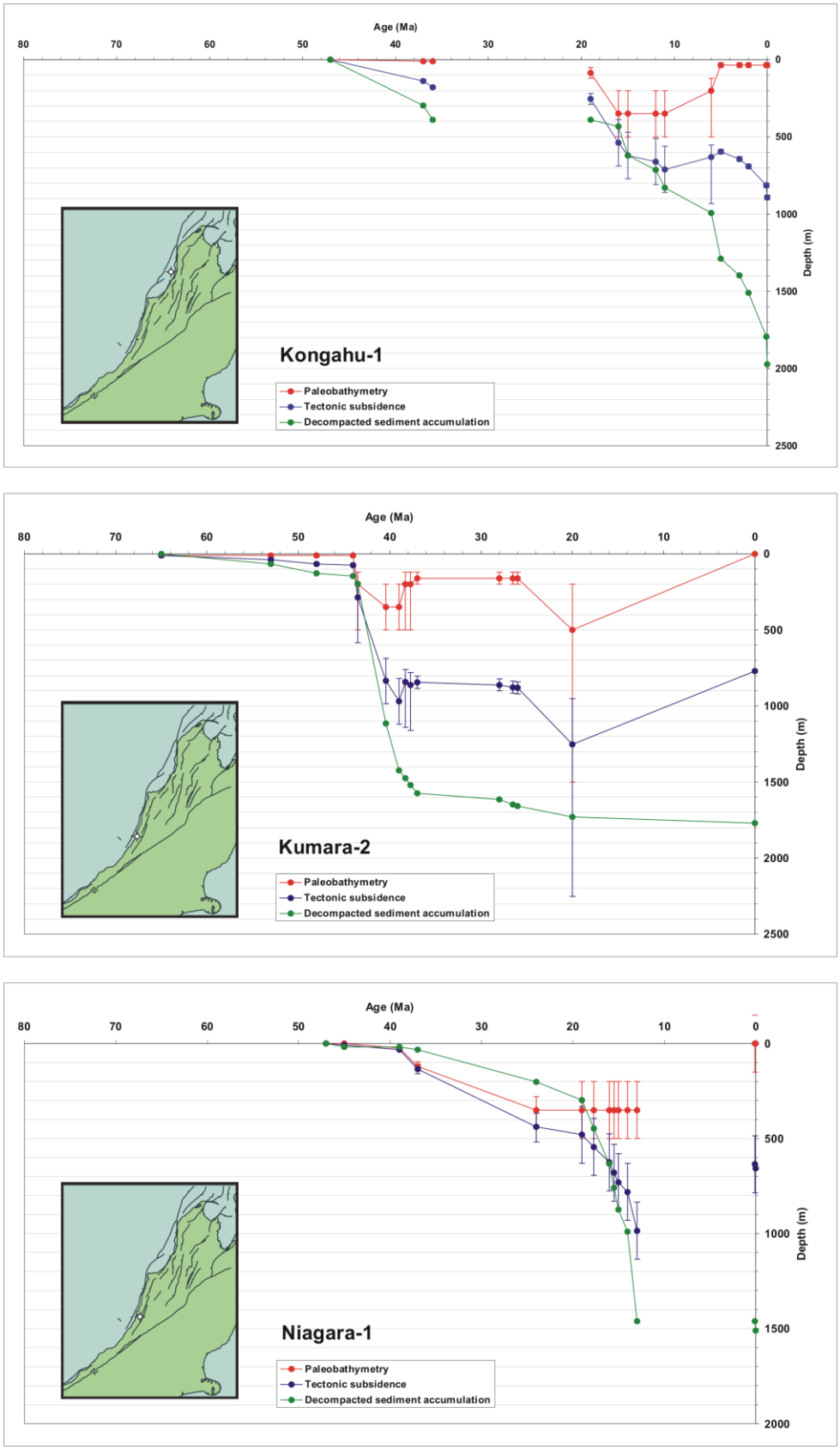

Figure 7.7: Geohistory plots of Kongahu-1, Kumara-2 and Niagara-1, West Coast.

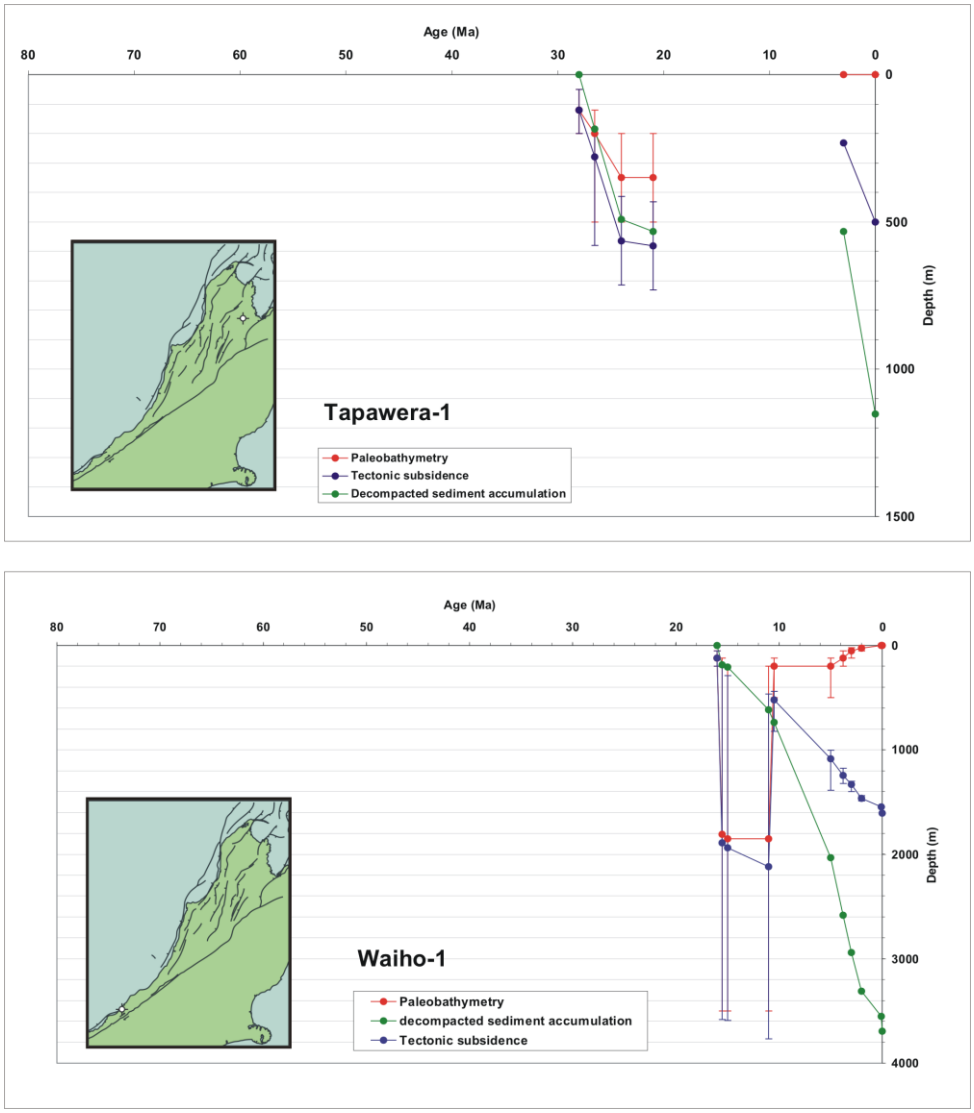

Figure 7.8: Geohistory plots for Tapawera-1 and Waiho-1, West Coast.

7. 5. 7: Waiho-1

Deposition does not occur at this locality until the middle of the Miocene (Fig 7.8). Initally there is an increase in sedimentation rates and water depth accompanied by a decrease in subsidence. At 11 Ma there is a rapid uplift and a decrease in water-depth leading to an increase in sedimentation. Following this event sedimentation increases, along with a decrease in water depth until present.

7. 6: INTERPRETATION AND DISCUSSION

Figure 7.9 show a subsidence curve characteristic of the West Coast region. The sedimentary record for the West Coast region generally begins towards the end of the Cretaceous, where there is a gradual decrease in subsidence related to heat loss following the break-up of Gondwana. At ~25 Ma a number of wells show an increase in subsidence, which is attributed to platform subsidence due to subduction initiation. A further increase is noted at ~20 Ma, possibly caused by the beginning of convergence between the Australian and Pacific Plates. A period of basin inversion occurred from ~15 Ma, followed by a rapid increase in sedimentation from 6 Ma, perhaps related to climate instability.

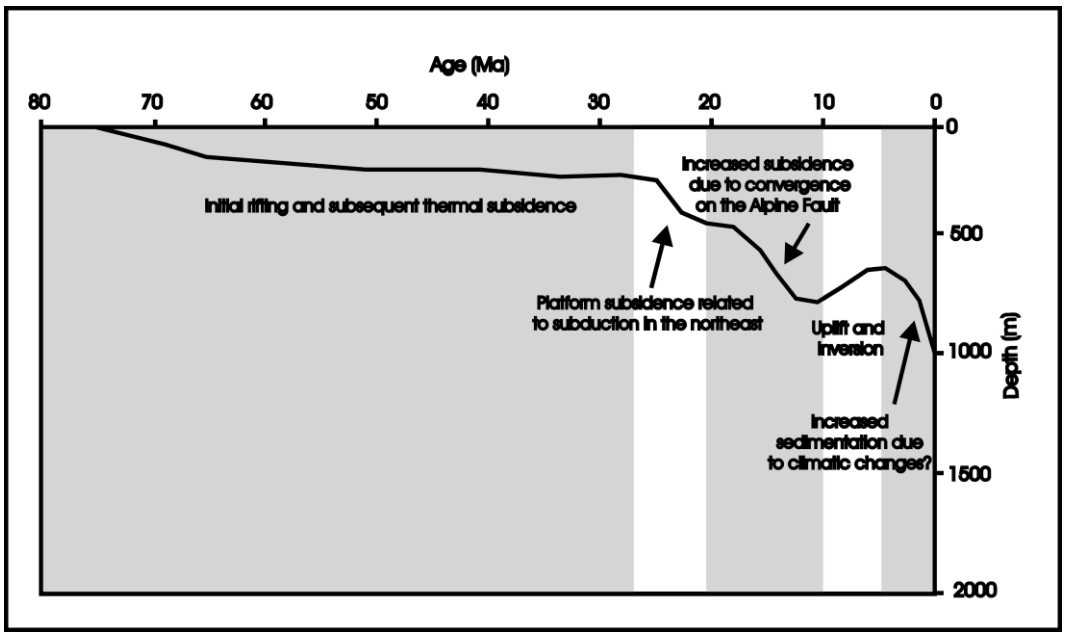

Figure 7. 9: Characteristic geohistory plot for the West Coast of the South Island, New Zealand.

7. 6. 1: Cretaceous

The sedimentary record for the early Cretaceous is limited in this region, with only the Motuan to early Ngaterian represented. Radiometric dates (Adams and Nathan, 1978; Adams and Raine, 1988) show a period of granite implacement, surface volcanism and metamorphic overprinting of older rocks between 110-105 m.y. (Nathan and others, 1986). A change in the tectonic pattern occurred at 105 ± 5 Ma., with extension

replacing convergence (Laird, 1993). This extension produced a series of WNW-trending half grabens. The grabens filled with non-marine sediments, which display a fan-shape in seismic cross-section, suggesting deposition was simultaneous with motion on bounding faults (Nathan and other, 1986). K-Ar and Rb-Sr biotite ages of 92-102 Ma. suggests that the Paparoa Metamorphic Core Complex was also forming at this time, with extension consistent with the direction shown by the half grabens (Tulloch and Kimbrough, 1989).

Uplift slowed in the late Ngaterian, and was followed by a period of little tectonic activity which lasted 20 m.y. (Nathan et. al, 1986). During this time there was widespread erosion of Cretaceous sediments and emplacement of basic dykes from 78-84 m.y.. A change in extension direction appears to occur during the Haumurian (84-65 Ma.). By studying the isopach patterns (Fig. 7.10), and paleocurrent and provenance directions, Laird (1993) showed that there was a dramatic change basin trend during the deposition of the Paparoa Coal Measures. The WNW-trend of mid Cretaceous fault bound grabens was approximately parallel, and therefore likely related to the Cretaceous spreading axis in the Tasman Sea, however, these West Coast features appear to predate the formation of the oldest sea-floor by 20 Ma. (Laird, 1993).

The second set of faults, those that bound the NNE-trending basins were parallel to the transfer fault systems, which offset the Tasman spreading axis and the New Caledonia Basin. This change appears to occur concurrently with the formation of sea-floor at the Tasman Ridge (Laird, 1993). This event is particularly important in the formation of the Taranaki Basin, and will therefore be explained further in the Taranaki Basin chapter (Chapter 8).

From Haumurian to Teurian was a time of uplift and basin subsidence. Non-marine coals were being deposited in the fault-controlled Paparoa Trough, Pakawau and Greville Basins (Nathan et. al., 1986) as seen at Aratika-2, in the southeast of the trough. In the south of the region a transgressive sequence was being deposited, with non-marine coals passing up to deep-marine mudstones. In South Westland and the Paparoa Trough mildly alkaline basalts were also erupted during this period (Coombs et. al., 1976).

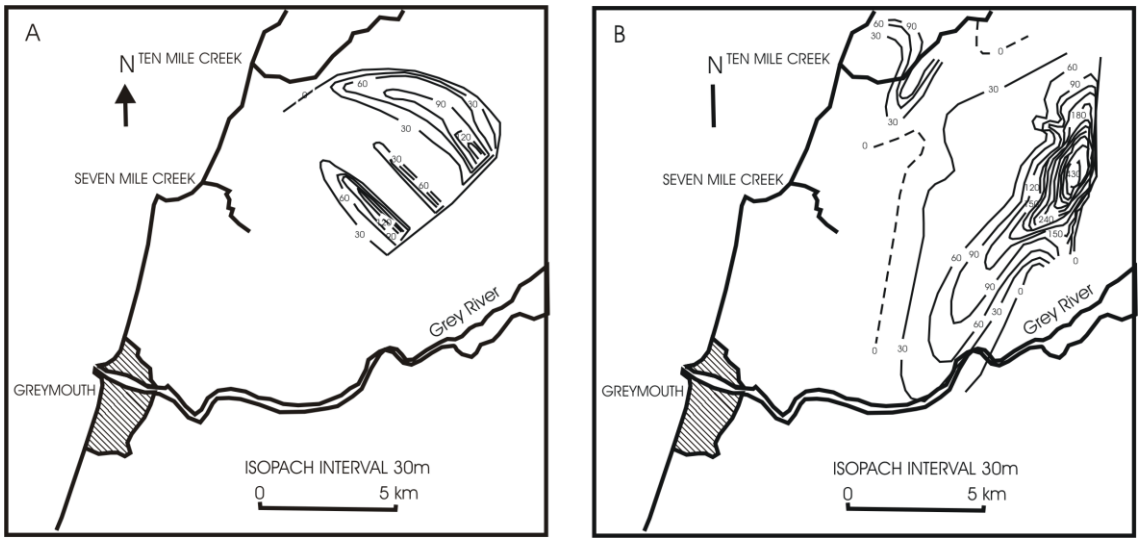

Figure 7. 10: Map of the Greymouth region showing the change in faulting trends seen with the help of isopachs during the deposition of the Paparoa Coal Measures (From Laird, 1993).

A Isopach showing mid Cretaceous sedimentation of the Paparoa Coal Measures

B Isopachs show a change in deposition and faulting, which occurred during mid-late Cretaceous.

7. 6. 2: Paleocene

The majority of subsidence was occurring in three basins during the Paleocene: The Pakawau and Grenville Basins, the Paparoa Trough, and on the Southwestern Embayment. Across the rest of the region there appears to have been wide spread erosion and peneplaination, in some places ranging from mid Cretaceous to mid Eocene (Flores and Sykes, 1993).

The Pakawau Basin was bound by major faults on the east and west. Provenance studies and paleocurrent reconstructions suggest that sediment was eroded from pre-Cretaceous basement to the south and east, and deposited in the basin by braided river systems (Titheridge, 1977). The Paparoa Coal Measures were being deposited in the Paparoa Trough during the Paleocene by fluvial and lacustrine systems (Laird, 1993). These systems appear to have fed the area from the east and northeast (Nathan and others, 1986). It is during the Paleocene that subsidence began at Kumara-2, located in

the southwest of the basin, perhaps reflecting lateral progradation of the clastic wedge, located adjacent to the easterly controlling fault.

Sedimentation on the Western Embayment (not strictly a basin hence the term 'embayment') thickens towards the present day shelf edge, and changes from terrestrial coal measures at the base, into shallow marine, and finally deep marine deposits during the late Paleocene (Nathan and others, 1986). The sediments in these basins, including the largely unexplored Grenville Basin, gradually become more quartzose towards the top (Nathan et. al., 1986). It has been suggested that this was caused by a dwindling sediment supply, and considerable chemical weathering.

7. 6. 3: Eocene

Tectonic activity had almost ceased by the early Eocene, with much of the area undergoing slow chemical weathering (Nathan and others, 1986). This lack of fault motion is probably due to the cessation of spreading in the Tasman Sea, which occurred at this time. The only place where sediment of early Eocene is preserved is in the south, where the foraminiferal limestone is thin and likely incomplete (Nathan, 1977).

Along with uplift, small fault bound basins began to form during the mid to late Eocene, this coincides with the extension and rift event seen to the southwest of New Zealand. Kumara-2, the southern-most subsiding well at this time shows a rapid increase in water depth, and subsidence and sedimentation rates, similar to the wells located in the Great South Basin. It is inferred that Kumara-2 represents the northernmost extent of deformation, related to the creation of the plate boundary in the south.

Subsidence continued in the Paparoa Trough, the largest of the subsiding areas, which expanded north and south from its Paleocene extent. Subsidence also began in the Reefton and Murchison Basins at this time, which were probably connected by a shallow sea (Czochanska et. al., 1987). Regional transgression, which began in the middle Eocene led to the inundation of areas previously exposed during the early Eocene (Nathan et. al, 1986), this may be the cause of subsidence initiation at Kongahu-1, located in the margin of the Murchison Basin. The result was numerous low-lying

islands located within a shallow sea. The units typically deposited over the peneplain surface are generally quartzose coal measures and then shallow marine sediments (Flores and Skyes, 1993). Poor water circulation lead to the deposition of dark brown carbonaceous muds, which dominate lithologies of this age.

7. 6. 4: Oligocene

Transgression continued into the Oligocene. Gradual drowning eventually led to almost all areas inundated by the middle Oligocene. As the terriginous sediment supply decreased, and water circulation improved, sedimentation fell into two categories; First, platform facies, shallow marine bioclastic limestones, which formed region wide, and second, basinal facies, calcareous mudstones, dominated by deep-water foraminifera, which were laid down in the basins (Nathan et. al., 1986).

Subsidence and deposition continued in the Murchison Basin, with a probable southward expansion. The onset of subsidence at Tapawera-1 suggests the basin extended to east at this time also. In the Paparoa Trough sedimentation also continued. However, no sediments are preserved in the axial area of the basin, with coal rank studies suggesting subsequent erosion, rather than a lack of deposition (Nathan, et. al., 1986). Sedimentation begin at both Kokiri-1 and Aratika-3 during the mid to late Oligocene. As these wells are located within the Paparoa Trough, it is inferred that sedimentation began earlier, possibly as early as the Cretaceous, but was subsequently removed by erosion.

Isopach reconstruction shows that the Murchison Basin appears to have merged with the Pararoa Trough during the Oligocene (Nathan et. al., 1986). It is probable that a seaway linked these two basins with the Reefton Basin as well. Subsidence also continued in the region surrounding present day Nelson. Breccia and conglomerate are present at basin margins and adjacent to major faults, suggesting localized uplift and erosion continued in the largely submerged area.

During the late Oligocene, a number of wells on the West Coast show a rapid increase in water depth, which in most cases predates an increase in sedimentation. This event

occurs at 26.5 ± 0.5 Ma., approximately coinciding with subduction initiation to the northeast of New Zealand, and with broad subsidence seen in the Taranaki Basin (Holt and Stern, 1994). Due to its proximity to Aratika-3, it is probable that the increase in water depth seen at Aratika-2 occurred at a similar time, with a lack of data preventing better resolution of the event. This will be further discussed in the Taranaki Basin chapter, and also in the discussion chapter (Chapters 8 and 10, respectively).

7. 6. 5: Miocene

An increase in terrigeonous sediments due to regression and uplift characterizes early Miocene deposits. Land emerged in the south, in the area immediately surrounding Nelson, and in a narrow strip, parallel to the Alpine Fault (Nathan et. al, 1986). The lack of erosion of underlying Oligocene sediments suggests that the subaerial regions had relatively subdued topography.

Subsidence ceased in all but the Murchison Basin, which saw an increase in subsidence rates. Rapid shallowing of the basin accompanied by increase subsidence attests to the huge influx of sediments from an eastern source. The Paparoa Trough ceased to subside in the Miocene. However a new depo-centers, the Grey Valley Trough was created immediately to the east, when Cretaceous to early Tertiary faults were reactivated with a reverse sense of throw (Bishop, 1991). By the Altonian (19-16 Ma.) subsidence had also begun northwest of Nelson.

By the mid Miocene both the Murchison Basin and the Grey Valley Trough had extended considerably south, with terrestrial sedimentation occurring in each area (Bishop, 1991). On the Western Platform subsidence also began, with rates increasing southwards. Sircombe and Kamp (1998) suggested that the subsidence seen in the middle Miocene (16-11 Ma.) was the result of lithospheric flexure, related to loading of the margin by the reverse faulted Southern Alps which began at this time. However, the geohistory plots produced by this study using more wells appear to show a significant subsidence event earlier at 19 ± 4 Ma., coinciding with an increase in sedimentation. This suggests that the timing of convergence on the Alpine Fault began earlier than previously thought, as proposed by Cande and Stock (2004). Further evidence for

convergence on the plate boundary is supplied by uplift at Kongahu-1, Kokiri-1, Waiho and possibly at Kumara-2, which occurred at 11 Ma..

7. 6. 6: Pliocene to Recent

By the early Quaternary the new Miocene sedimentary basins were well established, but began to shallow as sedimentation exceeded subsidence (Nathan et. al., 1986). It is proposed that uplift began around this time on the eastern side of the Alpine Fault. As discussed earlier, the increase in sedimentation seen in the wells during the early to middle Miocene may represent the onset of uplift, with possible climatic effects (Molnar, 2004) or more efficient subaerial erosion causing the influx of sediment during the Pliocene. The flood of coarse sediment resulted in the formation of vast piedmont gravel fans, similar to the present-day Canterbury Plains. An abrupt increase in localised and regional uplift occurred onshore during the early Quaternary, as shown by tilted and faulted late Quaternary marine terraces and the Basin-and-Range topography that the area is well known for (Nathan et. al., 1986).

7. 6. 7: Beta Values

Unfortunately, faulting and erosion has removed much of the pre-Eocene strata in the wells on the West Coast, preventing the calculation of β values for much of the region. However, values were calculated at Aratika-2 and at Kumara-2, both located in the Paparoa Trough. They show β values between 1.1 and 1.25. Data gathered during the SIGHT experiment suggest the crust below the West Coast is ~25 km thick (Henrys et. al., 2004), suggesting the original thickness prior to rifting was between 28 and 32 km.

7. 7: CONCLUSIONS

- The sedimentary record presented in studied wells show subsidence was occurring at 75 Ma., however previous studies suggest rifting began earlier, related to the opening of the Tasman Sea.
- Rifting was followed by thermal subsidence until 25 Ma., however much of the sedimentary record pertaining to this time has subsequently been removed.
- Kumara-2 shows a dramatic increase in sedimentation and subsidence beginning at 45 Ma., similar to wells located in the Great South Basin. This increase coincides with the northward propagation of the Australian-Pacific plate boundary. It is inferred that this presents the northern extent of deformation related to this event.
- A number of wells show an increase in water depth at 26.5 ± 0.5 Ma.. Approximately coinciding with the initiation of subduction to New Zealand's northeast, this may be the southern limit of the broad subsidence seen in the Taranaki by Holt and Stern (1994).
- An increase in sedimentation and subsidence from 19 ± 4 Ma. creates a geohistory curve characteristic of foreland basins. This adds further support to Cande and Stock's hypothesis that convergence on the Alpine Fault began earlier than previously thought.
- Where sediment has been preserved, β values range from 1.1 to 1.25, meaning the original crustal thickness was between 28 and 32 km.

CHAPTER 8: TARANAKI BASIN

8. 1: INTRODUCTION

Located along the west coast of New Zealand's North Island, the Taranaki Basin covers approximately 100,000 km^2 (Fig. 8.1). The Taranaki Basin is bound in the east by the Taranaki Fault, and is given an arbitrary western boundary, for this study east of the continental shelf break. In the south the Taranaki Basin overlaps with the West Coast Basin discussed in a previous chapter. This investigation will include the wells of the Golden Bay region within the Taranaki Basin chapter. The Taranaki region consists of two tectonically distinct regions: the passive Western Stable Platform; and the active Eastern Mobile Belt, the structural elements of which include foreland basin, fold-thrust belt, volcanic arc, and back-arc extensional grabens.

8. 2: STRATIGRAPHY

As for the rest of New Zealand's sedimentary basins, the early history of the Taranaki Basin is dominated by the break-up of Gondwana. Cretaceous rifting associated with the opening of the Tasman Sea has created space for over 7000 m of Cretaceous and Cenozoic sediments (Palmer and Andrews, 1993).

The lithostratigraphic nomenclature for the Taranaki Basin is complex, due to the use of informal names by oil workers and the need to redefine many units based on new data from additional wells. The stratigraphy provided in this section is based on a summary by King and Thrasher (1996). The stratigraphy is broken into six groups:

8. 2. 1 The Pakawau Group

The Pakawau Group is a syn-rift deposit including all late Cretaceous sediments (Fig. 8.3). The group is further broken into the Rakopi Formation, dominated by coal measures, and the North Cape Formation, a shallow marine lithofacies. The Pakawau Group was deposited in isolated and interconnected depocenters which onlap basement, and also in N-NE fault-bound sub-basins (Palmer and Andrews, 1993).

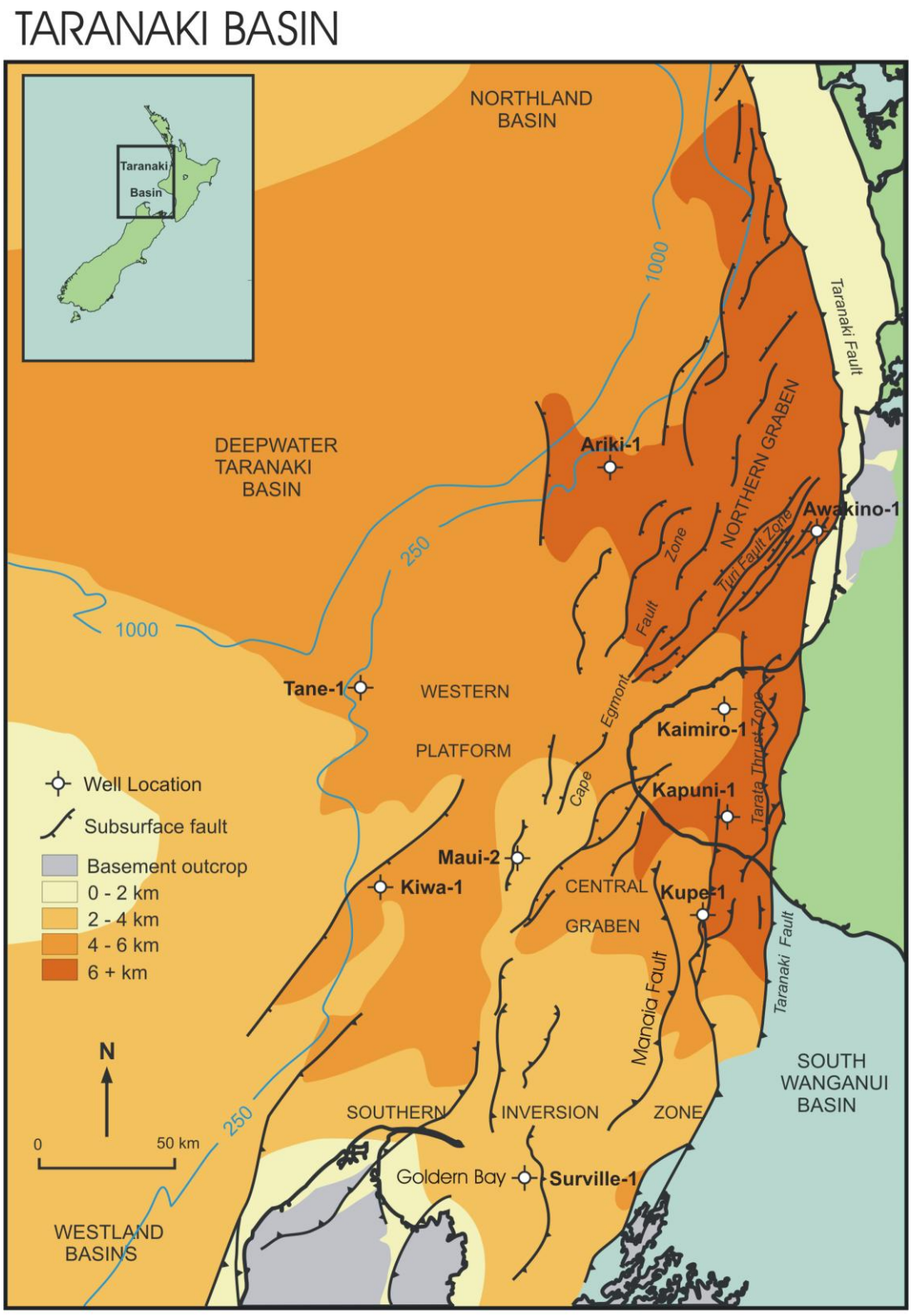

Figure 8.1: Map of the Taranaki Basin, showing location of wells, sedimentary thickness and major faults (from Explore New Zealand Petroleum 2003, Ministry of Economic Development, Crown Minerals, 2003).

8. 2. 2: The Kapuni Group

The Kapuni Group is a late-rift accumulation of Paleocene to Eocene sediment (King and Thrasher, 1996). The terrestrial to marginal-marine unit is further divided into the Farewell, Kaimiro, Mangahewa and McKee Formations. In the south of the basin the sedimentary pattern was inherited from the Cretaceous basin shapes, however, in the north deposition was increasingly dominated by the deepening marine basin and shore migration (Palmer and Andrews, 1993). The unit includes a variety of lithotypes, and is laterally equivalent in age to the Moa Group (discussed below) (King and Thrasher, 1996). The area of deposition for the Kapuni Group decreased with transgression during the Eocene, leading to an increase in depositional area of the Moa Group. Tilting of the region appears to occurred during the deposition of this unit, with the deeping of the basin in the north, while in the south there is a lack of sediment from the Eocene, and possible erosion (Funnel et. al., 1996).

8. 2. 3: The Moa Group

The Moa Group represents a post-rift transgressive sequence of Paleocene to Eocene age (King and Thrasher, 1996). The Turi and Tangaroa Formations consist of fine-grained calcareous siltstone and sandstone. The top of this unit is marked by an paraconformity providing evidence of waning subsidence and sediment supply. Carter and Landis (1982) suggested that this represents the Marshall Paraconformity seen in other basins of New Zealand.

8. 2. 4: The Ngatoro Group

The Ngatoro Group is a diachronous unit which ranges in age from early Oligocene to late Early Miocene in the west, to late Oligocene to earliest Miocene in the east (King and Thrasher, 1996). The thin, sediment-starved unit is high in calcium carbonate content, and is broken into the Otaraoa, Tikorangi and Taimana Formations. The deposition of the Ngatoro Group was accompanied by major changes in the tectonic influences. Deposition at the base of the group marked the beginning of renewed subsidence and marine inundation (King and Thrasher, 1996). This is followed by compression and erosion. The mid to late Oligocene sees rapid platform subsidence,

LINE NM 16

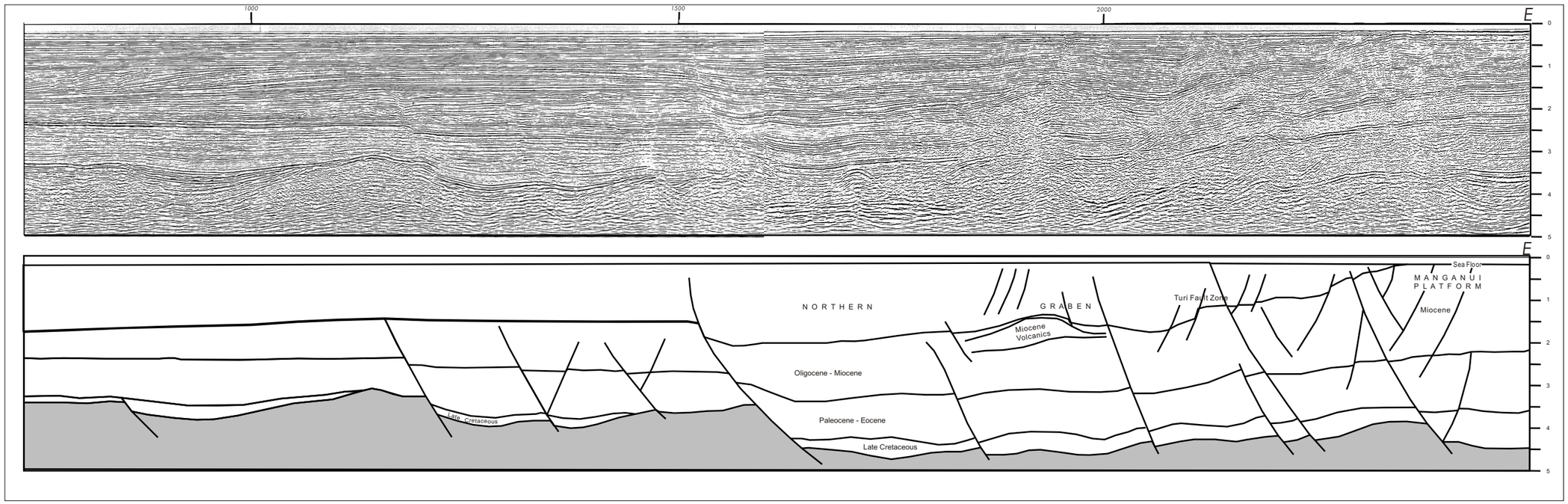

Figure 8.2: Seismic section across central Taranaki Basin, showing sediment to basement and faulting. With interpretation by King and Thrasher, 1996

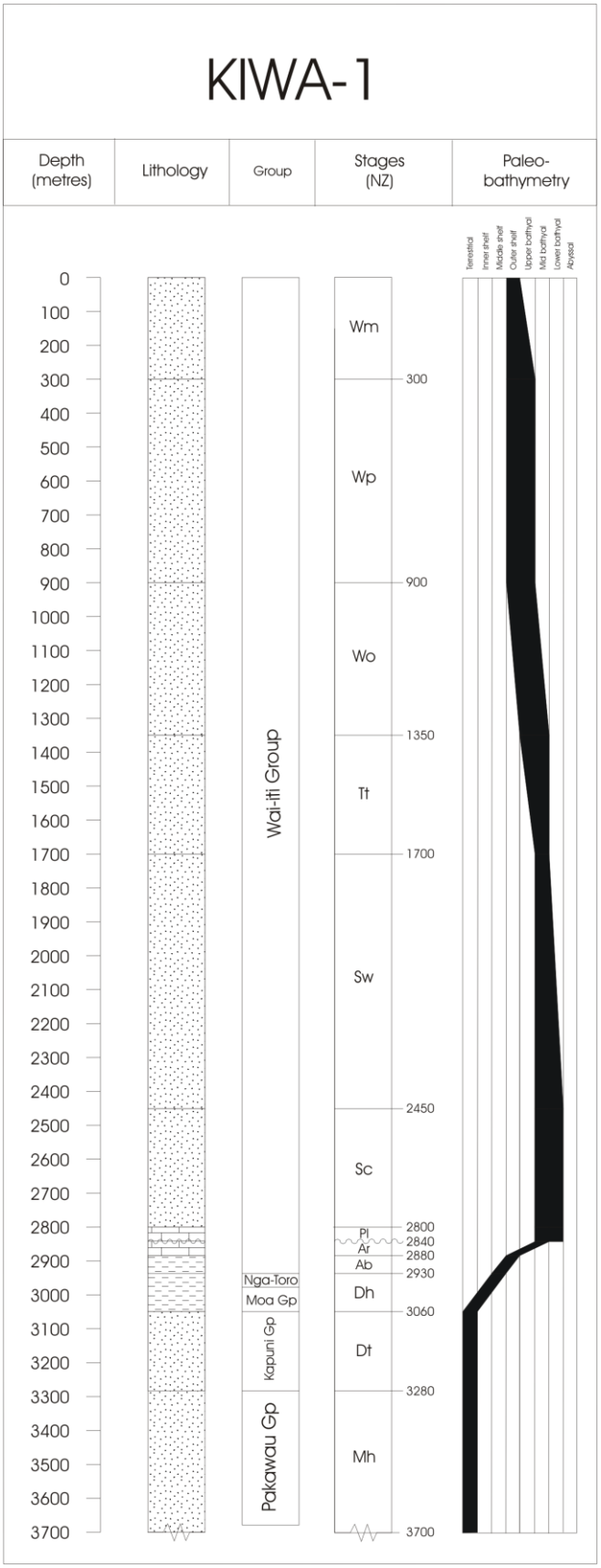

Figure 8.3: Stratigraphic column for Kiwa-1, typical of Taranaki, New Zealand.

and an increase in water depth, which is most dramatic in the east, where the region goes from subaerial or shallow marine to bathyal (Holt and Stern, 1994).

8. 2. 5: The Wai-iti Group

The Wai-iti Group represents the remainder of the Miocene sediments, and is divided into the Manganui, Moki, Mohakatino, Mount Messenger, Urenui and Ariki Formation. The regressive marine unit is clastic dominated and consists of shelf, slope and basin-floor silts, muds and sandstones (King, 1988a, 1988b). Deep water volcaniclastics also appear. The Wai-iti Group is characterized by high sedimentation rates, due to increased tectonism associated with the convergent plate boundary (King and Thrasher, 1996).

8. 2. 6: The Rotokare Group

The final group is the Rotokare Group. This regressive sequence is sourced from intra-basinal and hinterland regions of uplift and erosion, resulting in high sedimentation rates and deposition (Funnel et. al., 1996). The Matemateaonga, Tangahoe, Mangaa and Giant Foreset Formations make up this unit, which is thick (upto 4000 m) in all areas except southern Taranaki.

8. 3: LOCATION OF WELLS

Well	Lat/Long	Date spudded
Ariki-1	38 º 12’ 05” S 173 º 41’ 51” E	1983
Awakino-1	38 º 33’ 27” S 174 º 33’ 60” E	1985
Kaimiro-1	39 º 10’ 01” S 174 º 09’ 12” E	1982
Kapuni-13	39 º 29’ 14” S 174 º 10’ 20” E	1983
Kiwa-1	39 º 48’ 39” S 172 º 41’ 53” E	1981
Kupe-1	39 º 49’ 39” S 174 º 07’ 37” E	1975
Maui-2	39 º 36’ 46” S 173 º 26’ 58” E	1969
Surville-1	40 º 43’ 20” S 173 º 26’ 50” E	1976
Tane-1	38 º 56’ 20” S 172 º 38’ 20” E	1976

Table 8.1: Location and age of Taranaki Basin petroleum wells used for this study.

8. 4: QUALITY OF DATA FROM WELLS

The information in this section is based on data published in the individual well completion reports and from revised stratigraphic columns in King and Thrasher (1996). Paleontological data and correlation with onshore outcrops were used for age and paleowater depth determination. Seismic and lithological techniques, and to a lesser extent, down-hole logging were also used. As noted in other chapters, the wells were drilled over two decades, so there is a possibility of time-scale amendment. Ariki-1, Kiwa-1, Maui-2, Surville-1 and Tane-1 all reached basement. Awakino-1, Kaimiro-1, Kapuni-13 and Kupe-1 were not drilled to basement. Interpreted seismic data used by Hayward and Wood (1989) is utilized to estimate depth to basement in these cases.

Note: Kapuni-13 is also known as Kapuni Deep-1.

8. 5: RESULTS

The geohistory of the wells located on the Eastern Mobile Belt is shown in figure 8.4, while the Western Platform wells are represented in figure 8.5. Figures 8.6, 8.7 and 8.8 summarize the results from the individual wells used in this investigation.

8. 5. 1: Ariki-1

Sedimentation and subsidence began during the Haumurian (75 Ma) at Ariki-1 (Fig. 8.6). An increase in subsidence and water depth occurred at the beginning of the Paleocene. During the Eocene sedimentation and subsidence slowed. An increase in sedimentation and subsidence (up to 133 $m.Myr^{-1}$ and 51 $m.Myr^{-1}$ respectively) occurred during the mid to late Oligocene, continuing to increase until reaching a maximum of 430 $m.Myr^{-1}$ during the Pliocene period. Uplift occurred in the region from mid Miocene onwards, reaching a maximum rate during the late Pliocene. Water depth gradually decreased from early to mid Miocene until present.

Assumming thermal subsidence between 47 and 28 Ma and a maximum of 1301 m of tectonic subsidence, a β value of 1.9 was calculated.

8. 5. 2: Awakino-1

A lack of data during the Cretaceous and Paleocene periods mean details are difficult to resolve (Fig. 8.6), however, it is known that sedimentation and subsidence began during the Haumurian (70 Ma). Sedimentation and subsidence slowed until late Oligocene. An increase in sediment accumulation is seen at 19 Ma, which decreased until present. Subsidence followed a similar trend, with a maximum of 28 $m.Myr^{-1}$ reached during the Eocene, before a sudden increase in water depth and subsidence at 25 Ma. Initially rapid (~400 $m.Myr^{-1}$), subsidence gradually slows before uplift occurs from 16 Ma onwards.

Using a minimum of 100 m of tectonic subsidence and a maximum of 300 m between 43 and 33 Ma, a β value of 1.9 ± 0.3 was calculated.

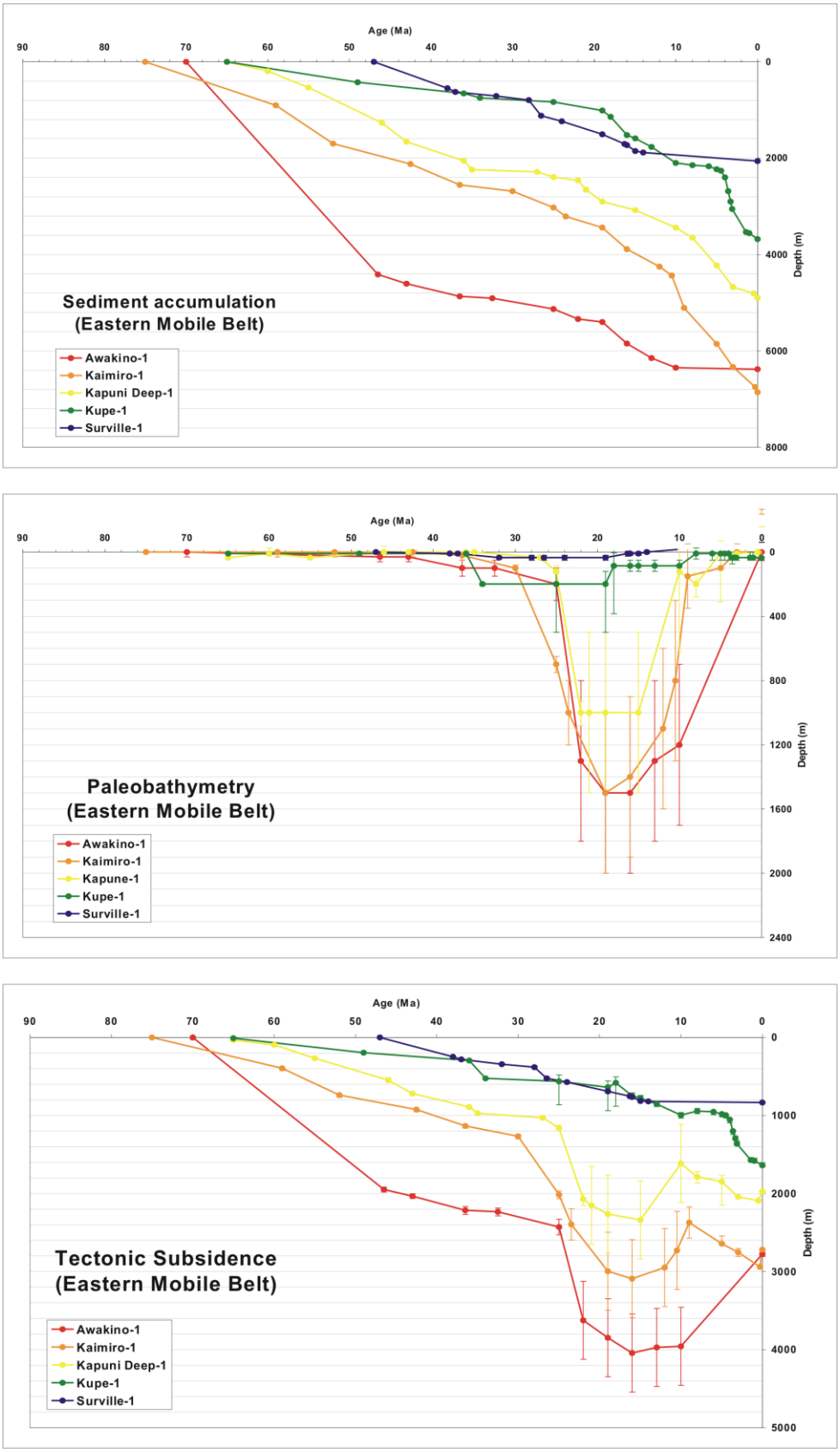

Figure 8.4: Geohistory plots for the wells located on the Eastern Mobile Belt, Taranaki Basin.

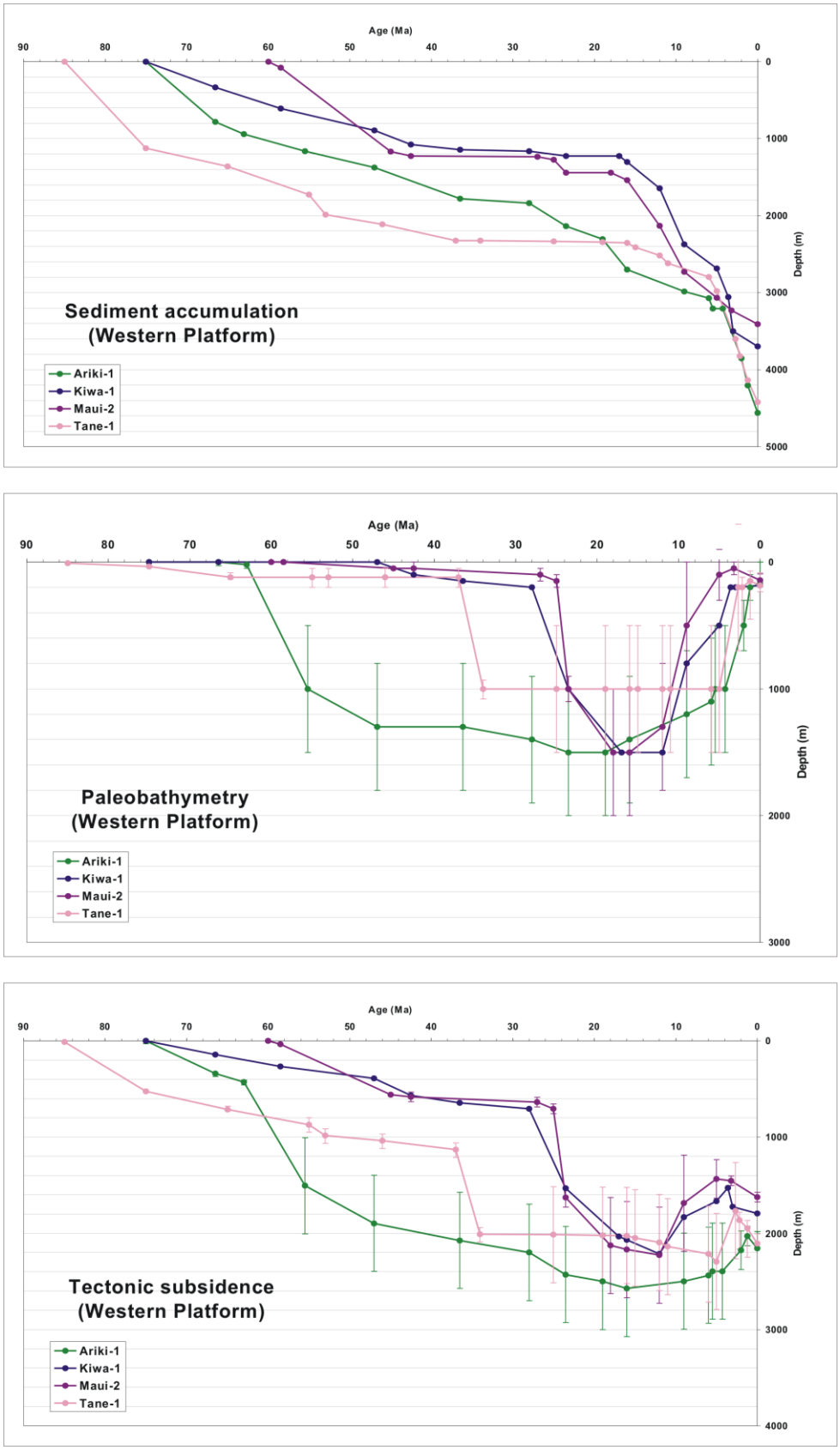

Figure 8.5: Geohistory plots for the wells located on the Western Platform, Taranaki Basin.

8. 5. 3: Kaimiro-1

Deposition and subsidence was initiated during the Haumurian (75 Ma) (Fig. 8.6). Overall, sedimentation and subsidence slowed until the middle Oligocene. 30 Ma saw a significant increase in subsidence, which was accompanied by an increase in water depth. This subsidence slowed during the early to mid Miocene, before uplift occurred between 16 and 10 Ma. Sedimentation also increased during the Oligocene to Miocene. Accumulation remained high until present, with a maximum of ~440 $m.Myr^{-1}$ reached at ~11 Ma, accompanying the re-establishment of subsidence, which followed the period of inversion.

A β value of 2.1 ± 0.1 was caluclated at Kaimiro, assuming rifting between 52 and 43 Ma, with a minimum tectonic subsidence value of 156 m and a maximum of 213 m.

8. 5. 4: Kapuni Deep-1

The boundary between the Cretaceous and Paleocene was when sedimentation began at Kapuni Deep-1 (Fig. 8.7). Barring a short pulse of increased sedimentation at the Eocene-Oligocene boundary, sedimentation and subsidence slowed until the end of the Oligocene. Kapuni Deep-1 shows a similar pattern to both Awakino-1 and Kaimiro-1, with an increase in water depth and subsidence rates near the Oligocene Miocene boundary. At Kapuni Deep-1 uplift occurs from 15 Ma, lasting 5 Myr. Subsidence resumes from 10 Ma

Assuming rifting between 43 and 27 Ma, and minimum of 290 m of tectonic subsidence and a maximum of 340 m, a β value of 2.0 ± 0.05 was calculated at Kapuni Deep-1.

8. 5. 5: Kiwa-1

Sedimentation began at Kiwa-1 during the Haumurian (75 Ma). The curves show an initial gradual decrease in subsidence until the Oligocene (Fig. 8.7), sedimentation increases during the Miocene. At 28 Ma, the pattern previously noted at Awakino-1, Kaimiro-1 and Kapuni Deep-1 is seen. Both subsidence rates and water depth rapidly increase. Sedimenation also increases, but not until 17 Ma and remains high until

present. Subsidence has slowed by 12 My where uplift occurs for 8 My. Subsidence resumes from 4 Ma until present.

A β value of 1.55 ± 0.15 was calculated at Kiwa-1. This was based on the assumption that tectonic subsidence of between 460 and 660m occurred between 66 and 28 Ma.

8. 5. 6: Kupe-1

Sedimentation and subsidence began at Kupe-1 at the Cretaceous-Paleocene boundary(Fig. 8.7). Both sedimentation and subsidence gradually slowed until the end of the Oligocene. Sedimentation and subsidence increase at the beginning of the Miocene. A brief period of uplift occurs at 10 Ma, which occurs at the same time as a decrease in sedimentation and water depth. Sedimentation and subsidence continue following this, with sedimentation reaching a maximum of over 700 $m.Myr^{-1}$ and subsidence reaching 360 $m.Myr^{-1}$. These rapid rates continue until present.

At Kupe-1 a β value of 1.75 ± 0.25 was calculated. This was calculated assuming tectonic subsidence of between 130 and 530 m between 49 and 19 Ma.

8. 5. 7: Maui-2

Sedimentation began at Maui-2 during the Teurian (60 Ma) (Fig. 8.8). By the middle of the Eocene these rates had dropped to 1 $m.Myr^{-1}$ of sedimentation, and 4 $m.Myr^{-1}$ of subsidence. Slow accumulation and subsidence continued until the end of the Oligocene, where a dramatic increase in both water depth and rate of subsidence occurred. At 18 Ma, sedimentation increased suddenly, followed by a rapid decrease in water depth. Uplift occurred from 12 Ma until 5 Ma, with subsidence resuming until present. Sedimentation has gradually slowed until present.

Using a minimum of 47 m of tectonic subsidence, and a maximum of 180 m, between 45 and 27 Ma, a β value of 1.7 ± 0.1 was calculated.

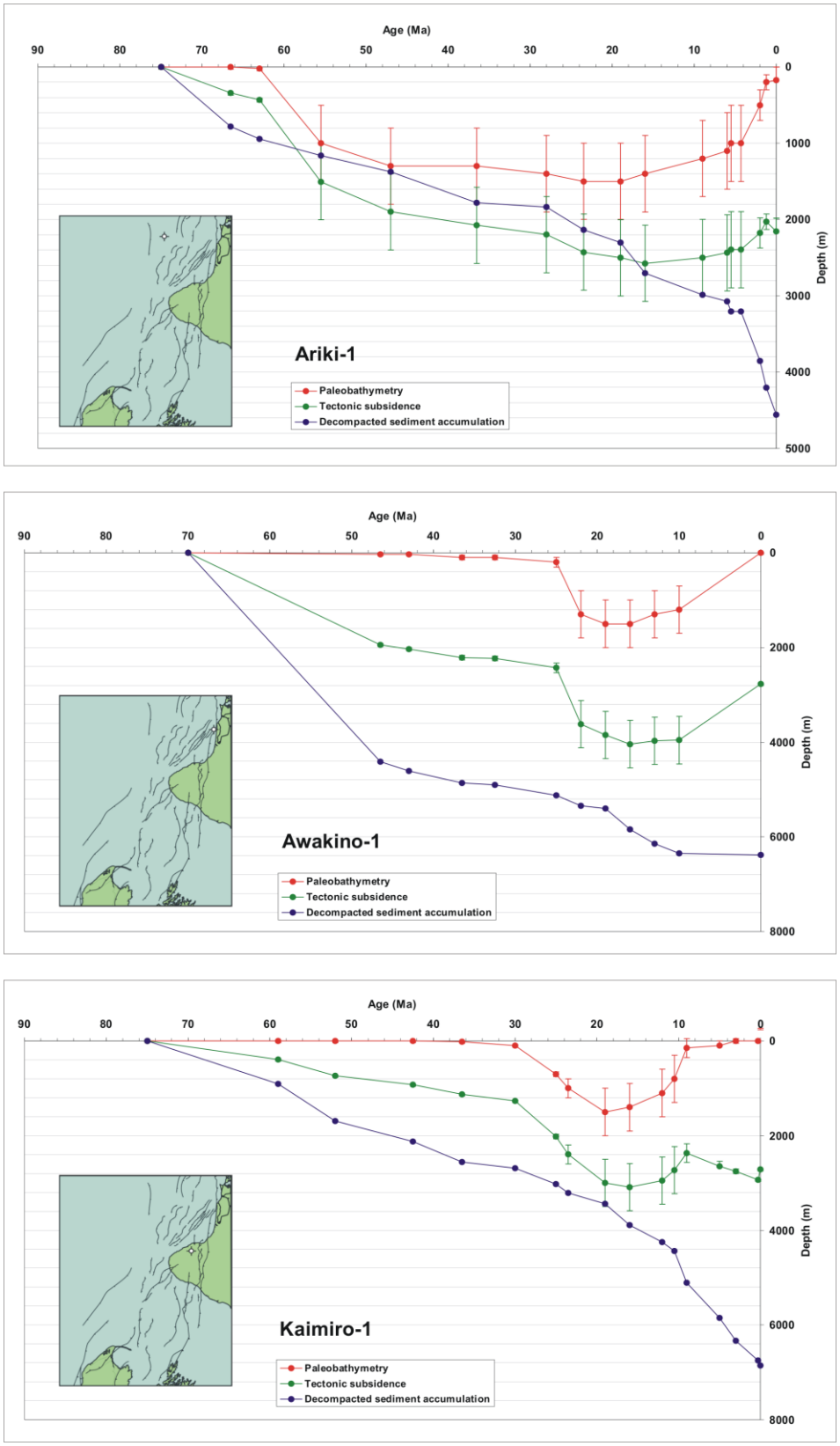

Figure 8.6: Geohistory Plots for Ariki-1, Awakino-1 and Kaimiro-1, Taranaki Basin.

8. 5. 8: Surville-1

The Heretaungan (47 Ma) was when sedimentation began to accumulate at Surville-1 (Fig. 8.8). Rates of both sedimentation and subsidence decreased until the end of the Oligocene. At 28 Ma, the curves of both sediment accumulation and subsidence show an increase in rate. From the end of the Oligocene until the middle of the Miocene rates gradually climb. From mid Miocene until present rates are much slower, with 12 $m.Myr^{-1}$ of sedimentation and only 1 $m.Myr^{-1}$ of subsidence.

A β value of 1.5 was calculated at Surville-1, this was assuming thermal subsidence of between 75 and 125 m, between 37 and 28 Ma.

8. 5. 9: Tane-1

Sediment accumulation at Tane-1 began during the Piripauan (85 Ma) (Fig. 8.8). With the exception of an increase at the Paleocene-Eocene boundary, subsidence rates slowed until the Oligocene. Sedimentation also slowed until the middle of the Miocene, where rates increase until present. A sudden increase in water depth and subsidence occurred at 37 Ma. At 5 Ma a period of uplift occurred, coinciding with a decrease in water depth.

At Tane-1 a β value of 1.75 ± 0.25 was calculated. Rifting occurred between 75 and 37 Ma, with a maximum of 690 m and a minimum of 490 m of tectonic subsidence.

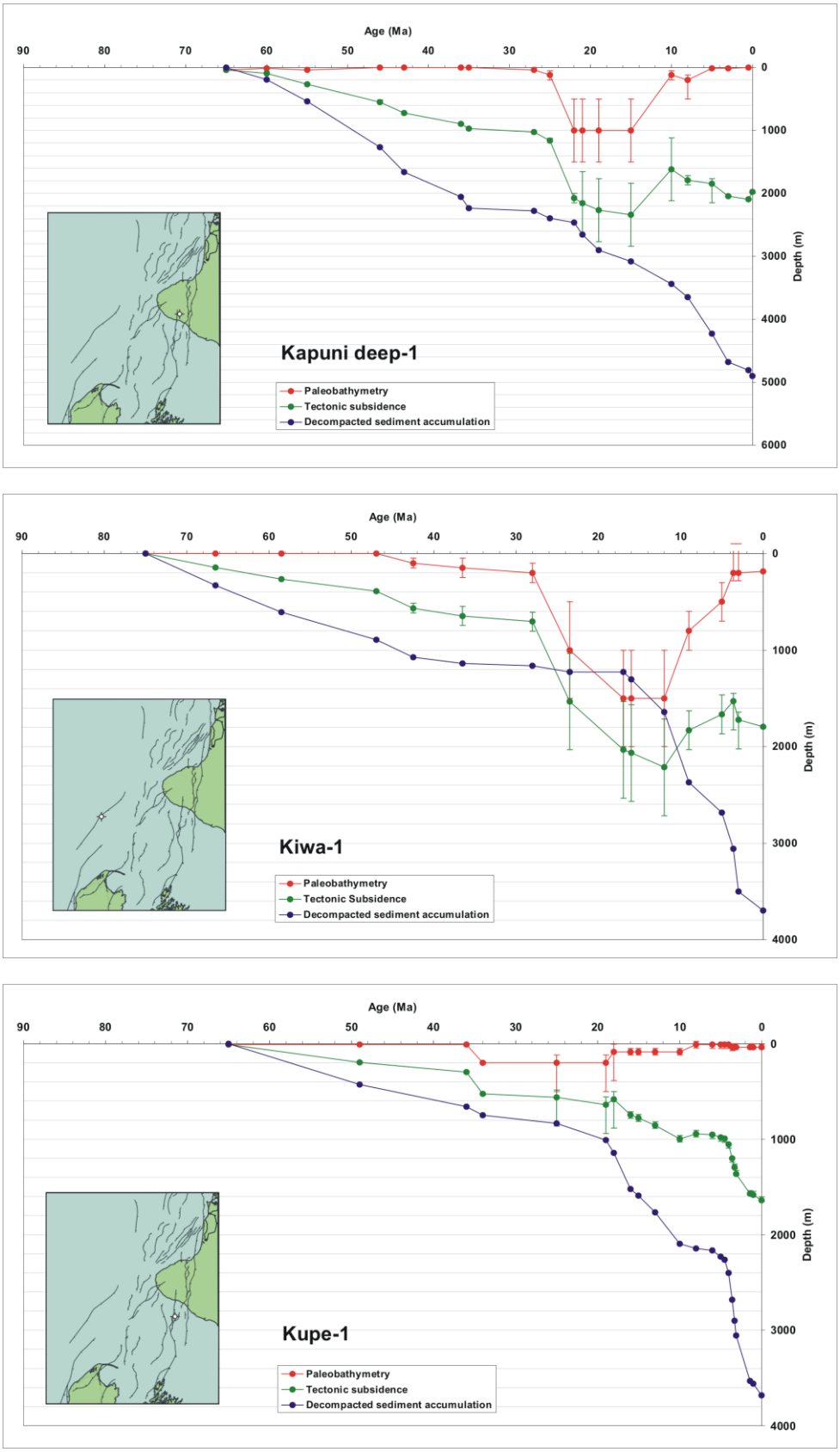

Figure 8.7: Geohistory Plots for Kapuni Deep-1, Kiwa-1 and Kupe-1, Taranaki Basin.

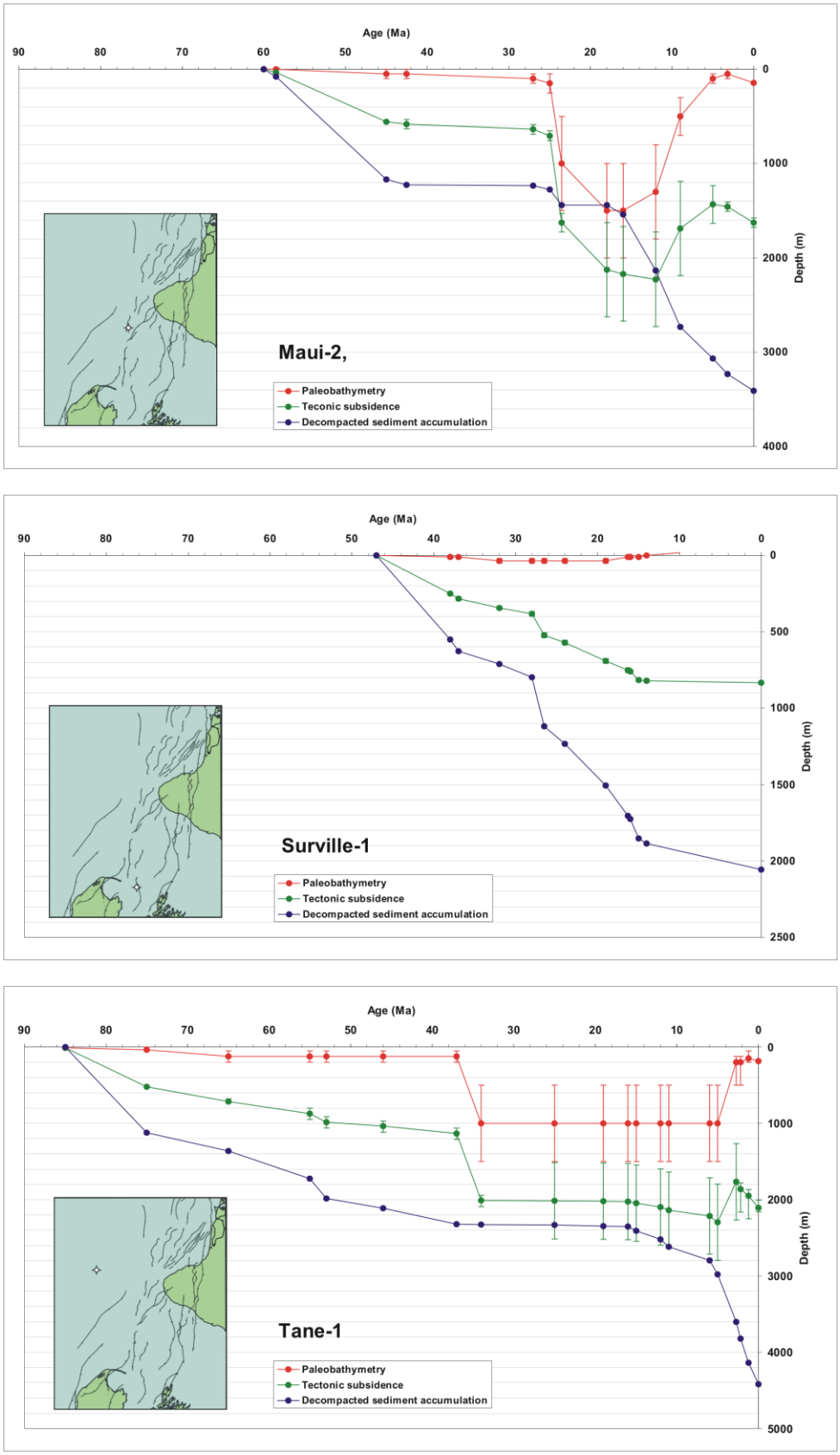

Figure 8.8: Geohistory Plots for Maui-2, Surville-1 and Tane-1, Taranaki Basin.

8. 6: INTERPRETATION AND DISCUSSION

A generic tectonic subsidence curve is provided for the Taranaki Basin in Figure 8.9. It shows that typical McKenzie style thermal subsidence follows initial rifting until 27.5 ± 2.5 Ma. At this point the curve changes from concave-up to convex up. As discussed below, it is assumed that this is related to the onset of subduction and related thrust-belt loading. A period of uplift follows, representing the migration of the thrust belt into the foreland basin.

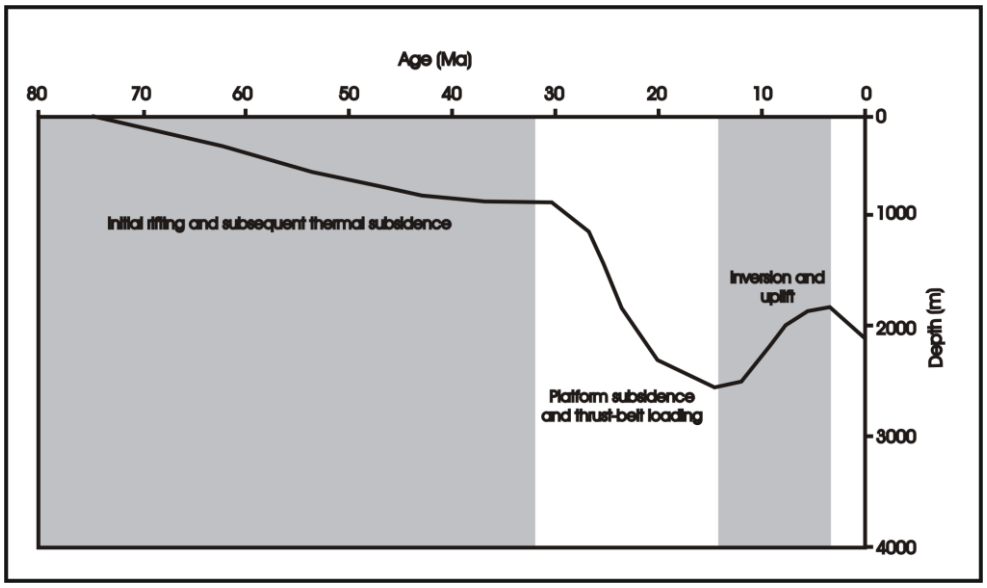

Figure 8.9: Generic tectonic subsidence curve for the Taranaki Basin.

8. 6. 1: Mid to Late Cretaceous

During the middle Cretaceous the west coast of New Zealand was located along the Pacific margin of Gondwana (Palmer and Andrews, 1993). The Taranaki basin developed as a passive margin, coinciding with extension and subsequent sea-floor spreading in the Tasman Sea, beginning at approximately 80 Ma (Palmer and Andrews, 1993). Laird (1981) considered the Taranaki Basin to be the consequence of a failed continental rift, however, King and Thrasher (1996) believe that the resulting basin is simply a rift transform system connected to the southern end of the Tasman Sea Ridge, which continues down the west coast of the South Island (fig. 8.10).

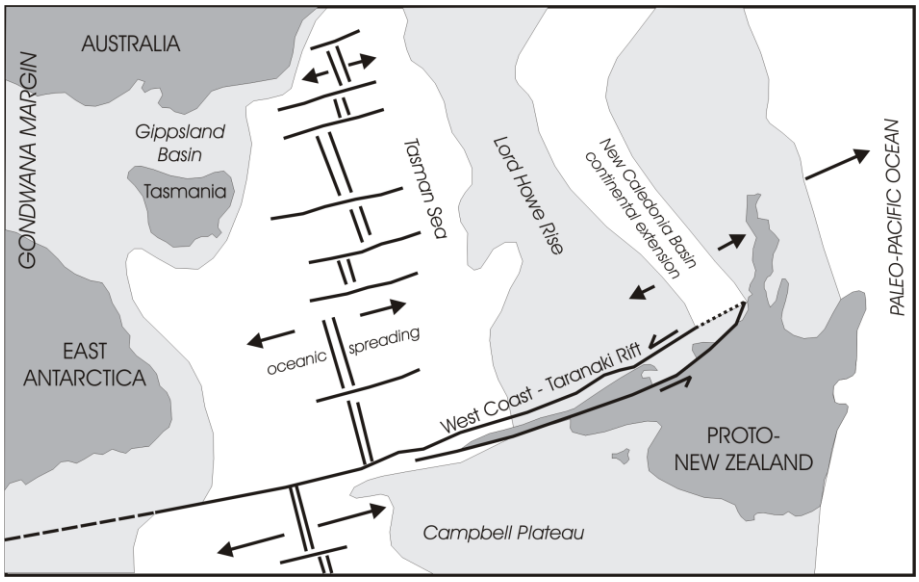

Figure 8.10: Tectonic reconstruction showing the setting of the West Coast-Taranaki rift transform system at 72 Ma, as suggested by King and Thrasher (1996).

The half grabens that comprise the late Cretaceous Taranaki Basin are either north-south trending normal faults, or northeast-southwest trending dip-slip faults with a lateral offset (Thrasher 1990, 1992). The pattern of these *en echelon* faults suggests that the basin formed with a component of sinistal shear. The opening of the New Caledonia Basin at this time provides the means for this offset. On the western side of the West Coast-Taranaki Rift system the net plate motion was affected by both the rapid spreading in the Tasman and by the relatively slower opening of the New Caledonia Basin (King and Thrasher, 1996). The outcome of these processes was still a northeast drift, albeit much slower than on the eastern side of the rift system, resulting in sinistal offset across the zone. A slight divergence in the component of drift resulted in extension and half-graben formation.

Based on characteristic deformation styles Knox (1982) broke the Taranaki region into three structural units (Fig. 8.11):

- The Western Unit
- The Southern Unit
- The Northern Unit

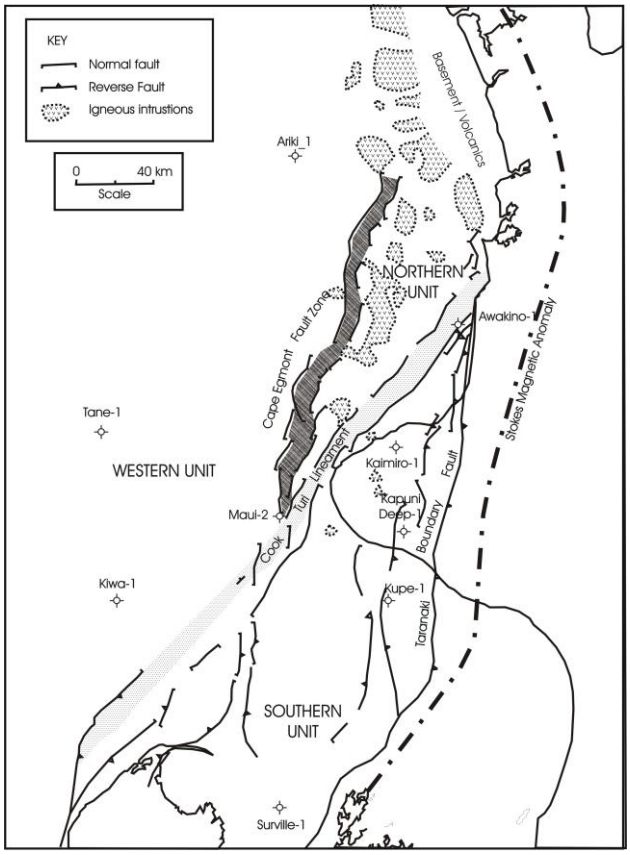

Figure 8.11: Structural units based on deformation style, as proposed by Knox (1982).

Located to the west of the Cape Egmont Fault Zone, the Western unit was folded during the late Jurassic-early Creaceous Rangitata Orogeny. Erosion occurred, and concurrent extension resulted in a fault-cut peneplain with subdued relief. This unit has been largely stable since the late Eocene.

To the east of the Cook-Turi lineament (Fig. 8.11; A boundary marking the northwestern extent of reverse faulting) is the Southern Unit, separated from the

Northern Unit by the Taranaki Boundary Fault. This unit has a similar late Cretaceous-early Tertiary history to that of the Western Unit, however reverse faulting and inversion occurred during the Cenozoic.

The Northern Unit formed by continuous subsidence and is defined by normal faults, some of which have an oblique component of slip. Several intermediate-basin intrusive bodied have distorted the region during the Cenozoic.

The half-grabens that formed in response to extension in these regions are typically asymmetric in cross-section, with significant faulting on only one side, usually the western side (King and Thrasher, 1996). The faults high angled at the surface, but block rotation suggests that angles shallow with depth (Thrasher, 1992). The graben fill is comprised of terrestrial conglomerate and coal measures, likely shed from the upthrown ranges onto the fault-bound lowlands (Palmer and Andrews, 1993).

The geohistory plots for the Cretaceous show that subsidence began in the west, with sediment accumulation at the westernmost well, Tane-1 beginning at 85 Ma. The onset of subsidence appears to move in a southeastern direction with Kiwa-1, Kaimiro-1 and Ariki-1 beginning to subside at 75 Ma and Awakino-1 at 70 Ma. The other wells show no subsidence during the Cretaceous, suggesting they are located on the uplift block of basement.

8. 6. 2: Paleocene

Continued subsidence in the north led to transgression in a southeastern direction, and the formation of an embayment open to the sea in the northwest. This can be seen in the geohistory plots, with sedimentation and subsidence beginning at Kupe-1 and Kapuni Deep-1 at the Cretaceous-Paleocene boundary. The presence of glauconite in the otherwise terrestrial deposits at Kapuni Deep-1 suggest that the shoreline fluctuated laterally during the Paleocene, eventually becoming established by late Paleocene and remaining until the middle Eocene (Palmer and Andrews, 1993). The resulting region represents the southernmost end of the New Caledonia Basin. It is therefore likely that the increase in both subsidence and water depth seen at Ariki-1 is the result of further

southward propagation of the feature at this time (Hayward, 1987). To the south and southeast of the shore expansive coastal plains formed. Several major river systems crossed the plains, with swamp and flood-plains forming, resulting in thick coalbeds and carbonaceous mudstones (Palmer and Andrews, 1993).

Due to lesser fault motion during the early to mid Paleocene, deposition of the Kapuni Group, unlike the underlying Pakawau Group, was not restricted to the Cretaceous grabens. Regional subsidence, rather than local prevailed, with grabens eventually filled and the intervening basement highs drowned by the widely distributed Kapuni Group (Palmer and Andrews, 1993). Towards the end of the Paleocene, however, there was reactivation of faults, which is shown by an onlap disconformity near the base of the Eocene (Knox, 1982). This provides a possible explanation for the increase in sedimentation seen at Kaimiro-1 and Tane-1 during the early Eocene.

Further evidence of an increase in tectonism at the end of the Paleocene is the warping that occurred. Biostratigraphic studies show that erosion occurred on several of the crests of the antiforms in the Southern Unit (Knox, 1982). Erosion may offer an explanation as to why sedimentation at Maui-2, located near the crest of the Moa-Maui Swell, appears not to follow the trend of southeastward transgression. There are two possible reasons for this warping. First, it maybe related to the dying phase of sea-floor spreading in the Tasman Sea. Alternatively, it has been attributed to the adjustment of crustal blocks due to Australia's separation from Antarctica, which occurred from 55 Ma (Knox, 1982).

8. 6. 3: Eocene

The Eocene period is characterised by coastal onlap (King and Thrasher, 1996). In this case, however, transgression is by no means simple, with three separate pulses of shoreline movement (Palmer and Andrews, 1993). These occurred during the late Cretaceous in the northwest, during the early to middle Eocene in the basins center, and finally, during the late Eocene where eastern onshore Taranaki was affected. Figure 8.12 shows the extent of the transgressional periods which occurred. It is suggested that the transgressions were separated by relatively 'quiet' periods, possibly with minor regression also occurring. King and Thrasher (1996) suggest a tectonic origin for this

observed shoreline migration, as it coincides with eustatic sea level fall in the curves created by Haq et. al. (1987). It is probable that the increase in water depth and subsidence seen at Tane-1 represents the final transgressional event, however, the change in water depth may have been overestimated, leading to an exaggerated subsidence rate.

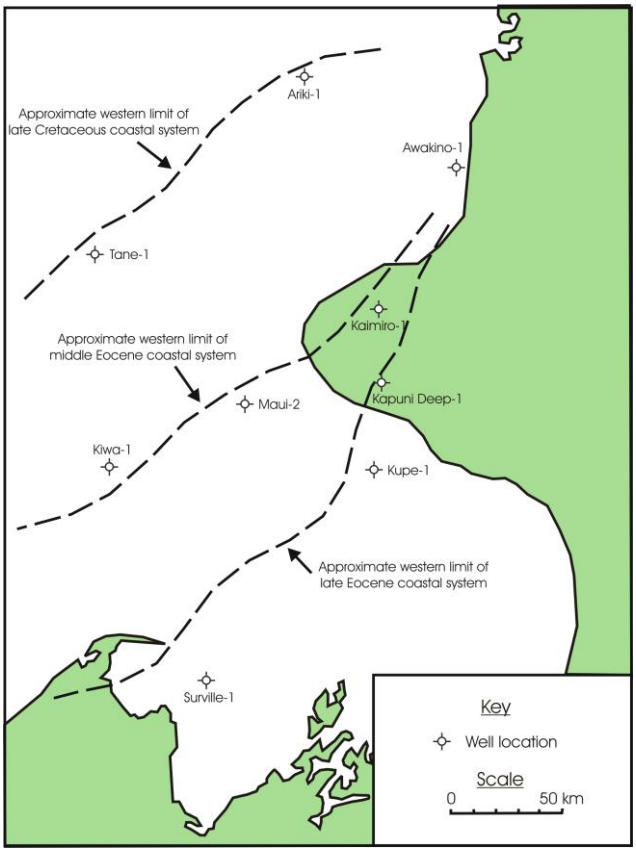

Figure 8.12: Extent of the Late Cretaceous to Eocene southeastward transgression.

During the early to middle Eocene fault activity was low, however synsedimentary faults did occur along the Cape Egmont Fault Zone, probably related to crustal events elsewhere in New Zealand (Knox, 1982). The Tane Member shows 'bowing', the result of post-rift sagging, the overlying unit infills the synform, thinning towards the basins edge where it onlaps an unconformity surface (King and Thrasher, 1996).

The latest Eocene-early Oligocene heralds the end of the Taranaki Basins extensional phase and the beginning of compressive tectonics in response to the developing

Australia-Pacific plate boundary. Folding occurred, producing a series of north-south trending anticlines, with thinning of sequences located on the crests (Palmer, 1985). It is feasible that the slow rates of sedimentation (1 $m.Myr^{-1}$) seen at Maui-2 represent erosion and subsequent deposition, however, a lack of data over this period prevents better distinction of events. The increase in sedimentation seen at Kiwa-1 and Kapuni Deep-1 may correspond to deposition of sediments eroded from anticlinal crests.

The change in the tectonic style is accompanied by a change in sedimentation style. In the south of the basin there is a break in the stratigraphic record from many wells (King and Thrasher, 1996). This depositional hiatus could be due to a lack of sediment supply, or conversely, due to erosion by deep bottom currents related to cooling in Antarctica (King and Robinson, 1988). The time-break coincides with the inferred onset of spreading in the Emerald Basin at 45 Ma. An alternative possibility is that the event was induced by uplift related to this event (King and Thrasher, 1996).

In the north of the basin the deposition of bathyal muds is interrupted by an influx of reworked Mesozoic sandstone. Uplift of the north end of the Taranaki Fault is inferred, as the eastern side of the fault constitutes the closest source of Mesozoic sediments (King and Thrasher, 1996).

8. 6. 4: Oligocene

When one looks at the geohistory plots for the Oligocene, it is obvious that a dramatic change in basin formation occurs in the Taranaki Basin. During the early Oligocene the Taranaki Basins is almost completely submerged (Fig. 8.13), and sedimentation changes from clastic to thin successions, dominated by calcareous deposits (Palmer and Andrews, 1993). As mentioned earlier, the latest Eocene-Oligocene signals the end of passive thermal-decay subsidence related to events in the Cretaceous, with the introduction of subsidence caused by tectonic forcing factors, which in most areas, is not immediately accompanied by sedimentation.

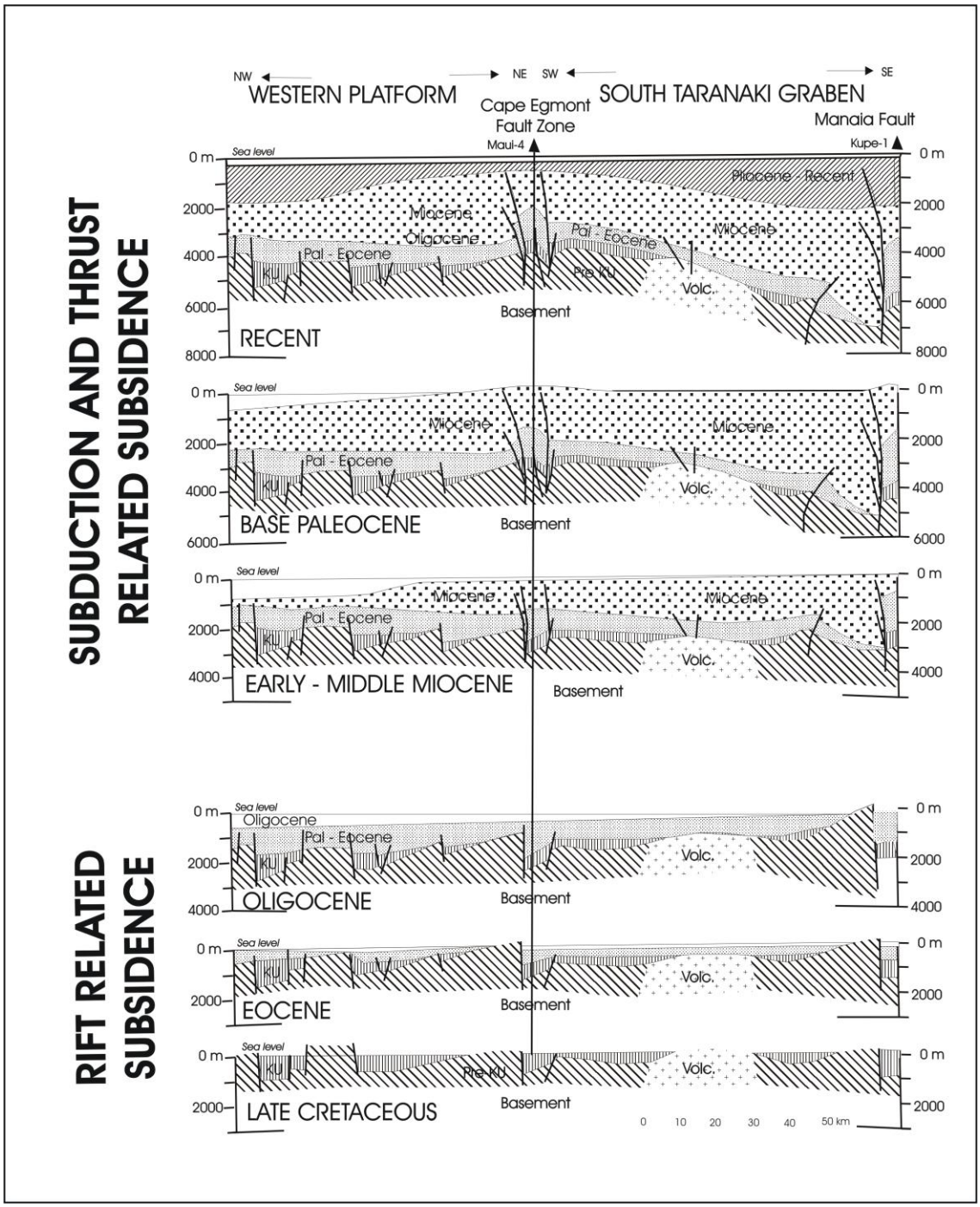

Figure 8.13: Reconstruction showing the magintude and distribution of subsidence. The figure clearly demonstrates the change from localised rift related to subsidence to region platform subsidence related to subduction. (From Pilaar and Wakefield, 1978).

The change in the tectonic regime is first seen in the west, with Tane-1 showing a dramatic increase in both subsidence and water-depth. King and Thrasher (1996) state that subsidence began in the north, moving south and east with time. If this is the case then Ariki-1 should be the first to show subsidence. This is possible, however this area is at bathyal depths both before and after the event, meaning large uncertainies probably prevent the event from being distinguished. At all other wells, with the exception of Kupe-1, the event takes place at 27.5 ± 2.5 Ma. At Kupe-1 and Surville-1, the two southernmost wells, the event doe not register as a change in water-depth. In the case of Surville-1 this is because the event at 28 Ma is accompanied by an increase in sedimentation, effectively filling the trough as it forms. At Kupe-1, where the event is not visible, King and Thrasher (1996) suggest that subsidence was counteracted by minor uplift along the Manaia Fault.

There are a number of theories accounting for the subsidence that occurs in Taranaki during the Oligocene, some complementary, others conflicting. Originally, King and Robinson (1988) attributed the subsidence to western down-throw on the Taranaki Fault, leading to the formation of a massive extensional half-graben. Calculations involving instantaneous poles of rotation suggests that the region was undergoing transpression at this time (Sutherland, 1995), not the extension required. Stern and Davey (1990) proposed that the subsidence was caused by isostatic loading, in response to the development of a westward propagating fold-thrust belt. If this were the sole reason for the subsidence one would expect the developing trough to spread westwards,rather than eastwards, as witnessed. The third hypothesis is that the subsidence was caused by mantle processes related to the onset of subduction along the Australian-Pacific plate boundary to the northeast of New Zealand (Stern and Holt, 1994). There is now general agreement that regional subsidence was caused by the onset of subduction, with local tectonic loading superimposed in places, predominately in the east of the basin close to the Taranaki Fault Zone. These theories will be discussed in greater detail in a following chapter.

8. 6. 5: Miocene

The tectonic condition which prevailed in the Miocene can best be described as variable. In the early Miocene movement along the Taranaki Fault Zone increased, with basement located to the east of the fault being thrust westward (King and Thrasher, 1996). This coincided with the emplacement of the Northland Allocthon (Isaac et. al., 1994). The increased load on the adjacent lithosphere lead to an increase in foreland subsidence and the northwestward propagation of a sedimentary wedge, commonly seen in foreland basin areas (Holt and Stern, 1994). On the geohistory plots the affects of this loading can be seen, with subsidence seen at all wells at this time. While uplift on the Taranaki Fault was well underway by the early Miocene, an increase in sedimentation is not seen on the geohistory plots for the region until 17.5 ± 1.5 Ma. The sudden increase in sedimentation may represent the subaerial emergence and subsequence erosion of providence regions previously below water (Holt and Stern, 1994). Palmer and Andrews (1993) also note a major influx of coarse sediment at this time, further evidence of emergence. From 14 ± 2 Ma local uplift on the Taranaki and associated fault systems dominates over regional subsidence, as seen as uplift on the geohistory plots for most wells. It is important to note, however, a built-in bias when using petroleum wells, as antiforms tend to be targeted due to trapping capabilities.

The compression causing this uplift in the region is thought to be related to the clockwise rotation of the Australia-Pacific plate boundary, due to the southward motion of the instantaneous pole of rotation (Sutherland, 1995). Tectonic reconstructions suggest that southward drift of the pole led to a south to southeastward shift in the focus of compression (King and Thrasher, 1996). A second hypothesis for this uplift is that the erosion of topography above sea level led to partial removal of the load over the thrust zone, resulting in limited rebound of the basin (Holt and Stern, 1994),

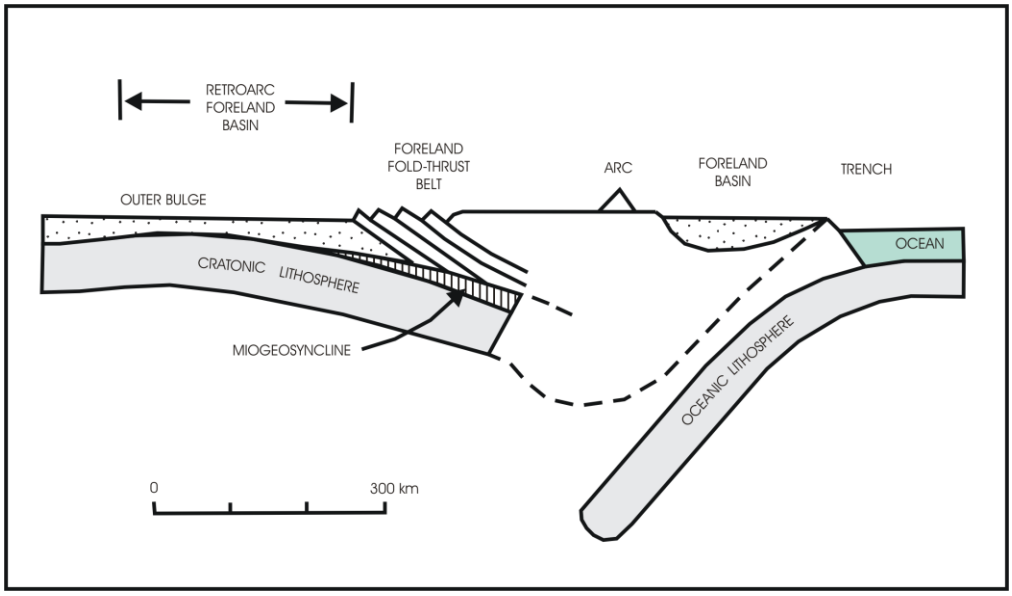

Figure 8.14: Model of the plate tectonic setting for a retroarc foreland basin (From Beaumont, 1981).

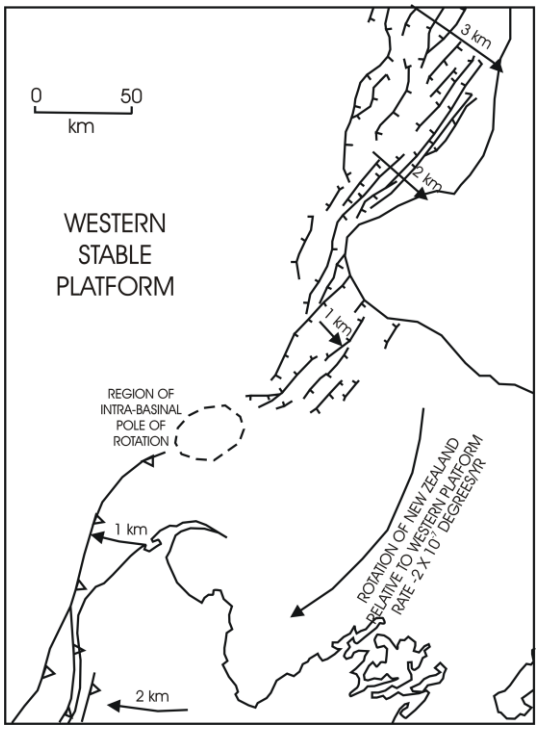

Figure 8.15: Schematic rotation model for post-Miocene horizontal deformation (From King and Thrasher, 1996).

In the south this compression led to the reverse reactivation of previously normal faults, and the inversion of late Cretaceous half-grabens. The region where this crustal shortening occurred is known as the Southern Inversion Zone.

In the north the uplift again gave way to extension and basin subsidence by latest Miocene, once again due to the southward movement of the Australian-Pacific pole of rotation (King and Thrasher, 1996). Extension appears to have propagated south in a fan-like opening leading to the formation of the Northern and Central Grabens (King and Thrasher, 1996). Due to the location of the Central and Northern Grabens, behind an active magmatic arc or convergent mountain range, these two basins fit the Beaumont (1981) definition of a retroarc foreland basin (Fig. 8.14). This subsidence can be seen in the geohistory plots for Kaimiro-1, Kapuni Deep-1, possibly Kupe-1 and slightly later at Maui-2, Kiwa-1 and Tane-1. Possible extension in the north is accompanied by the onset of andesitic volcanism and the emplacement of the Mohakatino Volcanics (Palmer and Andrews, 1993). The focus of volcanism moved south with time, the product of intra-arc magmatism derived from the subduction of the Pacific Plate beneath the Australian Plate (King and Thrasher, 1996).

8. 6. 6: Pliocene to Recent

The tectonics of the region continued to be shaped by deformation on the plate boundary in the Pliocene. While reverse faulting continued on some faults in the Southern Inversion Zone, the Taranaki Basin generally underwent extension (Armstrong et. al., 1998). Extension continued in the north, however many areas especially in the northeast underwent uplift and erosion due to regional tilting (King and Thrasher, 1996).

Miocene to Pliocene rocks in the region typically show a 2-4° southwest structural dip,towards an area of subsidence in the South Wanganui Basin (Armstrong et. al., 1998). Two possible mechanisms have been suggested for the observed tilting and subsidence, thermal uplift and flexural tilting. Porosity analysis (Fig. 8.16) show that exhumation increases towards the center of the North Island (Pulford and Stern, 2004), towards the southern apex of the Central Volcanic Region, an area renowned for a thin crust, high heat flow and extension (Stern, 1987). While uplift due to high heat flow explains the pattern of exhumation, it fails to explain the subsidence in the South Wanganui Basin. Modeling suggest a more likely mechanism, flexural tilting. Results suggest that tilting and

subsidence patterns can be explained by the slab-pull force of the subducting slab on the overriding plate (Stern et. al., 1992).

High sedimentation, as seen on all geohistory plots except Surville-1 and Awakino-1 can be explained by an increased clastic supply from rapidly rising sources areas to the south and east of the region and to an increase in accommodation space due to subsidence. In the regions to the east of the Cape Egmont Fault Zone this space is created by tectonic deformation, while to the west it is solely the result of sediment loading (Holt and Stern, 1991). Surville-1, the southern most well shows little subsidence or accumulation likely due to its position in the Southern Inversion Zone. At Awakino-1 the affects are also less pronounced, this is probably due to its northeasterly location, resulting in higher uplift due to flexural tilting explained above.

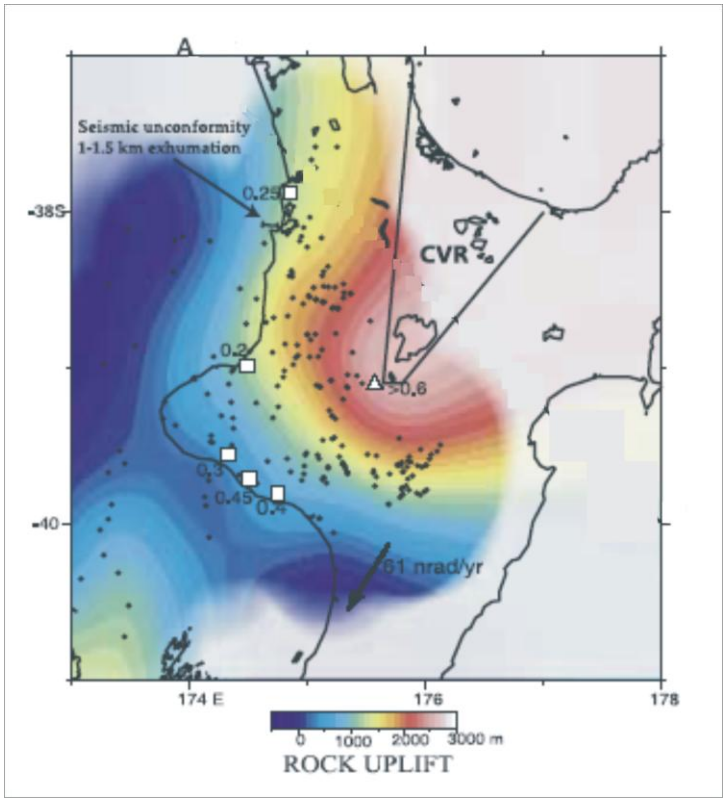

Figure 8.16: Rock uplift calculated from surface and exhumation. Black points are constrained by both surface and exhumation data. (From Pulford and Stern, 2004).

8. 7: BETA VALUES

As a general rule, the β values decrease to the south-west of the region, however, the highest β (2.1 ± 0.1) are located on Taranaki Peninsula, adjacent to the Tarata Thrust Zone. Compressive forces subsequently thickened this region during the Miocene, this combined with the eruption of volcanic deposits resulted in subaerial exposure. The contours of the β values, shown in figure 8.17, approximately follow the isopach thicknesses of the Cretaceous to early Paleogene basin (King and Thrasher, 1996).

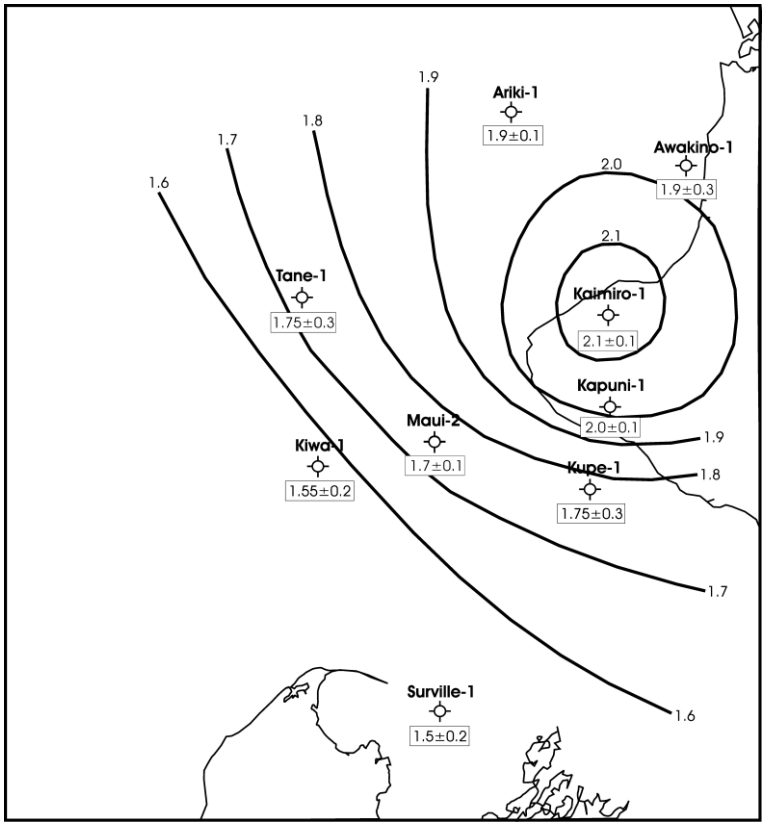

Figure 8.17: Map showing beta values calculated by this study. The distribution of contours approximately matches the shape of the Cretaceous to early Paleogene basin.

The β values calculated in this investigation compare well with β values calculated by Holt and Stern (1991). Their β values ranged from 1.5 to 2, meaning that crust on the Western Platform, which is now 25 to 30 km thick (Stern and Davey, 1990) was originally 40-55 km thick.

8. 8: CONCLUSIONS

- Rifting related to break-up of Gondwana leads to extension in the Taranaki Basin beginning at 80 ± 5 Ma.
- Rifting is followed by thermal subsidence until 27.5 ± 2.5 Ma, where a dramatic increase in water-depth occurs. It is likely this platform subsidence event is due to subduction related mantle flow.
- Subsidence at 27.5 ± 2.5 Ma appears to begin in the north, moving south and east with time.
- An increase in sedimentation occurs at 17.5 ± 1.5 Ma, representing the emergence of the Taranaki Fault Zone and subsequence subaerial erosion, resulting in the formation of a geohistory curve with a typical 'foreland basin' shape.
- Local uplift dominates over regional subsidence at the well sites from 14 ± 2 Ma.
- β values in the Taranaki Basin range from 1.5 to 2.1, implying crustal thickness prior to rifting was between 40 and 55 km thick.

CHAPTER 9: NORTHLAND BASIN

9. 1: INTRODUCTION

For the purpose of this study, the region of Northland extends north from latitude 37^{o} S ending at latitude 32^{o} S. Longitude 171^{o}42' E and 176^{o} E form the remaining boundaries of the region (Fig. 9.1). Included within this rectangle is the Northland Peninsula, which extends northwest 340 km from Auckland. In the east of the peninsula basement terranes outcrop, while 3-4 km thick sediment successions have accumulated to the west. Further offshore maximum sediment thickness exceeds 8 km. It is generally accepted that the west Northland region is part of a continuous sedimentary basin that includes hydrocarbon producing offshore Taranaki (Fig. 8.1). Despite this, the Northland region is largely unexplored, penetrated by only two post-1970 wells, Northland-1 and Waimamaku-2, of which Northland-1 was contaminated by slumping during the drilling process.

9. 2: STRATIGRAPHY

Due to the complex nature of Northland's geology, the stratigraphy will be broken into three sections: an autochthonous sequence, and allochthonous sequence and a post allochthonous sequence. The emplacement of these will be explained in further detail in this chapter.

9. 2. 1: The Autochthonous sequence

9. 2. 1. 1: The Houhora Complex

Located mainly in northern Northland, the Houhora Complex includes indurated sandstones, interbedded sandstone and mudstone, and conglomerate. The volcanic sequence includes basaltic flow deposits, rhyolitic volcanoclastic deposits, basaltic dykes and granophyric diorite intrustions (Issac, et. al, 1988). Deposition occurred in a marine basin, which had a continental source. Rhyolitic pyroclastics erupted in an adjacent subaerial region, and were emplaced by submarine pyroclastic flows (Hayward et. al., 1989). A Cretaceous age is suggested by the rare occurrence of *Inoceramus* fossils (Hayward et. al., 1989).

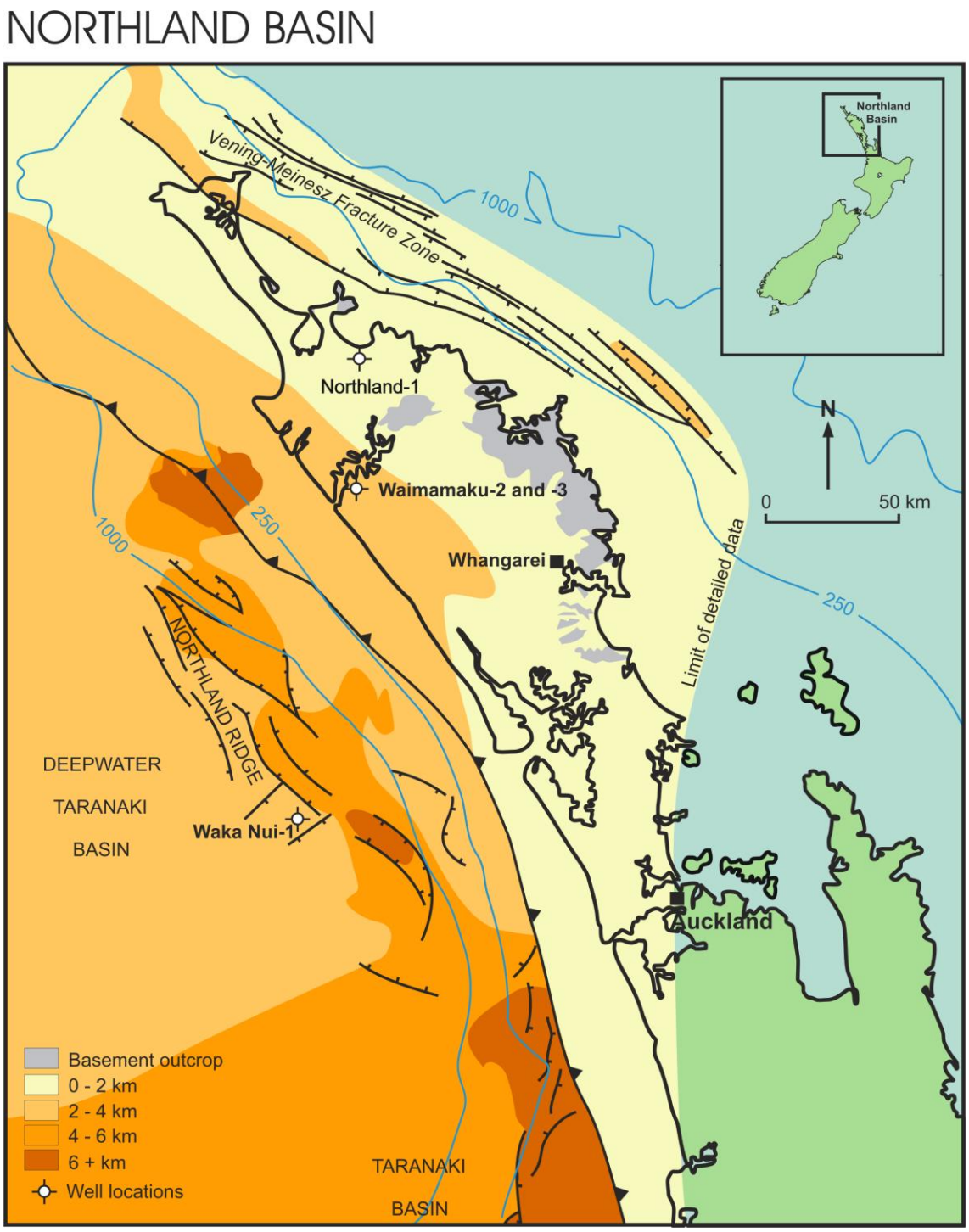

Figure 9. 1: Map of the Northland region, showing the location of wells, sedimentary thickness and major faults (From Explore New Zealand Petroleum 2003, Ministry of Economic Development, Crown Minerals, 2003).

Line 72-151 and 72-141

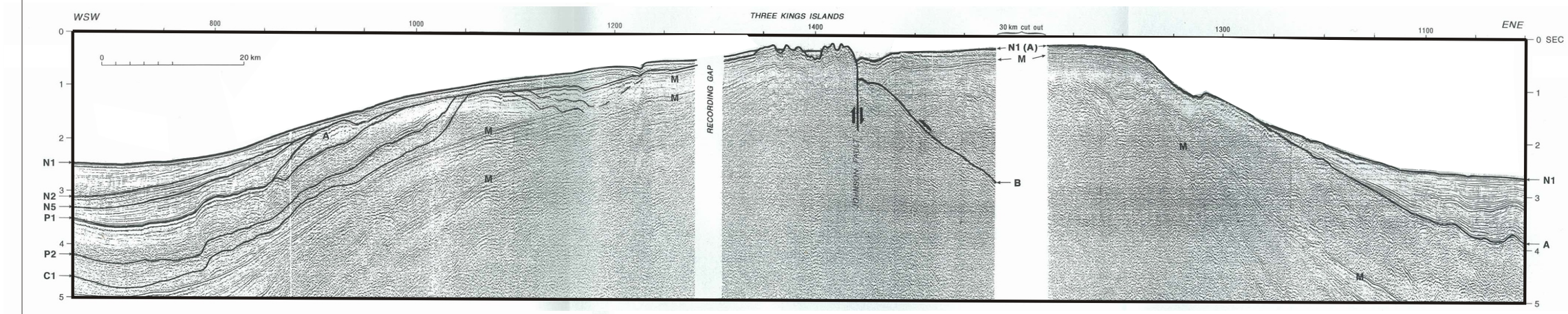

Figure **9. 2:** Seismic profile showing the Northland Allochthon.

This profile shows the Three Kings - Mount Camel basement high (centre) and thrust on it, the Northland Allochthon (right). The Northland Allochthon (top reflector A) is distinguished by the highly disrupted reflectors overlying a basal (B) and a higher decollement.
The reflectors labelled M are multiples.
(Isaac et. al., 1994)

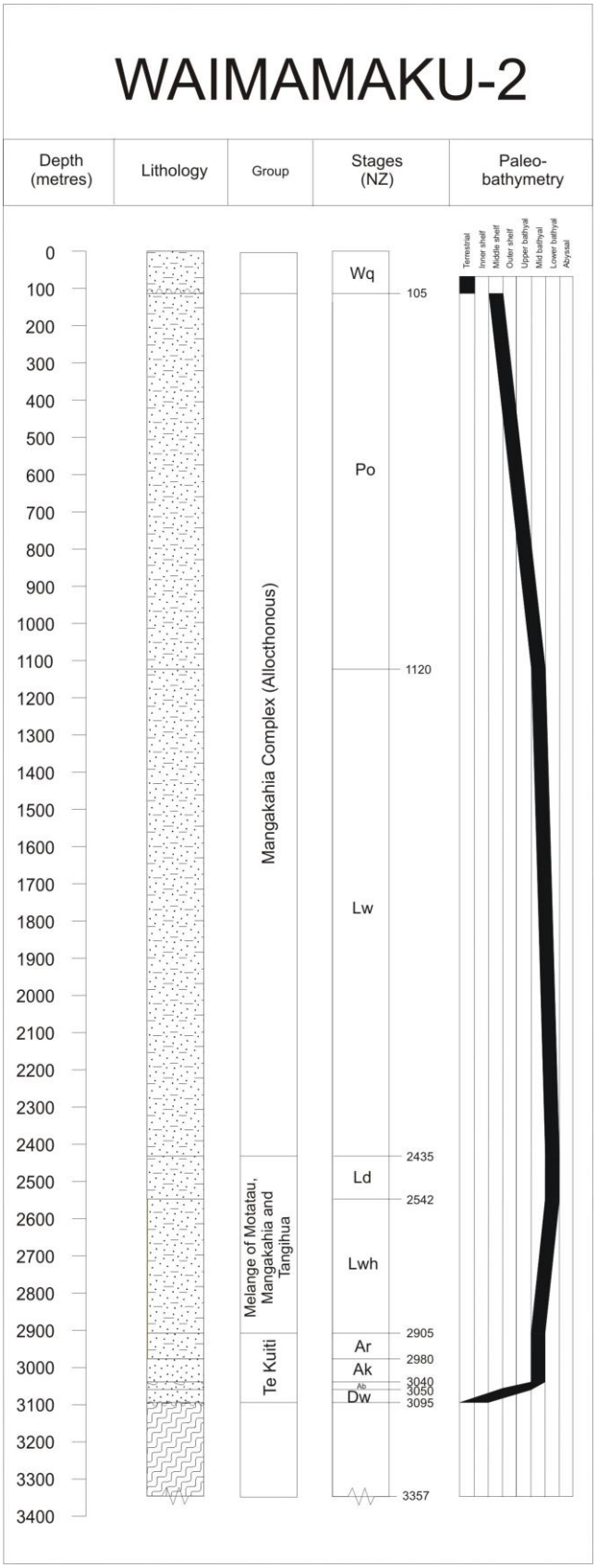

Figure 9.3: Stratigraphic column for Waimamaku-2, typical of the allochthonous region of Northland, New Zealand.

9. 2. 1. 2: The Te Kuiti Group

In the north and east, the Te Kuiti Group overlies pre-Cretaceous basement (Fig. 9.3), however, in the northwest, the group overlies Cretaceous to Paleocene sediments as seen in the Waimamaku-2 drillhole. In eastern Northland late Eocene coal measures, which include basement sourced sandstone and conglomerate, are overlain by and in places interfingered with calcareous and glauconitic sandstone (Gilbert et. al., 1989)). Atop of this is an Oligocene limestone, which in places onlaps basement highs. A fluvial environment is inferred for the deposition of the coal measures, with an increasing marine influence to the west. The sea encroached with the deposition of the sandstone, reaching an inner shelf depth by the deposition of the limestone (Hayward et. al., 1989)

In northern and western Northland the Te Kuiti sequence consists of bedded mid to late Eocene sandstones, which have a glauconitic component. Conformably overlying the sandstone is a calcareous mudstone, which indicates late Eocene subsidence from mid shelf to upper bathyal depth (Hayward et. al., 1989)

9. 2. 1. 3: Offshore western Northland

The geology off the west coast of Northland is known only from seismic profiles, and by comparisons with the contiguous Taranaki Basin. Data indicate the presence of an autochthonous sequence of Cretaceous coal measures, overlain by 1 to 2.5 km of Paleocene to Eocene deep bathyal, fine grained mudstones, similar to those seen in northern Taranaki (Hayward, 1987a). A fine grained, bathyal biogenic limestone can be traced north on seismic profiles, from northern Taranaki into Northland. This is overlain by Miocene volcanics off the Waitakere Ranges, Kaipara and the Waipoua areas (Hayward, 1987b).

9. 2. 2: The Allochthonous sequence

Poor exposures and a complicated structure prevent accurate descriptions of original sequences; for this reason the rocks of the allochthonous sequence are grouped into four complexes.

9. 2. 2. 1: The Tupou Complex

The Tupou complex consists of strongly deformed sandstones, interbedded sand and mudstones, and of conglomerates . The complex is jointed in many places, and layer-parallel shear and boudinage is common (Brook and Hayward, 1989). The unit accumulated in a marine setting adjacent to a landmass, with sediment deposited by gravity flows . An early Cretaceous age is inferred from a single *Aucellina euglypha* fossil (Isaac et. al., 1994). It is thought that this unit represents displaced youngest basement rocks (Brook and Hayward, 1989).

9. 2. 2. 2: The Tangihua Complex

The Tangihua Complex is thought to be early Cretaceous to Paleocene in age. It consists of a submarine basalt with dolerite and gabbro intrustions (Parker et. al., 1989)). Minor pelagic mudstone and micritic limestones are also present. The complex is cut by numerous faults and sub-parallel to bedding shear zones (Larsen and Sporli, 1989).

9. 2. 2. 3: The Mangakahia Complex.

Rocks pertaining to the Mangakahia Complex are abundant in the allochthonous sequences of Northland. The complex, thought to be of late Cretaceous to Eocene in age, consists of four major lithofacies: A clastic flysch association, a siliceous mudstone, a muddy limestone and a non-calcareous mudstone. The complex shows a general fining upwards trend, interpreted as basinal deepening, with depths increasing from outer shelf conditions to bathyal to possibly abyssal (Hayward et. al., 1989).

9. 2. 2. 4: The Motatau Complex

Again abundant in the allochthonous sequence, the Motatau Complex consists of early Eocene to early Miocene carbonate rich mudstones and limestones. Sediments were deposited above the CCD, and the decreasing terrigeous content is thought to represent a reduction in areal extent and relief of subaerial source areas (Hayward et. al., 1989). Lithologically similar to the underlying Mangakaia Complex, the base of the Motatau also shows an overlay in the age of deposition. Due to this it is thought the two complexes accumulated in stratigraphic succession (Isaac et. al., 1994).

9. 2. 3: The post-allochthonous sequence

9. 2. 3. 1: The Akarana Supergroup

This Supergroup unconformably overlies the allochthonous units of Northland. In the far north latest Oligocene shallow water bioclastic and lithic breccia are overlain by early Miocene mudstone, which is interbedded with tuff and andesitic volcanoclastic deposits (Brook and Thrasher, 1991). Upwardly shallowing andesitic conglomerate and sandstone are then located stratigraphically above.

In the region surrounding Whangarei the allochthonous and autochthonous units are cut by early Miocene dykes and intrusions (Smith et. al., 1986). Deposited ontop are terrestrial and localized lacustrine deposits and predominately coarse grained andesitic volcaniclastic deposits (Brook and Thrasher, 1991).

In the vicinity of Hokianga, the units are overlain by early Miocene shelfal deposits, while in southern Northland early Miocene bathyal flysch deposits are found (Isaac et. al, 1994)

9. 3: LOCATION OF WELL

Well	Lat/Long	Date spudded
Waimamaku-2	173˚ 28’ 1.7” E 35˚ 34’ 9.5” S	1972

Table 9. 1: Location and age of Waimamaku-2 petroleum well used for this study.

9. 4: QUALITY OF DATA FROM WELLS

The data compiled in the following chapter was gathered from the individual well completion reports available on the Crown Minerals website. Age and paleobathymetic estimations are based on foraminifera and macrofossils. Seismic correlation between laterally continuous units found in the Taranaki Basin is also used. Rather than providing an overall view, it is important to note that a lack of wells in the region will have resulted in a biased analysis of basin development. Waimamaku-2 was drilled to basement.

9. 5: RESULTS

The geohistory of Waimamaku-2, the only well studied in the Northland region, is provided in figure 9.4.

9. 5. 1: Waimamaku-2

Deposition began at Waimamaku-2 during the Waipawan (55 Ma). Initially sedimentation did not keep up with subsidence, with the area subsiding at up to 130 $m.Myr^{-1}$, while sedimentation was at less than 6 $m.Myr^{-1}$. There was an increase in the rate of deposition at 37 Ma, and another dramatic increase at 25 Ma, where rates increased to almost 500 $m.Myr^{-1}$ for a period of 4 Myr. Following a plateau during the late Eocene to early Oligocene subsidence increased again at 34 Ma. This was accompanied by a decrease in water depth from lower bathyal to upper middle bathyal. Following the rapid increase in sedimentation at 25 Ma, both sedimentation and subsidence slowed before an unconformity removed much of the rocks pertaining to the Miocene.

Assuming 85 m of subsidence between 37 and 34 Ma, a β value of 1.8 ± 0.1 was calculated based on McKenzie's (1978) model.

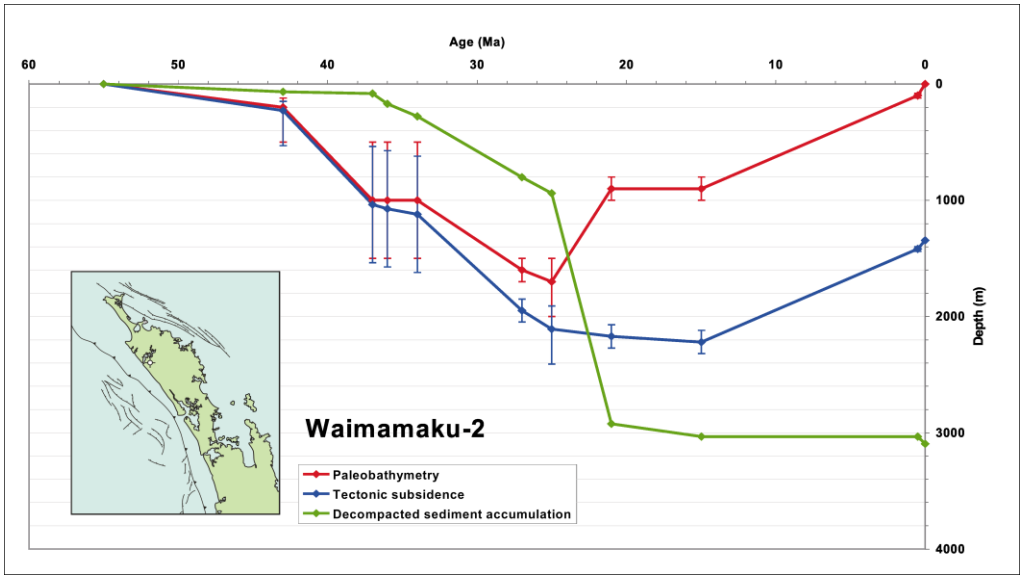

Figure 9.4: Geohistory plot for Waimamaku-2, Northland, New Zealand.

9. 6: INTERPRETATION AND DISCUSSION

Figure 9.5 shows a total subsidence curve characteristic of the Northland well. Thermal subsidence follows rifting, initially subsidence was initially faster than sedimentation. During the early Miocene the emplacement of the Northland Allochthon occurred, represented by the sudden increase in subsidence seen at 25 Ma. Erosion from the adjoining landmass led to a decrease in water depth seen from ~15 Ma.

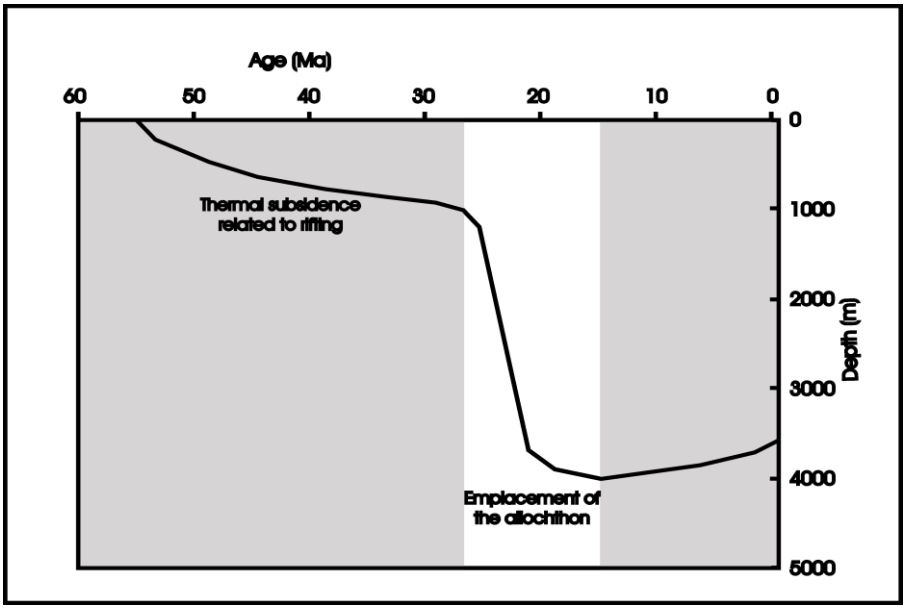

Figure 9.5: Characteristic total subsidence curve for the Northland region.

9. 6. 1: Early to late Cretaceous

Pre-Cretaceous rocks were severely deformed during an early Cretaceous period of south to southwest-directed accretion and overthrusting. Initial rifting in the Northland Basin is thought to have begun at 95-110 Ma., prior to spreading in the Tasman Sea (Isaac et. al, 1994), however without a number of exploration wells it is difficult to derive the exact timing of extension. The subsidence history for some of the region has been determined from seismic investigations (Isaac et. al., 1994), which suggests rifting began at ~100 Ma, however this subsidence is not preserved at Waimamaku-2.

A second period of faulting during the late Cretaceous further complicates the matter. As explained in the previous chapter the Taranaki Rift System formed in response to rifting in the New Caledonia Basin. Isaac et. al. (1994) proposed the presence of a bounding fault, located west of and parallel to the present day Northland Peninsula. They suggest that this fault, orientated NNW, approximately parallel to the axis of spreading, accommodated extension, with uplift to the northeast, rather than strike-slip seen in Taranaki. They cite several lines of evidence adding credibility to this hypothesis. Seismic sections west of the present day coastline show high amplitude, parallel reflectors, which dip to the south and southwest, inferred to be submarine fans. Geometry and sediment volumes in these structures suggest the presence of a rapidly eroding high-standing landmass to the east. A lack of Cretaceous deposits located on the Northland Peninsula suggest uplift to the east of the inferred fault. The depth to basement varies widely across the basin. Near south Manakau basement was reached at 340m, while on 40 km offshore the depth to basement is 4200 m. At Waimamaku-2 basement was struck at 2942 m, while 50 km to the west it is located at over 8000 m below sea level. The presence of diffraction hyperbole in unmigrated seismic sections also suggest the presence of a major fault.

Sedimentation during the Cretaceous occurred primarily in fault controlled basins (Brook and Thrasher, 1991). Trangression during the late Cretaceous lead to the submergence of low lying land, and the formation of numerous islands, which show erosion surfaces (Isaac et. al, 1994). Bourma Sequences suggest sediments were deposited by gravity flow mechanisms, in fans located in a slope or bathyal setting. A

second phase of faulting occurred during the latest Cretaceous, reactivating and lengthening existing faults, and creating new ones (Isaac et. al., 1994).

9. 6. 2: Paleocene

Thermal subsidence dominates in the Paleocene, following the rifting of the Cretaceous. By the Paleocene most uplifted fault blocks had been drowned by sediments, and a thin sedimentary succession was deposited over most of the region (Isaac et. al., 1994). A single broad basin formed, accumulating more than 1200 m of sediment, with a long axis close to the present day coastline. Isaac et. al. (1994) suggest the basin was the result of a delta or submarine fan rather than by faulting as the long axis only partially overlaps with basin sedimentation of the Cretaceous.

Transgression continued into the Paleocene, with inundation of coastal plains surrounding the Cretaceous landmass, and the deposition of paralic coal measures. Sedimentation slowed (Hayward et. al., 1989), probably the result of erosion creating a more subdued topography. Further offshore glauconitic sandstones and anoxic mudstones suggest poor oceanic circulation (Hayward et. al., 1989).

9. 6. 3: Eocene

There appears to have been no faulting to the west of the landmass during the Eocene. Subsidence and sedimentation continued, with the last Cretaceous high buried. The Paleocene depo-center moved northwards, in response to the formation of a northward-draining fluvial system (Isaac et. al., 1994). A number of shallow depo-centers formed a belt west of the present coastline, and shallow shelf sandstones were overlain by conformable bathyal mudstones (Isaac et. al., 1994), indicating that transgression continued. Deposition of the Avoca Coal Measures may have occurred on the northeastern margin of the landmass, however a lack of other coal measures in the region suggests they accumulated on the west coast, later to be incorporated into the Northland Allocthon (Issac et. al, 1994). This hypothesis requires exposure or near exposure during Miocene thrusting, which is consistent with slow sedimentation during the Oligocene.

A dissected landmass persisted from present-day eastern Northland to the Coromandel Peninsula (Hayward et. al., 1994). Faulting suggests a minor reactivation of tectonism, which resulted in the formation of half grabens, and the likely deposition of sediment at Waimamaku-2. This may have been the result of changes in the Pacific Plate vector at this time (Isaac et. al., 1994). These grabens filled with terrestrial material deposited by a west draining fluvial system, eventually becoming the Kamo Coal Measures. This is then overlain by glauconitic shelf sandstones (Isaac et. al., 1994). South of Auckland a northward draining river deposited the Waikato Coal Measures.

East of the landmass stable bathyal to abbsysal conditions prevailed, with calcareous muds accumulating. Hayward et. al., (1989) suggest strong bottom currents prevent deposition in this area during the late Eocene. However a planar truncation surface suggest that this maybe due to marine regression (Isacc et. al., 1994).

9. 6. 4: Oligocene

Changes in plate tectonics during the Oligocene appear to have little effect on the Northland Basin, with gradual subsidence continuing. To New Zealand's northeast the opening of the South Fiji Basin began, magnetic anomalies suggest rifting occurred between 32 and 26 Ma. (Davey, 1982; Malahoff et. al., 1982). It is possible that the increase in subsidence and water depth seen at Waimamaku-2 at 34 Ma is related to these changes in the tectonic vectors at this time.

Deposition during the Oligocene was largely calcareous, and occurred in wide stable basins, most of which were under shelf or bathyal conditions. Sediment starvation in the basins and limestone deposition on the Coromandel Peninsula during the early to middle Oligocene suggest all or almost all of the region was submerged due to continued transgression (Sporli, 1989). This appears to contradict the fact that subduction to the north was required to start sufficiently early in the Oligocene to produce calc-alkaline magma for early Miocene eastern and western belt volcanics (Isaac et. al., 1994).

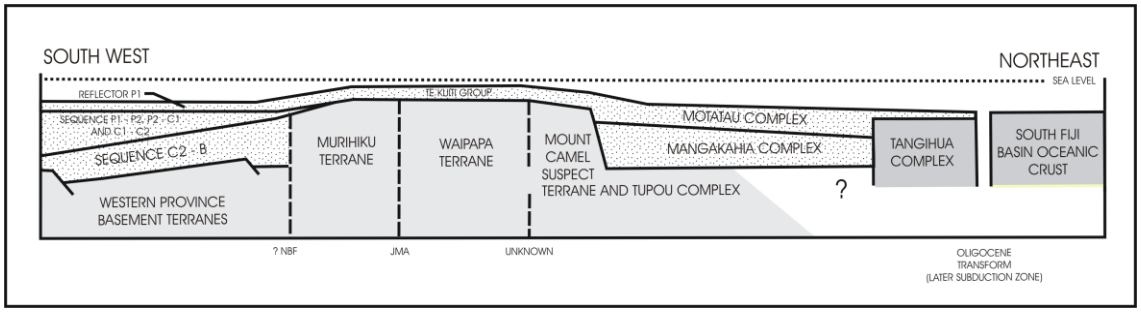

Figure 9.6: Schematic cross-section of Northland, showing extent and distribution of basement and Cretaceous-Cenozoic sediments prior to late Oligocene subduction and obduction. No scale is implied. (From Isaac et. al, 1994).

By latest Oligocene the affects of the developing convergent margin are seen. In places uplift and erosion occur (Hayward et. al., 1989), while the majority of the region rapidly subsides (Isaac et. al., 1994). This subsidence and faulting is likely the first indication of the evolving margin, with subsidence caused by the subducting plate dragging the region downwards (Isaac, 1994), providing a second possible cause of subsidence at Waimamaku-2. The distribution of terranes prior to the Miocene is shown in Fig. 9.6.

9. 6. 5: Miocene

After tens of millions of years of relative quiescence, the Northland region was turned into a major depocenter with widespread volcanism, uplift and erosion. The subduction zone to the north of New Zealand may have become choked during the late Oligocene, with the continued compression manifest as uplift in the northeast of the Northland region (Brook and Hayward, 1989). Forces associated with this continued compression created numerous large scale (up to 1 km thick, and 100 km across) nappes, each deformed by heterogeneous layer-parallel shear (Hayward, 1993). Emplacement of these nappes provides the likely cause of the rapid increase in sedimentation seen at Waimamaku-2, where sedimentation rates reached almost 500 $m.Myr^{-1}$.

Based on the age of overlying, underlying and incorporated sediments, it is known that during the early Miocene these fault bound nappes slid to the south and the southeast into a bathyal basin, primarily due to gravity. Emplacement of the nappes began in the north, progressing south with time (Fig 9.7). Southern subsidence is likely due to

loading, and to the subducting slab pulling the overriding plate downwards (Hayward et. al., 1989).

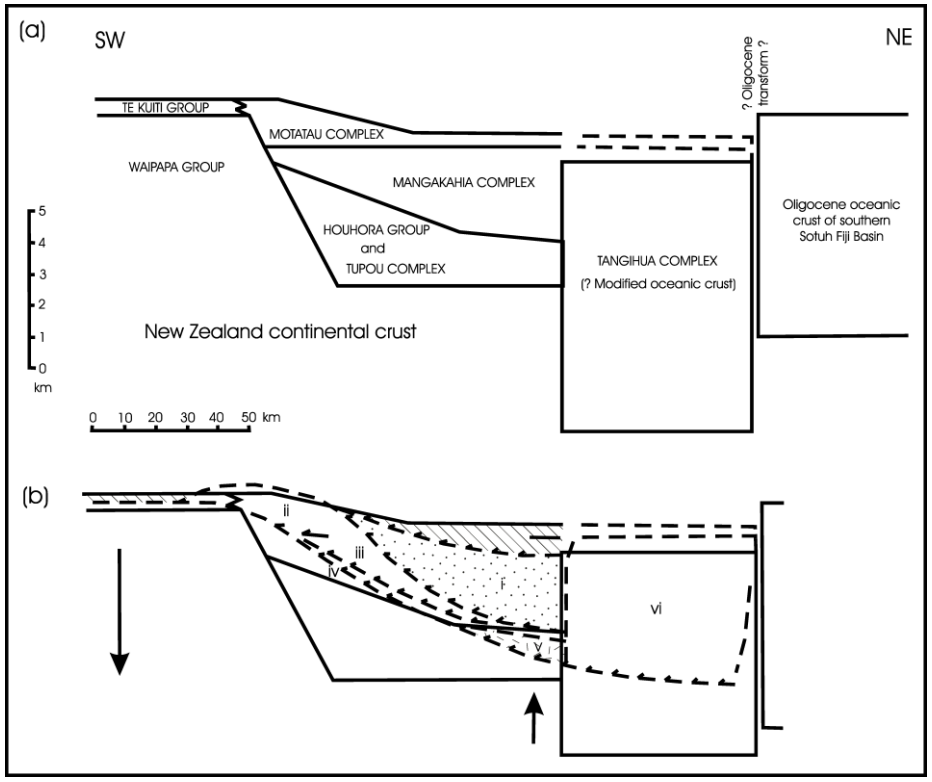

Figure 9.7: Schematic cross-section through northern Northland, showing inferred origin of nappes involved in the Allochthon movement. (From Brook and Hayward, 1989).

A Inferred stratigraphy prior to nappe emplacement.

B Uplift in the north results in nappes 'sliding' south. Roman numerals denote the order of emplacement.

Shelf and upper bathyal marine deposits accumulated in 'piggy back' basins, on top of the still moving allocthon (Brook and Thrasher, 1991). These basins, including the Parengarenga and Otaua basins later became incorporated into the allocthon (Hayward, 1993). By the middle of the Otaian the southern front of the allocthon had reached Kaipara, with the Waitemata depocentre forming to the south of this, in the region of Auckland (Hayward, 1993). A second pulse of tectonism during the latest Otaian led to renewed uplift in the north, and further thrusting and nappe emplacement (Hayward, 1993).

9. 6. 6: Pliocene to Recent

During this period clastic sediment was eroded from a landmass similar to the present-day Northland peninsula. These sediments accumulated on a western continental shelf, in embayments and in basins between partially buried volcanic blocks. Sedimentation was greater in the south, but was redistributed to some extent, by long shore drift, which created a series of well developed canyons and slope channel systems.

Onshore subaerial basalts flowed onto the allochthonous rocks near Kerikeri. Tilting occurred over large areas. In the far north planed surfaces were exposed with southwest tilting. Normal faulting related to the development of the Taupo Volcanic Zone was occurring at this time.

9. 6. 7: Beta values

A β value of 1.8 ± 0.1 was calculated for the Northland region; unfortunately this was based on the subsidence history of one well. Horspool et. al. (2006) interpreted shearwave velocities for the region, and gave a crustal thickness of 26 ± 1 km for the area. This means that prior to rifting the crust in Northland was ~45 km thick, similar to values estimated for the adjoining Taranaki Basin.

9. 7: CONCLUSIONS

- The Northland Basin initially shows a signature typical of thermal subsidence, which followed rifting beginning at ~100 Ma.
- The geohistory plot for Waimamaku-2 is dominated by the emplacement of the Northland Allochthon, a series of nappes emplaced from the southwest during the earliest Miocene.
- The basin gradually filled from ~15 Ma, as sediment eroded from the adjacent landmass was redeposited by long shore drift.
- A β value of 1.8 ± 0.1 was calculated for Waimamaku-2. This suggests that the initial crustal thickness prior to rifting was ~45 km, within the range of values calculated for the adjoining Taranaki Basin.

CHAPTER 10: DISCUSSION

The following chapter revisits a number of points raised in the discussion section of individual basin chapters, combining data from other basins. The subjects that are elaborated on are:

- The development of the southern Boundary during the Eocene
- Possible convergence on the Alpine Fault at 19 Ma
- The nature of the Marshall Paraconformity evident in a number of South Island wells
- Mechanical properties of the Northland crust, determined by load induced subsidence
- The possibility of platform subsidence affecting the West Coast
- A summary of β values from basins surrounding New Zealand.

10. 1 DEVELOPMENT OF THE SOUTHERN BOUNDARY

The geohistory plots for the Great South Basin are dominated by a rapid subsidence event (with a rate of 190 $m.Myr^{-1}$ at Pakaha-1) beginning at 51 ± 2 Ma. Due to the timing of this subsidence, it is assumed that it is related to rifting in the Emerald Basin, and the formation of the southern Australian-Pacific boundary. Fortunately, the Eocene-Miocene sea floor south of New Zealand still exists, constraining the development of the Southeast Tasman Oceanic Crust (STOC).

The STOC is a triangular portion of crust created as the result of Eocene spreading along the Macquarie Ridge system (Figure 10.1). Changes in the Tasman region near the end of the Paleocene resulted in the reorganization of plate boundaries (Weissel, et. al., 1977). Rifting ceased along the Tasman Ridge at 53 Ma (Weissel et. al.,1977), allowing for the propagation of a spreading ridge south of New Zealand. The geometry of the feature suggests it was influenced by existing faults of the Emerald Fracture Zone, transform faults of the Tasman Ridge. It has been suggested that significant differences in mechanical properties between the two sides of these faults, combined

with movement of the pole of rotation may have induced rifting (Wood, et. al., 1996; Sutherland et. al., 2000).

Cessation of rifting in the Tasman is well constrained. However, the onset of the next phase of rifting is less well constrained. Identification of magnetic anomaly 22 (50 Ma) adjacent to the southwestern margin of the STOC by Weissel et. al. 1977, has been considered by Lawver and Gahagan (1994), who reinterpreted the sequence, including anomaly 24 (53 Ma). The distinctive geometry of the rift margins allows for reconstruction, based on a three-plate model. Sutherland's (1995) reconstruction closes the rift at 45 ± 5 Ma, prior to anomaly 18 (42 Ma). Wood et. al. (1996), identified anomaly 18 as the oldest sea floor, however, this was located to the northeast of the previous studies. This decrease in age adjacent to the boundary indicates that the ridge propagated north along the transform.

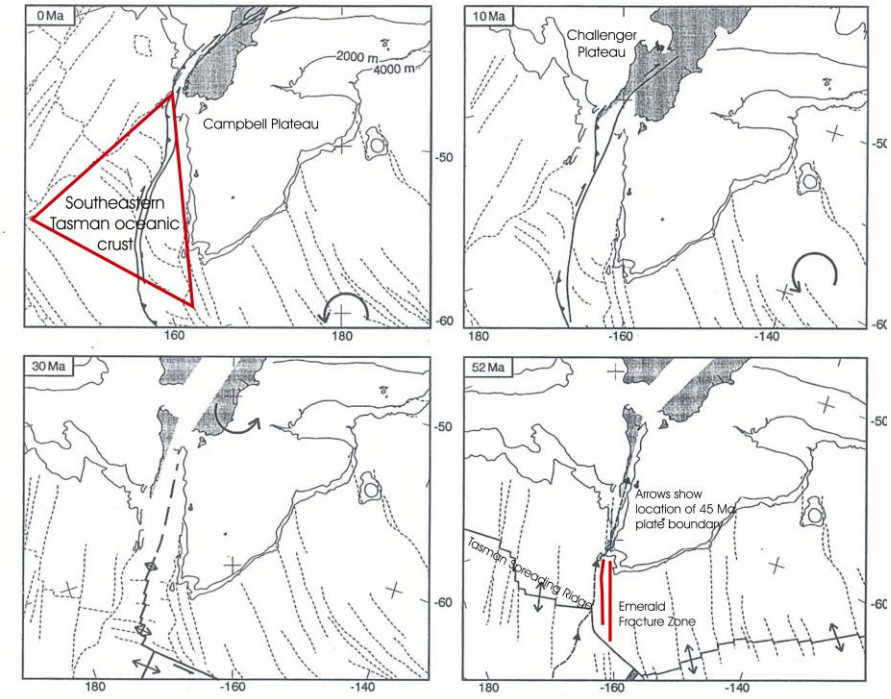

Figure 10.1: Cenozoic plate reconstructions of southern New Zealand (From Sutherland, 1995). Active boundaries are shown in bold, while dash lines show satellite-derived fracture zones. Circular arrow shows the approximate location of the instantaneous rotation pole for Australia-Pacific boundary

Data complied by this study show an increase in tectonic subsidence at 51 ± 2 Ma, approximately coinciding with two major tectonic events in the Tasman region. First,

the end of spreading along the Tasman Ridge at 53 Ma, and second, the northward propagation of Australia-Pacific boundary. It is plausible that the event seen in the subsidence curves represents the onset of tensional forces, rather than the formation of sea floor. In either case, it appears that extensional forces came into play in the Great South Basin immediately following (~1-2 Myr) the conclusion of Tasman centered spreading, with the subsidence curves clearly showing a extensional signature from 51 ± 2 Ma. If this event represents sea-floor spreading, it adds weight to data complied by Lawver and Gahagan (1994), but it also falls within the range of error calculated by Sutherland (1995).

A second scenario for this Eocene event is supplied by Cook et. al. (1999). They propose that the subsidence is the result of dynamic topography. They envisage a mantle plume, present since the earlier Cretaceous rifting event, which die away during the Eocene resulting in 400-800 m of subsidence. While plausible, this suggestion requires further investigation.

10. 2: MOVEMENT ON THE ALPINE FAULT AT ~20 Ma

Many of the subsidence curves from the South Island show a gradual increase in sedimentation (e.g: The Canterbury Basin) from ~20 Ma. The presence of the Alpine Fault has played an important role in the geological evolution of the South Island; however, the timing of motion, particularly surface and rock uplift, on this dramatic feature is still debated in scientific circles (i.e: Molnar et. al., 1975; Stock and Molnar, 1982; Kamp, 1986; Bradshaw, 1989; Sutherland, 1995; King, 2000, Cande and Stock, 2004). This section will briefly summarize the major theories related to the motion on the Alpine Fault.

During the middle to late Eocene sea-floor spreading in the southern Tasman Sea marked the initial stages in the development of the Australia-Pacific plate boundary (Sutherland, 1995). Southeastern movement of the instantaneous pole caused spreading along the boundary to become more oblique with time (Sutherland, 1995)(Figure 10.2). At the same time, the Hikurangi subduction zone began to encroach upon northern New Zealand from the middle Oligocene (King, 2000). Formed as a transfer system, the Alpine Fault links two subduction zones of opposite polarity; the east-dipping Fiordland system to the south of New Zealand, and west-dipping Hikurangi system to the north (Norris et. al., 1990).

Inception of the Alpine Fault during the early Miocene is well constrained by changes in basin geometry (Sircombe and Kamp, 1998; Nathan et. al., 1986), the intrusion of a suite of lamprophyre dykes (Cooper et. al., 1987), and localized inversion of basins (Kamp et. al., 1996; Kamp et. al., 1999). The discussion, however, surrounding the timing of uplift initiation tends to fall within three major schools of thought. First, that of Walcott (1998), suggests that 90 km of shorting has occurred since 6.4 Ma, with only 25 km of shortening occurring in the 12 Myr prior to 6.4 Ma. Alternatively, Kamp et. al. (1996) suggests that a major phase of uplift related to compression on the Australia-Pacific boundary occurred from 13-8 Ma. Finally, that of Cande and Stock (2004), suggests there has been little change in the rate of convergence over the last 20 Myr.

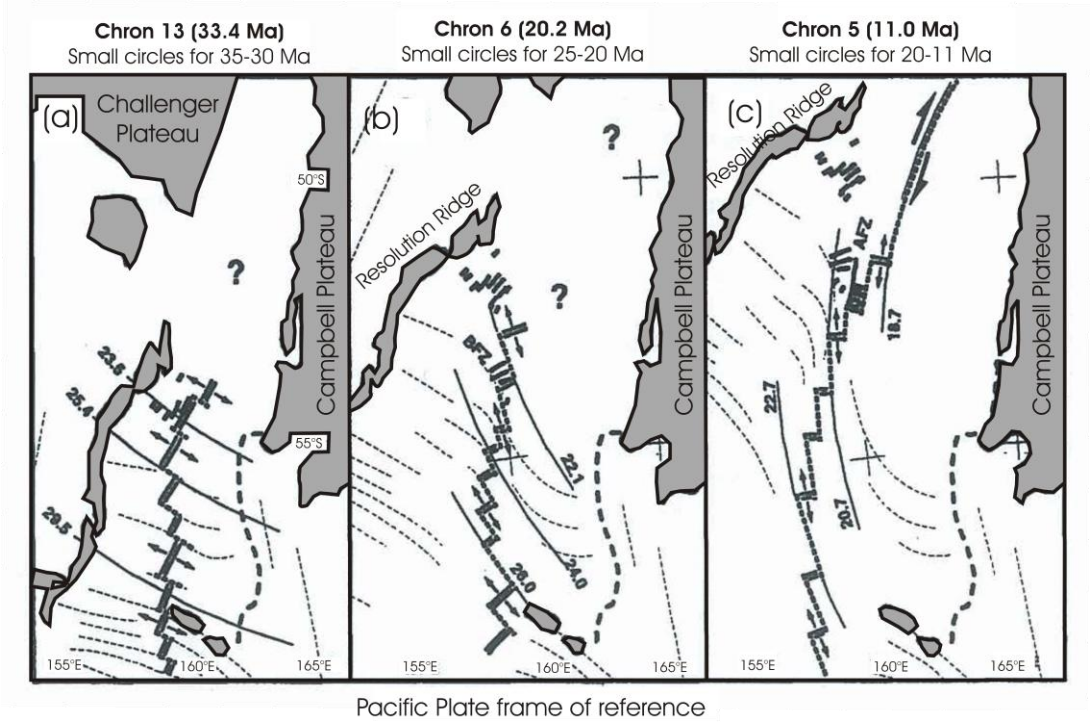

Figure 10.2: Tectonic reconstructions of the PAC-AUS plate boundary, showing the change from rifting to transcurrent motion. The change in orientation of fracture zone small circles document the southeastern migration of the boundary's instantaneous rotation pole. Grey areas, represent continental blocks and togographic highs. (From Lamarche et. al., 1997)

Based on a change in the sea-floor spreading direction highlighted by gravity anomalies, data presented by Walcott (1998) suggest that at 6.4 Ma a significant change in the relative motion of the Pacific and Australian plates resulted in the uplift of the Southern Alps. Interpretations of $^{40}Ar/^{39}Ar$, fission track and (U-Th)/He ages provided by Batt et. al. (2004) support Walcott's theory. Their data show two distinct phases of cooling, inferred to be due to exhumation. The first, which begins at 23-25 Ma is believed to be due to the inception of the Alpine Fault; resulting from uplift and exhumation of reactivated misaligned structures and at restraining bends. The second regional synchronous phase beginning at ~ 8 Ma, is assumed to be due to the previously mentioned changes in plate motion. Although obscured by marked cooling occurring from ~8 Ma, a prominent 5-6 Ma signal is observed in the $^{40}Ar/^{39}Ar$ age spectra of a number of samples, suggesting that structural adjustment to the new regime occurred over an extended period (Batt et. al., 2004)

Rather than representing a period of tectonic quiescence, the cessation of cooling between these two phases is construed to be the result of a progressive focus of deformation from an initially distributed regional network to discrete fault structures, primarily the Alpine Fault. A northward shift in the plate motion of the Pacific plate relative to the North American plate is thought to have occurred at this time (Atwater and Stock, 1998), providing further support for this theory.

Using fission track and vitrinite reflectance data from the Buller Coalfield, Kamp et. al. (1996), created a thermal history for the region. Interpretations of the data suggest two compressional phases. The first, which lasted from 24-19 Ma is likely related to the inception of the through-going boundary, and corresponds with an increase in terrigenous sediment. The second compressional phase, lasting from 13-9 Ma, is assumed by the authors to represent the initiation of convergence between the two plates. Similar data has been collected in the Greymouth coalfield. Kamp et. al. (1999), compiled fission track and virtrinite reflectance data from drill hole and outcrop samples. Three cooling phases, interpreted as exhumation events were deduced: 20-15 Ma, 12-7 Ma, and ~2 Ma to the present, each with an interpretation similar to previous models. It is suggested that the 1-2 Myr delay between events in the Buller Coalfield and similar events in the Greymouth Coalfield are the result of deformation beginning in the north, and progressing southward with time (Kamp et. al., 1999); conflicting with Batt et. al. (2004) theory of simultaneous deformation along the length of the Alpine Fault.

This southward shift in deformation, however, is confirmed by Sircombe and Kamp (1998), who used seismic reflections from the West Coast to study the geohistory of the South Westland Basin. They propose that the South Westland Basin is the result of flexural downwarping through thrusting at is southeastern margin, beginning during the middle Miocene. A large unfilled depression is known to have been present prior to the onset of rapid deposition, and loading by sediments alone has been shown to be sufficient to form the basin, without the need for plate boundary thrusting (Sutherland, 1996).

In further support of Kamp's theory is clast composition within middle Miocene sediments, which show reverse faulting in the South Westland Fault Zone, and uplift southeast of the Alpine Fault at this time (Sutherland, 1996). Uplift southeast of the Alpine Fault may be the result of a restraining bend geometry associated with the transfer of dextral slip from the eastern margin of Fiordland to the Alpine Fault (Norris and Turnbull, 1993).

Revisions in the Pacific-Australia plate rotations calculated by Cande and Stock (2004) may have implications for the interpretations of previously discussed fission track and virtrinite reflectance data. Using magnetic anomalies and fracture zone data they found that there has been little change in relative displacement along the Alpine Fault in the last 20 Myr, and that the average rate of convergence over the last 6 Myr is about 40 per cent smaller than in previous models. If so, the phase of cooling thought to represent the inception of the Alpine Fault as a purely strike-slip feature may in fact represent the start of convergence along the boundary.

Geohistory plots produced by this study show an increase in sedimentation and subsequent subsidence rates during the early Miocene, particularly in the Canterbury (at Kowai-1 sedimentation increased from ~3 $m.Myr^{-1}$ during the Oligocene, to ~50 $m.Myr^{-1}$ during the early Miocene) and West Coast regions (at Niagara-1 sedimentation increased from ~10 $m.Myr^{-1}$ over the Oligocene, to over 130 $m.Myr^{-1}$ during the Miocene). This investigation favors the Cande and Stock (2004) theory to explain this phenomena. It is unlikely that localized uplift would be capable of supplying these regions with the considerable amount of sediment seen, which resulted in significant basin growth. In Canterbury these clastic sediments fine to the east, and seismic sections have shown they form a prograding wedge (Field et. al., 1989) suggesting a considerable subaerially exposed source to the west. Isopach maps show that extensive basin growth occurred in the South Westland Basin, the Murchison Basin, the Grey Valley Trough and the Greville Basin, again suggesting an extensive source area.

10. 3: THE MARSHALL PARACONFORMITY

Several of the southern South Island subsidence curves show an unconformity over the Oligocene, which this investigation interprets as the Marshall Paraconformity. The Marshall Paraconformity is one of a number of unconformities that disrupt Oligocene sedimentation in the southwestern Pacific (Carter, 1985). While the presence of these hiatuses is not contested, the cause of them is. Debate surrounds the importance of sea level fluctuations as a controlling factor, particularly whether the sedimentary break represents a period of transgression or regression.

The Marshall Paraconformity typically separates onlapping, trangressive, terrigenous sediments, from blanket-like glauconitic and bioclastic sediments above (Carter, 1985). Thalassinidean and crab burrows usually mark the surface of the lower sediments, with infilling by the overlying greensands (Carter, 1985). In some places the above units display dune cross-bedding, with sets up to 2 m thick and tens of metres long (Ward and Lewis, 1975). A time gap of at least 4 m.y. is inferred, with sediments of mid-late Oligocene removed from ~32 Ma, however, in places late Eocene rocks are present immediately below the surface, suggesting a duration of at least 15 m.y. (Carter, 1985).

A number of hypotheses have been suggested and debated for the cause of the paraconformity. These include eustatic sea level fall, transgression, and the initiation of erosional circum-Antarctic currents, related to the separation of Australia from Antarctica, or the glaciation of Antarctica. Each of these theories will briefly be discussed below.

Carter and Landis (1972) originally suggested that the Marshall Paraconformity was the result of regional tectonics, in particular, the complete separation of Australia and Antarctica, which occurred during the Oligocene. The New Zealand plateau lay directly east of the ‘channel’ that opened between the two continents, thereby subjecting the region to the full force of the evolving current flowing between (Molnar et. al., 1975). The unconformity can also be interpreted to be due to deep-sea erosion and non-deposition caused by an increased supply of deep-bottom water, caused by the glaciation of the isolated Antarctic continent (Kennett et. al., 1974). The deposition of cross-bedded units above the unconformity surface is perhaps evidence of current influence during deposition, and it is possible that these two current forming processes occurred simultaneously.

Fulthorpe et. al. (1996) point out that relating the origin of the Marshall Paraconformity to oceanic currents does not exclude involvement of a major sea level event.

A lack of widespread erosional features and the condensed nature of the Marshall Paraconformity led to the assumption that the break was due to a regional highstand, resulting in sediment starvation, hence it was non-depositional rather than erosional. Subsidence curves provided in earlier chapters show that thermal relaxation and subsidence followed Cretaceous rifting (Chapters 4, 5, 8 and 9). The interval occupied by the mid Oligocene limestones has long been interpreted as reflecting extreme restriction of terrigenous sediment, resulting from maximum flooding of the landmass during a relative highstand (Schofield, 1951; in Fulthorpe et. al., 1996). Eustatic sea level curves, however, appear to contradict this assumption.

Publication of the first detailed global eustatic sea level curve by Vail et. al. (1977) provided a third hypothesis for the formation of the Marshall Paraconformity. Loutit and Kennett (1981) noted that the paraconformity appeared to coincide with a significant drop in global sea level at 29 Ma. The complete separation of Antarctica resulted in the thermal isolation and development of glaciation (Shackleton and Kennett, 1975; Barrett et. al., 1989). The formation of an ice-cap must inevitably have been accompanied by a eustatic sea level drop.

Initial estimates provided by Vail and Hardenbohl (1979) suggested a 400m sea level drop, sufficient to expose the continental shelf. This lead to the assumption that subaerial erosion was responsible for the hiatus. More recent calculations based on oxygen isotopes indicate a maximum sea level drop of 90m (Miller et. al., 1991). Assuming paleobathymetric estimations of ~250m prior to the event are correct, this drop is insufficient to expose the region subaerially. Localized areas of subaerial erosion surrounding Oamaru have been attributed to uplift associated with late Eocene to Oligocene volcanism (Carter, 1985).

Fulthorpe et. al. (1996) provide a means to reconcile this contradictory evidence. They propose that the origin of the sedimentary break is independent of the regional condensed sequence it is contained within. Strontium ages supplied confirm that the 2-4 My hiatus overlaps the mid Oligocene sea level low (Haq, 1987, 1988), and also the Oi2 oxygen isotope event noted by Miller et. al. (1991). They suggest that the break in limestone

production, located within the regional transgressional mega-sequence was caused by mid Oligocene glacio-eustatic fall and related oceanic current processes.

Sedimentation rates over the proposed period of the Marshall Paraconformity are in many locations the slowest in basin history. In the Canterbury basin sediment representing late Whaingaroan to Duntroonian is missing from Ealing-1, Leeston-1, Kowai-1 and Resolution-1, coinciding with the Marshall Paraconformity. Lewis (1984) suggested that uplift, and subsequent subaerial erosion led to the removal of sediment at Ealing-1 and Leeston-1, however, the occurrence of subaerial erosion at these locations is debated by Carter (1985). Fulthorpe et. al, (1996) note the presence of a strongly burrowed surface at a number of onshore outcrops in the Canterbury area. An increase in semi-opaque debris seen in Canterbury sediments immediately following the hiatus indicates a change in paleocurrents (Smale, 1987).

In the Great South Basin sedimentation and subsidence are slow, with water-depth at a maximum in most locations. Sediments are missing over period at Hoiho-1C and Tara-1, while the record at Kawau-1A is condensed (Cook, 1999). Seismic sections show complex bedforms in the Penrod Group, indicative of strong currents (Cook, 1999), the timing of which is consistent with the inception of the Antarctic Circum-polar Current.

Oligocene erosional unconformities occur over much of Western Southland (Turnbull et. al, 1993). Sediment is missing from the center and eastern sides of both the Te Anau and Waiau Basins, and from along the flanks of the Solander Ridge. A condensed succession is interpreted in Solander-1, and a drop in sea level is interpreted at Parara-1 (Turnbull et. al., 1993), which is not resolved by data presented here. It has been proposed that the continental shelf in western Southland was broken into blocks by northwest trending faults. Some of these blocks were affected by submarine currents resulting in unconformities (Turnbull et. al, 1993). Evidence for these marine currents is provided by the occurrence of trough cross-bedded sandstones (Norris and Turnbull, 1993).

Erosion in places, and slow sedimentation in others suggest that the Marshall Paraconformity represents an increase in deep marine currents. Data presented in this investigation combined with eustatic sea level data suggest a decrease in water depth within a regional trangressive phase. This is in agreement with data presented by Fulthorpe et. al. (1996).

10. 4: LOADING BY THE NORTHLAND ALLOCTHON

The subsidence data in conjunction with maps of the areal extent of the Northland Allochthon provide us with an opportunity to study the flexural properties of the lithosphere. We will consider the Northland Allochthon as a load instantaneously emplaced on the lithosphere. The degree of subsidence is then a function of several factors:

- Thickness of the load
- Lateral extent and width of the load
- Density of the material constituting the load
- And the flexural rigidity of the lithosphere

Flexural rigidity (*D*) is defined by the equation:

$$D = \frac{ET_e^3}{12(1-\upsilon^2)} \quad \text{(Nm)} \tag{10.1}$$

where T_e represents elastic thickness, and E and υ are Young's modulus and Poisson's ratio respectively.

The flexural parameter (α), required by this investigation for the calculation of *D*, is expressed by the following equation (Walcott, 1970):

$$\alpha = \left(\frac{4D}{(\rho_m - \rho_f)g} \right)^{1/4} \quad \text{(km)} \tag{10.2}$$

where g is gravitational acceleration, and ρ_m and ρ_f represent the density of the mantle and load respectively. For this investigation ρ_m is taken to be 3300 kg/m^3, and based on calculations by Watts (2001) ρ_f is taken to be 2850 kg/m^3.

As discussed in the preceding chapter (Chapter 9), the Northland Allochthon consists of a series of nappes, emplaced during the Miocene, over what is now the Northland Peninsula. Figure 10.3 shows the present day extent of the allochthon. The width of the Allochthon is about 80 km, and its length is ~350 km. For the purpose of this analysis we will assume the load is 2D.

In order to calculate the flexural rigidity and elastic thickness of the lithosphere below Northland, it is necessary to estimate from subsidence data the amplification factor (Φ) in the region. Amplification is the ratio of maximum amplitude after loading to the amplitude before loading, shown by figure 10.4(a) and defined by the following equation:

$$\phi_{obs} = \frac{(H+Y)}{H} \tag{10.3}$$

Where H is the thickness of the load, and Y is the amount of total subsidence.

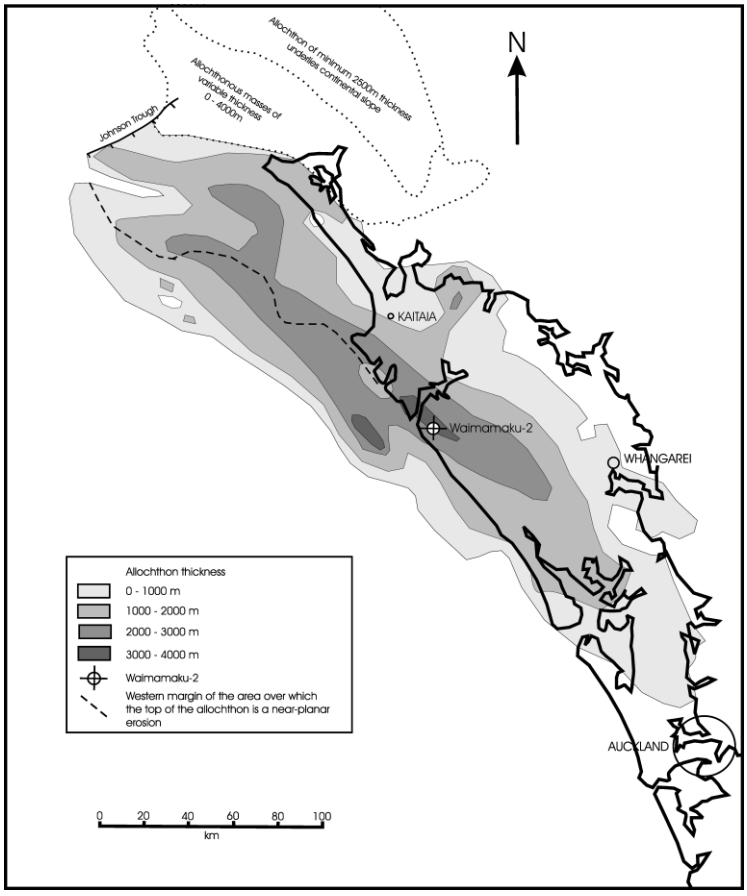

Figure 10.3: The present day extent of the Northland Allochthon. Isopachs were determined from seismic interpretations, drilling results and geological mapping (From Isaac et. al., 1994)

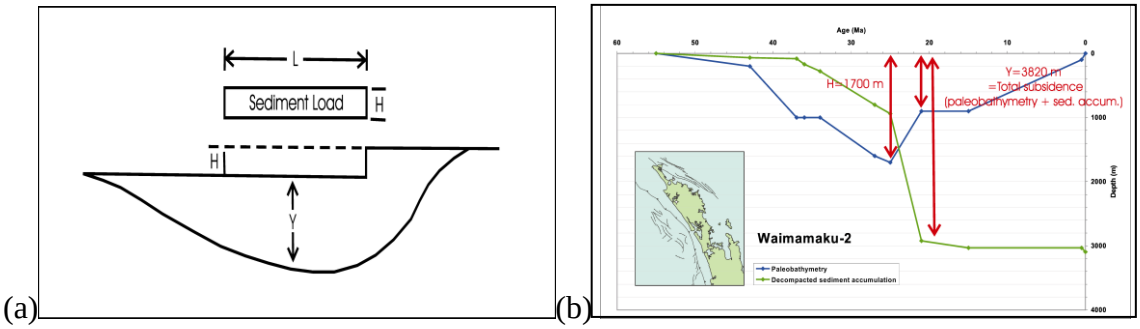

Figure 10.4: (a) Amplification factor for a loaded shelf margin is simply the ratio of the isopach thickness (Y + H) to the original water depth (H). The magnitude of the flexural response beneath the loads center is represented by the parameter Y. (From Holt and Stern, 1991).
(b) Decompacted sediment accumulation and paleobathymetry for Waimamaku-2, showing the derivation of values Y and H.

From the subsidence curve (Fig. 10.4(b)) for Waimamaku-2, near the center of the allochthon H = 1700 m, and Y = 3820 m, therefore ϕ_{obs}= 3.2

The amplification factor below the center of a 2D rectangular load of width L can be expressed by the following equation (Angevine et. al., 1990; Holt and Stern, 1991, Watts, 2001):

$$\phi = \rho_L /(\rho_m - \rho_f)\left[1 - e^{-L/2\alpha}\cos(L/2\alpha)\right] + 1 \qquad (10.4)$$

where ρ_L is the density of the load, ρ_m is the density of the mantle, ρ_f is the infill density and α is the flexural parameter. Figure 10.5 shows how the amplification factor changes with the dimensionless ratio L/α, where L is the load width, and α is the flexural parameter. As we know the observed amplification factor (ϕ_{obs}) from equation 10.3, and the load width, in this case approximately 80 km (from fig. 10.3), it is possible to calculate α from figure 10.5. Malpas et. al. 1992, showed that the bulk of the rocks comprising the Northland Allochthon are normal mid-ocean-ridge basalts, therefore, based on calculations by Watts (2001) the density of the load is taken to be 2850 kg/m^3.

Based on the use of equations 10.2, 10.3 and 10.4, the lithospheric rigidity of Northland is estimated to be 1.5×10^{22} Nm. Using this value and equation 10. 1 an elastic thickness of 12 km is estimated for the lithosphere below the Northland Allochthon.

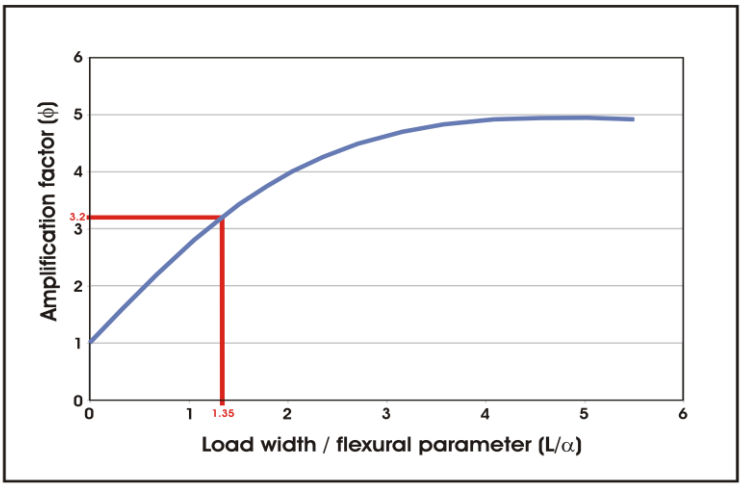

Figure 10.5: Plot from equation 10.4, showing amplification factor verse the dimensionless ratio L/α (load width over flexural parameter for the Northland region (mantle density = 3350 kg/m^3, infill density = 2850 kg/m^3 (Watts, 2001), load density = 1850 kg/m^3 (infill density – density of water).

This value is somewhat smaller than those calculated by Holt and Stern (1991). Based on the loading of the Western Platform by the Plio-Pleistocene Giant Foreset Formation an elastic thickness of 20-28 km was calculated. It is important, however, to note the relationship between rigidity and age of the lithosphere. Figure 10.6 demonstrates this association for oceanic lithosphere, while the scatter is more extensive for continental lithosphere, the thermal age of the crust remains the dominant control on rigidity (Watts, 2001).

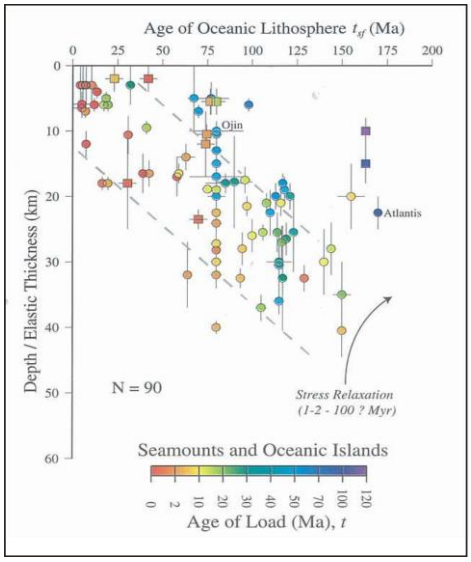

Figure 10.6: Elastic thickness verse age of oceanic lithosphere (From Watts, 2001)

The elastic thickness calculated for the Northland region represents that at the time of the Miocene allochthon emplacement, when the crust was significantly thinner and thermally young. Assuming the crust formed in both the Northland and Taranaki regions at ~65 Ma, at the time of emplacement (~25 Ma), the crust in Northland was ~40 Myr. The calculated elastic thickness for the Taranaki region denotes the value following the deposition of the Giant Foreset Formation (<5 Ma), some 20 Myr later, allowing further heat loss, and therefore increased rigidity.

10. 5: SUBSIDENCE IN TARNAKI AND THE WEST COAST

A number of subsidence curves complied by Hayward and Wood (1989) for the Taranaki Basin demonstrate region-wide simultaneous subsidence during the late Oligocene. This event has since been confirmed by other studies (e.g: Holt and Stern, 1994), and by this investigation (see chapter 8). Stern and Holt (1994) suggested that the initiation of subduction caused mantle flow, resulting platform subsidence and the basin-wide signature seen. This investigation explores the subsidence history of the West Coast, in an attempt to observe the event, and to approximate the wavelength of flexure.

Geological records and numerical modeling suggest broad areas, much larger than individual basins, have undergone subsidence in the past. Where these regions are associated with subduction zones the process has become known as platform subsidence, or more recently, dynamic topography. While various hypotheses have been offered, there is now general agreement that platform subsidence and dynamic topography is the result of sinking lithospheric slabs inducing flow in the mantle at subduction zones. This flow results in normal stresses, which create a low pressure region in the mantle, subsequently resulting in a broad topographic depression (Fig. 10.7) (Mitrovica and Jarvis, 1985), with possible uplift in the forebulge.

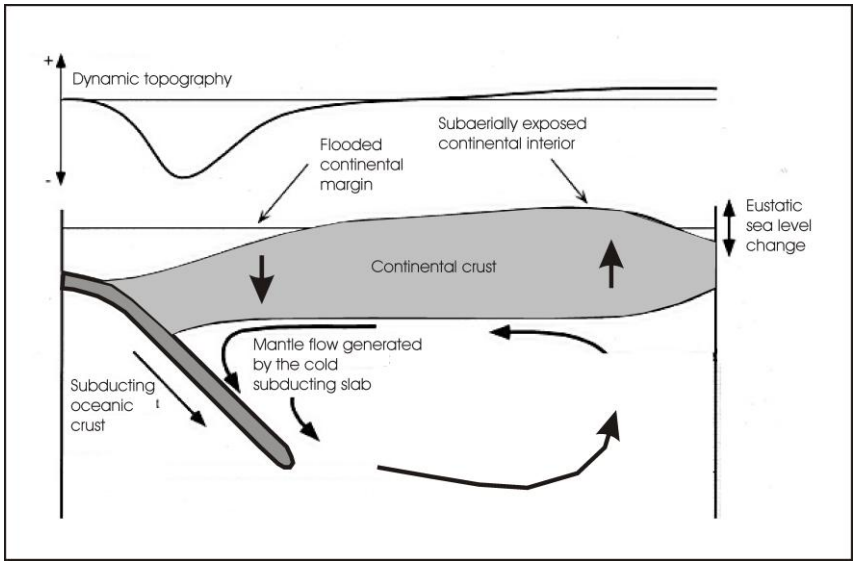

Figure 10.7: Cross-section of a subduction zone, showing how mantle flow can induce broad wavelength subsidence, with uplift on the forebulge (from Burgess, 1997).

This deformation typically has a wavelength of 500-1000km, although evidence for up to 1500km of warping is found in the western interior of North America (Mitrovica et. al., 1989). The wavelength of these features is an order of magnitude longer than that caused by lithospheric flexure (Coakley and Gurnis, 1995), and leads to sedimentation in craton interiors, far beyond the reach of flexural effects that are restricted to plate margins (Mitrovica et. al., 1989). The asymmetrical amplitude of deformation gently increases towards the trench, where subsidence of up to 2km, if filled with water may occur (Stern and Holt, 1994). The extent and rate of subsidence, and uplift at the cessation of subduction are associated with a number of variables such as rate and extent of slab penetration into the mantle, dip angle of the Benioff Zone related to the elastic thickness of the crust (Mitrovica et. al., 1989), and the temperature contrast between the slab and surrounding mantle (Mitrovica and Jarvis, 1985).

Evidence of platform subsidence has now been found in many localites, including the Russian Platform (Vinogradov, 1974; Nalivkin, 1976), the Iberian Margin (Janssen, 1993), the Canadian Rocky Foreland (Peper, 1994), in Eastern Australia (Gallagher, et. al., 1994; Russell and Gurnis, 1994), and in the Michigan Basin (Coakley and Gurnis, 1995).

A change in the tectonic regime of the New Zealand continent occurred during the late Oligocene. The microplates of the South Fiji Basin began to act as a single plate, leading to the cessation of sea-floor spreading (Malahoff et. al., 1982). Extension in the Norfolk Basin also began at this time (Mortimer, et. al., 1998). Convergence and the initiation of subduction to the north of proto-New Zealand resulted from the southward migration of the Australian-Pacific rotation pole (Sutherland, 1995). Evidence for the southward propagation of the plate boundary includes the establishment of andesitic magmatic arcs in western Northland (Hayward, 1993), the obduction of earlier passive margin sequences and some adjacent ocean floor in the north (Hayward et. al., 1989; Balance, 1993), and the imbrication of older passive margin sequences and the formation of thrust controlled slope basins on the North Island's east coast (Lewis and Pettinga, 1993).

As previously mentioned, a period of rapid subsidence occurred on the Taranaki Platform. It appears data from the West Coast of the South Island complied by this investigation also shows this trend, with an increase in water depth and subsidence occurring at 26 ± 2 Ma (Fig 10.8).

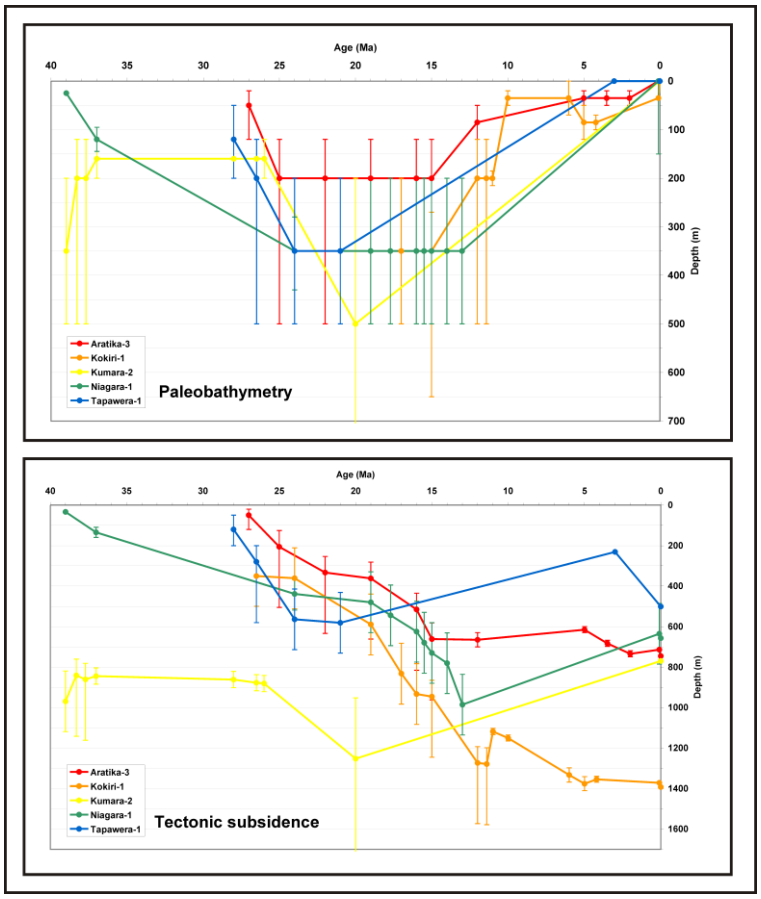

Figure 10.8: Paleobathymetry and tectonic subsidence for a number of wells on the West Coast of the South Island, which show subsidence occurring at 26 ± 2 Ma, interpreted as platform subsidence.

Niagara-1 has been included in the plot, although subsidence appears to occur prior to the Oligocene. Resolution of data at Niagara-1 is poor over this period, however, this well is located within the same basin as Aratika-3, Kokiri-1 and Kumara-2, and therefore it is assumed that subsidence occurred at approximately the same time.

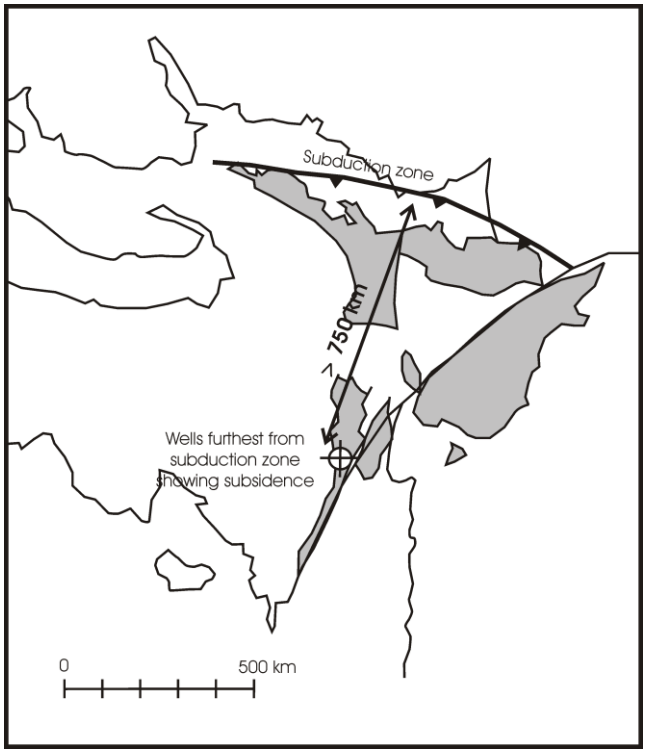

Figure 10.9: Tectonic reconstruction of New Zealand continent at 25 Ma, showing the wavelength of flexure related to the inception of subduction (from Stagpoole and Wood, G.N.S. website, 2007)

If this subsidence noted on the West Coast is due to viscous mantle flow, related to the onset of subduction, the wavelength of this subsidence is >750 km (Fig. 10.9). This value is within the expected range given by Gurnis (1992), and by Burgess and Gurnis (1995). To create subsidence over this distance by lithospheric flexure would require either extreme values of crustal rigidities, or the presence of a supercrustal load, for which there is no evidence. The fact that wells in the Canterbury and Great South Basins, located on the opposite side of the developing Alpine Fault, appear to show predominately decreasing water depths adds further weight to the argument that Taranaki and the West Coast are 'back-arc' to the evolving subduction zone.

10. 6: THE INCREASE IN SEDIMENTATION AT 6 Ma

Evidence presented in this study appears to confirm the conclusions of Cande and Stock (2004). Their revision of tectonic plate systems suggests that convergence began on the Alpine Fault prior to 20 Ma, with only a slight increase at 6 Ma. An alternative explanation is therefore required for the sudden increase in sedimentation and subsidence at 6 Ma seen in almost all wells around New Zealand, usually attributed to the start of uplift on the Alpine Fault. Isostatic rebounded caused by a change in climate is suggested.

Once formed, a mountain belt is vulnerable to erosion. The removal of crustal material disrupts the isostatic balance of a region. Based on the principles of isostacy, an increase in erosion (for example, due to climate change) will lead to an increased rate of rock uplift (Watt, 2001), bringing deeper levels of the crust to the earth's surface (Fig. 10.10).

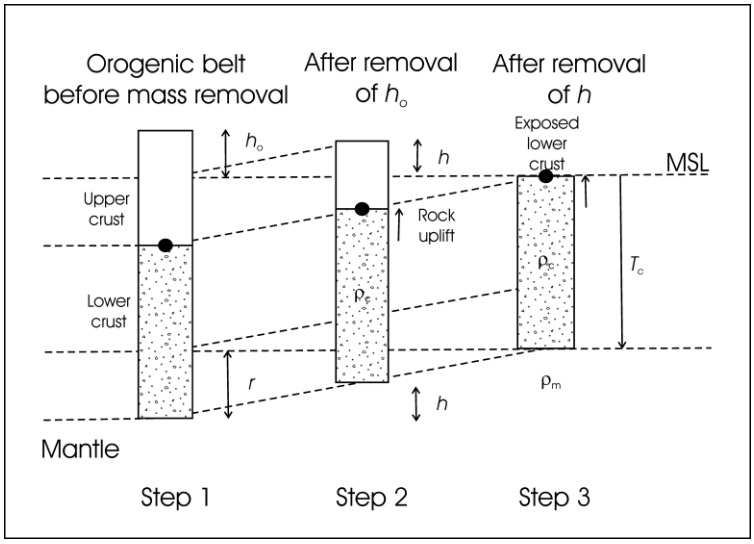

Figure 10.10: Isostatic response to erosion of an orogen. The earth's surface subsides with respect to the geoid, however, erosion results in rock uplift. (from Watts, 2001)

In an orogenic belt that is initially in isostatic equilibrium the total amount of material removed, S_e, is related to the initial elevation of the orogen, h_o, by the equation:

$$S_e = h_o\left(1+\frac{\rho_c}{\rho_m-\rho_c}\right) \qquad \text{(m)} \qquad (10.5)$$

where ρ_c and ρ_m are the densities of crust and mantle respectively. This means that if h_o = 5km, >20 km of material may have been removed by erosion.

Sediment thickness measured by the Deep-Sea Drilling Program (DSDP) indicates a rapid global increase in terrigenous accumulation on the ocean floor (Hay et. al., 1988). This marked increased was thought to be largely due to the growth of continental ice-sheets, resulting in subaerial erosion of the exposed continental margins. Molnar (2005), however, noted that this increase in sedimentation and subsidence also occurred in central Asian basins, far from the effects of marine regression. Formation of mountain glaciers may explain increased erosion at high altitudes, but increases are also noted at lower altitudes, and more significantly, low latitudes. While glaciation and sea level changes must account for some of the observed increases in sedimentation, neither explains it all, as some regions that show an increase appear independent of both glaciers and sea level fluctuations.

Climate variability provides a possible mechanism for increased global erosion. Figure 10.11 shows four standardised, 4-Myr-long high-resolution $\delta^{18}O$ time series, collected from a number of sites in the Pacific and Atlantic during the DSDP. When compared with the other graphs, graph A shows a general increase in frequency and amplitude of oxygen isotope events, a proxy for global climate change. Molnar (2004) suggests that rapid fluctuations in climate resulted in a state of disequilibria, where erosive processes were forced to continually adjust to changing conditions, resulting in increased erosion.

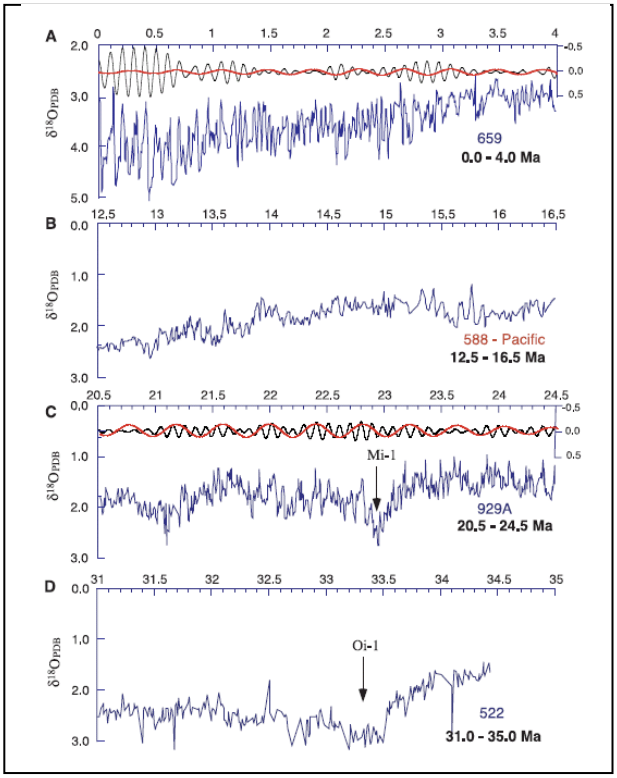

Figure 10.11: High resolution 4-Myr-long $\partial^{18}O$ time series for four intervals during the Cenozoic, showing the increase in amplitude and frequency of climatic events. Data is from DSDP and ODP: (a) Site 659, eastern equatorial Atlantic; (b) Site 588, from the southwest Pacific; (c) Site 929, western equatorial Atlantic; and (d) Site 522, south Atlantic. (from Zachos, et. al., 2001)

In the North Alpine Foreland Basin adjacent to the European Alps, mineral cooling ages show that during the Pliocene the region underwent 1-3 km of erosion, coinciding with a decline in tectonic activity. Cederbom et. al. (2004) inferred that this was due to the intensification of the Atlantic Gulf Stream, which caused an increase in precipitation with increased erosion, and hence isostatic rock uplift in the neighbouring alps. Thiede et. al., (2005) also suggest climate as a driving factor for exhumation in the Himalayas since the Pliocene.

Using the bed-load of streams in the Southern Alps, and sediment accumulations in adjacent basins, Adams (1980) showed that the region's erosion rate was approximately equal to the rate of rock uplift. Therefore, the observed uplift of marine terraces must be in part the result of isostatic uplift due to erosion (Molnar and England, 1990). It is

not suggested that erosion alone is responsible for rock uplift in the Southern Alps since 6 Ma. Plate motion reconstructions show that convergence was occurring along the Alpine Fault at this time (i.e.: Sutherland, 1995; King, 2000), providing a tectonic source for uplift. The Cande and Stock (2004) reconstruction actually shows an increase in the angle of convergence. Nevertheless, the effects of climate variability are likely to contribute, at least in part, to the increase in sedimentation seen at 6 Ma

10. 7: BETA VALUES

The β values in the extension basins surrounding New Zealand are generally below 2, with the only exceptions found by this investigation being in the center of the Taranaki (β = 2.1) and in the Central sub-basin of the Great South Basin (β = 2.5). As expected, β is highest in the large offshore basins of Canterbury, Great South Basin and Taranaki, with contours closely following the isopachs of the Cretaceous basins. Prior to Cretaceous rifting, the crustal thickness surrounding New Zealand generally ranged from 35 to 50 km. The values calculated for the West Coast Basin are slightly lower, however, this may reflect sediment removal, as only two wells contain sediment pertaining to the Cretaceous.

Data from the Canterbury and Great South Basin can be compared with that from West Antarctica, as these regions were separated by the Cretaceous rifting of Gondwana. Based on gravity anomalies in the Ross Sea region Karner et. al. (2005) concluded that undeformed crust on the flanks of the Ross Sea Basins is ~40 km thick, and that the basins are generally extended by a factor of ~2 in their centres. These values are comparable with the 35-50 km thickness, and 1.8-2.4 β value calculated by this investigation for the Canterbury and Great South Basins.

The crustal thicknesses and β values from western New Zealand can be compared with continental lithosphere of eastern Australia, as these regions were also adjoined prior to the separation of Gondwana. Seismic evidence suggests that non-rifted continental crust in eastern Australia is between 30 and 45 km thick (Collins, 1991). The values estimated by this investigation are similar and envelop the range provided by Collins (1991).

CHAPTER 11: CONCLUSIONS

- The most common feature to all New Zealand subsidence curves is the signal associated with rifting due to break up of Gondwana. This sharp onset of subsidence at ~80-65 Ma seen in wells from most basins around New Zealand is then followed by a slow thermal subsidence, related to cooling of the lithosphere.

- Subsidence curves for the Great South Basin show an additional rapid subsidence beginning at 51 ± 2 Ma. This coincides with the cessation of rifting in the Tasman Sea, onset of rifting and the formation of oceanic crust in the Emerald Basin. It is assumed that the extension signature is the result of tensional forces, related to plate reorganization in the region at this time.

- An increase in sedimentation at ~20 Ma is noted in the sedimentary basins of the South Island. Convergence on the Alpine Fault, leading to increased erosion is cited as a mechanism for this period of basin growth. This is consistent with the Cande and Stock (2004) model of plate motions.

- Sedimentation breaks seen in the Canterbury, Great South and Western Southland Basins during the late Oligocene are interpreted as the Marshall Paraconformity. Based on decreasing sedimentation prior to the event, it is suggested that the region was undergoing a transgressive phase. However, it is likely that the break itself represents a decrease in water-depth, and the formation of erosive bottom currents.

- An example of using paleobathymetry and subsidence data to constrain the mechanical properties of the lithosphere is provided. Based on paleobathymetry and subsidence at Waimamaku-2, near the center of the Northland Allochthon load, a lithospheric rigidity of 1.5×10^{22} Nm is estimated. An elastic thickness of ~12 km was estimated. This is lower than values calculated for the Plio-

Pleistocene loading of the Taranaki Platform, reflecting a younger, hotter crust in Northland at the time of loading.

- With the exception of the central Taranaki and Great South Basins, β for the sedimentary basins surrounding New Zealand are below 2, suggesting crustal thickness prior to rifting was between 35 and 50 km. These values are consistent with data from conjugate margins of Australia and Antarctica.

- This investigation confirms subsidence, expressed as excess paleobathymetry, in Taranaki during the late Oligocene, as noted by other authors (i.e.: Hayward and Wood, 1989; Holt and Stern, 1994). Wells located on the west coast of the South Island also demonstrate this event at 26 ± 2 Ma. Due to this event approximately coinciding with the Taranaki Basin subsidence at 25 ± 3 Ma, it is assumed this broad flexure (wavelength >750 km) is the result of subduction related mantle flow.

- An increase in sedimentation is noted in most wells at ~6 Ma, coinciding with a change in the frequency and wavelength of climatic events. It is proposed that part of this increase is the result of climate-driven erosion, forcing isostatic uplift of the Southern Alps.

REFERENCES

Adams, R. D. (1962). Thickness of the earth's crust beneath the Campbell Plateau. *New Zealand Journal of Geology and Geophysics* **5**: 78-85.

Allen, P. A., and Allen, J. R. (2005). *Basin Analysis: Principles and Applications.* Blackwell Publishing Company, Padstow.

Andrews, P. B., Field, B. D., Browne, G. H., and McLennan, J. M. (1987). *Lithostratigraphic nomenclature for the upper Cretaceous and Tertiary sequence of central Canterbury, New Zealand*, New Zealand Geological Survey; Record 24. New Zealand Geological Survey, Lower Hutt.

Angevine, C. L., Heller, P. L., and Paola, C. (1990). *Quantitative Sedimentary Basin Modelling*, Continuing Education Course Note Series # 32. American Association of Petroleum Geologists.

Armstrong, P. A., Allis, R. G., Funnel, R. H., and Chapman, D. S. (1998). Late Neogene exhumation patterns in the Taranaki Basin (New Zealand): Evidence from offset porosity-depth trends. *Journal of Geophysical Research* **103**: 30269-82.

Athy, L. F. (1930). Density, porosity andcompaction of sedimentary rocks. *Bulletin American Association of Petroleum Geologists* **14**: 1-24.

Atwater, T., and Stock, T. (1998). Pacific-North American plate tectonics of the Neogene southwestern United States- An update. *International Geological Review* **40**: 375-402.

Ballance, P. F. (1993). The Paleo-Pacific, post-subduction, passive margin thermal relaxation sequence (Late Cretaceous-Paleogene) of the drifting New Zealand continent. In: *South Pacific Sedimentary Basin. Sedimentary Basins of the World* (eds. P. F. Ballance). **2:** 93-110. Elsevier Science Publishers, Amsterdam.

Barrett, P. J., Hambrey, M. J., Harwood, D. M., Pyne, A. R., and Webb, P. N. (1989). Antarctic Cenozoic history from the CIROS-1 drillhole, McMurdo Sound. *DSIR Bulletin* **245**: 241-251.

Batt, G. E., Baldwin, S. L., Cottam, M. A., Fitzgerald, P. G., Brandon, M. T., and Spell, T. L. (2004). Cenozoic plate boundary evolution in the South Island of New Zealand: New thermochronological constrains. *Tectonics* **23**.

Baxter, A. K. (1993). *Analysis of the rifting history of the Great South Basin, New Zealand*, BSc (Honors) thesis, Victoria University of Wellington.

Beavan, J., Denham, M., Denys, P., Hager, B., Herring, T., Kurnick, C., Matheson, D., Molnar, P., and Pearson, C. (2002). A direct geodetic measurement of the uplift rate of the Southern Alps. *EOS (Transactions) AGU* **83**(22).

Beggs, J. M. (1993). Depositional and Tectonic History of the Great South Basin. In: *South Pacific Sedimentary Basins. Sedimentary Basins of the World.* (eds. P. F. Ballance). **2:** 365-373. Elsevier Science Publications, Amsterdam.

Bradshaw, J. D. (1989). Cretaceous geotectonic patterns in the New Zealand region. *Tectonics* **8**(4): 803-820.

Brook, F. J., and Hayward, B. W. (1989). Geology of autochthonous and allocthonous sequences between Kaitaia and Whangaroa, Northern New Zealand. *New Zealand Geological survey record* **36**.

Brook, F. J., and Thrasher, G. P. (1991). Cretaceous and Cenozoic geology of northernmost New Zealand. *New Zealand Geological survey record* **41**.

Browne, G. H., and Field, B. D. (1985). *The lithostratigraphy of late Cretaceous to early Pleistocene rocks of northern Canterbury, New Zealand*, New Zealand Geological Survey; Record 6. New Zealand Geological Survey, Lower Hutt.

Burgess, P. M., and Gurnis, M. (1995). Mechanisms for the formation of cratonic stratigraphic sequences. *Earth and planetary science letters* **136**(3-4): 647-663.

Burgess, P. M., Gurnis, M., and Moresi, L. (1997). Formation of sequences in the cratonic interior of North America by interaction between mantle, eustatic, and stratigraphic processes. *Geological Society of America Bulletin* **108**: 1515-1535.

Cande, S. C., and Stock, J. M. (2004). Pacific-Antarctic-Australian motion and the fromation of the Macquarie Plate. *Geophysical Journal International* **157**: 399-414.

Carter, M./ Petroleum Corporation of New Zealand Exploration Ltd., (1983); Kaimiro-1 Well Completion Report. PPL 38091. Ministry of Economic Development New Zealand unpublished petroleum report. PR936

Carter, M., and Rainey, S./ Petroleum Corporation of New Zealand Exploration Ltd., (1988); Well Completion Report, Happy Valley-1, -1A, -1B, -1C. PPL38074. Ministry of Economic Development New Zealand unpublished petroleum report. PR1382

Carter, M., and Rainey, S./ Petroleum Corporation of New Zealand Exploration Ltd., (1988); Well Completion Report, Upukerora-1. PPL38074. Ministry of Economic Development New Zealand unpublished petroleum report. PR1381

Carter, M., Kelly, M., Hillyer, M., and McDowell, P./ Petroleum Corporation of New Zealand Exploration Ltd., (1986); Kumara-2, -2A Well Completion Report. PPL38070. Ministry of Economic Development New Zealand unpublished petroleum report. PR1183

Carter, M. J./ Petroleum Corporation of New Zealand Explorarion Ltd., (1981); Kokiri-1 Well Completion Report, PPL38038. Ministry of Economic Development New Zealand unpublished petroleum report. PR799

Carter, R. M. (1985). The mid Oligocene Marshall Paraconformity, New Zealand: Coincidence with global eustatic sea-level fall of rise? *Journal of Geology* **93**: 359-371.

Carter, R. M. (1988). Post-breakup stratigraphy of the Kaikoura Synthem (Cretaceous-Cenozoic), continental margin, southeastern New Zealand. *New Zealand Journal of Geology and Geophysics* **31**: 405-429.

Carter, R. M., and Landis, C. A. (1972). Correlative Oligocene unconformities in southern Australia. *Nature* **237**: 12-13.

Carter, R. M., and Landis, C. A. (1982). Oligocene unconformities in the South Island. *Journal of the Royal Society* **12**: 42-46.

Carter, R. M., and Norris, R. J. (1976). Cenozoic history of southern New Zealand: an accord between geological observations and plate-tectonic predictions. *Earth and planetary science letters* **31**: 85-94.

Cederbom, C. E., Sinclair, H. D., Schlunegger, F., and Rahn, M. K. (2004). Climate induced rebound and exhumation of the European Alps. *Geology* **32**(8): 709-712.

Clarke, K. J., Sporli, K. B., and Gibson, G. W (1989). Structure of Oligocene limestones in the Mangamuka Bridge area, Northland Allocthon, New Zealand. *The Royal Society of New Zealand Bulletin* **26**: 75-84.

Coakley, B., and Gurnis, M. (1995). Far-field tilting of Laurentia during the Ordovician and constraints on the evolution of a slab under an ancient continent. *Journal of Geophysical Research* **100**: 6313-27.

Cochran, J. R. (1983). Effects of finite extension times on the development of sedimentary basins. *Earth and planetary science letters* **66**: 289-302.

Collins, C. D. N. (1991). The nature of the crust-mantle boundary under Australia from seismic evidence. In: *The Australian Lithosphere* (eds. B. J. Drummond). **17:** 67-80. Geological Society of Australia special publication,

Cook, R. A., and Greggs, R. (1997). Overview of New Zealand's petroleum systems, potential. *Oil and Gas Journal* **95**(1): 55-58.

Cook, R. A., Sutherland, R., Zhu, H., and others (1999). *Cretaceous and Cenozoic geology and petroleum systems of the Great South Basin, New Zealand*, Institute of Geological and Nuclear Sciences; monograph 20. Institute of Geological and Nuclear Sciences Limited, Lower Hutt.

Cooper, A. F., Barreiro, B. A., Kimbrough, D. L., and Mattinson, J. M. (1987). Lamprophyre dike intrusion and the age of the Alpine Fault, New Zealand. *Geology* **15**: 941-944.

Davey, F. J., and Smith, E. G. C. (1983). The tectonic setting of the Fiordland region, southwest New Zealand. *Geophysical Journal of the Royal Astronomical Society.* **72**: 23-38.

De Dock, J. F., True, T., Lammerink, W., Kelly, C., and McDowell, P./ Petroleum Corporation of New Zealand Exploration Ltd., (1985); Awakino-1 Well Completion Report. PPL38094. Ministry of Economic Development New Zealand unpublished petroleum report. PR1140

Dickinson, W. R. (1976). *Plate tectonic evolution of sedimentary basins*, Continuing Education Course Note Series # 1. American Association of Petroleum Geologists.

Engmann, L. A., and Fenton, P. H./ BP Oil Exporation Company New Zealand Ltd., (1986); Well Completion Report, Solander-1. PPL38206. Ministry of Economic Development New Zealand unpublished petroleum report. PR1149

Falvey, D. A. (1974). The development of continental margins in plate tectonic theory. *Journal of Australian Petroleum Exploration Association* **14**: 95-106.

Field, B. D., and Browne, G. H. (1993). A subsidening platform adjacent to a plate boundary transpression zone: Neogene of Canterbury, New Zealand. In: *South Pacific Sedimentary Basins. Sedimentary Basins of the World.* (eds. P. F. Ballance). **2:** 271-278. Elsevier Science Publishers, Amsterdam.

Field, B. D., and Uruski, C. I. (1991). Middle Miocene to Recent development of the Solander Basin: structure and sequence stratigraphy. *New Zealand Geological survey record* **43**(117-122).

Field, B. D., Browne, G. H. and others (1989). *Cretaceous and Cenozoic sedimentary basins and geological evolution of the Canterbury Region, South Island, New Zealand*, New Zealand Geological Survey Basin Studies; 2. New Zealand Geological Survey, Lower Hutt.

Fulthorpe, C. S., and Carter, R. M. (1991). Continental-shelf propradation by sediment-drift accretion. *Geological Society of America Bulletin* **103**: 300-309.

Fulthorpe, C. S., Carter, R. M., Miller, K. G., and Wilson, J. (1996). Marshall Paraconformity: a mid-Oligocene record of inception of the Antarctic Circumpolar Current and coeval glacio-eustatic lowstand? *Marine and Petroleum Geology* **13**(1): 61-77.

Funnel, R., Chapman, D., Allis, R., and Armstrong, P. (1996). Thermal state of the Taranaki Basin, New Zealand. *Journal of Geophysical Research* **101**(B11): 25,197-25,215.

Gage, M. (1957). *The geology of the Waitaki subdivision*, New Zealand Geological survey bulletin. Department of Scientific and Industrial Research, Wellington, New Zealand.

Gaina, C., Muller, D. R., Royer, J. Y., Stock, J. Hardebeck, J., and Symonds, P. (1998). The tectonic history of the Tasman Sea: A puzzle with 13 pieces. *Journal of Geophysical Research* **103**: 12413-33.

Gallagher, K., Dumitru, T. A., and Gleadow, A. J. W. (1994). Constraints on the vertical motion of eastern Australia during the Mesozoic. *Basin Research* **6**: 77-94.

Gilbert, D. B., Ballance, P. F., and Sporli, K. B. (1989). Te Kuiti Group and Northland Allochthonous rocks on the north flank of the Omahuta Basement Block, Northland, New Zealand. *The Royal Society of New Zealand Bulletin* **26**: 65-74.

Giles, M. R. (1997). Diagenesis: A quantitive perspective. Implications for basin modeling and rock property predictions. In: (eds. Kluwer Academic Publishers, Dordrecht.

Gurnis, M. (1992). Rapid continental subsidence following the initiation and evolution of subduction. *Science* **255**: 1556-8.

Haq, B. U., Hardenbol, J., and Vail, P. R. (1987). Chronology of Fluctuating Sea-levels since the Triassic. *Science* **235**: 1156-1167.

Haq, B. U., Hardenbol, J., and Vail, P. R. (1988). Mesozoic and Cenozoic chronostratigraphy and cycles of sea-level change. In: *Sea-level Changes: An Intergrated Approach. Special Publication, Society of Economic Paleontology and Minerals* (eds. C. K. H. Wilgus, B. S.;Kendall, C. G. St. C.; Posamentier, H. W.; Ross, C. A.; Van Wagoner, J. C.). **42:** 71-108.

Harrison, J./ Offshore Mining Company Ltd., (1977); Well Completion Report, Aratika No. 2. Ministry of Economic Development New Zealand unpublished petroleum report. PR719

Haxby, W. F., Turcotte, D. L., and Bird, J. M. (1976). Thermal and mechanical evolution of the Michigan Basin. *Tectonophysics* **36**: 57-75.

Hay, W. W., Sloan, J. L., and Wold, C. N. (1988). Mass/age distribution and composition of sediment on the ocean floor and the global rate of sediment subduction. *Journal of Geophysical Research* **93**: 14933-40.

Hayward, B. W. (1987a). Paleobathymetry and structural and tectonic history of Cenozoic drillhole sequences in Taranaki Basin. In: *New Zealand Geological Survey Report, Pal 122.* (eds.

Hayward, B. W. (1987b). Letters to the Editor - Identity of igneous bodies beneath the continental shelf of west Northland, New Zealand. *New Zealand Journal of Geology and Geophysics* **30**: 93-95.

Hayward, B. W. (1993). The tempestuous 10 million year life of a double arc and intra-arc basin - New Zealand's Northland Basin in the early Miocene. In: *South Pacific Sedimentary Basins. Sedimentary Basins of the World, 2* (eds. P. F. Ballance). Elsevier, Amsterdam.

Hayward, B. W., and Wood, R. A. (1989). *Computer generated geohistory plots for Taranaki drill hole sequences, Rep*, PAL 147*.* Department of Science and Industrial Research, New Zealand, Lower Hutt.

Hayward, B. W., Brook, F. J., and Isaac, M. J. (1989). Cretaceous to middle Tertiary stratigraphy, paleogeography and tectonic history of Northland, New Zealand. *The Royal Society of New Zealand Bulletin* **26**: 47-64.

Heidlauf, D. T., Hsui, A. T., and Klein, G. D. (1986). Tectonic subsidence analysis of the Illinois Basin. *Journal of Geology* **94**: 779-794.

Henrys, S. A., Woodward, D. J., Okaya, D., and Yu, J. (2004). Mapping the Moho beneath the Southern Alps continent-continent collision, New Zealand, using wide-angle reflections. *Geophysical Research Letters* **31**.

Holt, W. E., and Stern, T. A. (1991). Sediment loading on the Western Platform of the New Zealand continent: implications for the strenght of a continental margin. *Earth and planetary science letters* **107**: 523-538.

Holt, W. E., and Stern, T. A. (1994). Subduction, platform subsidence, and foreland thrust loading: the late Tertiary development of Taranaki Basin, New Zealand. *Tectonics* **13**(1068-1092).

Hoolihan, K./ Offshore Mining Co. Ltd., (1978); Kowai-1 Well Completion Report. Ministry of Economic Development New Zealand unpublished petroleum report. PR722

Horspool, N. A., Savage, M. K., and Bannister, S. (2006). Implications for intraplate volcanism and back-arc deformation in northwestern New Zealand, from joint inversion of reciever functions and surface waves. *Geophysical Journal International* **166**: 1466-1483.

Hunt International Petroleum Company, N. Z. (1978); Hoiho-1C Well Completion Report. Ministry of Economic Development New Zealand unpublished petroleum report. PR730

Hunt International Petroleum Company, N. Z. (1977); Final Report, Kawau-1. Ministry of Economic Development New Zealand unpublished petroleum report. PR716

Hunt International Petroleum Company, N. Z. (1977); Pakaha-1 Well Completion Report. Ministry of Economic Development New Zealand unpublished petroleum report. PR703

Hunt International Petroleum Company, N. Z. (1978); Tara-1 well completion report. PPL740. Ministry of Economic Development New Zealand unpublished petroleum report. PR732

Hunt International Petroleum Company, N. Z. (1977); Toroa-1 Well Completion Report. Ministry of Economic Development New Zealand unpublished petroleum report. PR691

Hunt International Petroleum Company, N. Z. (1976); Well Completion Report , Parara-1. Ministry of Economic Development New Zealand unpublished petroleum report. PR673

Indo-Pacific Energy (New Zealand), (2000); Ealing-1 Well Completion Report. Ministry of Economic Development New Zealand unpublished petroleum report. PR2559

Isaac, M. J., Herzer, R. H., Brook, F. J., and Hayward, B. W. (1994). *Cretaceous and Cenozoic geology of Northland, New Zealand*, Institute of Geological and Nuclear Sciences Ltd. Monograph 8. Institute of Geological and Nuclear Sciences Ltd., Lower Hutt.

Jarvis, G. T., and McKenzie, D. P. (1980). Sedimentary basin evolution with finite extension rates. *Earth and planetary science letters* **48**: 42-52.

Jassen, M. E., Torne, M., Cloetingh, S., and Banda, E. (1993). Pliocene uplift of the eastern Iberian margin: Inferences from quantitative modelling of the Valencia Trough. *Earth and planetary science letters* **119**: 585-597.

Kamp, P. J. J. (1986). Late Cretaceous-Cenozoic tectonic development of the southwest Pacific region. *Tectonophysics* **121**: 225-281.

Kamp, P. J. J., Webster, K. S., and Nathan, S. (1996). Thermal history analysis by intergrated modelling of apatite fission track and vitrinite reflectance data: application to an inverted basin (Buller Coalfield, New Zealand). *Basin Research* **8**: 383-402.

Kamp, P. J. J., Whitehouse, I. W. S., and Newman, J. (1999). Constraints on the thermal and tectonic evolution of the Greymouth coalfield. *New Zealand Journal of Geology and Geophysics* **42**: 447-467.

Karner, G. D., Studinger, M., and Bell, R. E. (2005). Gravity anomalies of sedimentary basins and their mechanical implications: Applications to the Ross Sea basins, West Antarctica. *Earth and planetary science letters* **235**: 577-596.

Kennett, J. P., Houtz, R. E., Andrews, P. B., Edwards, A. R., Gostin, V. A., Margolis, S. V., Ovenshine, A. T., and Perch-Nielsen, K. (1974). Development of the Circum-Antarctic Current. *Science* **186**: 144-147.

King, P. R. (1988a). Well summary sheets, onshore Taranaki, New Zealand, Report #: G125. New Zealand Geological Survey report.

King, P. R. (1988b). Well summary sheets, offshore Taranaki, New Zealand, Report #: G127. New Zealand Geological Survey report.

King, P. R. (2000). Tectonic reconstructions of New Zealand: 40 Ma to the Present. *New Zealand Journal of Geology and Geophysics* **43**.

King, P. R., and Robinson, P. H. (1988). An overview of Taranaki region geology, New Zealand. *Energy exploration and exploitation* **6**: 213-232.

King, P. R., and Thrasher, G. P. (1996). *Cretaceous-Cenozoic geology and petroleum systems of the Taranaki Basin, New Zealand*, Institute of Geological and Nuclear Sciences; monograph 13. Institute of Geological and Nuclear Sciences Limited, Lower Hutt.

Knox, G. J. (1982). Taranaki Basin, structural style and tectonic setting. *New Zealand Journal of Geology and Geophysics* **25**: 125-140.

Korsch, R. J., and Wellman, H. W. (1988). The geological evolution of New Zealand and the New Zealand region. In: *The Ocean Basins and Margins* (eds. A. E. M. S. Nairn, F. G.; Uyeda, S.). **7B:** 411-482. Plenum Publishing, New York.

Kusznir, N. J., Marsden, G., and Egan, S. (1991). A flexural-cantilever simple-shear/ pure-shear model of continental lithosphere extension: Applications to the Jeanne d'Arc Basin, Grand Banks and Viking Graben, North Sea. In: *The Geometry of Normal Faults: Special Publication Geological Society* (eds. **56:** 41-60.

Laird, M. G. (1981). *The late Mesozoic fragmentation of the New Zealand segment of Gondwana*. Gondwana Five: proceedings of the Fifth International Gondwana Symposium, Wellington, Balkema, Rotterdam.

Laird, M. G. (1993). Cretaceous continental rifts: New Zealand region. In: *South Pacific Sedimentary Basin. Sedimentary Basins of the World* (eds. P. F. Ballance). **2:** 37-49. Elsevier Science Publishers, Amsterdam.

Laird, M. G. (1994). Geological aspects of the opening of the Tasman Sea. In: *Evolution of the Tasman Sea* (eds. G. J. S. Van der Lingen, K. M.; Muir, R. J.). 27-30. A. A. Balkema, Rotterdam.

Lamarche, G., Collot, J. Y., Wood, R. A., Sosson, M., Sutherland, R., and Delteil, J. (1997). The Oligocene-Miocene Pacific-Australia plate boundary, south of New Zealand: Evolution from oceanic spreading to strike-slip faulting. *Earth and planetary science letters* **148**: 129-139.

Larsen, J. M., and Sporli, K. B. (1989). Structure of the Tangihua Ophiolites at Ahipara, Northland, New Zealand. *The Royal Society of New Zealand Bulletin* **26**: 137-144.

Lawver, L. A., and Gahagan, L. (1994). *Simplified Cenozoic Antarctic-Australian-New Zealand tectonics (abstract)*. Eos Transactions AGU 73(44), Fall meeting suppliment.

Lewis, D. W., and Belliss, S. E. (1984). Mid Tertiary unconformities in the Waitaki Subdivision, North Otago. *Journal of the Royal Society of New Zealand* **14**: 251-276.

Lewis, D. W., and Pettinga, J. R.. (1993). The emerging, imbicated frontal wedge of the Hikurangi margin. In: *South Pacific Sedimentary Basins, Sedimentary Basins of the World, 2* (eds. P. F. Ballance). Elsevier, Amsterdam.

Loutit, T. S., and Kennett, J. P. (1981). New Zealand and Australian Cenozoic sedimentary cycles and global sea-level changes. *American Association of Petroleum Geologists Bulletin* **65**: 1586-1601.

Malahoff, A., Feden, R. H., and Fleming, H. S. (1982). Magnetic anomolies and tectonic fabric of marginal basins north of New Zealand. *Journal of Geophysical Research* **87**: 4109-4125.

Malpas, J., Sporli, K. B., Black, P. M., and Smith, I. E. M. (1992). Northland ophiolite, New Zealand, and implications for plate-tectonic evolution of the southwest Pacific. *Geology* **20**: 149-152.

Marks, K. M., and Stock, J. M. (1997). Early Tertiary gravity field reconstructions of the southwest Pacific. *Earth and planetary science letters* **152**: 267-274.

McKenzie, D. P. (1978). Some remarks on the development of sedimentary basins. *Earth and planetary science letters* **40**: 25-32.

Miller, K. G., Wright, J. D., and Fairbanks, R. G. (1991). Unlocking the ice house: Oligocene-Miocene oxygen isotope, eustasy, and margin erosion. *Journal of Geophysical Research* **96**: 6829-48.

Milne, A. D./ Shell BP Todd Canterbury Services Ltd., (1975); Resolution-1 Well Completion Report. Ministry of Economic Development New Zealand unpublished petroleum report. PR648

Mitrovica, J. X., and Jarvis, G. T. (1985). Surface deflections due to transient subduction in a convecting mantle. *Tectonophysics* **120**: 211-237.

Mitrovica, J. X., Beaumont, C., and Jaris, G. T. (1989). Tilting of continental interiors by the dynamical effects of subduction. *Tectonics* **8**(5): 1079-1094.

Molnar, P. (2004). Late Cenozoic increase in accumulation rates of terrestrial sediment: How might climate change have affected erosion rates? *Annual Review of Earth and Planetary Science* **32**: 67-89.

Molnar, P., and England, P. (1990). Late Cenozoic uplift of mountain ranges and global climate change: chicken or egg? *Nature* **346**: 29-34.

Molnar, P., Atwater, T., Mammerickx, A., and Smith, S. M. (1975). Magnetic anomalies, bathymetry and the tectonic evolution of the south Pacific since the late Cretaceous. *Geophysical Journal of the Royal Astronomical Society.* **40**: 383-420.

Nalivkin, V. D. (1976). Dynamic development of the Russian Platform structures. *Tectonophysics* **36**: 247-262.

Nathan, S., and others (1986). *Cretaceous and Cenozoic sedimentary basins of the West Coast Region, South Island, New Zealand*, New Zealand Geological Survey Basin Studies 1. New Zealand Geological Survey, Lower Hutt.

Norris, R. J., and Turnbull, I. M. (1993). Cenozoic basins adjacent to an evolving transform plate boundary, southwest New Zealand. In: *South Pacific Sedimentary Basin. Sedimentary Basins of the World* (eds. P. F. Ballance). **2:** 251-270. Elsevier Science Publishers, Amsterdam.

Norris, R. J., Koons, P. O., and Cooper, A. F. (1990). The obliquely-convergent plate boundary in southern New Zealand: implications for ancient collision zones. *Journal of Structural Geology* **12**: 715-725.

Palmer, J. A. (1985). Pre-Miocene lithostratigraphy of Taranaki Basin, New Zealand. *New Zealand Journal of Geology and Geophysics* **28**: 197-216.

Palmer, J. A., and Andrews, P. B. (1993). Cretaceous-Tertiary sedimentation and implied tectonic controls on the structural evolution of Taranaki Basin, New Zealand. In: *South Pacific Sedimentary Basins. Sedimentary Basins of the World.* (eds. P. F. Ballance). **2:** 309-328. Elsevier Science Publishers, Amsterdam.

Parker, R. J., Ballance, P. F., and Sporli, K. B. (1989). Small Tangihua volcanic masses at low levels in the Northland Allochthon, New Zealand: tectonic significance. *The Royal Society of New Zealand Bulletin* **26**: 127-136.

Peper, T. (1994). Tectonic and eustatic control on Albian shallowing (Viking and Paddy Formations) in Western Canada Foreland basin. *Geological Society of America Bulletin* **106**: 253-264.

Placid Oil Company (1984); Well Report, Rakiura-1, Great South Basin, New Zealand. Ministry of Economic Development New Zealand unpublished petroleum report. PR994

Pulford, A., and Stern, T. A. (2004). Pliocene exhumation and landscape evolution of central North Island, New Zealand: The role of the upper mantle. *Journal of Geophysical Research* **109**: F01016.

Rainey, S. W., D./ Petroleum Corporation of New Zealand Ltd., (1989); Tapawera-1 Well Completion Report. PPL38500. Ministry of Economic Development New Zealand unpublished petroleum report. PR1445

Royden, L., and Keen, C. E. (1980). Rifting processes and thermal evolution of the continental margin of eastern Canada determined from subsidence curves. *Earth and planetary science letters* **51**: 343-361.

Russell, M., and Gurnis, M. (1994). The planform of epeirogeny: Vertical motions of Australia during the Cretaceous. *Basin Research* **6**: 63-76.

Scherwath, M., Stern, T., Davey, F., Okaya, D., Holbrook, W. S., Davies, R., and Kleffmann, S. (2003). Lithospheric structure across oblique continental collision in New Zealand from wide-angle *P* wave modelling. *Journal of Geophysical Research* **108**(B12): 2566.

Schofield, J. C. (1951). Distribution of lower Oligocene volcanics in New Zealand. *New Zealand Journal of Science and Technology* **B33**: 201-217.

Sclater, J. G., and Christie, P. A. F. (1980). Continental stretching: an explanation of the post mid-Cretaceous subsidence of the central North Sea basin. *Journal of Geophysical Research* **85**: 3711-3739.

Shackleton, N. J., and Kennett, J. P. (1975). Paleotemperature history of the Cenozoic and the initiation of Antarctic glaciation: oxygen and carbon isotope analyses in DSDP sites 277, 279 and 281. In: *Initial reports of the Deep Sea Drilling Project* (eds. J. P. e. a. Kennett). **21**. U.S. Govt. Printing Office, Washington, D.C.

Shell B.P. and Todd Oil Services Ltd. (1976); Well Completion Report, Surville-1. Ministry of Economic Development New Zealand unpublished petroleum report. PR677

Shell B.P. and Todd Oil Services Ltd. (1984); Completion Report. Ariki-1 Well. PPL38048. Ministry of Economic Development New Zealand unpublished petroleum report. PR1038

Shell B.P. and Todd Oil Services Ltd. (1982); Well Resume Kiwa-1. PPL38055. Ministry of Economic Development New Zealand unpublished petroleum report. PR880

Shell B.P. and Todd Oil Services Ltd. (1976); Well Resume Kupe-1. Ministry of Economic Development New Zealand unpublished petroleum report. PR662

Shell B.P. and Todd Oil Services Ltd. (1970); Well Resume Maui-2. Ministry of Economic Development New Zealand unpublished petroleum report. PR541

Shell B.P. and Todd Oil Services Ltd. (1976); Well Resume, Tane-1 (Offshore). Ministry of Economic Development New Zealand unpublished petroleum report. PR698

Shell B.P. and Todd Oil Services Ltd. (1984); Drilling Completion Report, Clipper-1. Offshore Canterbury, South Island, New Zealand. PPL 38202. Ministry of Economic Development New Zealand unpublished petroleum report. PR1036

Sircombe, K. N., and Kamp, P. J. J. (1998). The South Westland Basin: seismic stratigraphy, basin geometry and evolution of a foreland basin within the Southern Alps collision zone, New Zealand. *Tectonophysics* **300**: 359-387.

Smale, D. (1987). Heavy minerals in Cretaceous-Cenozoic sandstones in Canterbury. *New Zealand Geological survey report* **SL17**.

Smart, G. M./ New Zealand Petroleum Exploration Company Ltd., (1972); Waiho-1 Exploratory Well, Westland, South Island, New Zealand. Ministry of Economic Development New Zealand unpublished petroleum report. PR529

Smith, I. E., Day, R. A., and Ashcroft, J. (1986). Volcanic Associations of Northland. *New Zealand Geological survey record* **12**: 5-32.

Smith, W. H. F., and Sandwell, D. T. (1995). Marine gravity field from declassified Geosat and ERS-1 altimetry. *EOS transactions AGU 1995, supplement* **156**.

Stagpoole, V., Hill, M., Thornton, S., Wood, R., and Funnel, R. (2002). *New Zealand basin development and depositional system evolution: quantification and visualisation*. New Zealand Petroleum Conference Proceedings.

Stern, T. A. (1987). Asymmetric back-arc spreading, heat flux and structure associated with the Central Volcanic Region of New Zealand. *Earth and planetary science letters* **85**: 265-276.

Stern, T. A., and Davey, F. J. (1990). Deep seismic expression of a foreland basin: Taranaki Basin, New Zealand. *Geology* **18**: 979-982.

Stern, T. A., and Holt, W. E. (1994). Platform subsidence behind an active subduction zone. *Nature* **368**: 233-236.

Stern, T. A., Quinlan, G. M., and Holt, W. E. (1992). Basin formation behind an active subduction zone: three-dimensional flexure modelling of the Wangnui Basin, New Zealand. *Basin Research* **4**: 197-214.

Stock, J., and Molnar, P. (1982). Uncertainties in the relative positions of the Australia, Antarctica, Lord Howe, and Pacific plates since the Late Cretaceous. *Journal of Geophysical Research* **87**: 4697-4717.

Sutherland, R. (1995). The Australia-Pacific boundary and Cenozoic plate motions in the SW Pacific: Some constraints from Geosat data. *Tectonics* **14**(4): 819-831.

Sutherland, R. (1999). Basement geology and tectonic development of the greater New Zealand region: an interpretation from regional magnetic data. *Tectonophysics* **308**: 341-362.

Sutherland, R., and Browne, G. (2003). Canterbury Basin offers potential on South Island, New Zealand. *Oil and Gas Journal* **101**(5): 45-49.

Sutherland, R., and Melhuish, A. (2000). Formation and evolution of the Solander Basin, southwestern South Island, New Zealand, controlled by a major fault in the continental crust and upper mantle. *Tectonics* **19**(1): 44-61.

Taylor, B., and Karner, G. D. (1983). On the evolution of marginal basins. *reviews of Geophysics and Space Physics* **21**: 1727-1742.

Thiede, R. C., Arrowsmith, J. R., Bookhagen, B., McWilliams, M. O., Sobel, E. R., and Strecker, M. R. (2005). From tectonically to erosionally controlled development of the Himilayan orogen. *Geology* **33**(8): 689-692.

Thrasher, G. P. (1990). *Tectonics of the Taranaki Rift*. 1989 New Zealand Oil Exploration Conference proceedings: 124-133., Ministry of Commerce, Wellington.

Thrasher, G. P. (1992). *Late Cretaceous geology of Taranaki Basin, New Zealand*, thesis, Victoria University of Wellington.

Turcotte, D. L., and Schubert, G. (1982). *Geodynamic Applications of Continuum Physics to Geological Problems.* John Wiley and Sons, New York.

Turnbull, I. M., Lindqvist, J. K., Norris, R. J., Carter, R. M., Cave, M. P., Sykes, R., and Hyden, F. M. (1989). Lithostratigraphic nomenclature of the Cretaceous and Tertiary sedimentary rocks of Western Southland, New Zealand. *New Zealand Geological survey bulletin* **13**.

Turnbull, I. M., Uruski, C. I., and others (1993). *Cretaceous and Cenozoic Sedimentary Basins of Western Southland, South Island, New Zealand.* Institute of Geological and Nuclear Sciences, Lower Hutt.

Vail, P. R., and Hardenbol, J. (1979). Sea-level changes during the Tertiary. *Oceanus* **22**(3): 71-79.

Vail, P. R., Mitchum, R. M., and Thompson, S. (1977). Seismic stratigraphy and global changes in sea level. Part 4: Global cycles of relative changes of sea level. *American Association of Petroleum Geologists Memoir* **26**: 83-97.

van Hinte, J. E. (1978). Geohistory analysis: application of micropaleontology in exploration geology. *Bulletin American Association of Petroleum Geologists* **62**: 201-222.

Walcott, R. I. (1970).Flexural rigidity, thickness and viscosity of the lithosphere. *Journal of Geophysical Research* **75**: 3941-3954.

Walcott, R. I. (1998). Modes of oblique compression: late Cenozoic tectonics of the South Island of New Zealand. *Reviews of Geophysics* **36**: 1-26.

Ward, C. M. (1988). Marine terraces of the Waitutu district and their relationship to the late Cenozoic tectonics of the southern Fiordland region, New Zealand. *Journal of the Royal Society of New Zealand* **18**: 1-28.

Ward, D. M., and Lewis, D. W. (1975). Paleoenvironmental implications of storm-scoured, ichnofossiliferous mid-Tertiary limestones, Waihao District, south Canterbury, New Zealand. *New Zealand Journal of Geology and Geophysics* **18**: 881-908.

Watts, A. B. (2001). *Isostasy and Flexure of the Lithosphere.* Cambridge University Press, Cambridge.

Weissel, J. K., and Hayes, D. E. (1972). Evolution of the Tasman Sea reappraised. *Earth and planetary science letters* **36**: 77-84.

Weissel, J. K., Hayes, D. E., and Herron, E. M. (1977). Plate tectonic synthesis: The displacement between Australia, New Zealand and Antarctica since the late Cretaceous. *Marine Geology* **25**: 231-277.

Wellman, H., W. (1979). An uplift map for the South Island of New Zealand, and a model for uplift of the Southern Alps. *Bulletin of the Royal Society of New Zealand* **18**: 13-20.

Wernicke, B. (1981). Low-angle normal faults in the Basin and Range province: nappe tectonics in an extending orogen. *Nature* **291**: 645-648.

Wilson, D. D. (1963). Geology of the Waipara Subdivison (Amberley and Motunau sheets S68 and S69). *New Zealand Geological survey bulletin* **64**.

Wilson, I. R., and others/ Shell BP Todd Canterbury Services Ltd., (1985); Well Completion Report, Galleon-1. PPL 38203. Ministry of Economic Development New Zealand unpublished petroleum report. PR1146

Wiltshire, M. J./ Home Energy New Zealand Ltd., (1984); Well Completion Report, Kongahu-1. PPL38058. Offshore, West Coast, South Island, New Zealand. Ministry of Economic Development New Zealand unpublished petroleum report. PR1035

Wood, B. L./ New Zealand Petroleum Exploration Co. Ltd., (1969); Leeston-1. Ministry of Economic Development New Zealand unpublished petroleum report. PR526

Wood, R., Lamarche, G., Herzer, R., Delteil, J., and Davy, B. (1996). Paleogene seafloor spreading in the southeast Tasman Sea. *Tectonics* **15**(5): 966-975.

Wood, R. A., Andrews, P. B., Herzer, R. H. and others (1989). *Cretaceous and Cenozoic Geology of the Chatham Rise Region, South Island, New Zealand*, New Zealand Geological Survey Basin Studies; 3*.* New Zealand Geological Society, Lower Hutt.

Zachos, J., Pagani, M., Sloan, L., Thomas, E., and Billups, K. (2001). Trends, rhythms, and aberrationa in global climate 65 Ma to present. *Science* **292**: 686-693.

APPENDIX A
STRATIGRAPHIC COLUMNS

CANTERBURY BASIN

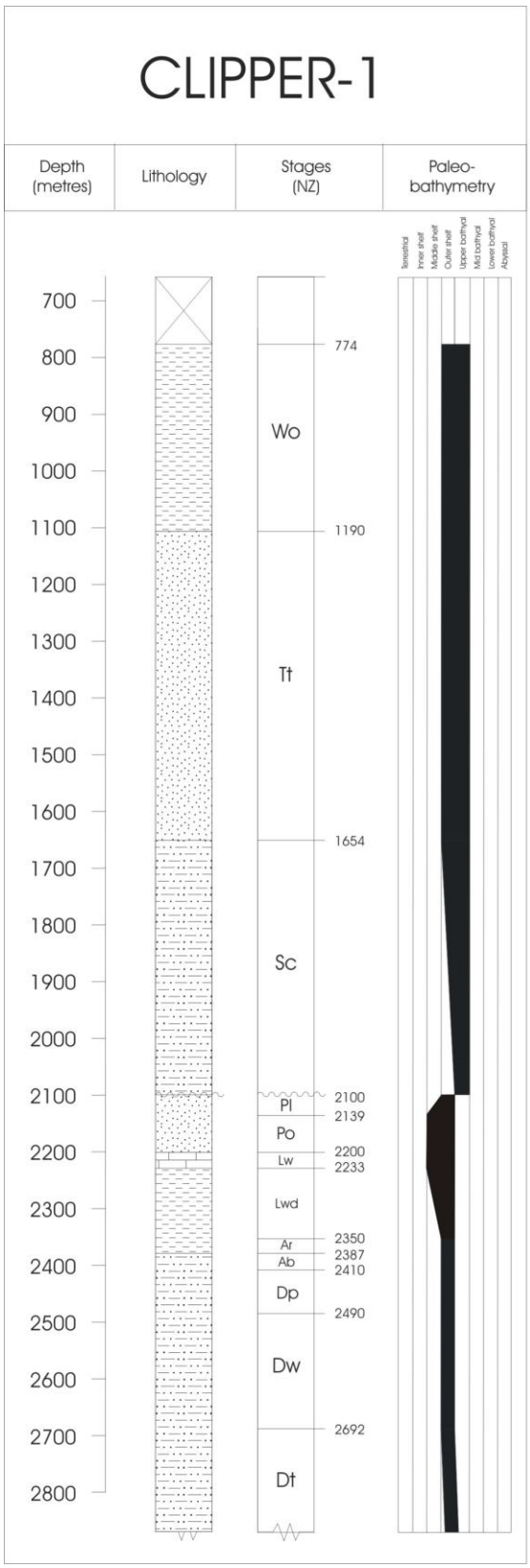
CLIPPER-1
Depth (metres)
Lithology
Stages (NZ)
Paleo-bathymetry
Terrestrial
Inner shelf
Middle shelf
Outer shelf
Upper bathyal
Mid bathyal
Lower bathyal
Abyssal
700
800
900
1000
1100
1200
1300
1400
1500
1600
1700
1800
1900
2000
2100
2200
2300
2400
2500
2600
2700
2800
774
Wo
1190
Tt
1654
Sc
2100
Pl
2139
Po
2200
Lw
2233
Lwd
2350
Ar
2387
Ab
2410
Dp
2490
Dw
2692
Dt

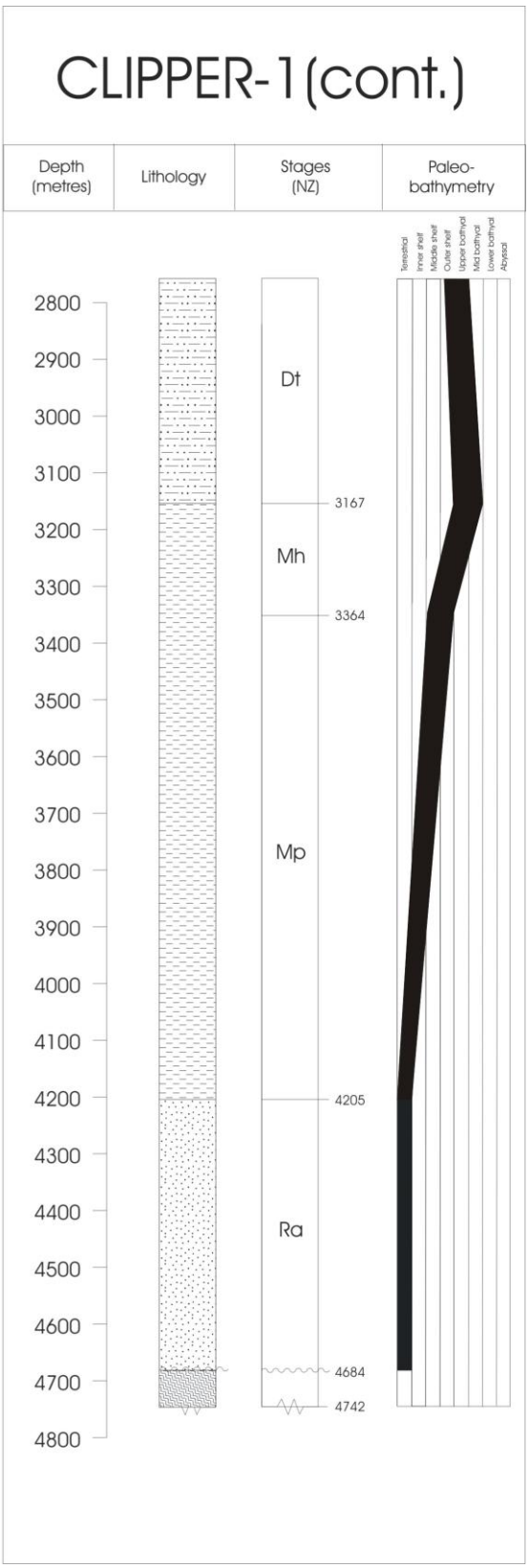
CLIPPER-1 (cont.)
Depth (metres)
Lithology
Stages (NZ)
Paleo-bathymetry
Terrestrial
Inner shelf
Middle shelf
Outer shelf
Upper bathyal
Mid bathyal
Lower bathyal
Abyssal
2800
2900
3000
3100
3200
3300
3400
3500
3600
3700
3800
3900
4000
4100
4200
4300
4400
4500
4600
4700
4800
Dt
3167
Mh
3364
Mp
4205
Ra
4684
4742

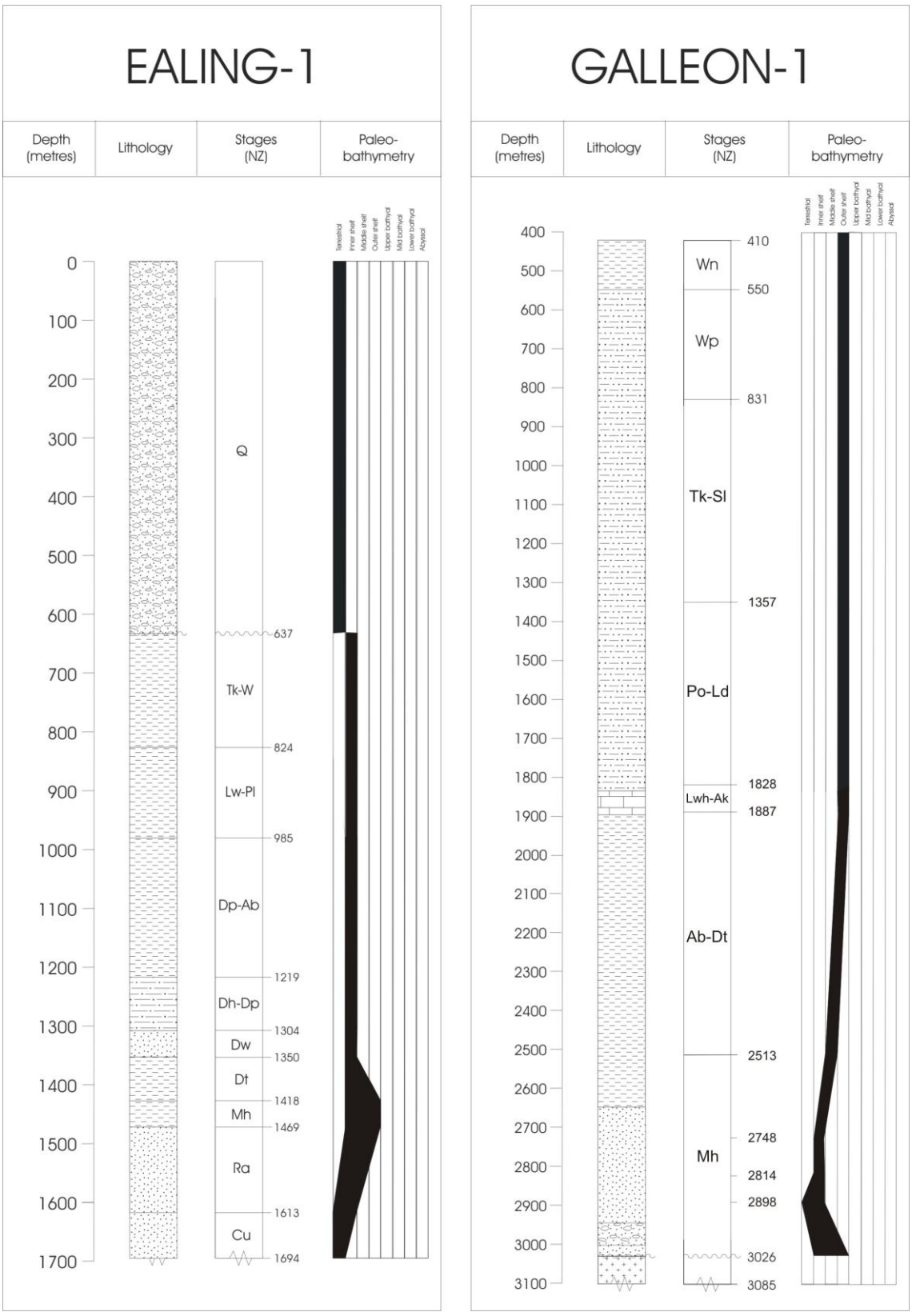
EALING-1
Depth (metres)
Lithology
Stages (NZ)
Paleo-bathymetry
Terrestrial
Inner shelf
Middle shelf
Outer shelf
Upper bathyal
Mid bathyal
Lower bathyal
Abyssal
0
100
200
300
400
500
600
700
800
900
1000
1100
1200
1300
1400
1500
1600
1700
Q
637
Tk-W
824
Lw-Pl
985
Dp-Ab
1219
Dh-Dp
1304
Dw
1350
Dt
1418
Mh
1469
Ra
1613
Cu
1694
GALLEON-1
Depth (metres)
Lithology
Stages (NZ)
Paleo-bathymetry
400
500
600
700
800
900
1000
1100
1200
1300
1400
1500
1600
1700
1800
1900
2000
2100
2200
2300
2400
2500
2600
2700
2800
2900
3000
3100
Wn
410
550
Wp
831
Tk-Sl
1357
Po-Ld
1828
Lwh-Ak
1887
Ab-Dt
2513
Mh
2748
2814
2898
3026
3085

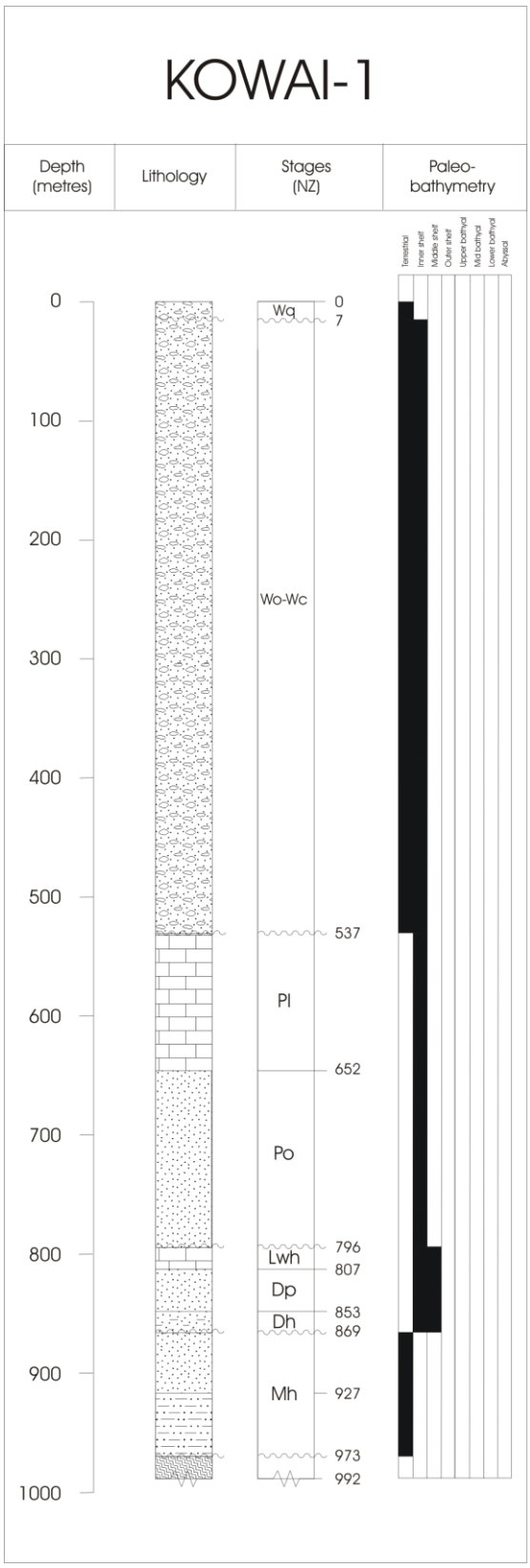
KOWAI-1
Depth (metres)
Lithology
Stages (NZ)
Paleo-bathymetry
Terrestrial
Inner shelf
Middle shelf
Outer shelf
Upper bathyal
Mid bathyal
Lower bathyal
Abyssal
0
100
200
300
400
500
600
700
800
900
1000
Wq
Wo-Wc
Pl
Po
Lwh
Dp
Dh
Mh
0
7
537
652
796
807
853
869
927
973
992

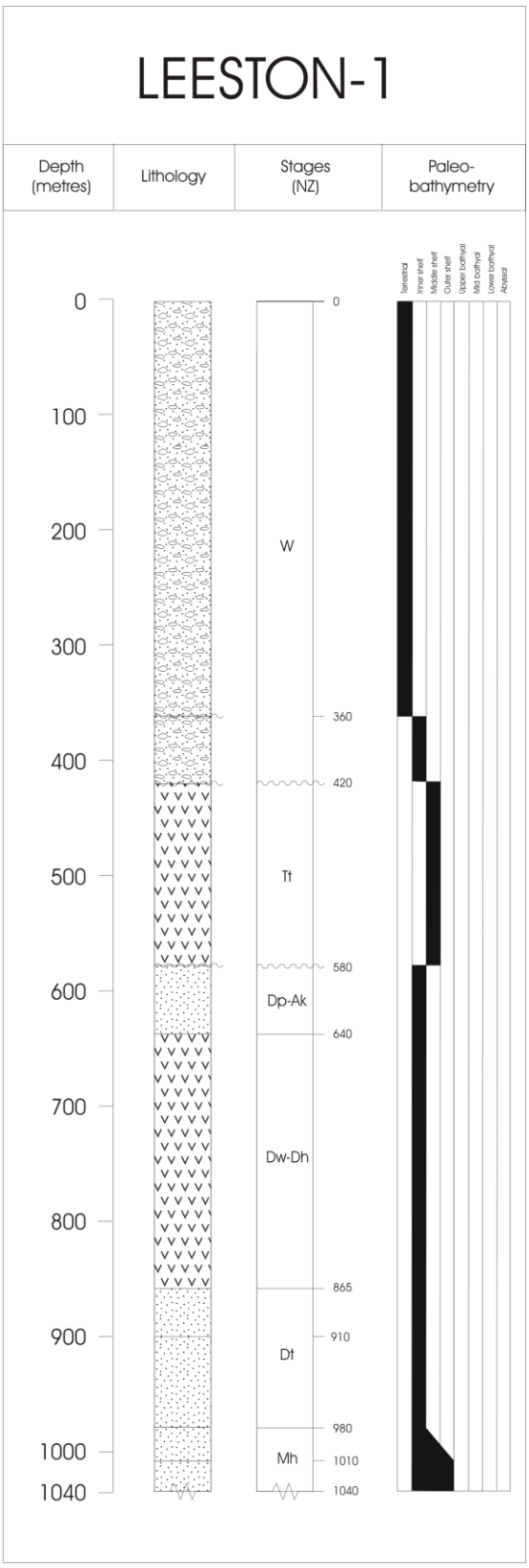
LEESTON-1
Depth (metres)
Lithology
Stages (NZ)
Paleo-bathymetry
Terrestrial
Inner shelf
Middle shelf
Outer shelf
Upper bathyal
Mid bathyal
Lower bathyal
Abyssal
0
100
200
300
400
500
600
700
800
900
1000
1040
W
Tt
Dp-Ak
Dw-Dh
Dt
Mh
0
360
420
580
640
865
910
980
1010
1040

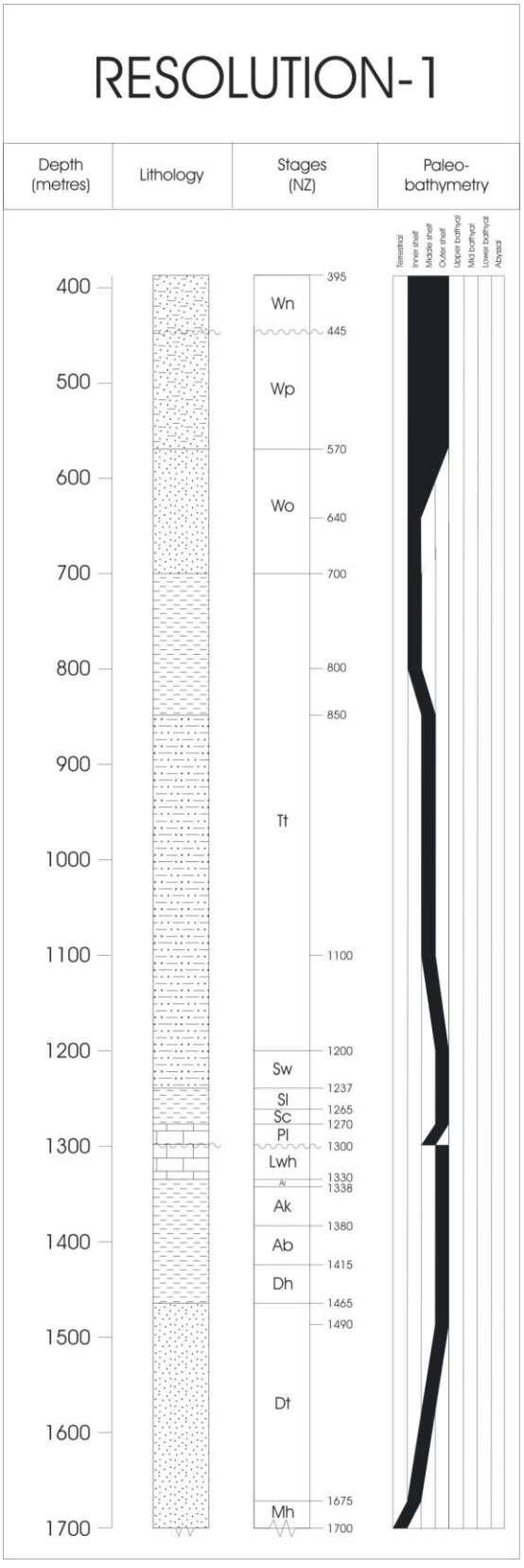
RESOLUTION-1
Depth (metres)
Lithology
Stages (NZ)
Paleo-bathymetry
Terrestrial
Inner shelf
Middle shelf
Outer shelf
Upper bathyal
Mid bathyal
Lower bathyal
Abyssal
400
500
600
700
800
900
1000
1100
1200
1300
1400
1500
1600
1700
Wn
Wp
Wo
Tt
Sw
Sl
Sc
Pl
Lwh
Ak
Ab
Dh
Dt
Mh
395
445
570
640
700
800
850
1100
1200
1237
1265
1270
1300
1330
1338
1380
1415
1465
1490
1675
1700

APPENDIX A
STRATIGRAPHIC COLUMNS

GREAT SOUTH BASIN

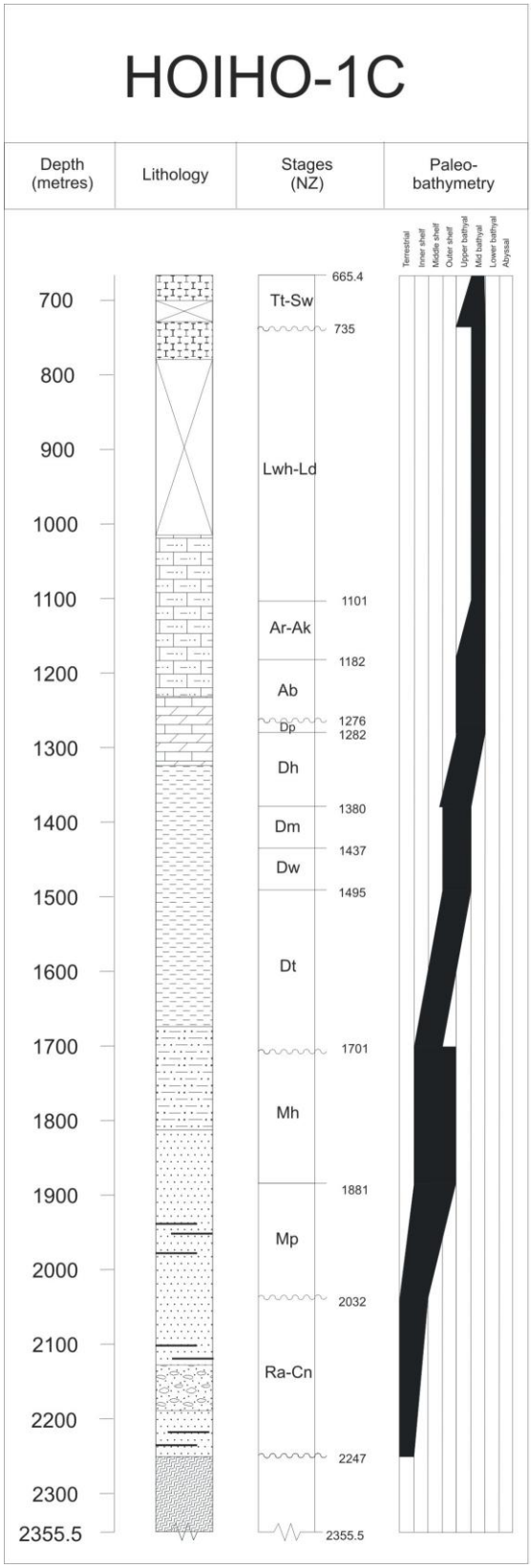
HOIHO-1C
Depth (metres)
Lithology
Stages (NZ)
Paleo-bathymetry
Terrestrial
Inner shelf
Middle shelf
Outer shelf
Upper bathyal
Mid bathyal
Lower bathyal
Abyssal
700
800
900
1000
1100
1200
1300
1400
1500
1600
1700
1800
1900
2000
2100
2200
2300
2355.5
665.4
Tt-Sw
735
Lwh-Ld
1101
Ar-Ak
1182
Ab
1276
Dp
1282
Dh
1380
Dm
1437
Dw
1495
Dt
1701
Mh
1881
Mp
2032
Ra-Cn
2247
2355.5

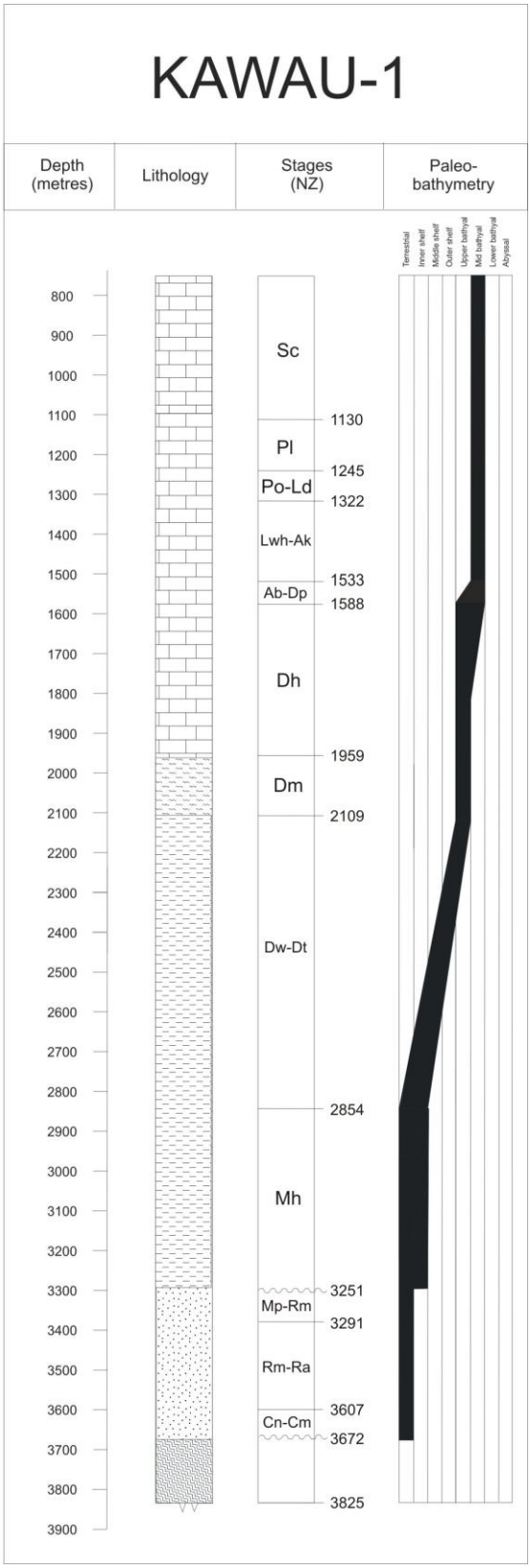
KAWAU-1
Depth (metres)
Lithology
Stages (NZ)
Paleo-bathymetry
Terrestrial
Inner shelf
Middle shelf
Outer shelf
Upper bathyal
Mid bathyal
Lower bathyal
Abyssal
800
900
1000
1100
1200
1300
1400
1500
1600
1700
1800
1900
2000
2100
2200
2300
2400
2500
2600
2700
2800
2900
3000
3100
3200
3300
3400
3500
3600
3700
3800
3900
Sc
1130
Pl
1245
Po-Ld
1322
Lwh-Ak
1533
Ab-Dp
1588
Dh
1959
Dm
2109
Dw-Dt
2854
Mh
3251
Mp-Rm
3291
Rm-Ra
3607
Cn-Cm
3672
3825

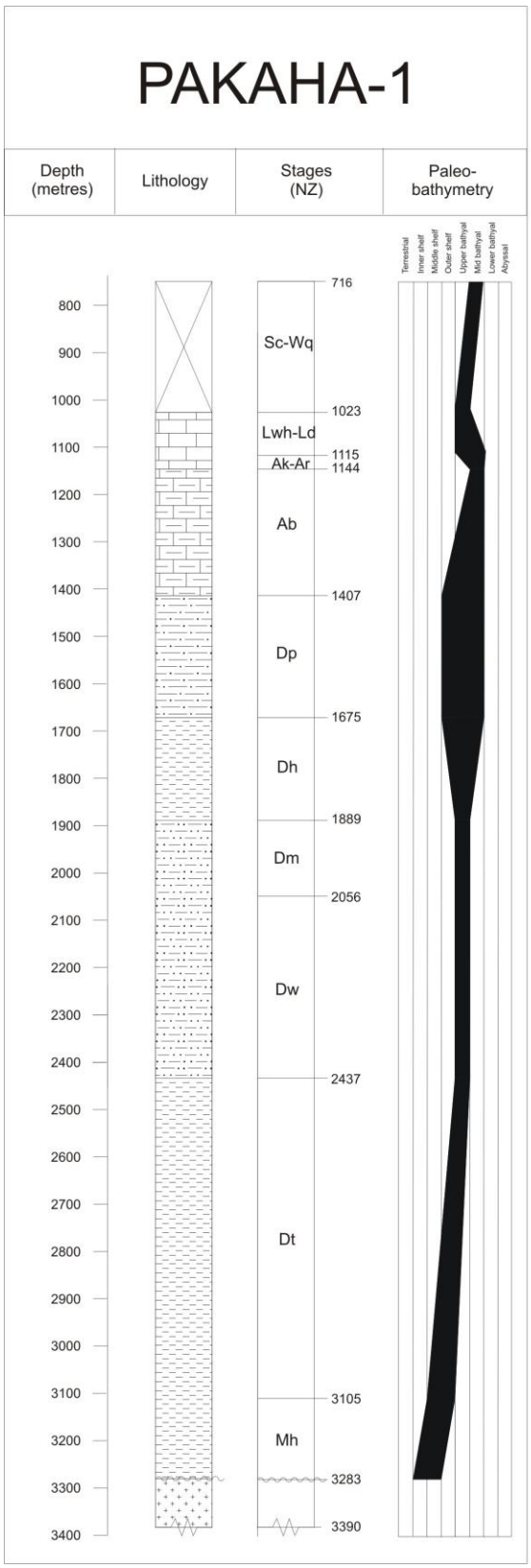
PAKAHA-1
Depth (metres)
Lithology
Stages (NZ)
Paleo-bathymetry
Terrestrial
Inner shelf
Middle shelf
Outer shelf
Upper bathyal
Mid bathyal
Lower bathyal
Abyssal
800
900
1000
1100
1200
1300
1400
1500
1600
1700
1800
1900
2000
2100
2200
2300
2400
2500
2600
2700
2800
2900
3000
3100
3200
3300
3400
716
Sc-Wq
1023
Lwh-Ld
1115
Ak-Ar
1144
Ab
1407
Dp
1675
Dh
1889
Dm
2056
Dw
2437
Dt
3105
Mh
3283
3390

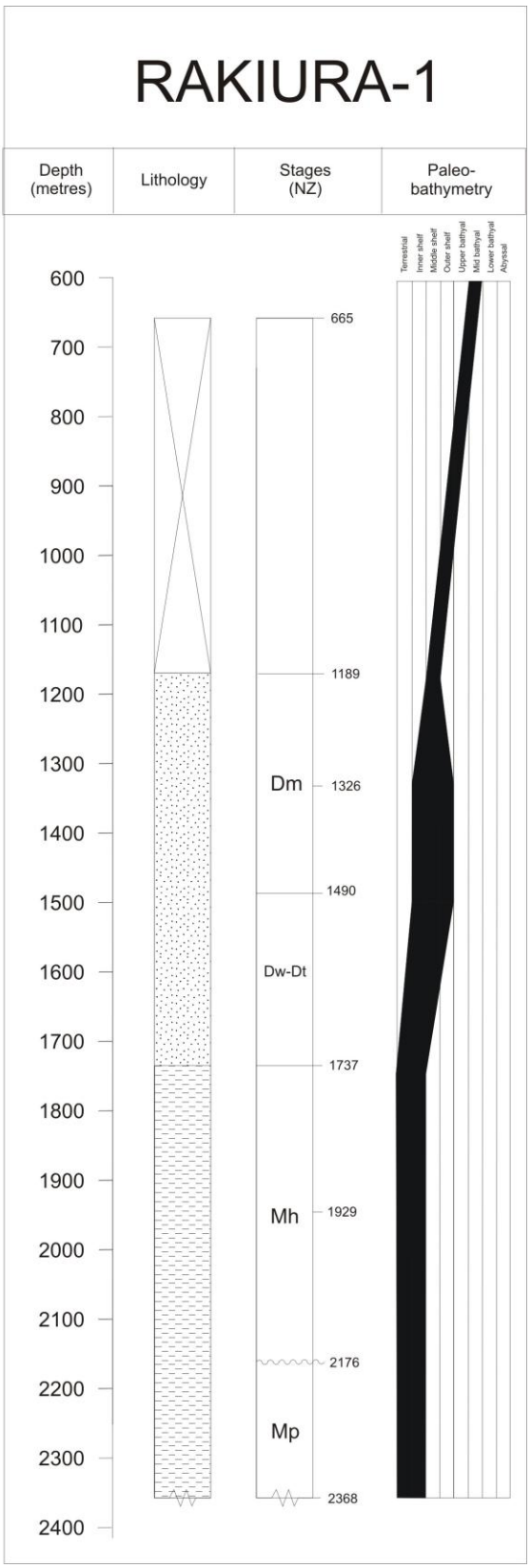
RAKIURA-1
Depth (metres)
Lithology
Stages (NZ)
Paleo-bathymetry
Terrestrial
Inner shelf
Middle shelf
Outer shelf
Upper bathyal
Mid bathyal
Lower bathyal
Abyssal
600
700
800
900
1000
1100
1200
1300
1400
1500
1600
1700
1800
1900
2000
2100
2200
2300
2400
665
1189
Dm
1326
1490
Dw-Dt
1737
Mh
1929
2176
Mp
2368

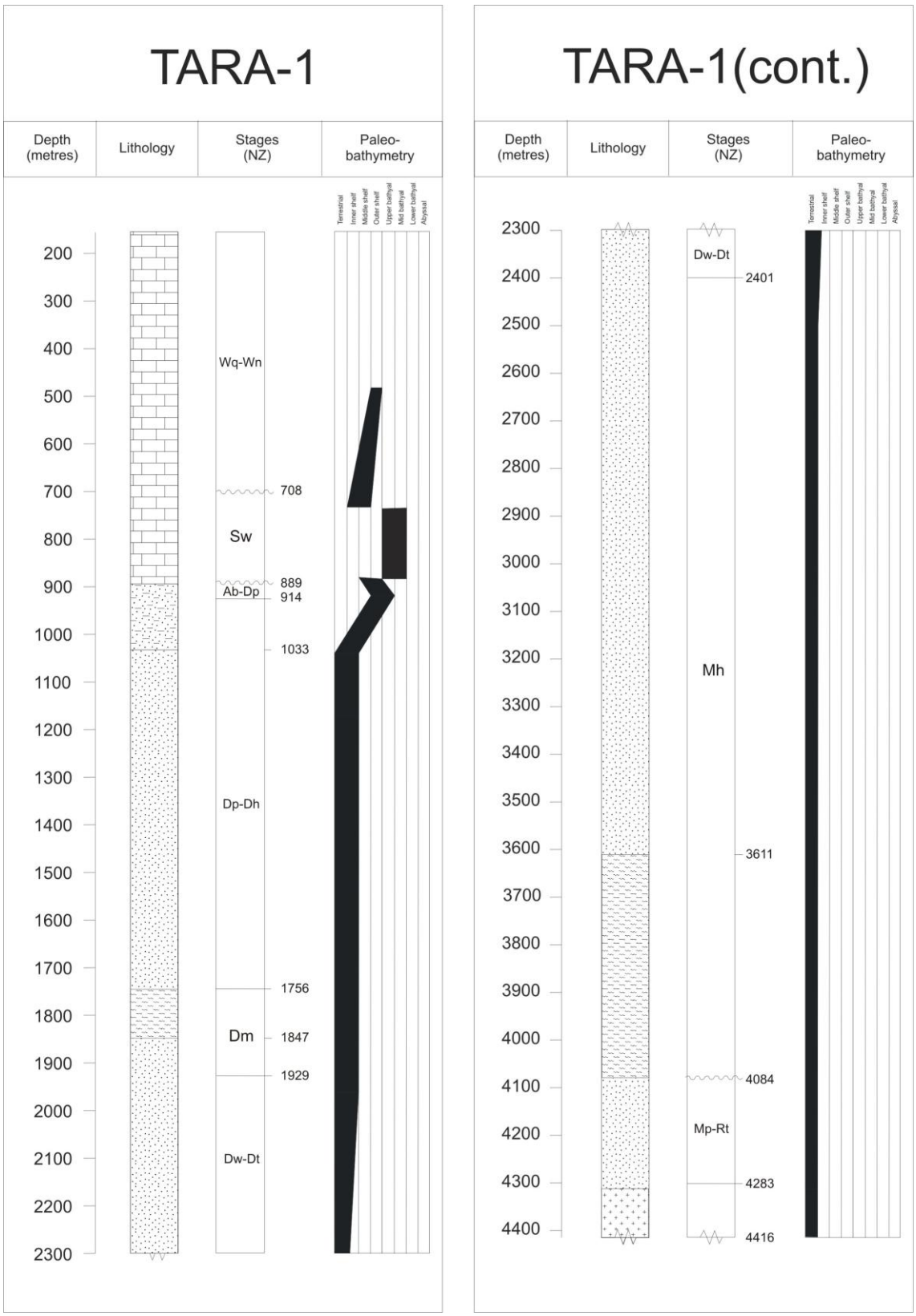
TARA-1
Depth (metres)
Lithology
Stages (NZ)
Paleo-bathymetry
Terrestrial
Inner shelf
Middle shelf
Outer shelf
Upper bathyal
Mid bathyal
Lower bathyal
Abyssal
200
300
400
500
600
700
800
900
1000
1100
1200
1300
1400
1500
1600
1700
1800
1900
2000
2100
2200
2300
Wq-Wn
708
Sw
889
Ab-Dp
914
1033
Dp-Dh
1756
Dm
1847
1929
Dw-Dt
TARA-1(cont.)
Depth (metres)
Lithology
Stages (NZ)
Paleo-bathymetry
2300
2400
2500
2600
2700
2800
2900
3000
3100
3200
3300
3400
3500
3600
3700
3800
3900
4000
4100
4200
4300
4400
Dw-Dt
2401
Mh
3611
4084
Mp-Rt
4283
4416

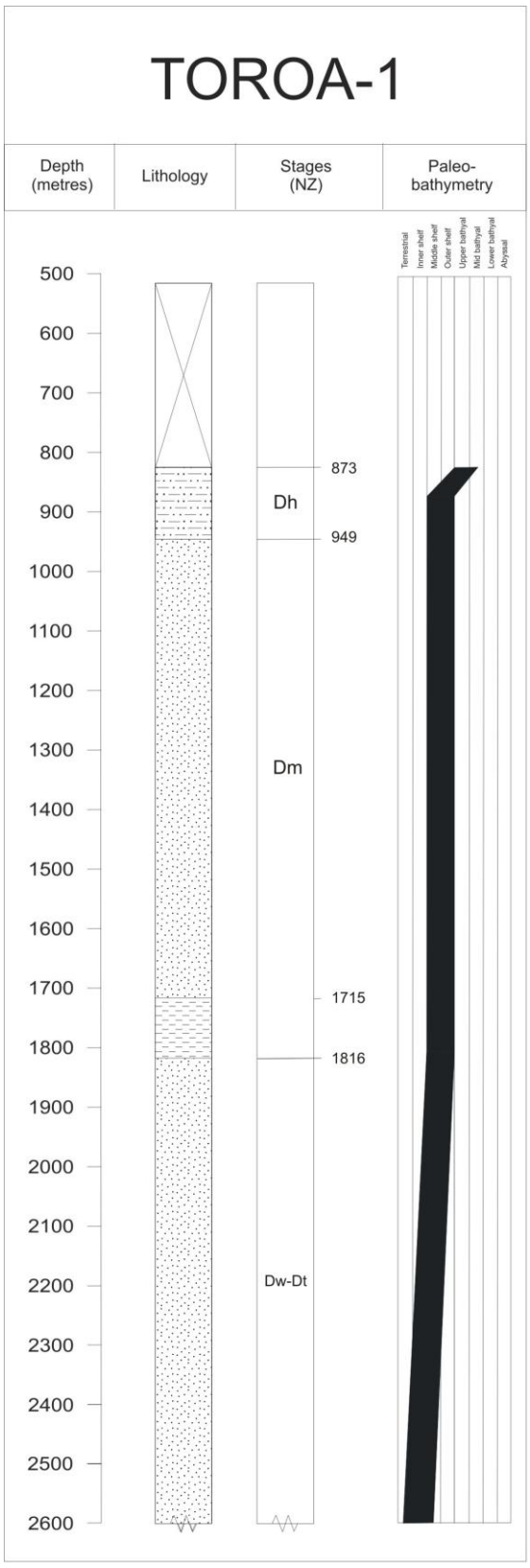
TOROA-1
Depth (metres)
Lithology
Stages (NZ)
Paleo-bathymetry
Terrestrial
Inner shelf
Middle shelf
Outer shelf
Upper bathyal
Mid bathyal
Lower bathyal
Abyssal
500
600
700
800
900
1000
1100
1200
1300
1400
1500
1600
1700
1800
1900
2000
2100
2200
2300
2400
2500
2600
873
Dh
949
Dm
1715
1816
Dw-Dt

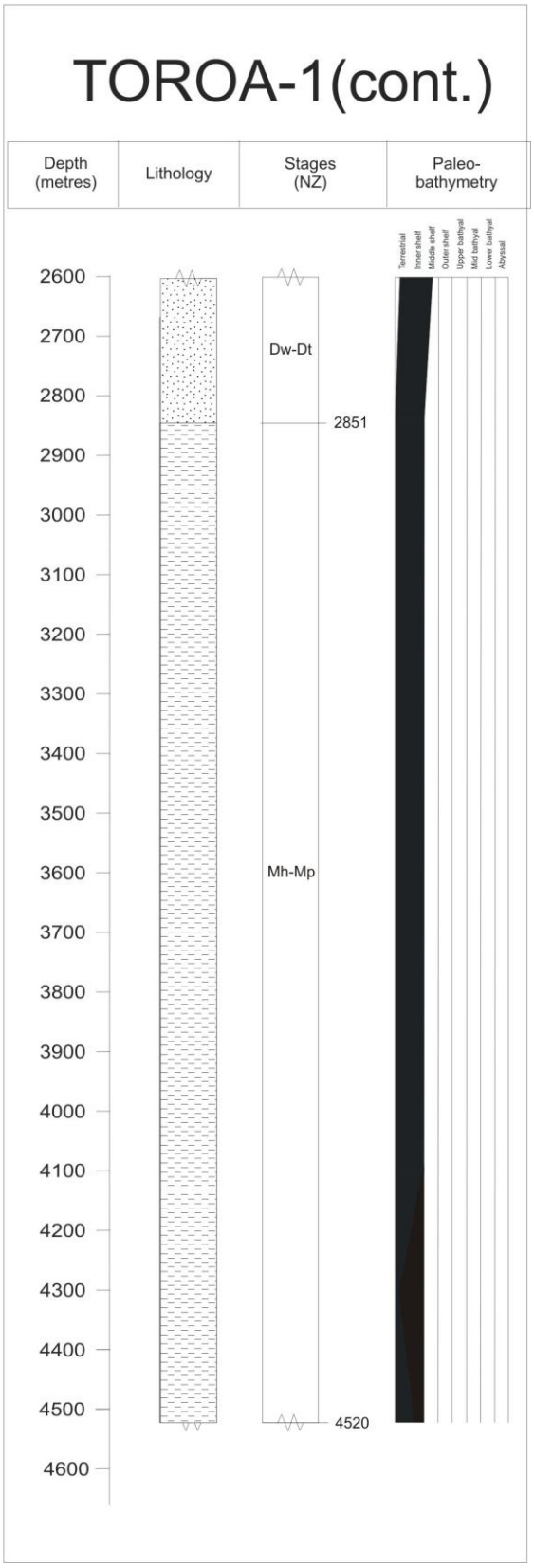
TOROA-1(cont.)
Depth (metres)
Lithology
Stages (NZ)
Paleo-bathymetry
Terrestrial
Inner shelf
Middle shelf
Outer shelf
Upper bathyal
Mid bathyal
Lower bathyal
Abyssal
2600
2700
2800
2900
3000
3100
3200
3300
3400
3500
3600
3700
3800
3900
4000
4100
4200
4300
4400
4500
4600
Dw-Dt
2851
Mh-Mp
4520

APPENDIX A
STRATIGRAPHIC COLUMNS

WESTERN SOUTHLAND BASIN

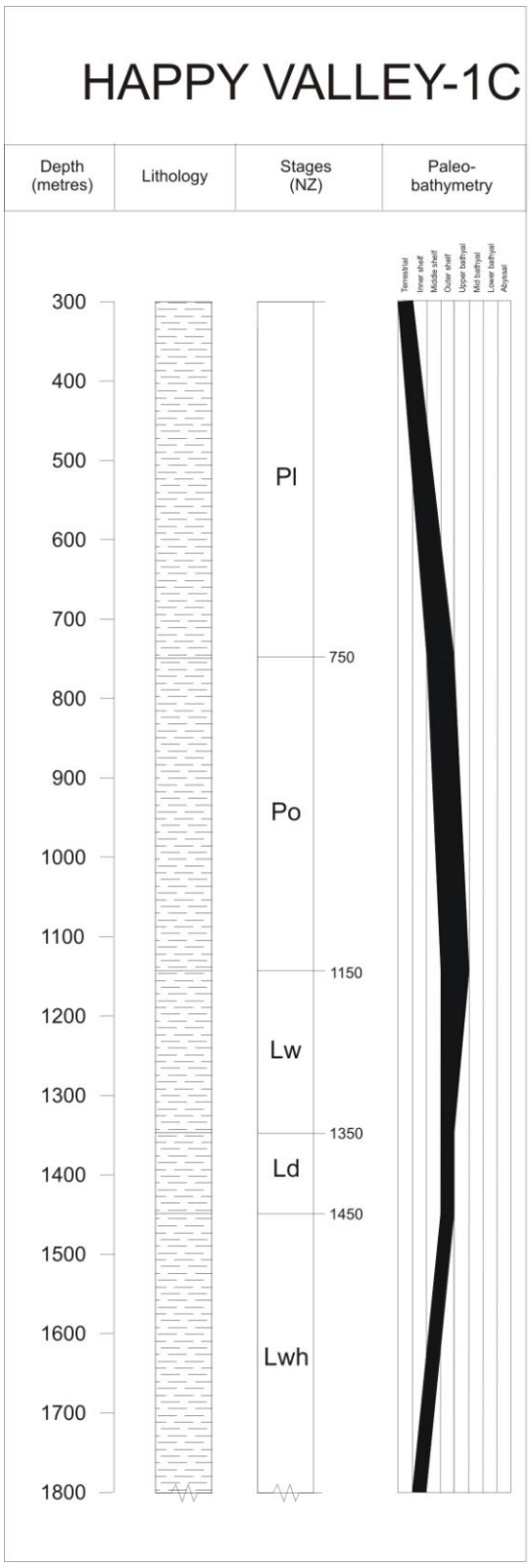
HAPPY VALLEY-1C
Depth (metres)
Lithology
Stages (NZ)
Paleo-bathymetry
300
400
500
600
700
800
900
1000
1100
1200
1300
1400
1500
1600
1700
1800
Pl
Po
Lw
Ld
Lwh
750
1150
1350
1450
Terrestrial
Inner shelf
Middle shelf
Outer shelf
Upper bathyal
Mid bathyal
Lower bathyal
Abyssal

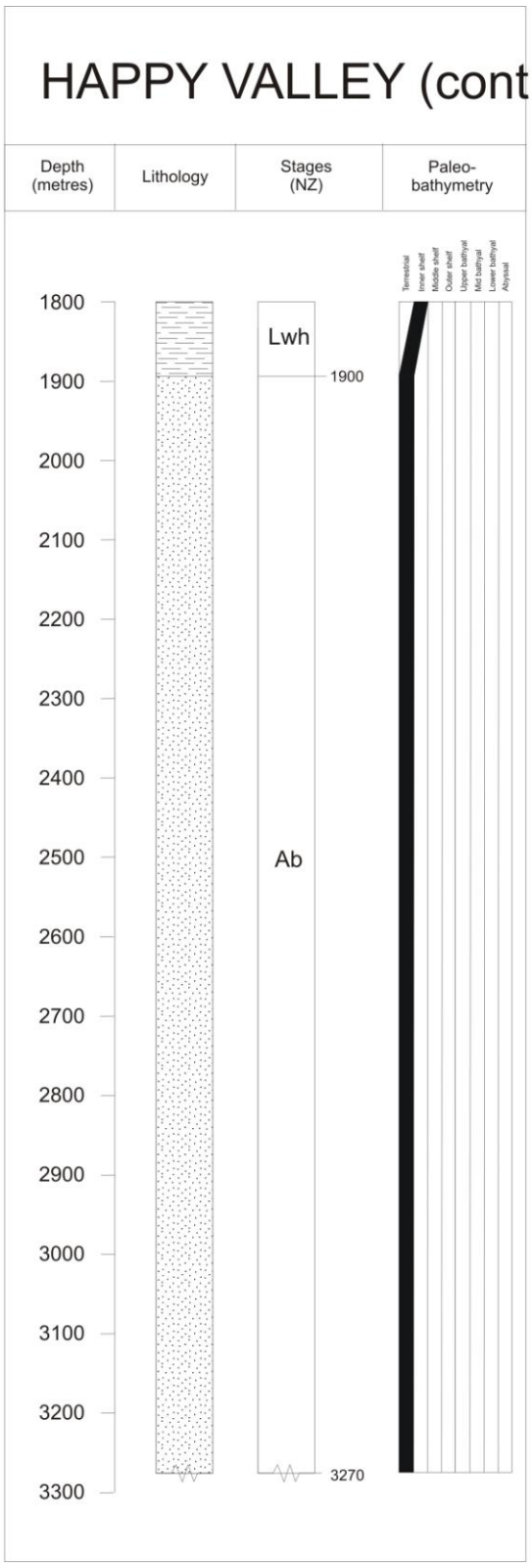
HAPPY VALLEY (cont.)
Depth (metres)
Lithology
Stages (NZ)
Paleo-bathymetry
1800
1900
2000
2100
2200
2300
2400
2500
2600
2700
2800
2900
3000
3100
3200
3300
Lwh
Ab
1900
3270
Terrestrial
Inner shelf
Middle shelf
Outer shelf
Upper bathyal
Mid bathyal
Lower bathyal
Abyssal

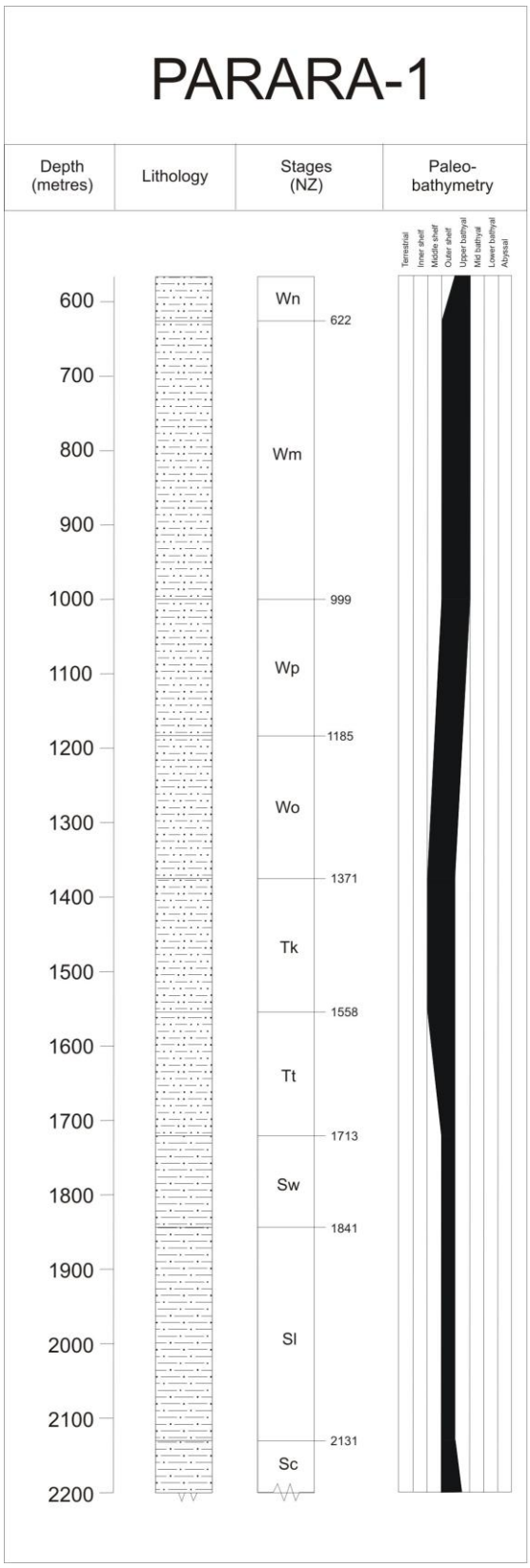
PARARA-1
Depth (metres)
Lithology
Stages (NZ)
Paleo-bathymetry
Terrestrial
Inner shelf
Middle shelf
Outer shelf
Upper bathyal
Mid bathyal
Lower bathyal
Abyssal
600
700
800
900
1000
1100
1200
1300
1400
1500
1600
1700
1800
1900
2000
2100
2200
Wn
622
Wm
999
Wp
1185
Wo
1371
Tk
1558
Tt
1713
Sw
1841
Sl
2131
Sc

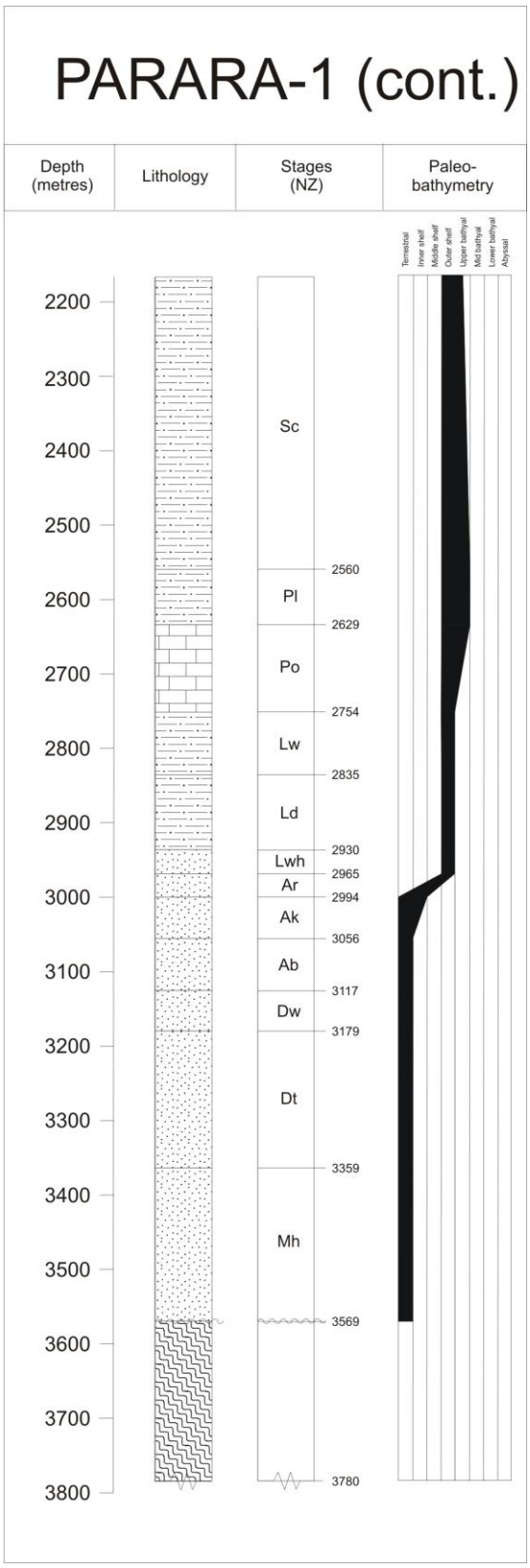
PARARA-1 (cont.)
Depth (metres)
Lithology
Stages (NZ)
Paleo-bathymetry
Terrestrial
Inner shelf
Middle shelf
Outer shelf
Upper bathyal
Mid bathyal
Lower bathyal
Abyssal
2200
2300
2400
2500
2600
2700
2800
2900
3000
3100
3200
3300
3400
3500
3600
3700
3800
Sc
2560
Pl
2629
Po
2754
Lw
2835
Ld
2930
Lwh
2965
Ar
2994
Ak
3056
Ab
3117
Dw
3179
Dt
3359
Mh
3569
3780

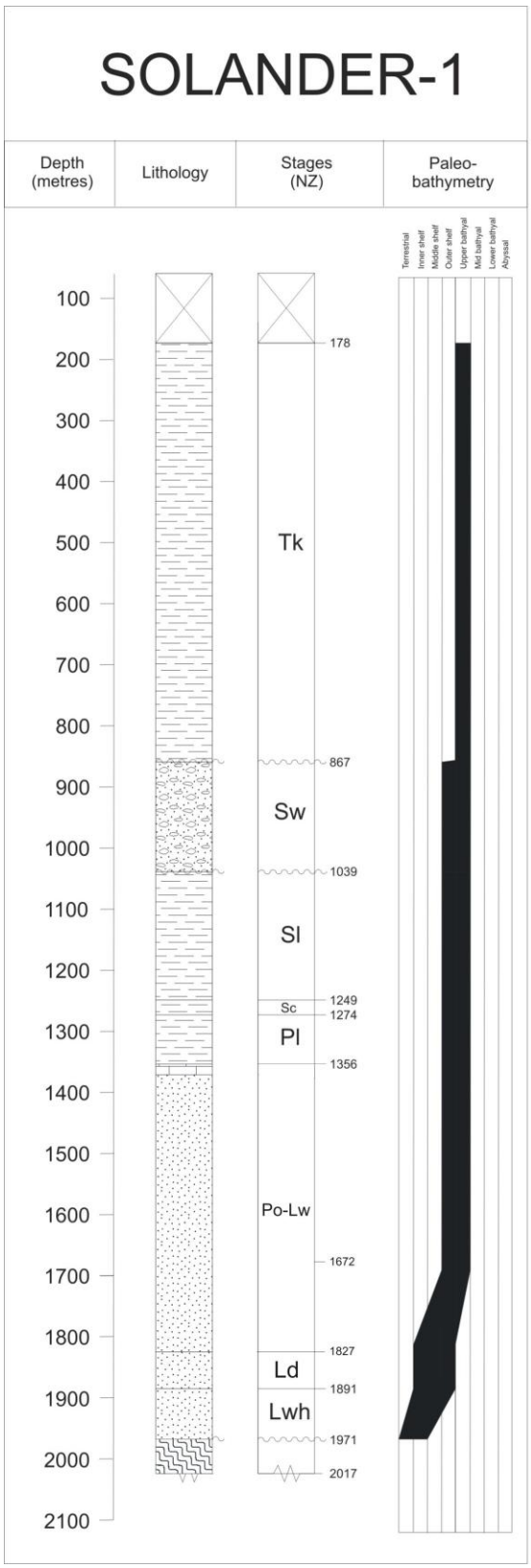
SOLANDER-1
Depth (metres)
Lithology
Stages (NZ)
Paleo-bathymetry
Terrestrial
Inner shelf
Middle shelf
Outer shelf
Upper bathyal
Mid bathyal
Lower bathyal
Abyssal
100
200
300
400
500
600
700
800
900
1000
1100
1200
1300
1400
1500
1600
1700
1800
1900
2000
2100
178
867
1039
1249
1274
1356
1672
1827
1891
1971
2017
Tk
Sw
Sl
Sc
Pl
Po-Lw
Ld
Lwh

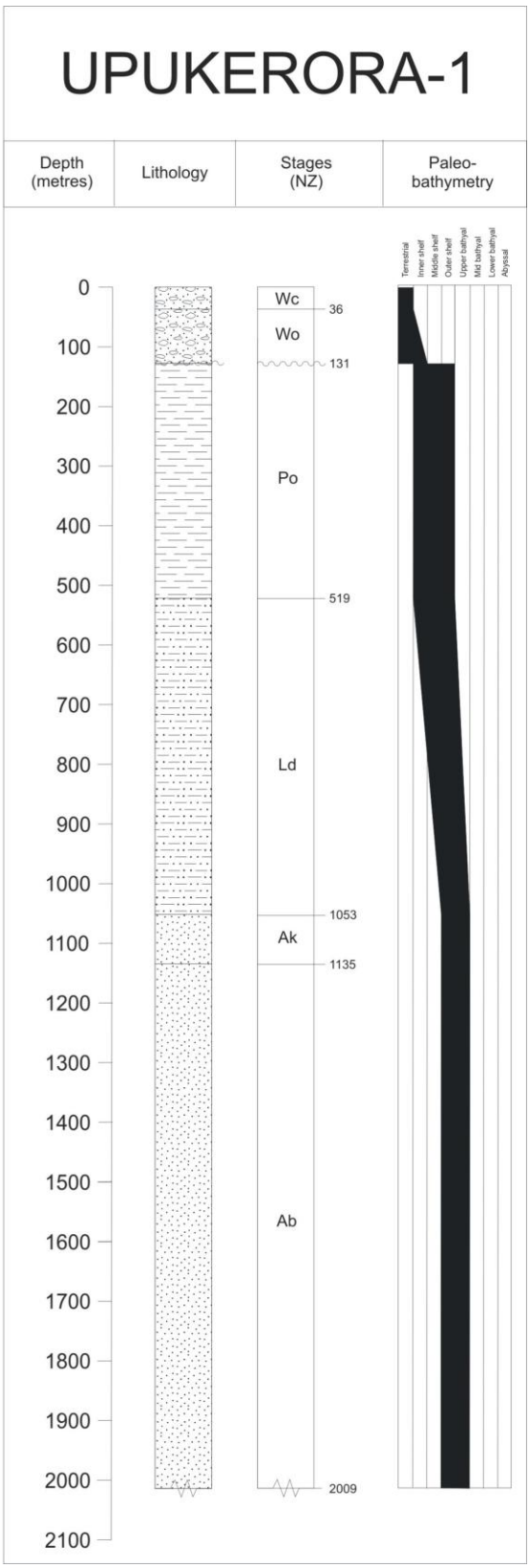
UPUKERORA-1
Depth (metres)
Lithology
Stages (NZ)
Paleo-bathymetry
Terrestrial
Inner shelf
Middle shelf
Outer shelf
Upper bathyal
Mid bathyal
Lower bathyal
Abyssal
0
100
200
300
400
500
600
700
800
900
1000
1100
1200
1300
1400
1500
1600
1700
1800
1900
2000
2100
Wc
36
Wo
131
Po
519
Ld
1053
Ak
1135
Ab
2009

APPENDIX A
STRATIGRAPHIC COLUMNS

WEST COAST BASIN

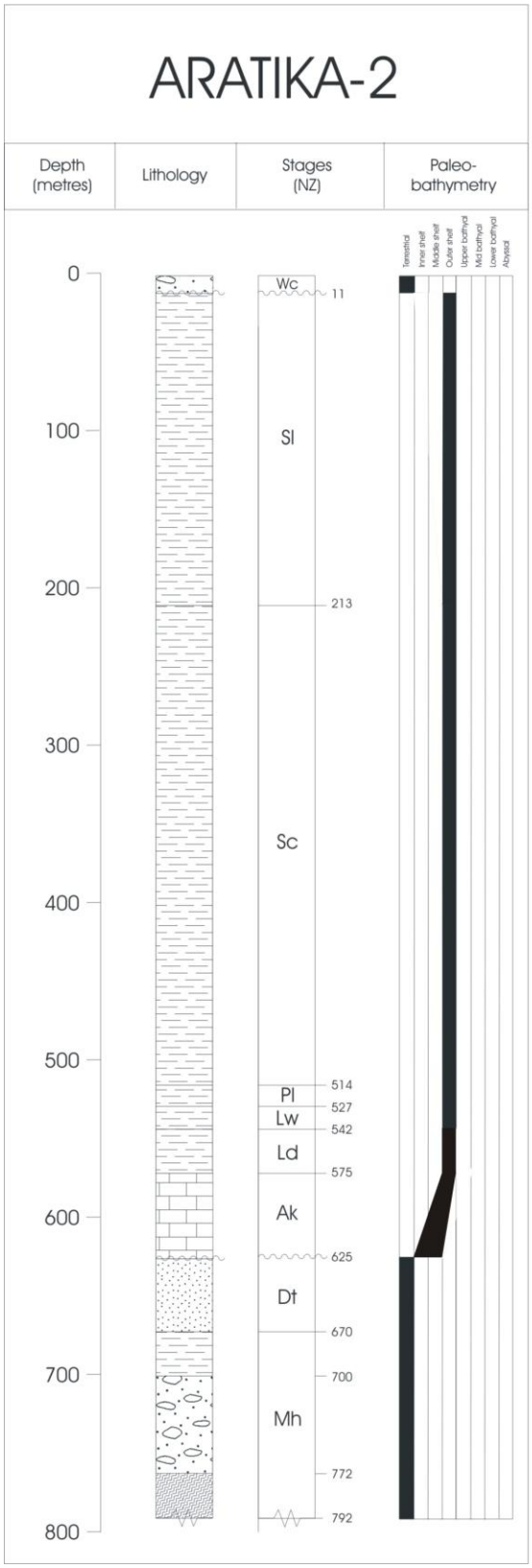
ARATIKA-2
Depth (metres)
Lithology
Stages (NZ)
Paleo-bathymetry
Terrestrial
Inner shelf
Middle shelf
Outer shelf
Upper bathyal
Mid bathyal
Lower bathyal
Abyssal
0
100
200
300
400
500
600
700
800
Wc
11
Sl
213
Sc
514
Pl
527
Lw
542
Ld
575
Ak
625
Dt
670
700
Mh
772
792

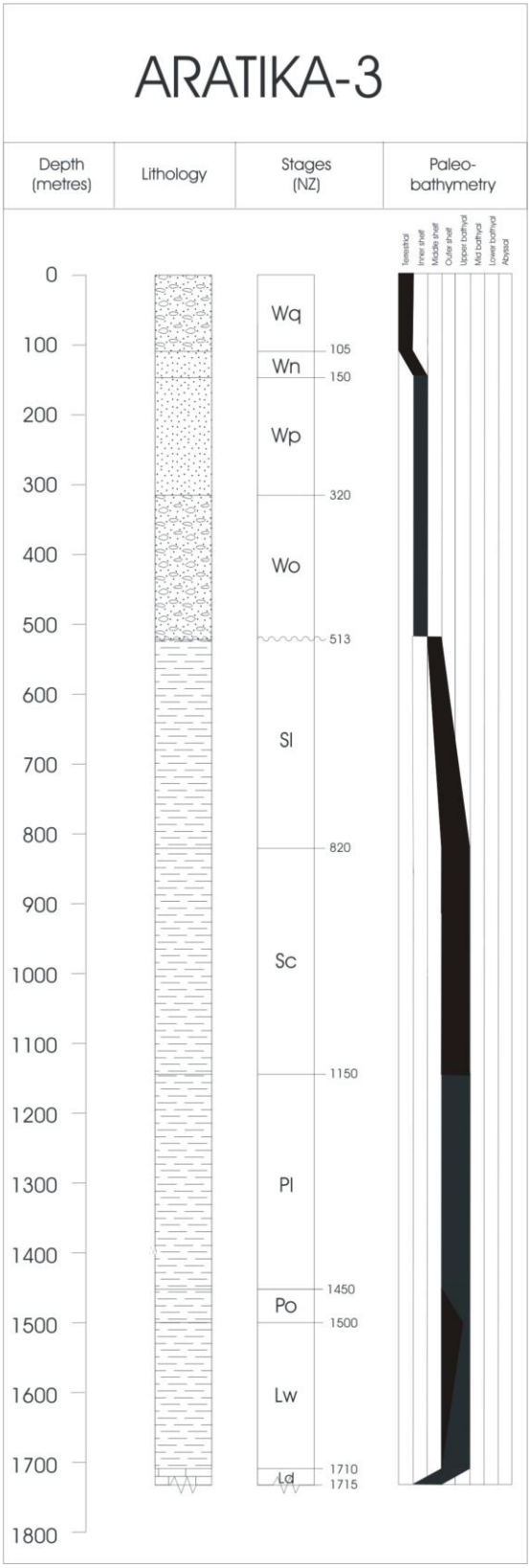
ARATIKA-3
Depth (metres)
Lithology
Stages (NZ)
Paleo-bathymetry
Terrestrial
Inner shelf
Middle shelf
Outer shelf
Upper bathyal
Mid bathyal
Lower bathyal
Abyssal
0
100
200
300
400
500
600
700
800
900
1000
1100
1200
1300
1400
1500
1600
1700
1800
Wq
105
Wn
150
Wp
320
Wo
513
Sl
820
Sc
1150
Pl
1450
Po
1500
Lw
1710
Ld
1715

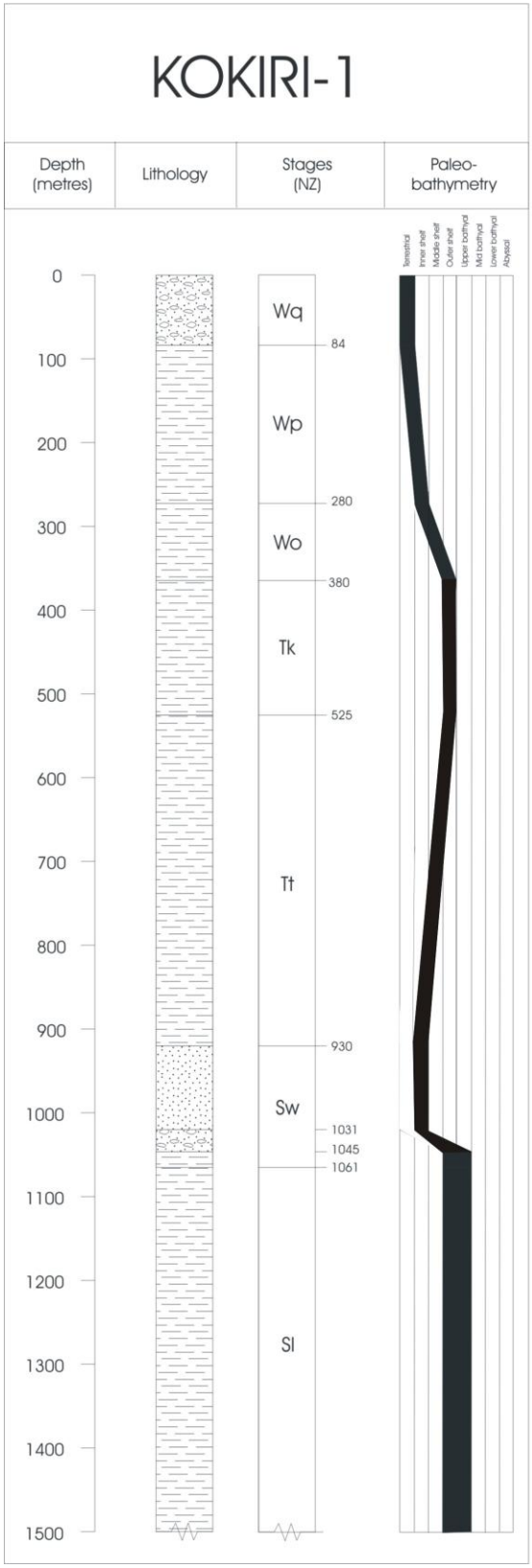
KOKIRI-1
Depth (metres)
Lithology
Stages (NZ)
Paleo-bathymetry
Terrestrial
Inner shelf
Middle shelf
Outer shelf
Upper bathyal
Mid bathyal
Lower bathyal
Abyssal
0
100
200
300
400
500
600
700
800
900
1000
1100
1200
1300
1400
1500
Wq
84
Wp
280
Wo
380
Tk
525
Tt
930
Sw
1031
1045
1061
Sl

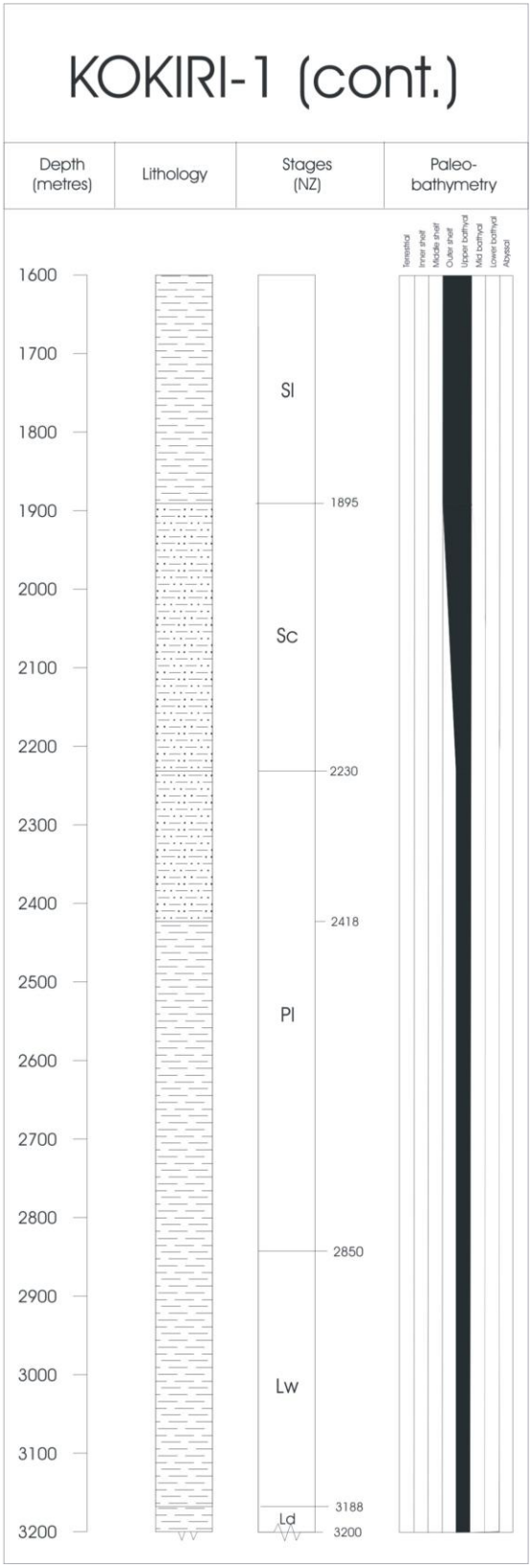
KOKIRI-1 (cont.)
Depth (metres)
Lithology
Stages (NZ)
Paleo-bathymetry
Terrestrial
Inner shelf
Middle shelf
Outer shelf
Upper bathyal
Mid bathyal
Lower bathyal
Abyssal
1600
1700
1800
1900
2000
2100
2200
2300
2400
2500
2600
2700
2800
2900
3000
3100
3200
Sl
1895
Sc
2230
2418
Pl
2850
Lw
3188
Ld
3200

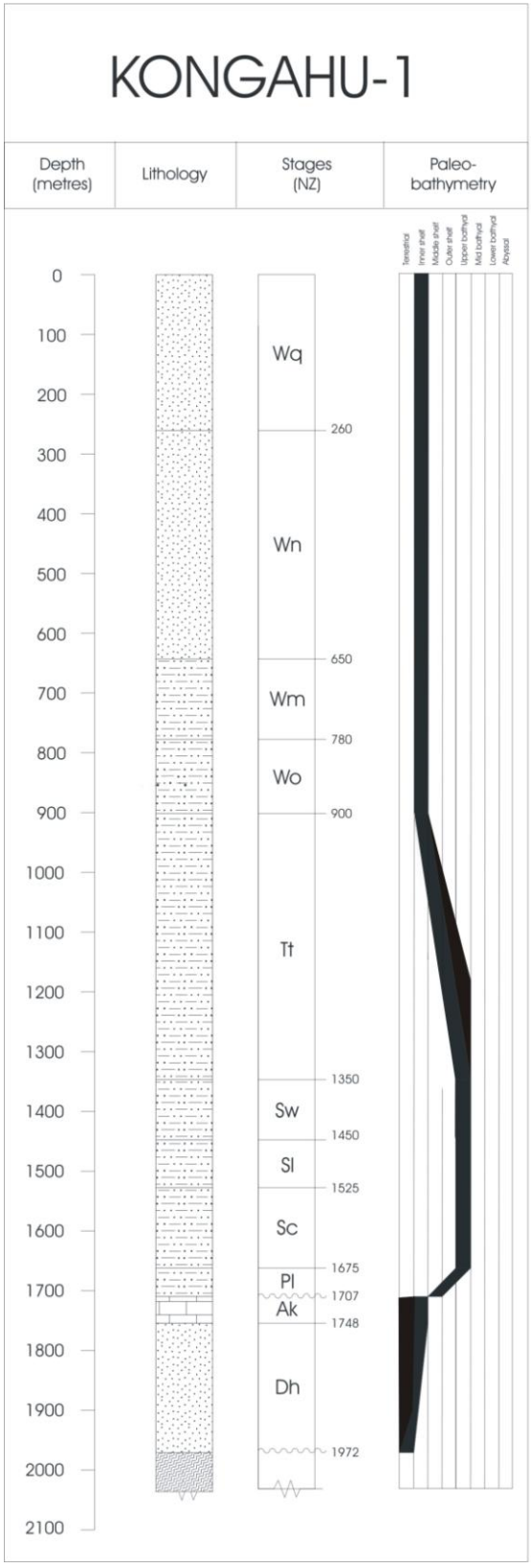
KONGAHU-1
Depth (metres)
Lithology
Stages (NZ)
Paleo-bathymetry
Terrestrial
Inner shelf
Middle shelf
Outer shelf
Upper bathyal
Mid bathyal
Lower bathyal
Abyssal
0
100
200
300
400
500
600
700
800
900
1000
1100
1200
1300
1400
1500
1600
1700
1800
1900
2000
2100
Wq
260
Wn
650
Wm
780
Wo
900
Tt
1350
Sw
1450
Sl
1525
Sc
1675
Pl
1707
Ak
1748
Dh
1972

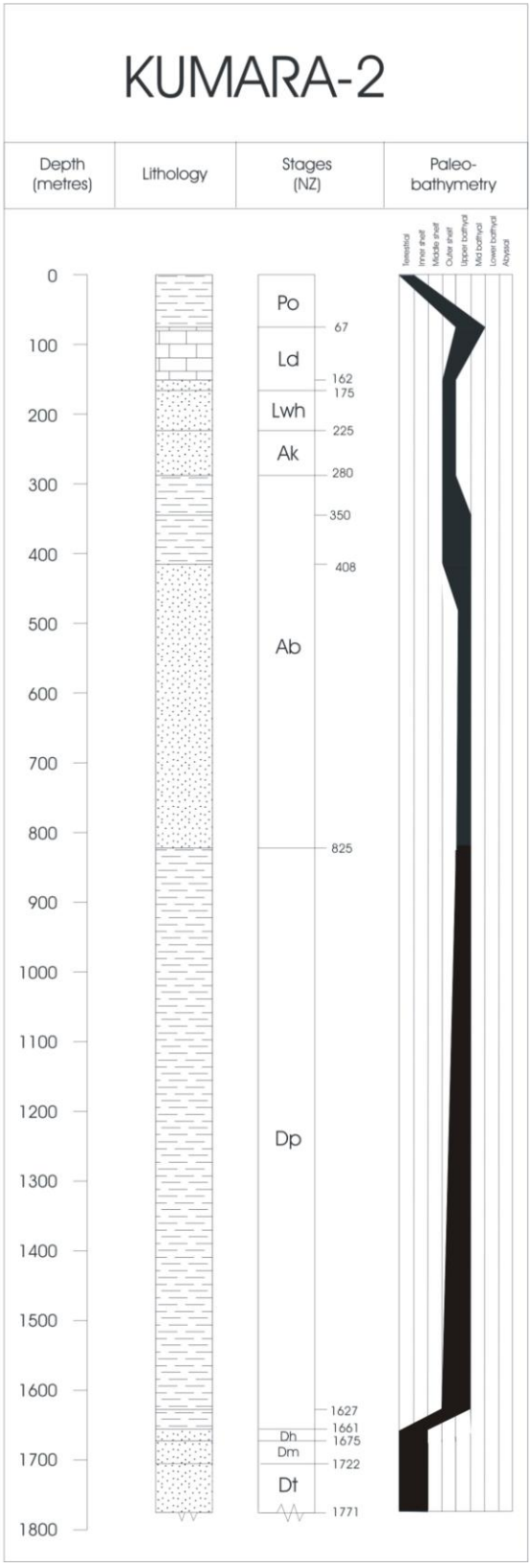
KUMARA-2
Depth (metres)
Lithology
Stages (NZ)
Paleo-bathymetry
Terrestrial
Inner shelf
Middle shelf
Outer shelf
Upper bathyal
Mid bathyal
Lower bathyal
Abyssal
0
100
200
300
400
500
600
700
800
900
1000
1100
1200
1300
1400
1500
1600
1700
1800
Po
67
Ld
162
175
Lwh
225
Ak
280
350
408
Ab
825
Dp
1627
Dh
1661
1675
Dm
1722
Dt
1771

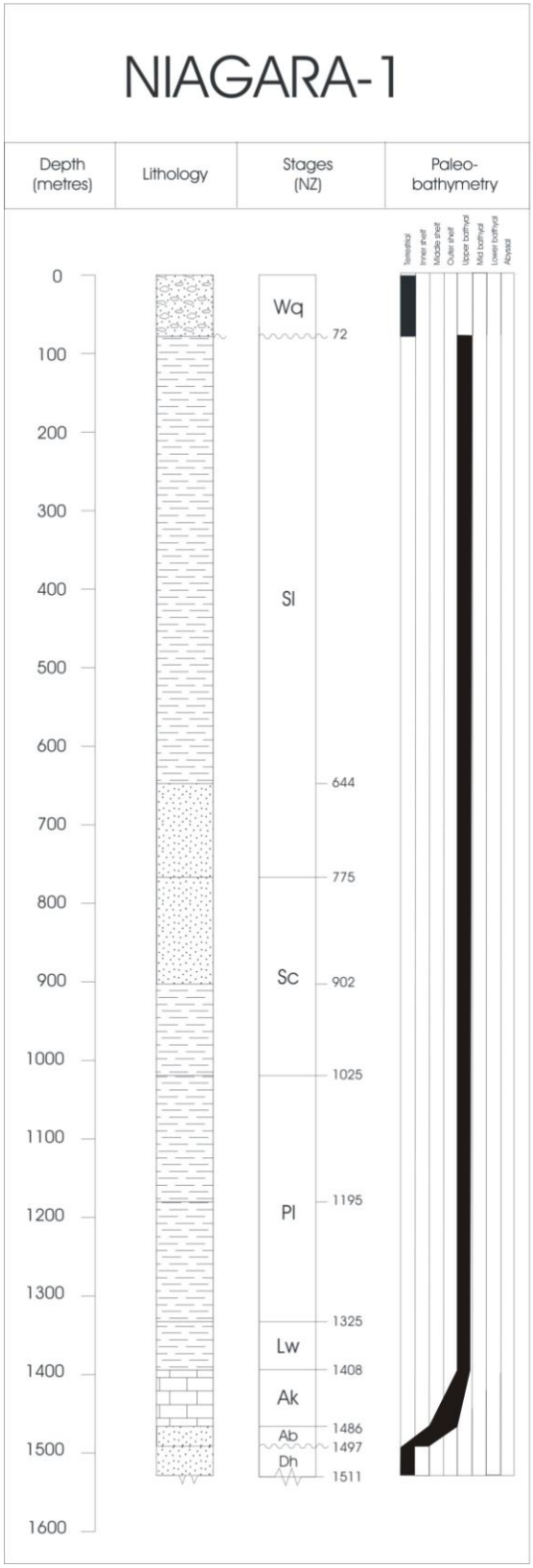
NIAGARA-1
Depth (metres)
Lithology
Stages (NZ)
Paleo-bathymetry
Terrestrial
Inner shelf
Middle shelf
Outer shelf
Upper bathyal
Mid bathyal
Lower bathyal
Abyssal
0
100
200
300
400
500
600
700
800
900
1000
1100
1200
1300
1400
1500
1600
Wq
72
Sl
644
775
Sc
902
1025
Pl
1195
1325
Lw
1408
Ak
1486
Ab
1497
Dh
1511

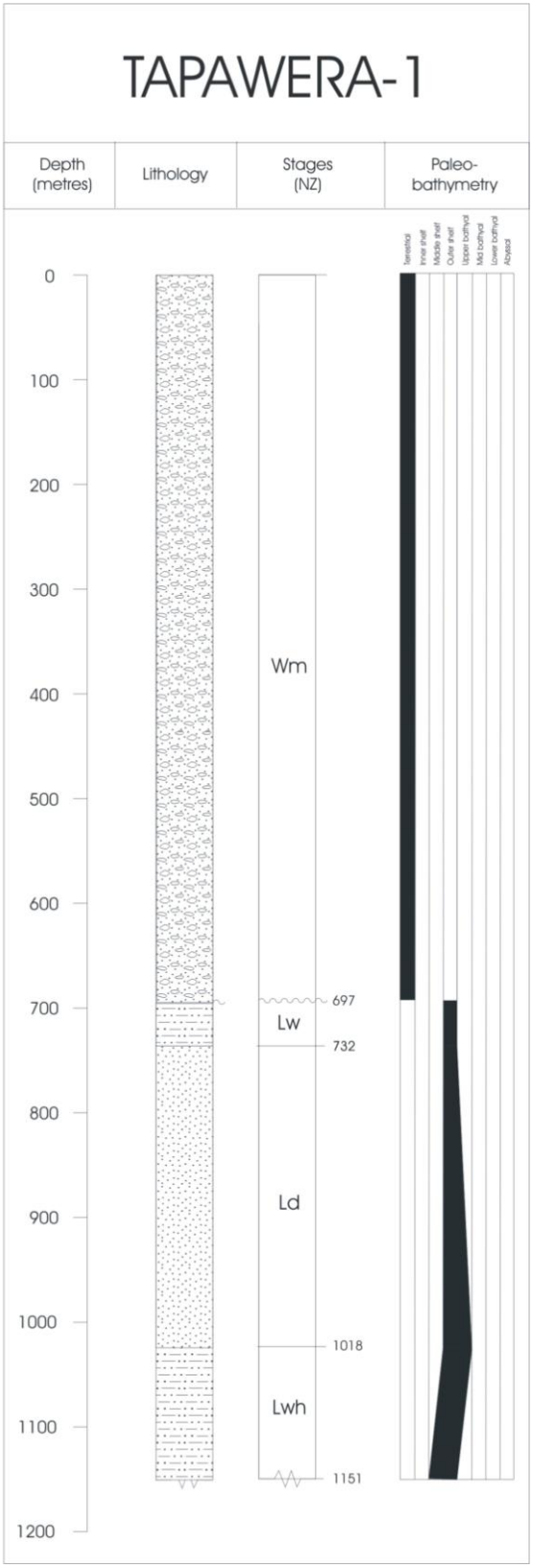
TAPAWERA-1
Depth (metres)
Lithology
Stages (NZ)
Paleo-bathymetry
Terrestrial
Inner shelf
Middle shelf
Outer shelf
Upper bathyal
Mid bathyal
Lower bathyal
Abyssal
0
100
200
300
400
500
600
700
800
900
1000
1100
1200
Wm
697
Lw
732
Ld
1018
Lwh
1151

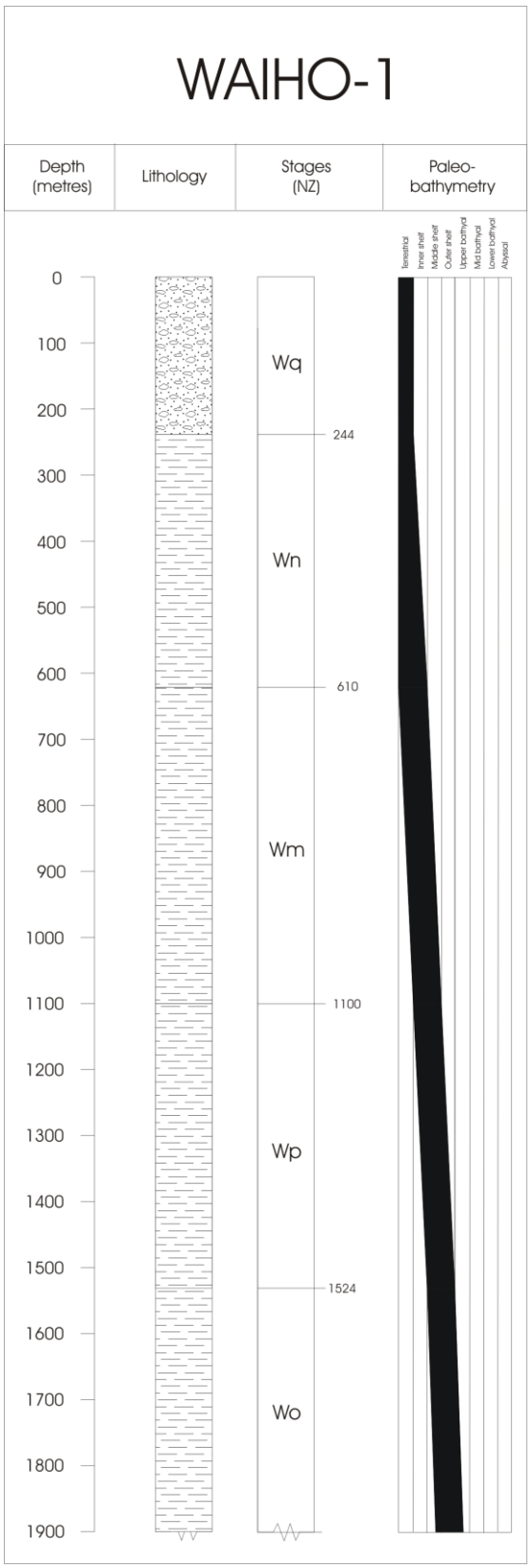
WAIHO-1
Depth (metres)
Lithology
Stages (NZ)
Paleo-bathymetry
Terrestrial
Inner shelf
Middle shelf
Outer shelf
Upper bathyal
Mid bathyal
Lower bathyal
Abyssal
0
100
200
300
400
500
600
700
800
900
1000
1100
1200
1300
1400
1500
1600
1700
1800
1900
Wq
244
Wn
610
Wm
1100
Wp
1524
Wo

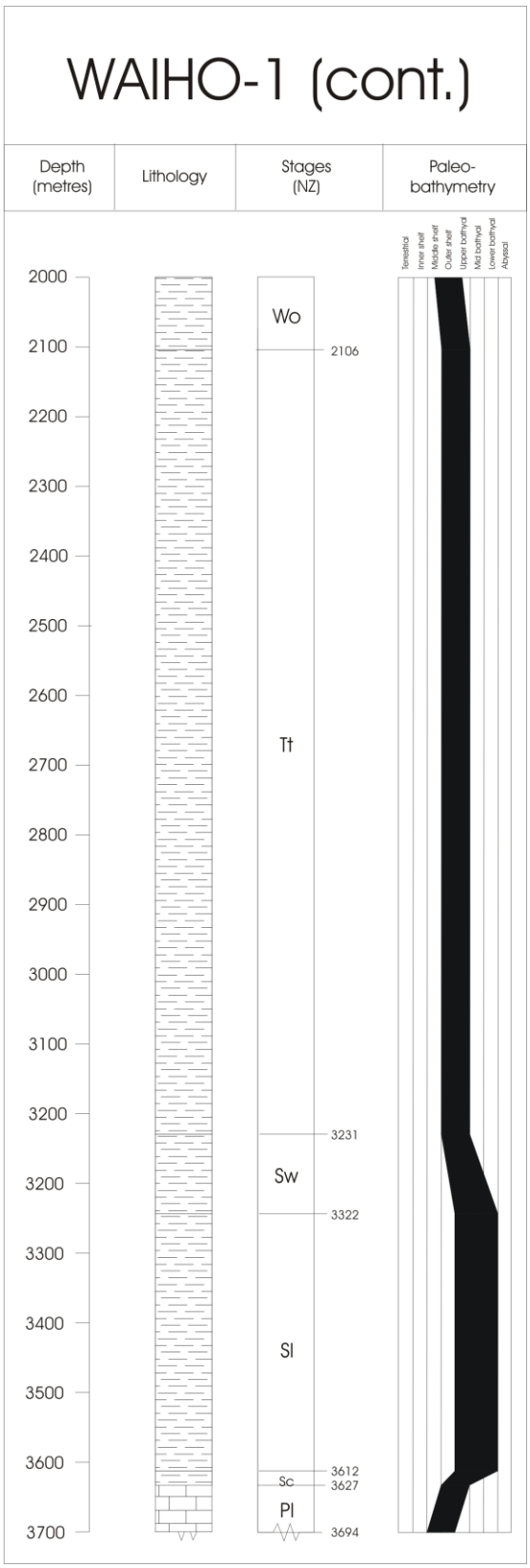
WAIHO-1 (cont.)
Depth (metres)
Lithology
Stages (NZ)
Paleo-bathymetry
Terrestrial
Inner shelf
Middle shelf
Outer shelf
Upper bathyal
Mid bathyal
Lower bathyal
Abyssal
2000
2100
2200
2300
2400
2500
2600
2700
2800
2900
3000
3100
3200
3200
3300
3400
3500
3600
3700
Wo
2106
Tt
3231
Sw
3322
Sl
3612
Sc
3627
Pl
3694

APPENDIX A
STRATIGRAPHIC COLUMNS

TARANAKI BASIN

NOTE: Columns provided for Awakino-1, Kaimiro-1, Kapuni-13 and Kupe-1 utilise seismic interpretations used by Hayward and Wood, 1989 to provide depths to basement. These drill holes were not drilled to depths shown on columns.

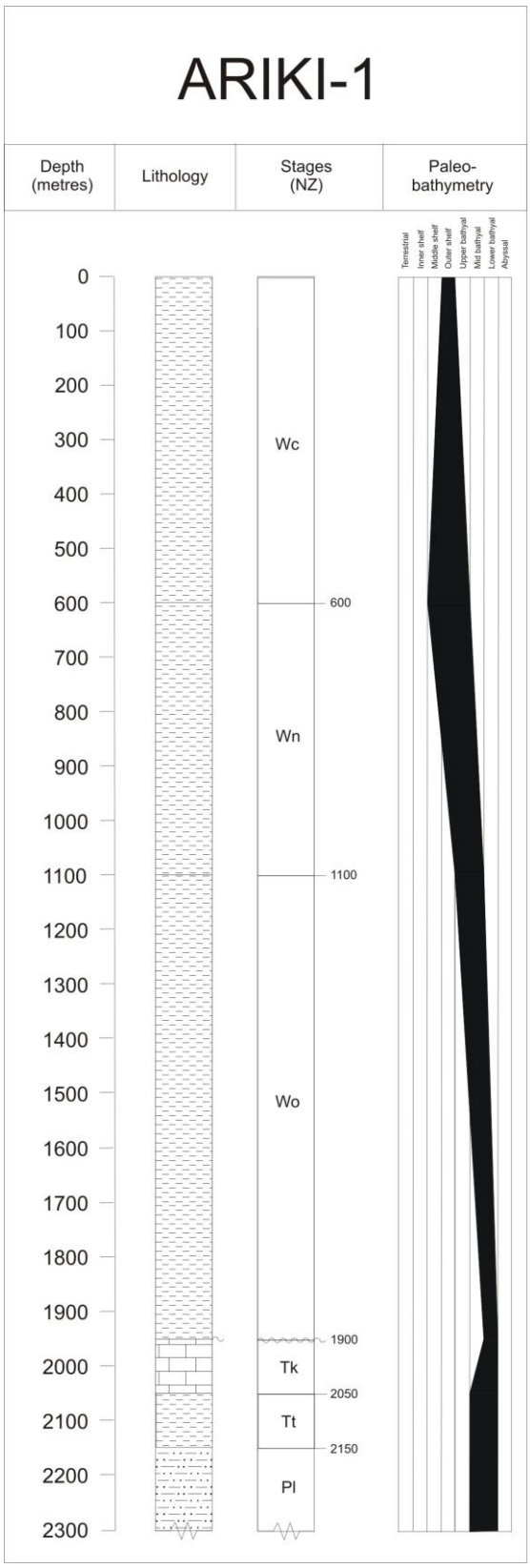
ARIKI-1
Depth (metres)
Lithology
Stages (NZ)
Paleo-bathymetry
Terrestrial
Inner shelf
Middle shelf
Outer shelf
Upper bathyal
Mid bathyal
Lower bathyal
Abyssal
0
100
200
300
400
500
600
700
800
900
1000
1100
1200
1300
1400
1500
1600
1700
1800
1900
2000
2100
2200
2300
Wc
Wn
Wo
Tk
Tt
Pl
600
1100
1900
2050
2150

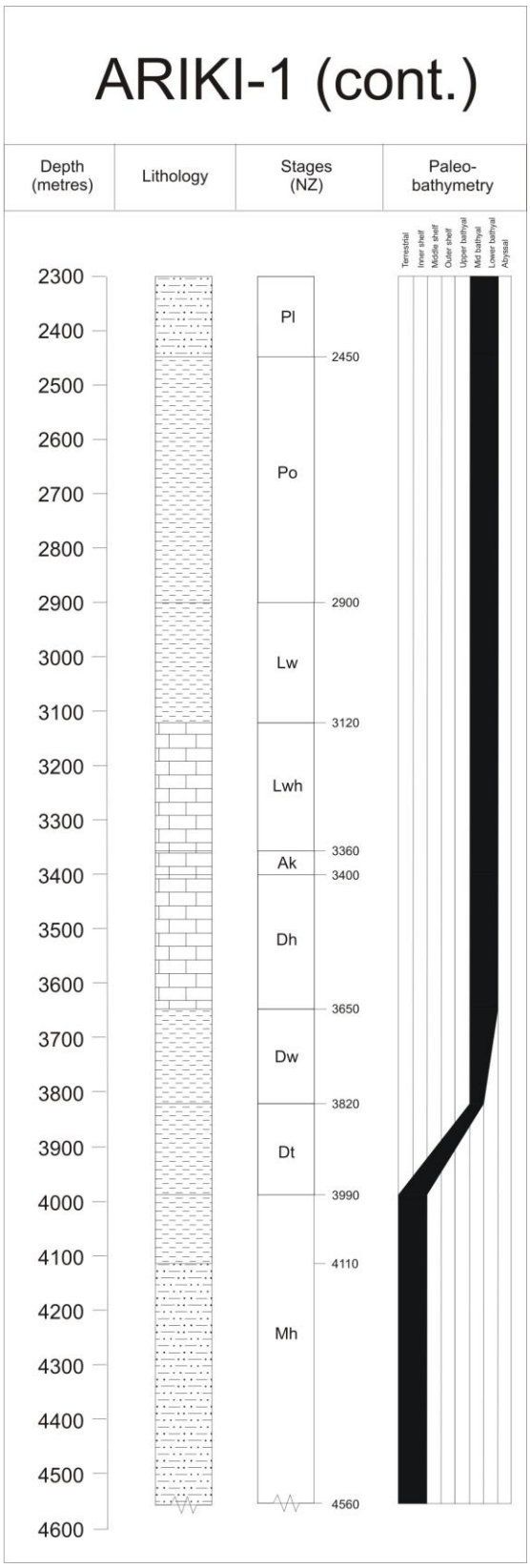
ARIKI-1 (cont.)
Depth (metres)
Lithology
Stages (NZ)
Paleo-bathymetry
Terrestrial
Inner shelf
Middle shelf
Outer shelf
Upper bathyal
Mid bathyal
Lower bathyal
Abyssal
2300
2400
2500
2600
2700
2800
2900
3000
3100
3200
3300
3400
3500
3600
3700
3800
3900
4000
4100
4200
4300
4400
4500
4600
Pl
Po
Lw
Lwh
Ak
Dh
Dw
Dt
Mh
2450
2900
3120
3360
3400
3650
3820
3990
4110
4560

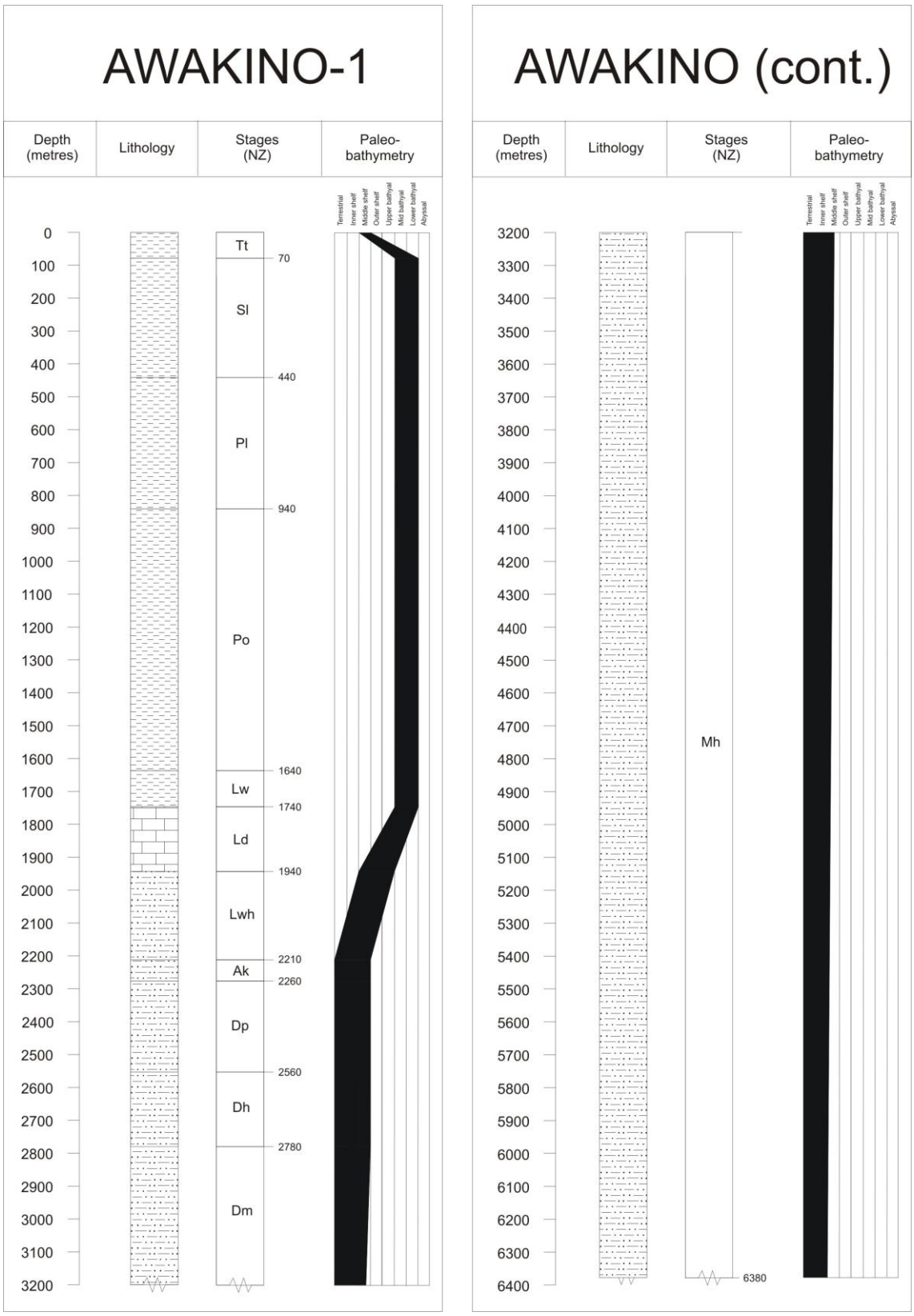
AWAKINO-1
Depth (metres)
Lithology
Stages (NZ)
Paleo-bathymetry
Terrestrial
Inner shelf
Middle shelf
Outer shelf
Upper bathyal
Mid bathyal
Lower bathyal
Abyssal
0
100
200
300
400
500
600
700
800
900
1000
1100
1200
1300
1400
1500
1600
1700
1800
1900
2000
2100
2200
2300
2400
2500
2600
2700
2800
2900
3000
3100
3200
Tt
70
Sl
440
Pl
940
Po
1640
Lw
1740
Ld
1940
Lwh
2210
Ak
2260
Dp
2560
Dh
2780
Dm
AWAKINO (cont.)
Depth (metres)
Lithology
Stages (NZ)
Paleo-bathymetry
3200
3300
3400
3500
3600
3700
3800
3900
4000
4100
4200
4300
4400
4500
4600
4700
4800
4900
5000
5100
5200
5300
5400
5500
5600
5700
5800
5900
6000
6100
6200
6300
6400
Mh
6380

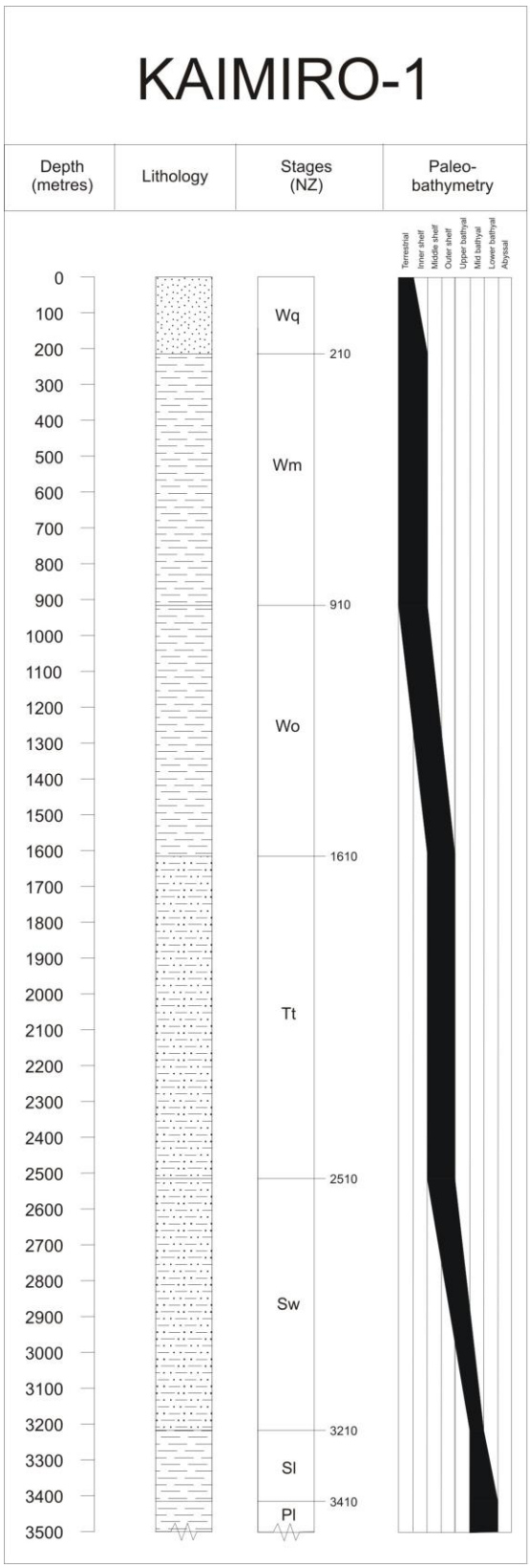
KAIMIRO-1
Depth (metres)
Lithology
Stages (NZ)
Paleo-bathymetry
Terrestrial
Inner shelf
Middle shelf
Outer shelf
Upper bathyal
Mid bathyal
Lower bathyal
Abyssal
0
100
200
300
400
500
600
700
800
900
1000
1100
1200
1300
1400
1500
1600
1700
1800
1900
2000
2100
2200
2300
2400
2500
2600
2700
2800
2900
3000
3100
3200
3300
3400
3500
Wq
210
Wm
910
Wo
1610
Tt
2510
Sw
3210
Sl
3410
Pl

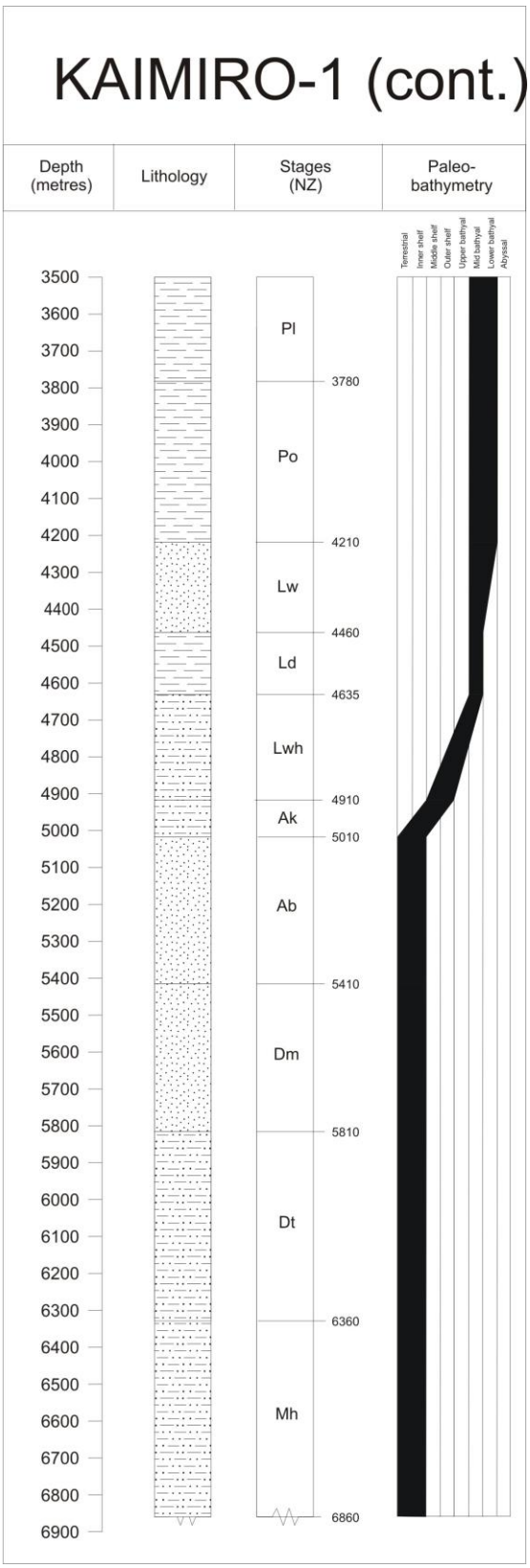
KAIMIRO-1 (cont.)
Depth (metres)
Lithology
Stages (NZ)
Paleo-bathymetry
Terrestrial
Inner shelf
Middle shelf
Outer shelf
Upper bathyal
Mid bathyal
Lower bathyal
Abyssal
3500
3600
3700
3800
3900
4000
4100
4200
4300
4400
4500
4600
4700
4800
4900
5000
5100
5200
5300
5400
5500
5600
5700
5800
5900
6000
6100
6200
6300
6400
6500
6600
6700
6800
6900
Pl
3780
Po
4210
Lw
4460
Ld
4635
Lwh
4910
Ak
5010
Ab
5410
Dm
5810
Dt
6360
Mh
6860

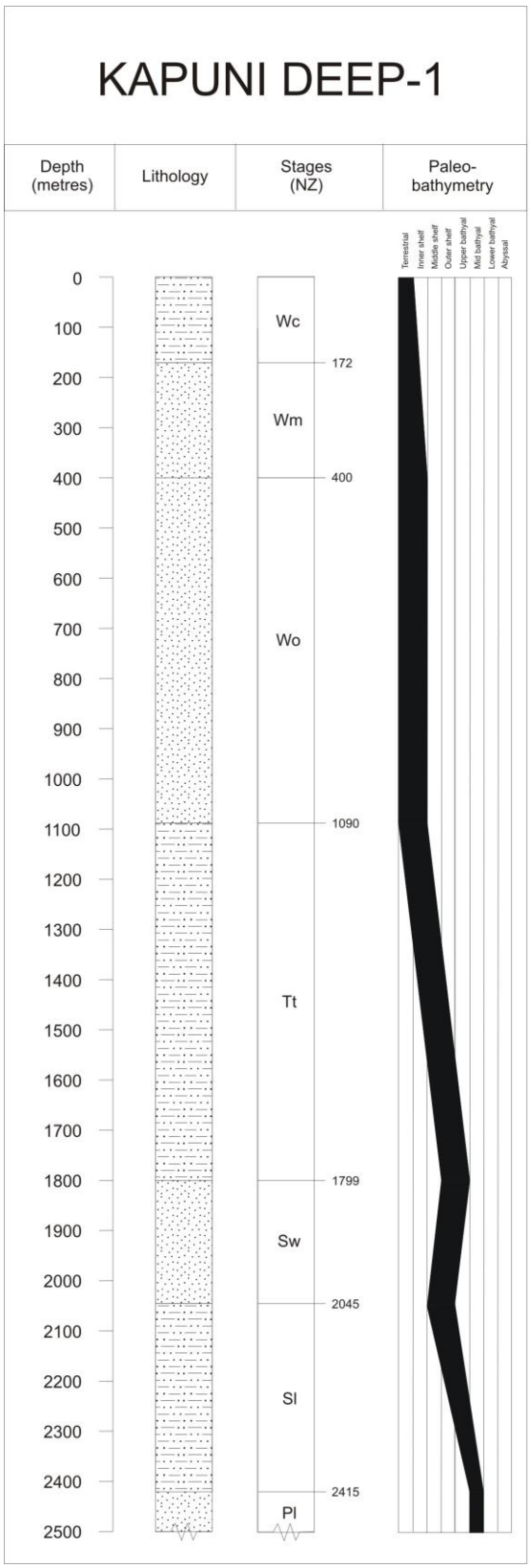
KAPUNI DEEP-1
Depth (metres)
Lithology
Stages (NZ)
Paleo-bathymetry
Terrestrial
Inner shelf
Middle shelf
Outer shelf
Upper bathyal
Mid bathyal
Lower bathyal
Abyssal
0
100
200
300
400
500
600
700
800
900
1000
1100
1200
1300
1400
1500
1600
1700
1800
1900
2000
2100
2200
2300
2400
2500
Wc
172
Wm
400
Wo
1090
Tt
1799
Sw
2045
Sl
2415
Pl

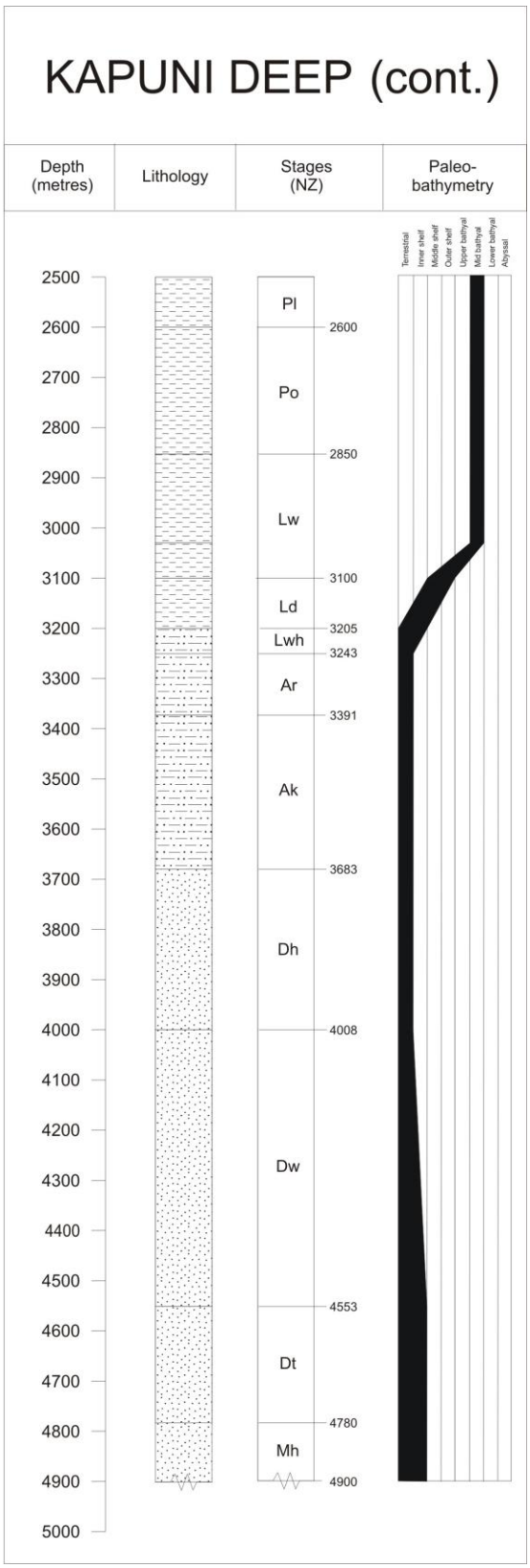
KAPUNI DEEP (cont.)
Depth (metres)
Lithology
Stages (NZ)
Paleo-bathymetry
Terrestrial
Inner shelf
Middle shelf
Outer shelf
Upper bathyal
Mid bathyal
Lower bathyal
Abyssal
2500
2600
2700
2800
2900
3000
3100
3200
3300
3400
3500
3600
3700
3800
3900
4000
4100
4200
4300
4400
4500
4600
4700
4800
4900
5000
Pl
2600
Po
2850
Lw
3100
Ld
3205
Lwh
3243
Ar
3391
Ak
3683
Dh
4008
Dw
4553
Dt
4780
Mh
4900

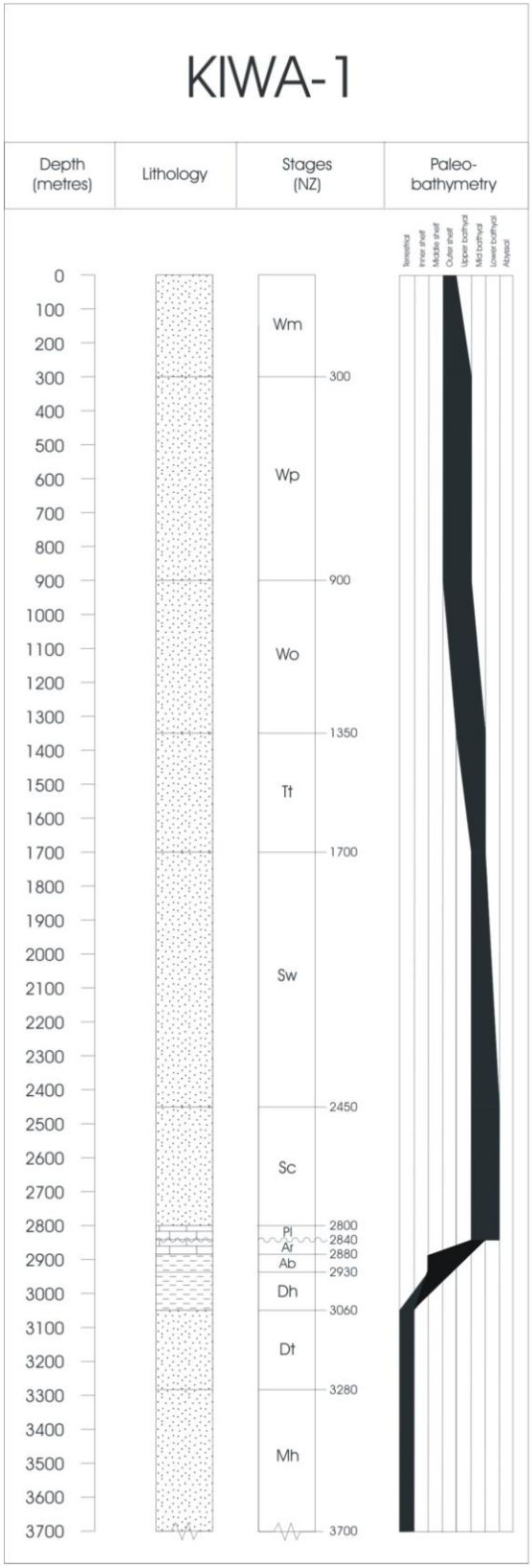
KIWA-1
Depth (metres)
Lithology
Stages (NZ)
Paleo-bathymetry
Terrestrial
Inner shelf
Middle shelf
Outer shelf
Upper bathyal
Mid bathyal
Lower bathyal
Abyssal
0
100
200
300
400
500
600
700
800
900
1000
1100
1200
1300
1400
1500
1600
1700
1800
1900
2000
2100
2200
2300
2400
2500
2600
2700
2800
2900
3000
3100
3200
3300
3400
3500
3600
3700
Wm
300
Wp
900
Wo
1350
Tt
1700
Sw
2450
Sc
2800
Pl
2840
Ar
2880
Ab
2930
Dh
3060
Dt
3280
Mh
3700

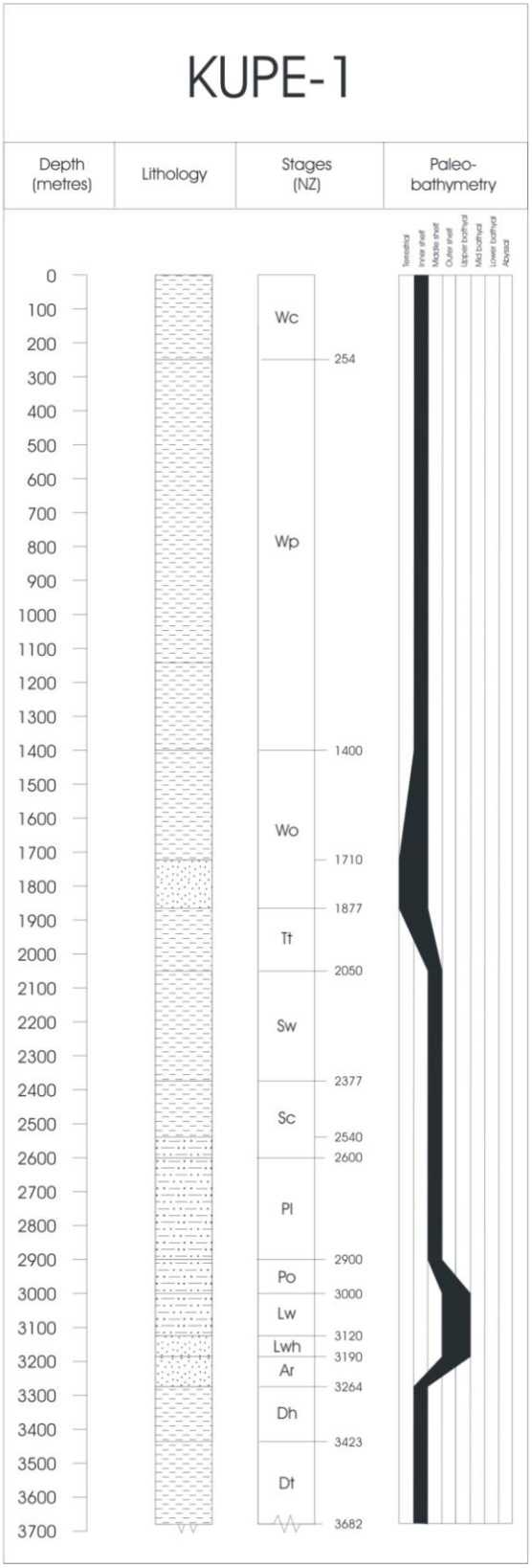
KUPE-1
Depth (metres)
Lithology
Stages (NZ)
Paleo-bathymetry
Terrestrial
Inner shelf
Middle shelf
Outer shelf
Upper bathyal
Mid bathyal
Lower bathyal
Abyssal
0
100
200
300
400
500
600
700
800
900
1000
1100
1200
1300
1400
1500
1600
1700
1800
1900
2000
2100
2200
2300
2400
2500
2600
2700
2800
2900
3000
3100
3200
3300
3400
3500
3600
3700
Wc
254
Wp
1400
Wo
1710
Tt
1877
Sw
2050
Sc
2377
Pl
2540
Po
2600
Lw
2900
Lwh
3000
Ar
3120
Dh
3190
Dt
3264
3423
3682

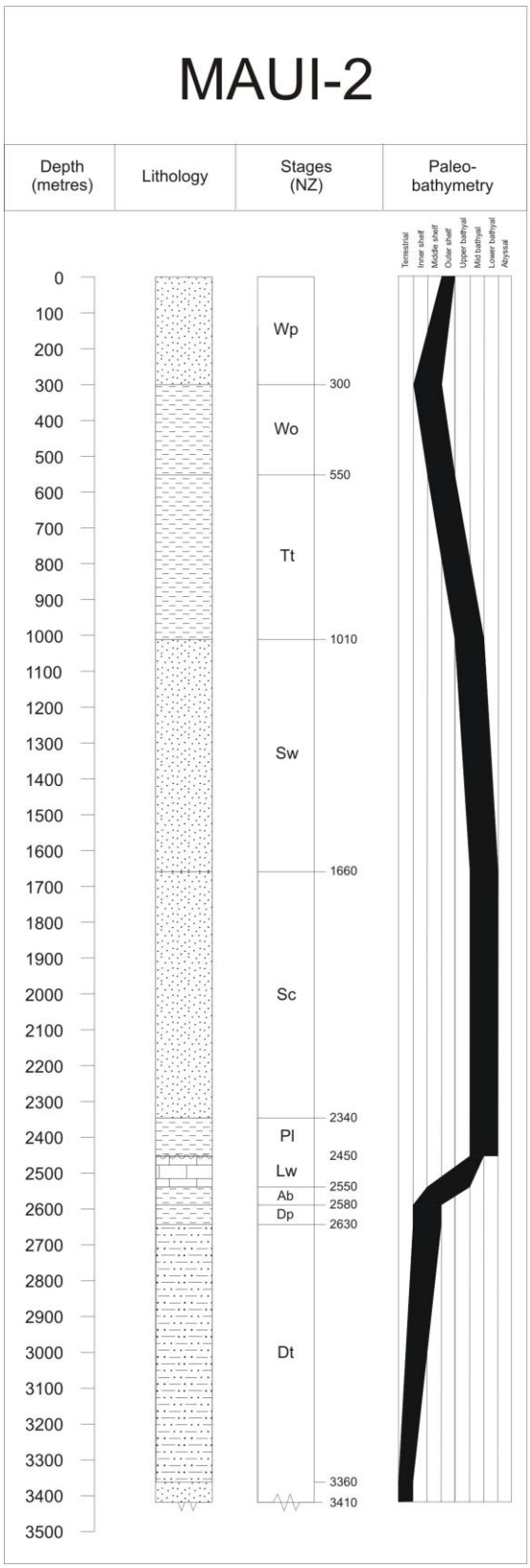
MAUI-2
Depth (metres)
Lithology
Stages (NZ)
Paleo-bathymetry
Terrestrial
Inner shelf
Middle shelf
Outer shelf
Upper bathyal
Mid bathyal
Lower bathyal
Abyssal
0
100
200
300
400
500
600
700
800
900
1000
1100
1200
1300
1400
1500
1600
1700
1800
1900
2000
2100
2200
2300
2400
2500
2600
2700
2800
2900
3000
3100
3200
3300
3400
3500
Wp
300
Wo
550
Tt
1010
Sw
1660
Sc
2340
Pl
2450
Lw
2550
Ab
2580
Dp
2630
Dt
3360
3410

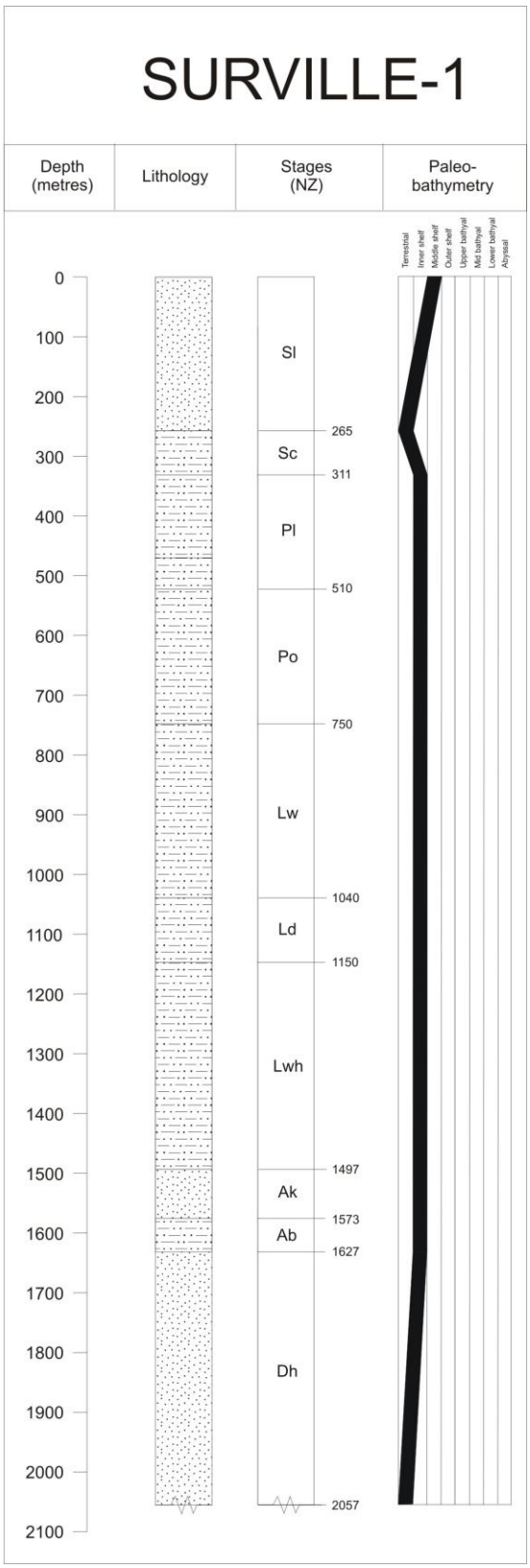
SURVILLE-1
Depth (metres)
Lithology
Stages (NZ)
Paleo-bathymetry
Terrestrial
Inner shelf
Middle shelf
Outer shelf
Upper bathyal
Mid bathyal
Lower bathyal
Abyssal
0
100
200
300
400
500
600
700
800
900
1000
1100
1200
1300
1400
1500
1600
1700
1800
1900
2000
2100
Sl
265
Sc
311
Pl
510
Po
750
Lw
1040
Ld
1150
Lwh
1497
Ak
1573
Ab
1627
Dh
2057

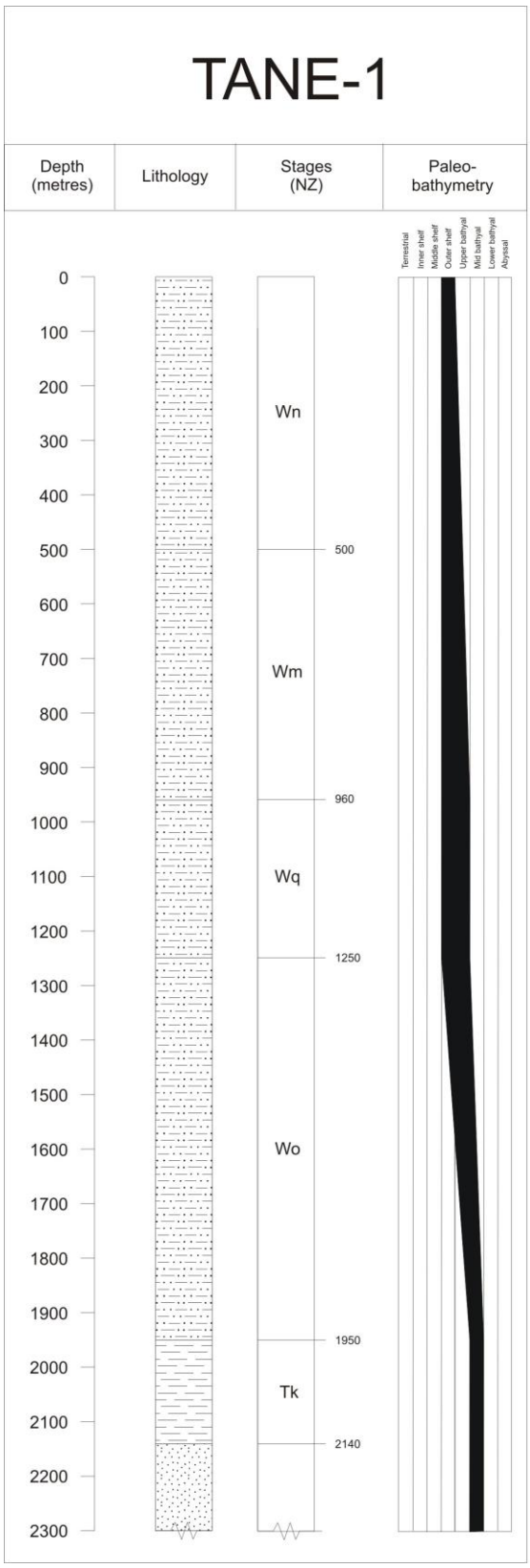
TANE-1
Depth (metres)
Lithology
Stages (NZ)
Paleo-bathymetry
Terrestrial
Inner shelf
Middle shelf
Outer shelf
Upper bathyal
Mid bathyal
Lower bathyal
Abyssal
0
100
200
300
400
500
600
700
800
900
1000
1100
1200
1300
1400
1500
1600
1700
1800
1900
2000
2100
2200
2300
Wn
Wm
Wq
Wo
Tk
500
960
1250
1950
2140

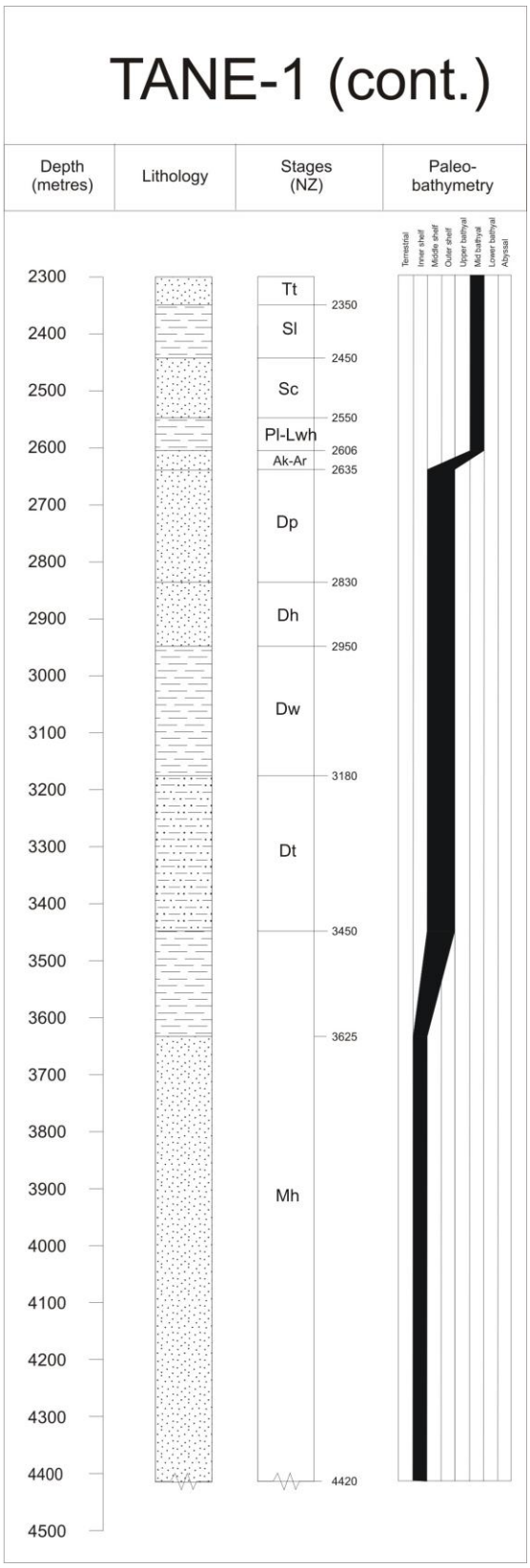
TANE-1 (cont.)
Depth (metres)
Lithology
Stages (NZ)
Paleo-bathymetry
Terrestrial
Inner shelf
Middle shelf
Outer shelf
Upper bathyal
Mid bathyal
Lower bathyal
Abyssal
2300
2400
2500
2600
2700
2800
2900
3000
3100
3200
3300
3400
3500
3600
3700
3800
3900
4000
4100
4200
4300
4400
4500
Tt
Sl
Sc
Pl-Lwh
Ak-Ar
Dp
Dh
Dw
Dt
Mh
2350
2450
2550
2606
2635
2830
2950
3180
3450
3625
4420

APPENDIX A
STRATIGRAPHIC COLUMNS

NORTHLAND BASIN

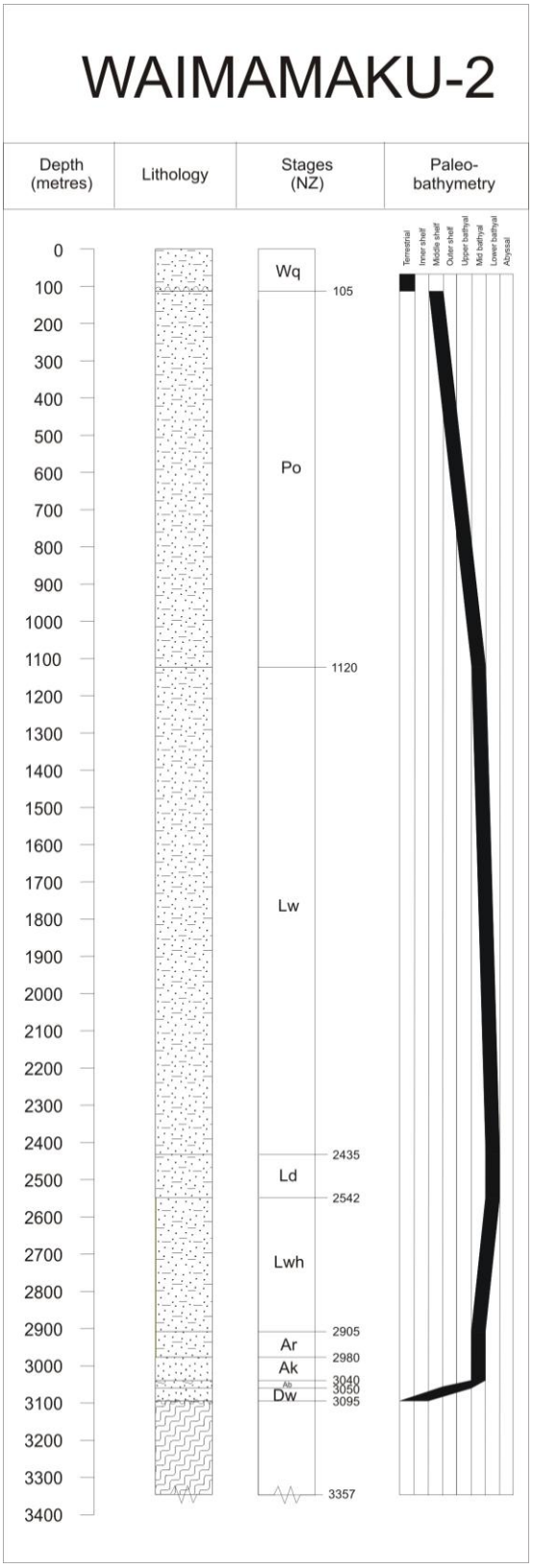
WAIMAMAKU-2
Depth (metres)
Lithology
Stages (NZ)
Paleo-bathymetry
Terrestrial
Inner shelf
Middle shelf
Outer shelf
Upper bathyal
Mid bathyal
Lower bathyal
Abyssal
0
100
200
300
400
500
600
700
800
900
1000
1100
1200
1300
1400
1500
1600
1700
1800
1900
2000
2100
2200
2300
2400
2500
2600
2700
2800
2900
3000
3100
3200
3300
3400
Wq
105
Po
1120
Lw
2435
Ld
2542
Lwh
2905
Ar
2980
Ak
3040
Ab
3050
Dw
3095
3357

APPENDIX B
DATA ENTRY

CANTERBURY BASIN

CLIPPER-1						CANTERBURY BASIN		
Age	**Depth**	**In. Poro.**	**C-value**	**Progressive decomp. Thickness**	**Tec. Sub.**	**Bath.**	**Min.**	**Max.**
0	0			4684	2237	177	177	177
3	774			4207	2029	200	120	500
5	1190	0.5	0.00044	3898	1895	200	120	500
11	1654	0.45	0.00033	3570	1752	200	120	500
15	2100	0.56	0.00039	3199	1741	350	200	500
19	2100	0.56	0.00039	3199	1551	160	120	200
22	2139	0.45	0.00033	3174	1500	120	50	200
24	2201	0.45	0.00033	3135	1483	120	50	200
26.5	2233	0.7	0.00071	3096	1466	120	50	200
37	2350	0.7	0.00071	2933	1435	160	120	200
44	2387	0.5	0.00044	2899	1420	160	120	200
47	2410	0.56	0.00039	2876	1411	160	120	200
49	2490	0.56	0.00039	2796	1376	160	120	200
53	2692	0.56	0.00039	2587	1285	160	120	200
65	3167	0.56	0.00039	2052	1242	350	200	500
75	3364	0.5	0.00044	1828	915	120	50	200
85	4205	0.5	0.00044	716	311	0	0	0
94	4684	0.45	0.00033	0	0	0	0	0

EALING-1						CANTERBURY BASIN		
Age	**Depth**	**In. Poro.**	**C-value**	**Progressive decomp. Thickness**	**Tec. Sub.**	**Bath.**	**Min.**	**Max.**
0	0			1694	737	0	0	0
2	637			1201	522	0	0	0
3	637	0.5	0.00044	1201	532	10	0	20
4	824	0.5	0.00044	1027	457	10	0	20
5.5	985	0.5	0.00044	865	386	10	0	20
7	1219	0.5	0.00044	606	273	10	0	20
16	1219	0.5	0.00044	606	298	35	0	50
25	1304	0.56	0.00039	498	251	35	0	50
43	1304	0.56	0.00039	498	251	35	0	50
46	1350	0.45	0.00033	446	229	35	0	50
56	1418	0.5	0.00044	358	256	100	20	200
65	1469	0.5	0.00044	289	226	100	20	200
84	1613	0.45	0.00033	107	57	10	0	20
108	1694	0.45	0.00033	0	0	0	0	0

GALLEON-1						CANTERBURY BASIN		
Age	**Depth**	**In. Poro.**	**C-value**	**Progressive decomp. Thickness**	**Tec. Sub.**	**Bath.**	**Min.**	**Max.**
0	0			3026	1476	117	117	117
3	410			2778	1368	160	120	200
4	550	0.5	0.00044	2685	1327	160	120	200
5	831	0.56	0.00039	2478	1237	160	120	200
15	1357	0.56	0.00039	2034	1045	160	120	200
19	1357	0.56	0.00039	2034	1045	160	120	200
28	1828	0.56	0.00039	1584	849	160	120	200
39	1887	0.7	0.00077	1483	805	160	120	200
65	2513	0.5	0.00044	736	405	85	50	120
69.7	2748	0.5	0.00044	397	198	25	0	50
71	2814	0.45	0.00033	307	143	10	0	20
72.7	2898	0.45	0.00033	189	82	0	0	0
75	3026	0.45	0.00033	0	110	110	20	200

KOWAI-1						CANTERBURY BASIN		
Age	**Depth**	**In. Poro.**	**C-value**	**Progressive decomp. Thickness**	**Tec. Sub.**	**Bath.**	**Min.**	**Max.**
0	0			973	423	0	0	0
0.01	7			967	430	10	0	20
3	7	0.45	0.00033	967	430	10	0	20
5	537	0.45	0.00033	537	243	10	0	20
19	537	0.45	0.00033	537	243	10	0	20
22	652	0.7	0.00071	374	173	10	0	20
25	795.5	0.45	0.00033	223	117	20	0	50
28	795.5	0.45	0.00033	223	147	50	20	120
37	806.5	0.7	0.00071	202	138	50	20	120
46	852.5	0.45	0.00033	150	115	50	20	120
50	869	0.5	0.00044	130	106	50	20	120
65	869	0.5	0.00044	130	56	0	0	0
70	926.5	0.5	0.00044	56	24	0	0	0
75	972.5	0.45	0.00033	0	0	0	0	0

LEESTON-1						CANTERBURY BASIN		
Age	**Depth**	**In. Poro.**	**C-value**	Progressive decomp. Thickness	**Tec. Sub.**	**Bath.**	**Min.**	**Max.**
0	0			1040	452	0	0	0
2.5	360			728	316	0	0	0
3	360	0.45	0.00033	728	351	35	20	50
5	420	0.45	0.00033	671	327	35	20	50
7	420	0.45	0.00033	671	377	85	50	120
11	580	0.45	0.00033	514	309	85	50	120
37	580	0.45	0.00033	514	259	35	20	50
46	640	0.45	0.00033	453	232	35	20	50
56	865	0.45	0.00033	208	125	35	20	50
60	910	0.45	0.00033	156	103	35	20	50
65	980	0.45	0.00033	73	67	35	20	50
75	1010	0.45	0.00033	37	116	100	20	200
84	1040	0.45	0.00033	0	100	100	20	200

RESOLUTION-1						CANTERBURY BASIN		
Age	**Depth**	**In. Poro.**	**C-value**	**Progressive decomp. Thickness**	**Tec. Sub.**	**Bath.**	**Min.**	**Max.**
0	0			1700	839	74	74	74
1	395			1414	715	100	0	200
2	445	0.5	0.00044	1374	697	100	0	200
3	570	0.5	0.00044	1270	652	100	0	200
4.2	640	0.45	0.00033	1214	553	25	0	50
5	700	0.45	0.00033	1165	517	10	0	20
6	800	0.5	0.00044	1075	493	25	0	50
6.5	850	0.5	0.00044	1029	533	85	50	120
9	1100	0.56	0.00039	776	422	85	50	120
12	1237	0.56	0.00039	627	433	160	120	200
15	1265	0.5	0.00044	598	420	160	120	200
16	1270	0.5	0.00044	592	418	160	120	200
19	1300	0.7	0.00071	538	319	85	50	120
28	1300	0.7	0.00071	538	394	160	120	200
37	1330	0.7	0.00071	478	368	160	120	200
39	1338	0.5	0.00044	468	363	160	120	200
44	1380	0.5	0.00044	414	340	160	120	200
47	1415	0.5	0.00044	369	320	160	120	200
50	1465	0.5	0.00044	301	291	160	120	200
51.5	1490	0.45	0.00033	271	278	160	120	200
65	1675	0.45	0.00033	34	50	35	20	50
75	1700	0.45	0.00033	0	0	0	0	0

APPENDIX B
DATA ENTRY

GREAT SOUTH BASIN

HOIHO-1						GREAT SOUTH BASIN		
Age	**Depth**	**In. Poro.**	**C-value**	Progressive decomp. Thickness	**Tec. Sub.**	**Bath.**	**Min.**	**Max.**
0	0			2247	1677	688	688	688
12	734			1791	1279	500	200	1500
28	734	0.7	0.00071	1791	1779	1000	500	1500
37	1101.1	0.7	0.00071	1372	1597	1000	500	1500
44	1182	0.5	0.00044	1292	1062	500	200	1500
47	1276	0.5	0.00044	1195	1019	500	200	1500
48	1276	0.5	0.00044	1195	1019	500	200	1500
49	1282	0.5	0.00044	1188	1017	500	200	1500
50	1380	0.5	0.00044	1082	671	200	120	500
51	1437	0.5	0.00044	1019	643	200	120	500
53	1495	0.5	0.00044	952	614	200	120	500
65	1701	0.5	0.00044	698	354	50	20	120
70	1701	0.5	0.00044	698	404	100	20	200
75	1881	0.45	0.00033	484	310	100	20	200
85	2032	0.45	0.00033	293	152	25	0	50
97	2247	0.45	0.00033	0	0	0	0	0

KAWAU-1						GREAT SOUTH BASIN		
Age	**Depth**	**In. Poro.**	**C-value**	Progressive decomp. Thickness	**Tec. Sub.**	**Bath.**	**Min.**	**Max.**
0	0			3672	2297	714	714	714
15	699			3335	2450	1000	500	1500
16	1130	0.7	0.00071	3029	2317	1000	500	1500
19	1245	0.7	0.00071	2936	2276	1000	500	1500
28	1322	0.7	0.00071	2869	2248	1000	500	1500
37	1533	0.7	0.00071	2675	2163	1000	500	1500
44	1588	0.7	0.00071	2620	1639	500	200	1500
47	1800	0.7	0.00071	2384	1386	350	200	500
48	1853	0.7	0.00071	2317	1358	350	200	500
49	1959	0.7	0.00071	2160	1289	350	200	500
54	2109	0.56	0.00039	2001	1220	350	200	500
65	2854	0.5	0.00044	1158	528	25	0	50
75	2957	0.5	0.00044	1025	471	25	0	50
80	3251	0.5	0.00044	609	290	25	0	50
85	3251	0.45	0.00033	609	265	0	0	0
90	3291	0.45	0.00033	555	241	0	0	0
91	3508	0.45	0.00033	250	109	0	0	0
93	3607	0.45	0.00033	101	44	0	0	0
102	3672	0.45	0.00033	0	0	0	0	0

PAKAHA-1						GREAT SOUTH BASIN		
Age	**Depth**	**In. Poro.**	**C-value**	Progressive decomp. Thickness	**Tec. Sub.**	**Bath.**	**Min.**	**Max.**
0	0			3284	2128	715	715	715
26.5	1024			2616	1488	350	200	500
28	1115	0.7	0.00071	2508	1590	500	200	1500
44	1145	0.56	0.00039	2482	2079	1000	500	1500
47	1408	0.56	0.00039	2245	1776	800	120	1500
48	1676	0.5	0.00044	1995	1667	800	120	1500
49	1889	0.5	0.00044	1783	1125	350	200	500
51	2057	0.5	0.00044	1609	1049	350	200	500
53	2438	0.5	0.00044	1180	863	350	200	500
65	3105	0.5	0.00044	264	235	120	50	200
75	3284	0.45	0.00033	0	50	50	20	120

RAKIURA-1						GREAT SOUTH BASIN		
Age	**Depth**	**In. Poro.**	**C-value**	Progressive decomp. Thickness	**Tec. Sub.**	**Bath.**	**Min.**	**Max.**
0	0			2368	1730	672	672	672
49	1189			1444	713	85	50	120
50	1189	0.45	0.00033	1444	678	50	20	200
51	1326	0.45	0.00033	1326	626	50	20	200
53	1490	0.45	0.00033	1183	564	50	20	200
65	1737	0.45	0.00033	975	459	35	0	50
75	1929	0.63	0.00051	731	353	35	0	50
85	2176	0.63	0.00051	363	193	35	0	50
85.1	2176	0.63	0.00051	363	193	35	0	50
87	2368	0.63	0.00051	0	35	35	0	50

TARA-1						GREAT SOUTH BASIN		
Age	**Depth**	**In. Poro.**	**C-value**	Progressive decomp. Thickness	**Tec. Sub.**	**Bath.**	**Min.**	**Max.**
0	0			4283	2012	155	155	155
2	708			3869	1732	50	20	120
11	708	0.7	0.00071	3869	2182	500	200	1500
12	889	0.7	0.00071	3681	2101	500	200	1500
39	889	0.7	0.00071	3682	1721	120	50	200
44	914	0.5	0.00044	3662	1752	160	120	500
47	1033	0.5	0.00044	3562	1574	25	0	50
48	1342	0.45	0.00033	3316	1467	25	0	50
49	1756	0.45	0.00033	2967	1315	25	0	50
51	1847	0.56	0.00039	2870	1273	25	0	50
53	1929	0.45	0.00033	2796	1241	25	0	50
65	2401	0.45	0.00033	2348	1021	0	0	0
75	3611	0.45	0.00033	1061	461	0	0	0
85	4084	0.56	0.00039	309	134	0	0	0
85.1	4084	0.56	0.00039	309	134	0	0	0
88	4283	0.45	0.00033	0	0	0	0	0

TOROA-1						GREAT SOUTH BASIN		
Age	**Depth**	**In. Poro.**	**C-value**	Progressive decomp. Thickness	**Tec. Sub.**	**Bath.**	**Min.**	**Max.**
0		0.56	0.00039	4520	2465	511	511	511
49	873	0.56	0.00039	3935	1831	120	50	200
49.1	949	0.56	0.00039	3871	1803	120	50	200
50	1715	0.45	0.00033	3275	1544	120	50	200
53	1816	0.63	0.00051	3152	1490	120	50	200
65	2851	0.45	0.00033	2206	994	35	0	50
75	3596	0.5	0.00044	1357	615	25	0	50
87	4520	0.5	0.00044	0	25	25	0	50

APPENDIX B
DATA ENTRY

WESTERN SOUTHLAND BASIN

HAPPY VALLEY-1			WESTERN SOUTHLAND BASINS					
Age	**Depth**	**In. Poro.**	**C-value**	Progressive decomp. Thickness	**Tec. Sub.**	**Bath.**	**Min.**	**Max.**
0	0			3270	1422	0	0	0
16	300			3086	1442	100	0	200
19	750	0.5	0.00044	2766	1323	120	50	200
22	1150	0.5	0.00044	2437	1260	200	120	500
25	1350	0.5	0.00044	2256	1141	160	120	200
27	1450	0.5	0.00044	2161	1100	160	120	200
34	1900	0.5	0.00044	1687	734	0	0	0
40	3270	0.45	0.00033	0	0	0	0	0

PARARA-1			WESTERN SOUTHLAND BASINS					
Age	**Depth**	**In. Poro.**	**C-value**	Progressive decomp. Thickness	**Tec. Sub.**	**Bath.**	**Min.**	**Max.**
0	0			3780	1943	147	147	147
1	622			3419	1687	200	120	500
1.36	999	0.56	0.00039	3160	1574	200	120	500
2	1185	0.56	0.00039	3024	1435	120	50	200
3	1371	0.56	0.00039	2883	1374	120	50	200
5	1558	0.56	0.00039	2740	1312	120	50	200
6	1713	0.56	0.00039	2622	1300	160	120	200
11	1841	0.63	0.00051	2503	1248	160	120	200
12.5	2131	0.63	0.00051	2213	1122	160	120	200
15	2560	0.63	0.00051	1726	950	200	160	500
16	2629	0.63	0.00051	1641	914	200	160	500
19	2754	0.63	0.00051	1481	764	120	50	200
24	2835	0.7	0.00071	1334	700	120	50	200
26.5	2930	0.63	0.00051	1177	672	160	120	200
28	2965	0.63	0.00051	1113	644	160	120	200
37	2994	0.45	0.00033	1078	479	10	0	20
39	3056	0.45	0.00033	1002	436	0	0	0
44	3117	0.45	0.00033	926	402	0	0	0
47	3179	0.45	0.00033	847	368	0	0	0
53	3359	0.45	0.00033	611	266	0	0	0
65	3569	0.45	0.00033	318	138	0	0	0
75	3780	0.45	0.00033	0	0	0	0	0

SOLANDER-1				WESTERN SOUTHLAND BASINS				
Age	**Depth**	**In. Poro.**	**C-value**	Progressive decomp. Thickness	**Tec. Sub.**	**Bath.**	**Min.**	**Max.**
0	0			1971	957	81	81	81
5	178			1850	1155	350	200	500
6	867	0.5	0.00044	1274	904	350	200	500
11	867	0.5	0.00044	1274	754	200	120	500
12.5	1039	0.45	0.00033	1117	686	200	120	500
15	1249	0.5	0.00044	893	588	200	120	500
16	1274	0.5	0.00044	865	576	200	120	500
19	1356	0.5	0.00044	771	535	200	120	500
24	1672	0.7	0.00071	438	391	200	120	500
25.8	1827	0.45	0.00033	294	238	110	20	200
26.5	1891	0.45	0.00033	209	201	110	20	200
37	1971	0.45	0.00033	0	10	10	0	20

UPUKERORA-1				WESTERN SOUTHLAND BASINS				
Age	**Depth**	**In. Poro.**	**C-value**	Progressive decomp. Thickness	**Tec. Sub.**	**Bath.**	**Min.**	**Max.**
0	0			2009	874	0	0	0
2	6.4			2005	872	0	0	0
2.5	36	0.45	0.00033	1986	863	0	0	0
5	131	0.45	0.00033	1923	846	10	0	20
19	131	0.45	0.00033	1923	946	110	20	200
22	519	0.5	0.00044	1633	820	110	20	200
28	1053	0.56	0.00039	1315	772	200	120	500
37	1135	0.45	0.00033	1033	649	200	120	500
44	2009	0.45	0.00033	0	200	200	120	500

APPENDIX B
DATA ENTRY

WEST COAST BASIN

ARATIKA-2						WEST COAST BASIN		
Age	**Depth**	**In. Poro.**	**C-value**	Progressive decomp. Thickness	**Tec. Sub.**	**Bath.**	**Min.**	**Max.**
0	0			792	344	0	0	0
1	11			784	341	0	0	0
12	11	0.45	0.00033	784	501	160	120	200
14	213	0.5	0.00044	618	429	160	120	200
16	514	0.5	0.00044	337	307	160	120	200
19	527	0.5	0.00044	324	301	160	120	200
24	542	0.5	0.00044	309	294	160	120	200
26.5	575	0.5	0.00044	276	280	160	120	200
37	625	0.7	0.00071	196	135	50	20	120
65	625	0.7	0.00071	196	85	0	0	0
67.7	670	0.45	0.00033	147	64	0	0	0
69.5	700	0.45	0.00033	113	49	0	0	0
73	772	0.5	0.00044	24	10	0	0	0
75	792	0.45	0.00033	0	0	0	0	0

ARATIKA-3						WEST COAST BASIN		
Age	**Depth**	**In. Poro.**	**C-value**	Progressive decomp. Thickness	**Tec. Sub.**	**Bath.**	**Min.**	**Max.**
0	0			1715	746	0	0	0
0.1	105			1641	713	0	0	0
2	150	0.45	0.00033	1608	734	35	20	50
3.5	310	0.45	0.00033	1490	683	35	20	50
5	513	0.45	0.00033	1334	615	35	20	50
12	513	0.45	0.00033	1334	665	85	50	120
15	820	0.5	0.00044	1061	661	200	120	500
16	1150	0.5	0.00044	725	515	200	120	500
19	1450	0.5	0.00044	371	361	200	120	500
22	1500	0.5	0.00044	307	333	200	120	500
25	1710	0.5	0.00044	13	206	200	120	500
27	1715	0.7	0.00071	0	50	50	20	120

KOKIRI-1						WEST COAST BASIN		
Age	**Depth**	**In. Poro.**	**C-value**	Progressive decomp. Thickness	**Tec. Sub.**	**Bath.**	**Min.**	**Max.**
0	0			3203	1393	0	0	0
0.1	84			3154	1372	0	0	0
4.2	280	0.5	0.00044	3034	1354	35	20	50
5	380	0.5	0.00044	2968	1376	85	50	120
6	525	0.5	0.00044	2869	1333	85	50	120
10	930	0.5	0.00044	2565	1150	35	20	50
11	1031	0.45	0.00033	2491	1118	35	20	50
11.4	1045	0.45	0.00033	2480	1278	200	120	500
12	1061	0.5	0.00044	2467	1273	200	120	500
15	1895	0.5	0.00044	1715	946	200	120	500
16	2230	0.56	0.00039	1341	933	350	200	500
17	2418	0.56	0.00039	1109	832	350	200	500
19	2850	0.5	0.00044	551	590	350	200	500
24	3188	0.5	0.00044	26	361	350	200	500
26.5	3203	0.5	0.00044	0	350	350	200	500

KONGAHU-1						WEST COAST BASIN		
Age	**Depth**	**In. Poro.**	**C-value**	Progressive decomp. Thickness	**Tec. Sub.**	**Bath.**	**Min.**	**Max.**
0	0			1972	892	123	123	123
0.1	260			1794	815	35	20	50
2	650	0.45	0.00033	1509	691	35	20	50
3	780	0.56	0.00039	1398	643	35	20	50
5	900	0.56	0.00039	1290	596	35	20	50
6	1200	0.56	0.00039	993	632	200	120	500
11	1350	0.56	0.00039	829	710	350	200	500
12	1450	0.56	0.00039	712	660	350	200	500
15	1525	0.56	0.00039	622	620	350	200	500
16	1675	0.56	0.00039	432	538	350	200	500
19	1707	0.56	0.00039	390	255	85	50	120
36	1707	0.56	0.00039	390	180	10	0	20
37	1748	0.7	0.00071	297	139	10	0	20
47	1972	0.45	0.00033	0	0	0	0	0

KUMARA-2						WEST COAST BASIN		
Age	**Depth**	**In. Poro.**	**C-value**	Progressive decomp. Thickness	**Tec. Sub.**	**Bath.**	**Min.**	**Max.**
0	0			1771	770	0	0	0
20	67			1730	1252	500	200	1500
26	162	0.7	0.00071	1658	881	160	120	200
26.5	175	0.45	0.00033	1649	877	160	120	200
28	225	0.45	0.00033	1614	862	160	120	200
37	280	0.45	0.00033	1574	844	160	120	200
37.7	350	0.5	0.00044	1520	861	200	120	500
38.3	408	0.5	0.00044	1474	841	200	120	500
39	475	0.45	0.00033	1423	969	350	200	500
40.4	825	0.5	0.00044	1116	835	350	200	500
43.5	1627	0.5	0.00044	195	285	200	120	500
44	1661	0.5	0.00044	146	74	10	0	20
48	1675	0.45	0.00033	128	66	10	0	20
53	1722	0.45	0.00033	66	39	10	0	20
65	1771	0.45	0.00033	0	10	10	0	20

NIAGARA-1						WEST COAST BASIN		
Age	**Depth**	**In. Poro.**	**C-value**	Progressive decomp. Thickness	**Tec. Sub.**	**Bath.**	**Min.**	**Max.**
0	0			1511	657	0	0	0
0.1	72			1461	635	0	0	0
13	72	0.45	0.00033	1461	985	350	200	500
14	644	0.5	0.00044	991	781	350	200	500
15	775	0.45	0.00033	874	730	350	200	500
15.5	902	0.45	0.00033	759	680	350	200	500
16	1025	0.5	0.00044	632	625	350	200	500
17.7	1195	0.5	0.00044	447	544	350	200	500
19	1325	0.5	0.00044	298	480	350	200	500
24	1408	0.5	0.00044	203	438	350	200	500
37	1486	0.7	0.00071	33	134	120	50	200
39	1497	0.45	0.00033	18	33	25	0	50
45	1497	0.45	0.00033	18	8	0	0	0
47	1511	0.45	0.00033	0	0	0	0	0

TAPAWERA-1						WEST COAST BASIN		
Age	**Depth**	**In. Poro.**	**C-value**	Progressive decomp. Thickness	**Tec. Sub.**	**Bath.**	**Min.**	**Max.**
0	0			1152	501	0	0	0
3	697			532	231	0	0	0
21	697	0.45	0.00033	532	581	350	200	500
24	732	0.56	0.00039	492	564	350	200	500
26.5	1018	0.45	0.00033	184	280	200	120	500
28	1151.5	0.56	0.00039	0	120	120	50	200

WAIHO-1						WEST COAST BASIN		
Age	**Depth**	**In. Poro.**	**C-value**	Progressive decomp. Thickness	**Tec. Sub.**	**Bath.**	**Min.**	**Max.**
0	0			3694	1606	0	0	0
0.1	244			3551	1544	0	0	0
2	610	0.5	0.00044	3311	1464	25	0	50
3	1100	0.5	0.00044	2942	1329	50	20	120
3.8	1524	0.5	0.00044	2584	1244	120	50	200
5	2106	0.5	0.00044	2034	1084	200	120	500
10.5	3231	0.5	0.00044	738	521	200	120	500
11	3322	0.5	0.00044	614	2117	1850	200	3500
15	3612	0.5	0.00044	206	1940	1850	200	3500
15.5	3627	0.5	0.00044	185	1890	1810	120	3500
16	3694	0.7	0.00071	0	120	120	50	200

APPENDIX B
DATA ENTRY

TARANAKI BASIN

ARIKI-1						TARANAKI BASIN		
Age	**Depth**	**In. Poro.**	**C-value**	Progressive decomp. Thickness	**Tec. Sub.**	**Bath.**	**Min.**	**Max.**
0	0			4561	2156	173	173	173
1.2	600			4203	2027	200	100	300
2	1100	0.5	0.00044	3853	2175	500	300	700
4.3	1950	0.5	0.00044	3207	2395	1000	1895	2895
5.5	1951	0.5	0.00044	3207	2394	1000	1894	2894
6	2051	0.7	0.00071	3073	2436	1100	1936	2936
9	2151	0.5	0.00044	2986	2498	1200	1998	2998
16	2451	0.56	0.00039	2701	2574	1400	2074	3074
19	2901	0.5	0.00044	2303	2501	1500	2001	3001
23.5	3121	0.5	0.00044	2135	2428	1500	1928	2928
28	3361	0.7	0.00071	1836	2198	1400	1698	2698
36.5	3401	0.7	0.00071	1782	2075	1300	1575	2575
47	3651	0.7	0.00071	1374	1897	1300	1397	2397
55.5	3821	0.5	0.00044	1163	1506	1000	1006	2006
63	3991	0.5	0.00044	942	430	20	0	50
66.5	4111	0.5	0.00044	780	339	0	0	30
75	4561	0.56	0.00039	0	0	0	0	30

AWAKINO-1						TARANAKI BASIN		
Age	**Depth**	**In. Poro.**	**C-value**	Progressive decomp. Thickness	**Tec. Sub.**	**Bath.**	**Min.**	**Max.**
0	0	0.5	0.00044	6380	2836	62	62	62
10	70	0.5	0.00044	6345	3959	1200	700	1700
13	440	0.5	0.00044	6147	3973	1300	800	1800
16	940	0.5	0.00044	5846	4042	1500	1000	2000
19	1640	0.5	0.00044	5399	3847	1500	1000	2000
22	1740	0.5	0.00044	5342	3622	1300	800	1800
25	1940	0.7	0.00071	5127	2429	200	100	300
32.5	2210	0.56	0.00039	4907	2233	100	50	150
36.5	2260	0.56	0.00039	4865	2215	100	50	150
43	2560	0.56	0.00039	4608	2034	30	0	60
46.5	2780	0.56	0.00039	4413	1949	30	0	60
70	6380	0.56	0.00039	0	0	0	0	30

KAIMIRO-1						TARANAKI BASIN		
Age	**Depth**	**In. Poro.**	**C-value**	Progressive decomp. Thickness	**Tec. Sub.**	**Bath.**	**Min.**	**Max.**
0	0			6860	2983	0	0	0
0.3	210	0.45	0.00033	6752	2936	0	0	30
3	910	0.5	0.00044	6335	2755	0	0	30
5	1610	0.5	0.00044	5852	2644	100	50	150
9	2510	0.56	0.00039	5105	2370	150	50	150
10.5	3210	0.56	0.00039	4439	2730	800	600	1000
12	3410	0.5	0.00044	4250	2948	1100	600	1600
16	3780	0.5	0.00044	3889	3091	1400	900	1900
19	4210	0.5	0.00044	3444	2998	1500	1000	2000
23.5	4460	0.45	0.00033	3211	2396	1000	500	1500
25	4635	0.5	0.00044	3025	2015	700	500	900
30	4910	0.56	0.00039	2687	1268	100	50	150
36.5	5010	0.56	0.00039	2556	1131	20	0	50
42.5	5410	0.45	0.00033	2124	923	0	0	30
52	5810	0.45	0.00033	1694	737	0	0	30
59	6360	0.56	0.00039	906	394	0	0	30
75	6860	0.56	0.00039	0	0	0	0	30

KAPUNI DEEP-1						TARANAKI BASIN		
Age	**Depth**	**In. Poro.**	**C-value**	Progressive decomp. Thickness	**Tec. Sub.**	**Bath.**	**Min.**	**Max.**
0	0			4900	2131	0	0	0
0.5	172	0.56	0.00039	4809	2091	0	0	0
3	400	0.5	0.00044	4678	2044	10	0	20
5	1090	0.5	0.00044	4225	1847	10	0	20
8	1799	0.56	0.00039	3650	1787	200	120	500
10	2045	0.5	0.00044	3440	1616	120	50	200
15	2415	0.56	0.00039	3082	2340	1000	500	1500
19	2600	0.5	0.00044	2904	2263	1000	500	1500
21	2850	0.5	0.00044	2654	2154	1000	500	1500
22	3034	0.5	0.00044	2463	2071	1000	500	1500
25	3100	0.5	0.00044	2393	1161	120	50	200
27	3205	0.5	0.00044	2280	1026	35	0	50
35	3243	0.56	0.00039	2235	972	0	0	0
36	3391	0.56	0.00039	2053	893	0	0	0
43	3683	0.56	0.00039	1658	721	0	0	0
46	4008	0.45	0.00033	1265	550	0	0	0
55	4553	0.45	0.00033	535	268	35	0	50
60	4780	0.45	0.00033	193	94	10	0	20
65	4900	0.45	0.00033	0	35	35	0	50

KIWA-1						TARANAKI BASIN		
Age	**Depth**	**In. Poro.**	**C-value**	Progressive decomp. Thickness	**Tec. Sub.**	**Bath.**	**Min.**	**Max.**
0	0			3700	1794	185	185	185
3	300	0.45	0.00033	3501	1722	200	120	500
3.6	900	0.45	0.00033	3057	1529	200	120	500
5	1350	0.45	0.00033	2683	1667	500	300	700
9	1700	0.45	0.00033	2371	1831	800	600	1000
12	2450	0.45	0.00033	1644	2215	1500	1000	2000
16	2800	0.45	0.00033	1303	2066	1500	1000	2000
17	2840	0.7	0.00071	1226	2033	1500	1000	2000
23.5	2840	0.7	0.00071	1226	1533	1000	500	1500
28	2870	0.7	0.00071	1163	706	200	100	300
36.5	2880	0.7	0.00071	1141	646	150	50	250
42.5	2930	0.5	0.00044	1074	567	100	50	150
47	3060	0.5	0.00044	894	389	0	0	0
58.5	3280	0.45	0.00033	608	264	0	0	0
66.5	3480	0.45	0.00033	331	144	0	0	0
75	3700	0.45	0.00033	0	0	0	0	0

KUPE-1						TARANAKI BASIN		
Age	**Depth**	**In. Poro.**	**C-value**	Progressive decomp. Thickness	**Tec. Sub.**	**Bath.**	**Min.**	**Max.**
0	0			3682	1639	38	38	38
1	213	0.45	0.00033	3559	1582	35	0	50
1.4	254	0.5	0.00044	3534	1571	35	0	50
3.1	944	0.5	0.00044	3055	1363	35	0	50
3.3	1140	0.5	0.00044	2900	1296	35	0	50
3.6	1400	0.5	0.00044	2682	1201	35	0	50
4	1710	0.5	0.00044	2402	1054	10	0	50
4.5	1877	0.45	0.00033	2263	994	10	0	50
5	1910	0.5	0.00044	2231	980	10	0	50
6	1980	0.5	0.00044	2164	951	10	0	50
8	2000	0.5	0.00044	2145	943	10	0	50
10	2050	0.5	0.00044	2096	996	85	50	120
13	2377	0.5	0.00044	1765	853	85	50	120
15	2540	0.5	0.00044	1592	777	85	50	120
16	2600	0.56	0.00039	1521	746	85	50	120
18	2900	0.56	0.00039	1144	582	85	50	120
19	3000	0.56	0.00039	1007	638	200	120	500
25	3120	0.56	0.00039	834	563	200	120	500
34	3190	0.45	0.00033	749	526	200	120	500
36	3264	0.45	0.00033	658	296	10	0	20
49	3423	0.5	0.00044	426	195	10	0	20
65	3682	0.5	0.00044	0	10	10	0	20

MAUI-2						TARANAKI BASIN		
Age	**Depth**	**In. Poro.**	**C-value**	Progressive decomp. Thickness	**Tec. Sub.**	**Bath.**	**Min.**	**Max.**
0	0			3410	1626	143	143	143
3.2	300	0.45	0.00033	3233	1456	50	0	100
5	550	0.5	0.00044	3069	1434	100	50	150
9	1010	0.5	0.00044	2731	1687	500	300	700
12	1660	0.56	0.00039	2133	2227	1300	800	1800
16	2340	0.45	0.00033	1539	2169	1500	1000	2000
18	2450	0.5	0.00044	1441	2126	1500	1000	2000
23.5	2450	0.7	0.00071	1441	1626	1000	500	1500
25	2550	0.7	0.00071	1275	704	150	50	250
27	2570	0.7	0.00071	1236	637	100	50	150
42.5	2580	0.5	0.00044	1224	582	50	0	100
45	2630	0.5	0.00044	1167	557	50	0	100
58.5	3360	0.56	0.00039	77	33	0	0	0
60	3410	0.45	0.00033	0	0	0	0	0

SURVILLE-1						TARANAKI BASIN		
Age	**Depth**	**In. Poro.**	**C-value**	Progressive decomp. Thickness	**Tec. Sub.**	**Bath.**	**Min.**	**Max.**
0	0			2057	894	0	0	0
14	265	0.45	0.00033	1886	820	0	0	0
15	311	0.56	0.00039	1853	816	10	0	20
16	484	0.56	0.00039	1725	760	10	0	20
16.3	510	0.56	0.00039	1705	751	10	0	20
19	750	0.56	0.00039	1506	690	35	20	50
24	1040	0.56	0.00039	1234	571	35	20	50
26.5	1150	0.56	0.00039	1120	522	35	20	50
28	1430	0.56	0.00039	797	382	35	20	50
32	1497	0.56	0.00039	711	344	35	20	50
37	1573	0.45	0.00033	626	282	10	0	20
38	1627	0.56	0.00039	551	250	10	0	20
47	2057	0.45	0.00033	0	0	0	0	0

TANE-1						TARANAKI BASIN		
Age	**Depth**	**In. Poro.**	**C-value**	Progressive decomp. Thickness	**Tec. Sub.**	**Bath.**	**Min.**	**Max.**
0	0			4420	2107	185	185	185
1.2	500	0.56	0.00039	4137	1949	150	50	200
2.2	960	0.56	0.00039	3823	1862	200	120	500
2.7	1250	0.56	0.00039	3600	1765	200	120	500
5	1950	0.56	0.00039	2977	2295	1000	500	1500
6	2140	0.5	0.00044	2796	2216	1000	500	1500
11	2350	0.45	0.00033	2616	2138	1000	500	1500
12	2450	0.5	0.00044	2518	2095	1000	500	1500
15	2550	0.56	0.00039	2411	2048	1000	500	1500
16	2606	0.5	0.00044	2353	2023	1000	500	1500
19	2614	0.5	0.00044	2345	2020	1000	500	1500
25	2626	0.5	0.00044	2333	2014	1000	500	1500
34	2632	0.5	0.00044	2326	2011	1000	500	1500
37	2635	0.5	0.00044	2323	1130	120	50	200
46	2836	0.5	0.00044	2111	1038	120	50	200
53	2950	0.5	0.00044	1986	984	120	50	200
55	3180	0.5	0.00044	1725	870	120	50	200
65	3450	0.56	0.00039	1362	712	120	50	200
75	3625	0.5	0.00044	1122	523	35	0	50
85	4420	0.45	0.00033	0	10	10	0	20

APPENDIX B
DATA ENTRY

NORTHLAND BASIN

WAIMAMAKU-2						NORTHLAND BASIN		
Age	**Depth**	**In. Poro.**	**C-value**	Progressive decomp. Thickness	**Tec. Sub.**	**Bath.**	**Min.**	**Max.**
0	0			3095	1346	0	0	0
0.5	105			3033	1419	100	80	120
15	105	0.5	0.00044	3033	2219	900	800	1000
21	1120	0.5	0.00044	2923	2171	900	800	1000
25	2434	0.5	0.00044	940	2109	1700	1500	2000
27	2542	0.5	0.00044	801	1948	1600	1500	1700
34	2905	0.5	0.00044	278	1121	1000	500	1500
36	2980	0.45	0.00033	171	1074	1000	500	1500
37	3040	0.45	0.00033	83	1036	1000	500	1500
43	3050	0.45	0.00033	68	229	200	120	500
55	3095	0.45	0.00033	0	0	0	0	0

APPENDIX C

WELL REPORT REFERENCES

Carter, M. J. / Petroleum Corporation of New Zealand Exploration Ltd.; 1983; Kaimiro-1 Well Completion Report. PPL 38091. Ministry of Economic Development, New Zealand. Unpublished Petroleum, Report # 936.

Carter, M. J. / Petroleum Corporation of New Zealand Explorarion Ltd.; 1981; Kokiri-1 Well Completion Report, PPL38038. Ministry of Economic Development, New Zealand. Unpublished Petroleum, Report # 799.

Carter, M. J.; Kelly, C.; Hillyer, M.; McDowell, P. / Petroleum Corporation of New Zealand Exploration Ltd.; 1986; Kumara-2, -2A Well Completion Report. PPL38070. Ministry of Economic Development, New Zealand. Unpublished Petroleum, Report # 1183.

Carter, M. J.; Rainey, S. / Petroleum Corporation of New Zealand Exploration Ltd.; 1988; Well Completion Report, Happy Valley-1, -1A, -1B, -1C. PPL38074. Ministry of Economic Development, New Zealand. Unpublished Petroleum, Report # 1382.

Carter, M. J.; Rainey, S. / Petroleum Corporation of New Zealand Exploration Ltd.; 1988; Well Completion Report, Upukerora-1. PPL38074. Ministry of Economic Development, New Zealand. Unpublished Petroleum, Report # 1381.

De Dock, J. F.; True, T.; Lammerink, W.; Kelly, C.; McDowell, P. / Petroleum Corporation of New Zealand Exploration Ltd.; 1985; Awakino-1 Well Completion Report. PPL38094. Ministry of Economic Development, New Zealand. Unpublished Petroleum, Report # 1140.

Engmann, L. A.; Fenton, P. H. / BP Oil Exporation Company New Zealand Ltd.; 1986; Well Completion Report, Solander-1. PPL38206. Ministry of Economic Development, New Zealand. Unpublished Petroleum, Report # 1149.

Harrison, J. / Offshore Mining Company Ltd.; 1977; Well Completion Report, Aratika No. 2. Ministry of Economic Development, New Zealand. Unpublished Petroleum, Report # 719.

Hoolihan, K. / Offshore Mining Company Ltd.; 1978; Kowai-1 Well Completion Report. Ministry of Economic Development, New Zealand. Unpublished Petroleum, Report # 722.

Indo-Pacific Energy (New Zealand); 2000; Ealing-1 Well Completion Report. Ministry of Economic Development, New Zealand. Unpublished Petroleum, Report # 2559.

Milne, A. D. / Shell BP Todd Canterbury Services Ltd.; 1975; Resolution-1 Well Completion Report. Ministry of Economic Development, New Zealand. Unpublished Petroleum, Report # 648.

New Zealand Aquitaine Petroleum Ltd.; 1976; Well Completion Report, Surville-1. Ministry of Economic Development, New Zealand. Unpublished Petroleum, Report # 677.

New Zealand Hunt International Petroleum Company; 1978; Hoiho-1C Well Completion Report. Ministry of Economic Development, New Zealand. Unpublished Petroleum, Report # 730.

New Zealand Hunt International Petroleum Company; 1977; Final Report, Kawau-1. Ministry of Economic Development, New Zealand. Unpublished Petroleum, Report # 716.

New Zealand Hunt International Petroleum Company; 1977; Pakaha-1 Well Completion Report. Ministry of Economic Development, New Zealand. Unpublished Petroleum, Report # 703.

New Zealand Hunt International Petroleum Company; 1978; Tara-1 well completion report. PPL740. Ministry of Economic Development, New Zealand. Unpublished Petroleum, Report # 732.

New Zealand Hunt International Petroleum Company; 1977; Toroa-1 Well Completion Report. Ministry of Economic Development, New Zealand. Unpublished Petroleum, Report # 691.

New Zealand Hunt International Petroleum Company; 1976; Well Completion Report , Parara-1. Ministry of Economic Development, New Zealand. Unpublished Petroleum, Report # 673.

Placid Oil Company; 1984; Well Report, Rakiura-1, Great South Basin, New Zealand. Ministry of Economic Development, New Zealand. Unpublished Petroleum, Report # 994.

Rainey, S.; Waghorn, D. / Petroleum Corporation of New Zealand Ltd.; 1989; Tapawera-1 Well Completion Report. PPL38500. Ministry of Economic Development, New Zealand. Unpublished Petroleum, Report # 1445.

Shell BP and Todd Oil Services Ltd.; 1984; Completion Report. Ariki-1 Well. PPL38048. Ministry of Economic Development, New Zealand. Unpublished Petroleum, Report # 1038.

Shell BP and Todd Oil Services Ltd.; 1982; Well Resume Kiwa-1. PPL38055. Ministry of Economic Development, New Zealand. Unpublished Petroleum, Report # 880.

Shell BP and Todd Oil Services Ltd.; 1976; Well Resume Kupe-1. Ministry of Economic Development, New Zealand. Unpublished Petroleum, Report # 662.

Shell BP and Todd Oil Services Ltd.; 1970; Well Resume Maui-2. Ministry of Economic Development, New Zealand. Unpublished Petroleum, Report # 541.

Shell BP and Todd Oil Services Ltd.; 1976; Well Resume, Tane-1 (Offshore). Ministry of Economic Development, New Zealand. Unpublished Petroleum, Report # 698.

Shell BP Todd Canterbury Services Ltd.; 1984; Drilling Completion Report, Clipper-1. Offshore Canterbury, South Island, New Zealand. PPL 38202. Ministry of Economic Development, New Zealand. Unpublished Petroleum, Report # 1036.

Smart, G. M. / New Zealand Petroleum Exploration Company Ltd.; 1972; Waiho-1 Exploratory Well, Westland, South Island, New Zealand. Ministry of Economic Development, New Zealand. Unpublished Petroleum, Report # 529.

Wilson, I. R. and others / Shell BP Todd Canterbury Services Ltd.; 1985; Well Completion Report, Galleon-1. PPL 38203. Ministry of Economic Development, New Zealand. Unpublished Petroleum, Report # 1146.

Wiltshire, M. J. / Home Energy New Zealand Ltd.; 1984; Well Completion Report, Kongahu-1. PPL38058. Offshore, West Coast, South Island, New Zealand. Ministry of Economic Development, New Zealand. Unpublished Petroleum, Report # 1035.

Wood, B. L. / New Zealand Petroleum Exploration Co. Ltd.; 1969; Leeston-1. Ministry of Economic Development, New Zealand. Unpublished Petroleum, Report # 526.